論文 / 著書情報
Article / Book Information

題目(和文)	高温多湿気候における潜熱蓄熱材を用いた自然換気住宅の熱環境性能評価に関する研究
Title(English)	Thermal performance evaluation of naturally ventilated buildings installed phase change materials in hot and humid climates
著者(和文)	北川遼
Author(English)	Haruka Kitagawa
出典(和文)	学位:博士(工学), 学位授与機関:東京工業大学, 報告番号:甲第12787号, 授与年月日:2024年3月26日, 学位の種別:課程博士, 審査員:淺輪 貴史,松岡 昌志,鍵 直樹,大風 翼,湯淺 和博
Citation(English)	Degree:Doctor (Engineering), Conferring organization: Tokyo Institute of Technology, Report number:甲第12787号, Conferred date:2024/3/26, Degree Type:Course doctor, Examiner:,,,,
学位種別(和文)	博士論文
Type(English)	Doctoral Thesis

Doctoral Dissertation

高温多湿気候における潜熱蓄熱材を用いた
自然換気住宅の熱環境性能評価に関する研究

Thermal performance evaluation of naturally ventilated buildings installed phase change materials in hot and humid climates

Haruka Kitagawa

School of Environment and Society
Department of Architecture and Building Engineering
Graduate major in Urban Design and Built Environment
Tokyo Institute of Technology

February 2024

Abstract

Currently, hot environments, which are caused by climate change and heat island effects, have become critical in various climate regions, and thus the rise in temperature results in an increase in electricity consumption for space cooling. In particular, the cooling demand in hot and humid climate regions tends to be high for an entire year because the daily maximum temperature usually exceeds 30 ℃ with a high humidity of 70–90%. Passive cooling methods utilize natural resources by means of architectural elements to reduce the cooling load in buildings. Previous studies have recommended the use of a combination of several passive cooling methods to improve the cooling effect because single passive cooling method alone is difficult to achieve thermal comfort during daytime in the hot and humid climates. Thus, it is particularly important to determine an effective combination of passive cooling methods to achieve thermal comfort in hot and humid climate regions throughout a year. The main objective of this study is to clarify a thermal performance of residential buildings with an effective combination of passive cooling methods for hot and humid climates in terms of thermal comfort. In particular, this study focuses on the combination of natural ventilation and phase change material (PCM), and then evaluates its cooling effect on residential buildings.

Firstly, the comprehensive overview of the passive cooling methods in hot and humid climates was presented using a text mining-based bibliometric analysis method in Chapter 2. The results using 39,604 publications showed that natural ventilation took a vital role in passive cooling methods improving thermal comfort in hot and humid climates. Meanwhile, the increase in thermal storage using PCM in low thermal mass buildings improves the cooling effect and is expected to compensate the disadvantage of natural

ventilation due to the fluctuations of wind conditions, and a number of studies on PCM has rapidly increased since the 2010s. This implies that the combination of natural ventilation and thermal storage of PCM is a promising option improving thermal comfort further under hot and humid conditions, although the combination of natural ventilation and PCM was not observed in the co-occurrence networks and previous research. Based on the results, Chapter 2 finally proposes a comprehensive floor cooling system that includes window systems, window-opening control, and PCMs for naturally ventilated buildings.

Based on the proposal, a field measurement was conducted to determine the window design that optimizes indoor air flow pattern to provide comfort ventilation while maintaining thermal storage effect of the proposed system in Chapter 3. The results showed that the horizontal pivot window is a preferable window system in the hot and humid climate. The horizontal pivot windows led to inflows to the occupied level regardless of the outdoor condition, while reducing the heat transfer coefficient on the floor was by 1.5 W/m^2K compared with that of the simple opening. Nevertheless, the increase in thermal storage owing to the PCMs had a greater effect on the retention of the floor cooling effect, compared with the effect of the window design.

Therefore, another field measurement was conducted to clarify the measures to ensure the thermal storage effect of the proposed system in Chapter 4. The thermal storage effect of latent heat with an appropriate phase change temperature is particularly influential in lowering the floor surface temperature. Although calm wind conditions and warm nocturnal ambient temperature are common in the hot and humid climate region and they prevented the PCMs from solidifying in case of natural ventilation for the underfloor space, forced ventilation for the underfloor space was effective in ensuring sufficient solidification.

Based on the results of the field measurements, a computational fluid dynamics (CFD) simulation coupled with a heat balance analysis was conducted to clarify the key parameter of thermal storage effect which cannot be investigated in the field measurements in Chapter 5. In the proposed floor cooling system, the air velocity that ensures the solidification of the PCMs in the underfloor space was found to be a key parameter, and thermal storage was maximized when the operational schedule of the underfloor ventilation was controlled by the outdoor temperature.

Referring to the results of the cooling method for the PCMs in Chapter 5, the thermal energy simulation (TES) was developed in Chapter 6 to evaluate the annual performance of the proposed floor cooling system that considers the hysteresis of PCM and to determine its design guidelines and indicators. Regarding the indicator of the phase change of the PCM, the daily maximum and minimum ambient temperatures of the PCMs significantly affected the maximum and minimum liquid fractions, respectively, and thus it can be a useful guideline for selecting a phase change temperature besides the daily average ambient temperature of PCMs. Moreover, the maximum liquid fraction strongly influenced the retention of the thermal storage effect of the PCM because its cooling effect decreased rapidly after the melted

completely. Based on the annual TES, a reasonable annual average utilization rate of approximately 70% was determined to maintain a low floor surface temperature throughout the year.

Finally, the annual TES was conducted to determine the optimum window-opening control that maximizes annual thermal comfort using the optimum window system and PCMs with the optimum operation in Chapter 7. The TES model developed in Chapter 6 was modified by coupling with the air flow network model. The resultant annual thermal comfort period based on the SET* increased up to 83.3% throughout the year, while the annual electricity consumption for space cooling in the test room with the proposed system was reduced by 41% compared with that of the control room. In the morning, the thermal storage effect of the PCMs using night ventilation extended the thermal comfort period and reduced the cooling load. As the outdoor air temperature increased, the outdoor wind speed tended to increase, and the ventilative cooling compensated for the increased room temperature. Considering the influences of room temperature and air velocity on the SET*, opening the windows when the indoor temperature exceeds 27 ℃ with night ventilation can maximize the annual thermal comfort in hot and humid climates.

When the above-mentioned findings for the combination of natural ventilation and PCM were applied, occupants in hot and humid climates can spend most of the year comfortably without ACs, thereby reducing the energy consumption. The results of the field measurements and simulation models constructed in this study can be used as a guideline for the installation of PCMs to naturally ventilated buildings in hot and humid climates.

Contents

Chapter 1
Introduction

Abstract

Chapter 1 provides a general background and discusses problems regarding buildings to determine the main focus of this thesis. In hot and humid climate regions, the daily maximum temperature usually exceeds 30 ℃ with a high humidity of 70–90% year-round. Chapter 1 discusses the situation in Indonesia, where typical issues of tropical developing countries, such as rapid economic growth and urbanization, have been experienced as an example to find a solution. They cause the increase in energy consumption and greenhouse gas emissions such as CO_2 which impacts the global warming and climate change. The global warming rises the monthly mean temperature in Indonesia by 1.4–1.6 ℃ (RCP 4.5) and 2.0–2.4 ℃ (RCP8.0) between present and 2065. Consequently, the building sector, which accounts for 19% of all global GHG emissions now, has great potential and can be a strong contributor. Passive cooling methods that can improve the thermal environment without much energy consumption are feasible measures in hot and humid climate regions where the demand for space cooling was occurred throughout a year. Based on the limitations and research gaps of the existing studies on passive cooling methods, the objective and framework of this study are described.

Key words
Energy consumption, GHG reduction, Developing countries, Passive cooling methods

1.1. Background

Today, according to the World Population Prospects suggested by the United Nations, the global population continues to grow [1.1]. Until 2050, world population is expected to reach approximately 10 billion. In particular, tropical regions strongly contribute to an increasing population. As the population increases, energy consumption rises, and it is projected that global energy consumption will increase by nearly 50% between 2018 and 2050 [1.2]. Nowadays, the global energy consumption of buildings accounts for more than 40% of the total primary energy consumption, and as much as one-third of global greenhouse gas emissions [1.3]. As shown in Fig 1.1, the energy consumed in the building sector increases by 1.3% per year in the reference case from 2018 to 2050 [1.2]. Moreover, due to the rapid growth, building energy consumption in non-OECD countries, including developing tropical countries, increases at about 2% per year, about five times faster than in OECD countries [1.2].

The sector of buildings is a significant energy consumer. The IPCC reported that greenhouse gas (GHG) emissions from the building sector have more than double since 1970 to reach 9.18 $GtCO_2$-eq in 2010, representing 19% of all global GHG emissions [1.4]. Moreover, approximately 32-34% of the global final energy consumption in both residential and commercial buildings were used for room air conditioning. Based on the prediction by the IPCC, the use of energy for cooling and heating in commercial and residential buildings would increase by 79% and 83%, respectively, from 2010 to 2050. Nevertheless, the building sector is considered to have the largest potential for reducing greenhouse gas emissions compared to other major emitting sectors [1.5].

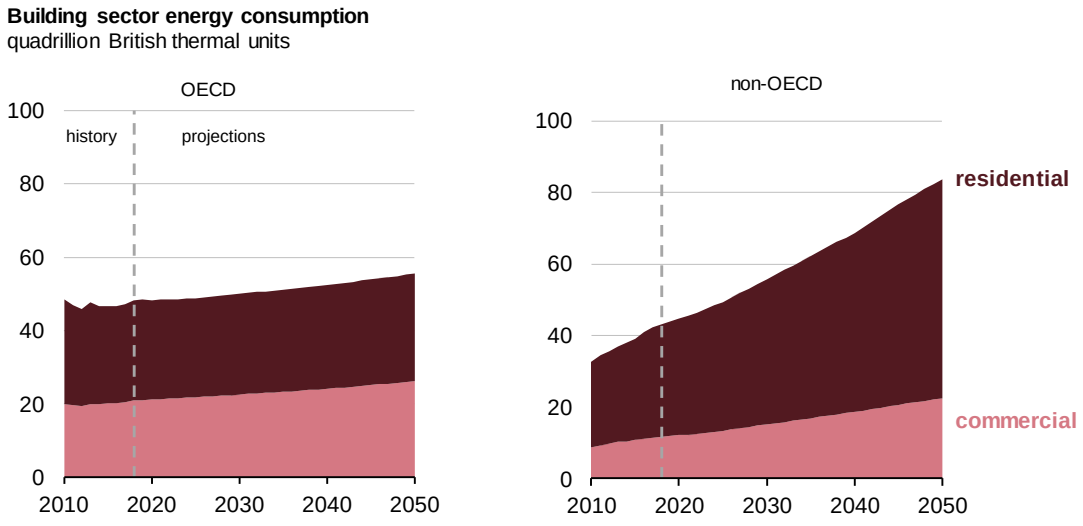

Fig. 1.1. Global energy consumption in building sector in OECD countries and non-OECD contries [1.2].

The Paris Agreement was proposed in November 2016. Now all the signatory parties, a total of 189 parties, including developing countries, need to keep the increase in global average temperature below 2 ℃ above preindustrial levels and put forward their best efforts to limit the temperature increase by 1.5 ℃ above preindustrial levels after 2020. GHG reduction is necessary to cope with climate change and pursue a sustainable low-carbon future.

1.2. Energy consumption and CO_2 emission in hot and humid regions

The rapid increase in population was particularly observed in tropical developing countries. Here, the situation in Indonesia, where typical issues of tropical developing countries have been facing, is brought up as an example in Chapter 1 to find a solution. Population of Indonesia exceeded 250 million and is the fourth-largest nation on the number of populations all over the world [1.1]. Moreover, it is projected that the population of Indonesia will reach more than 310 million people by 2045 [1.6]. The percentage of urban population is projected to increase from 49.8% in 2010 to 66.6% in 2035 [1.6].

Owing to the increase in population, urbanization, economic growth and poor environmental performance, the energy consumption has rapidly increased. The total final energy consumption (without traditional biomass) in 2018 was approximately 114 Mtoe. Based on the energy demand projection under three different scenarios, i.e., Business as Usual (BaU), Sustainable Development (PB), and Low Carbon (RK), the national energy demand will be 548.8 Mtoe (BaU), 481 Mtoe (PB) and 424.2 Mtoe (RK) in 2050 [1.7]. Similarly, GHG emissions in Indonesia are projected to increase to 2,869 million tons of CO_2 in 2050.

The use of the air conditioning also increases the GHG emission [1.8]. The IEA reported that the number of ACs for households in the Southeast Asia will increase from 40 million in 2018 to 350 million in 2040 [1.9]. Based on the number of ACs, electricity consumption will increase by 250 TWh. Moreover, a higher temperature will accelerate the electricity consumption for cooling further. Compared to present weather condition, the

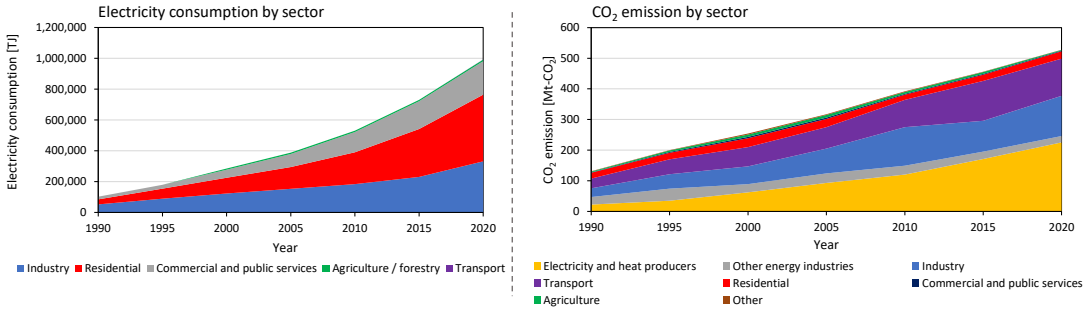

Fig. 1.2. Electricity consumption and CO_2 emission by sectors, Indonesia 1990–2020.

monthly mean temperature in Jakarta, calculated by morphing method [1.10], will increase by 1.4–1.6 ℃ under representative concentration pathways 4.5 (RCP 4.5) and 2.0–2.4 ℃ under RCP 8.0 by 2065. Although the cooling demand will become larger due to the higher temperature, the GHG reduction is necessary to suppress the temperature rise. To reduce the GHG emission, utilization of renewable energy can be a solution. However, the renewable energy generation in Indonesia accounted for only 5.5% of total energy generation in 2018 [1.11]. Therefore, reducing energy consumption on the demand side is necessary for the GHG reduction.

1.3. Urban housing in hot and humid regions

As discussed, the population of Indonesia which can be regarded as an example of a developing tropical country is continuously increasing. Most major cities in Indonesia are densely populated now. Therefore, the demand for apartments is expected to increase in the future because of the increase in the population and the limited capacity of land. Meanwhile, the economic growth of Indonesia has been being relatively high and stable growth rates in recent years, with an annual average economic growth of around 5%, and it is projected to see higher economic growth after recovery from the COVID-19 outbreak [1.12]. The government of Indonesia aims to earn its place as one of the world's developed countries by 2025, with an expected per capita income of USD 14,250–15,500 [1.13]. The increase in both population and economic growth in Indonesia brings the rise of the middle-class particularly in urban areas. Today, more than 150 million people, which is over half of the population of Indonesia, live in cities and it is projected that approximately 220 million people will live in urban areas by 2045 [1.14]. In 2016, the Indonesian Central Bureau of Statistics reported that nationwide housing shortages reached 11.6 million [1.15].

Private and public organizations conducted a housing project to meet the rapid demands for housing due to the growth of the population and the rise in the middle class. The central government developed the rental apartments, *Rusunawa* (hereafter, public apartments), and then managed them by the local governments (Fig. 1.3a,b). Meanwhile, the most owned apartments, *Rusunami* (private apartments), were designed and owned by private companies (Fig. 1.3c). Generally, most affordable apartments are constructed with a double-loaded corridor to maximize the ratio of occupied areas [1.16, 1.17]. However, double-loaded apartments often experience poor environmental conditions, such as daylighting, thermal comfort, ventilation, and indoor air quality [1.18–1.20].

Alfata et al. [1.21, 1.22] reported that the air temperature in the old public apartment under unoccupied condition was 3.1–6.9℃ lower than the corresponding outdoor air temperature during the peak hours. However, the air temperature maintained high under occupied conditions because of the small room area and heat generation from the occupants

(a) Old public rental apartment in Indonesia (*Rusunawa*) **(b) New public rental apartment in Indonesia (*Rusunawa*)** **(c) Private built-for-sale apartment in Indonesia (*Rusunami*)**

Fig. 1.3. Pictures of exterior and interior of a building and floor plan in (a,b) old and new public rental apartments in Indonesia *(Rusunawa*) and (c) private built-for-sale apartments in Indonesia (*Rusunami*) [1.21]

[1.7]. Meanwhile, the air temperature in both new public and private apartments was higher than the outdoor air temperature for most of the measurement periods [1.21,1.22]. There is a positive correlation between the AC ownership and the household income levels [1.23]. The rise of middle-class and hot condition in modern apartments can accelerate energy consumption for air conditioning. The energy conservation strategy while satisfying thermal comfort needs to be investigated.

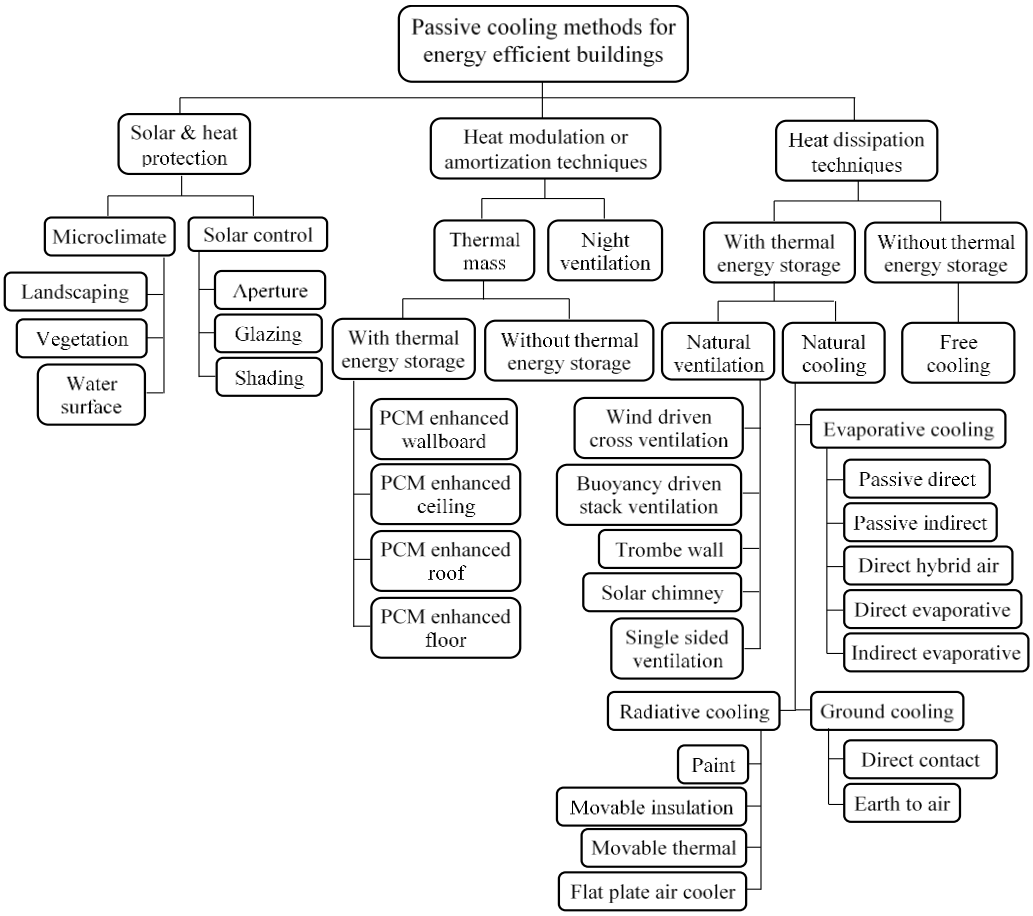

Fig. 1.4. Framework of passive cooling methods for energy efficient buildings [1.26].

1.4. Passive cooling methods and research scope

Passive cooling methods utilize natural resources by means of architectural elements, thereby reducing the cooling load in buildings [1.24, 1.25]. The determination of effective passive cooling methods for hot and humid climates where the demand for space cooling was occurred throughout a year can significantly contribute to reducing the energy consumption of space cooling while maintaining thermal comfort. Fig. 1.4 depicts representative passive cooling methods [1.26]. Several studies have comprehensively reviewed individual passive cooling methods under different climatic conditions, including hot and humid climates [1.25, 1.27, 1.28]. Moreover, researchers have published various review papers on passive cooling methods that can adapt to hot and humid conditions, such as the building envelope [1.29–1.32], shading devices [1.33–1.35], radiant cooling [1.16, 1.37], evaporative cooling [1.38–1.40],

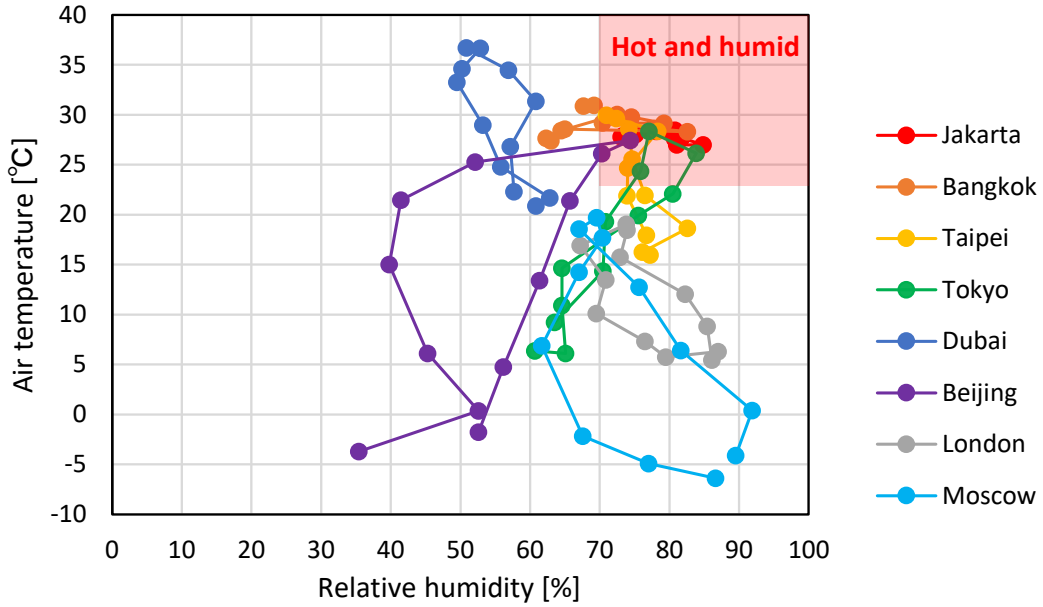

Fig. 1.5. Climographs of major cities.

and natural ventilation [1.40–1.43]; and each passive cooling method was systematically organized into subcategories based on its characteristics and principles. For instance, regarding natural ventilation, previous studies have widely investigated both methods and principles of comfort ventilation [1.43], night ventilation [1.44], wind-driven ventilation [1.45], buoyancy ventilation [1.46, 1.47], opening systems that assist in improving the ventilation performance [1.43, 1.48], and wind catchers [1.49, 1.50]. A tremendous number of studies on passive cooling methods have been published in both reviews and original papers. Samtamouris and Kolokotsa concluded that passive cooling methods are reaching a phase of maturity [1.40]. However, few comprehensive and systematic reviews on passive cooling methods have focused on hot and humid climates, although literature reviews of each passive cooling method alone have been frequently conducted. In hot and humid climates, such as Southeast Asia, it is difficult to achieve the thermal comfort of occupants using a single passive cooling method alone because the daily maximum air temperature and relative humidity usually exceed 30 ℃ and 70%, respectively [1.21, 1.22]. Previous studies have recommended the use of a combination of several passive cooling methods to improve the cooling effect [1.51, 1.52]. Therefore, it is particularly important to find an optimum combination of passive cooling methods to achieve thermal comfort in hot and humid climatic regions.

1.5. Research objective

The main objective of this study is to clarify a thermal performance of residential buildings with an effective combination of passive cooling methods for hot and humid climates in terms of thermal comfort. The results of the field investigations in modern apartments in Indonesia showed that thermal environments were often out of the comfort zone [1.21, 1.22]. Nevertheless, previous studies indicated that single passive cooling method alone was difficult to achieve thermal comfort. Given the need to reduce energy consumption, determination of effective passive cooling methods to satisfy thermal comfort is required. This study focuses on the combination of natural ventilation and phase change material (PCM), and then evaluates its cooling effect. This study provides a useful design guideline for naturally ventilated buildings installed PCMs. The specific objectives of this study are as follows:

- To provide the comprehensive overview of passive cooling methods in hot and humid climates, and to propose a feasible combination of passive cooling methods that have not been investigated in previous studies.
- To determine window systems that can optimize the indoor air flow pattern for achieving better thermal comfort satisfaction of the occupants, while maintaining the thermal storage effect during daytime.
- To clarify the measures to ensure the thermal storage effect of the proposed floor cooling system during daytime for naturally ventilated rooms. The field measurement was conducted to analyze the relationship between the indoor vertical temperature distributions and heat flows of the proposed system. Then, the key parameters and effective operation of the proposed system were determined.
- To evaluate the annual performance of the proposed floor cooling system that considers the hysteresis of the PCM and to determine its design guidelines and indicators for maximizing the thermal storage effect throughout a year.
- To determine the optimum window-opening control that maximizes the annual thermal comfort using the thermal storage effect of the proposed floor cooling system using the PCMs and ventilative cooling.

Fig. 1.6 shows the flow of this research. In Chapter 2, the comprehensive overview of passive cooling methods is conducted using 39,604 documents. Based on the comprehensive overview, possible combinations of passive cooling methods for hot and humid climates are discussed, and then a feasible combination of passive cooling methods are proposed. Based on the proposal in Chapter 2, Chapter 3 focus on a window system for comfort ventilation. In Chapter 3, the results of the field measurement of the window systems are

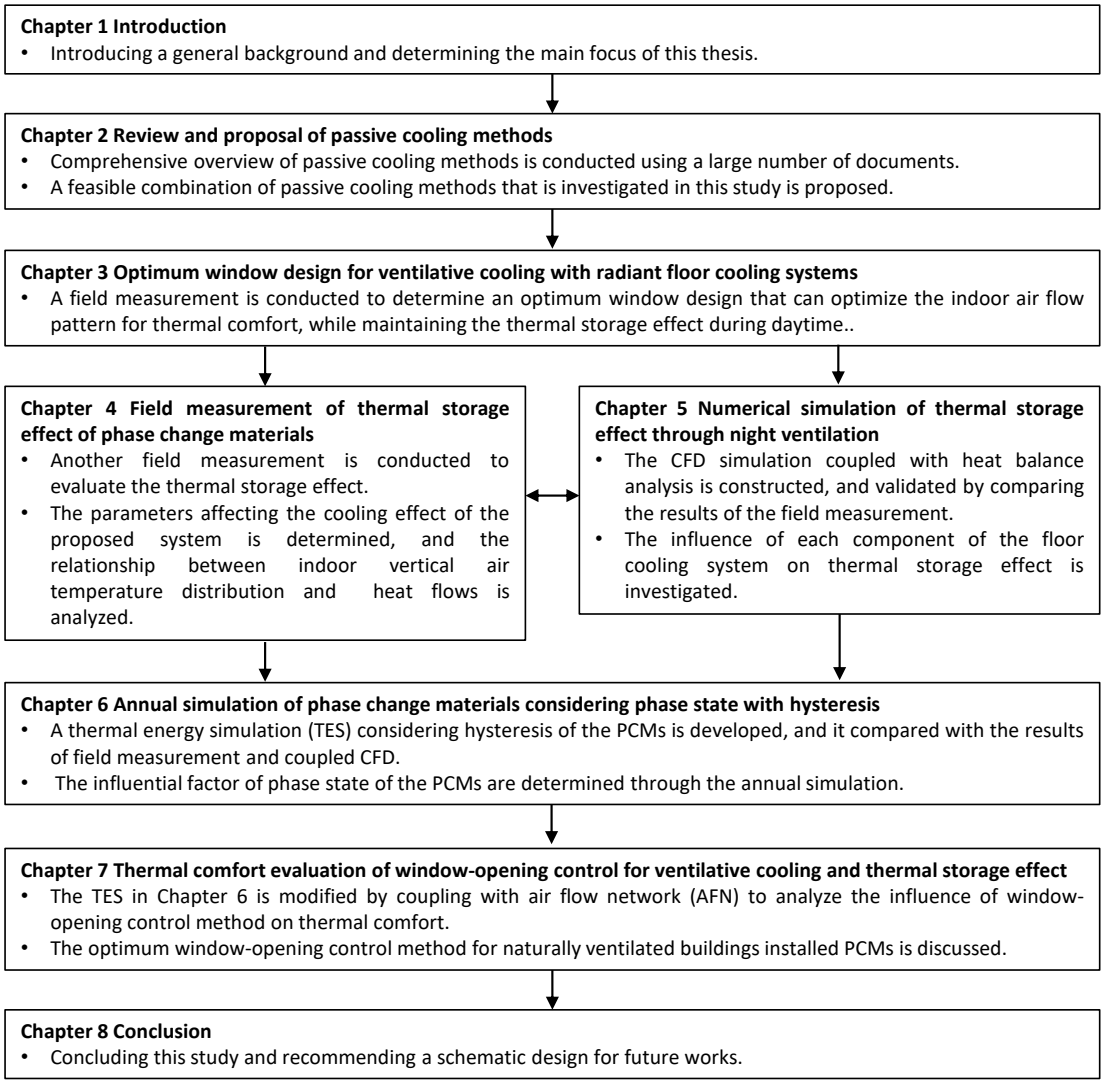

Fig. 1.6. Flow of this research.

analyzed particularly in terms of indoor air flow patterns, heat transfer coefficients of the floor, and floor surface temperatures. The influence of the window systems on thermal comfort was evaluated in the subsequent section. In Chapter 4, another field measurement is conducted to evaluate the thermal storage effect which may be combined with comfort ventilation through the filed measurement. To determine the parameters affecting the cooling effect of the proposed system, several operations of the room windows, louver windows, and exhaust fans are considered, and the relationship between the indoor vertical air temperature distributions and heat flows of the proposed floor cooling system is analyzed. Chapter 5 clarifies the key

parameters of a radiant floor cooling system using PCMs which cannot be investigated in Chapter 4 because of the limited time and cost. In Chapter 5, the computational fluid dynamics (CFD) simulation coupled with heat balance analysis is constructed, and it is validated by comparing with the field measurement results in Chapter 3. The influence of each component of the floor cooling system, i.e., ventilation fan, wind fin, and PCM thickness, on the thermal storage effect is investigated based on the validated model. In Chapter 6, annual performance of the proposed floor cooling system was evaluated using the thermal energy simulation (TES) considering hysteresis of the PCM that cannot consider in the coupled CFD (Chapter 5). The results of the TES are compared with those of the field measurement (Chapter 3) and coupled CFD (Chapter 5) to discuss the validity and applicability of the simulation method for naturally ventilated buildings. The influential factors of the phase state of the PCMs which are often affected by history in previous days are determined through the annual simulation. Furthermore, the TES is coupled with an air flow network (AFN) to analyze the influence of the window-opening control method on thermal comfort in Chapter 7. The optimum window-opening control method for naturally ventilated buildings with PCMs is discussed. Chapter 8 concludes this study and recommends a schematic design for future studies.

Chapter 2
A review and proposal of passive cooling methods

Abstract

The comprehensive overview of the passive cooling methods in hot and humid climate was shown using a text mining-based bibliometric analysis method in Chapter 2. First, comprehensive overview analysis clarifies the trend in the studies on passive cooling methods between 1970 and 2022. Second, 15 coding rules are constructed to perform the detailed analysis, and possible combination of passive cooling methods are discussed based on the comprehensive overview and the coding roles. To obtain the overview of the existing studies on passive cooling methods, 39,604 publications are sampled. The increase in the number of sampled publications between 1990s and 2010s is 2.6 times higher than that of the publications in Construction & Building technology field categorized in Web of Science. The publications obtained under 15 coding rules, which comprise only 26 compound words, account for 16.1–17.9% of the sampled publications between 2015 and 2021, mainly owing to the rapid increase in the studies on phase change material (PCM) in recent years. Further analysis of the co-occurrence network based on the coding rules shows that the recent studies on thermal energy storage mainly focus on PCM, which is latent heat storage materials, rather than sensible heat storage materials such as concrete. The analysis of the co-occurrence network of natural ventilation indicates that natural ventilation maintains the vital role of passive cooling methods by improving thermal comfort in hot climates. Moreover, passive cooling methods are frequently derived from cultural background and historical experience. Based on the results using the constructed method and detailed literature reviews, a feasible combination of passive

cooling methods which has not been investigated in previous studies for achieving thermal comfort in hot and humid climates was proposed.

Keywords
Bibliometric analysis, Text mining, Co-occurrence network, Coding rule.

2.1. Introduction

Comprehensive reviews are one of the methods used to find an optimum combination of passive cooling methods. Passive cooling methods are often constructed based on traditional knowledge and experience [2.1]; thus, it is important to analyze long-term references and their transitions until recent years. In general, passive cooling methods aim to 1) prevent heat gain, 2) modulate heat, and 3) dissipate internal heat [2.2]. Based on this principle, passive cooling methods have been classified, and researchers have often examined the optimum combination of passive cooling methods based on this classification [2.2–2.5]. Historically, such comprehensive reviews have also been conducted using qualitative approaches. In 1992, as a pioneering attempt, Antinucci et al. [2.6] reviewed 119 references on heat dissipation and protection design manually. Tejero-González et al. [2.7] conducted a literature review on 124 studies in 2016. In 2017, Panchabikesan et al. [2.8] investigated the potential of passive cooling methods by reviewing 127 documents. Bhamare et al. [2.3] reviewed 255 studies to provide the overview of passive cooling methods. However, Miranda et al. [2.9] indicated that the limitations of the previous qualitative literature reviews are time and cost, and a potential bias for selecting publications cannot be undeniable. In general, the number of publications has dramatically increased in recent years; however, the number of reviewed qualitative literature papers cannot dramatically increase because of the limited time and cost. A qualitative literature review based on sophisticated researcher knowledge and experience is undoubtedly valuable; nevertheless, a quantitative and systematic literature review method is required to capture comprehensive overviews of the research trends in response to the recent rapid increase in publications.

Bibliometric analysis using text mining methods can be an effective approach for conducting quantitative and systematic literature reviews in a wide range of research fields. Nie and Sun [2.10] used a text mining method to identify trends in research design, such as product design and information design, over the last 12 years. They concluded that text mining can help researchers obtain a comprehensive understanding of the knowledge on a certain field that is hidden in a large number of studies [2.10]. Donthu et al. [2.11] handled 5,344 documents published in the Journal of Business Research between 1973 and 2017 to analyze prominent topics and prolific authors [2.11]. Therefore, a bibliometric analysis using text mining is suitable for providing an overview of wide- and long-term information without certain bias. Because text mining can organize a considerable amount of text information, it helped doctors

to understand medical researches comprehensively [2.12], executives to decide on international strategic management [2.13], and marketers to gain insight into market advantages regarding consumer behavior [2.14]. Nevertheless, few studies in the building field have been conducted on bibliometric analyses using the text mining method [2.15], and an effective process for bibliometric analysis that can be applied to passive cooling methods has yet to be established. Previous bibliometric analyses categorized publications based on the author names, journal names, and existing categories in search engines such as medical science, business science, and building technology [2.9, 2.16]. Vanhala et al. [2.14] used single terms in a text mining-based bibliometric analysis to clarify latent topics in business research. However, a single term cannot express passive cooling methods such as ventilation, and most methods consist of multiple terms, such as comfort ventilation and night ventilation. It is necessary to determine the type of bibliometric analysis that has a combination of multiple terms that are effective for passive cooling field.

2.1.1. Objective

Chapter 2 aims to provide the comprehensive overview of passive cooling methods for buildings that adapt to hot and humid climates through the text-mining-based bibliometric analysis and to propose a feasible combination of passive cooling methods that has not been investigated in previous studies. First, the bibliometric analysis method using text mining was constructed to quantitatively handle the considerable number of publications on passive cooling methods for buildings. In this comprehensive review, the overall trends in the passive cooling methods that have been investigated since 1970s are analyzed. Second, coding rules consisting of compound words are built based on the quantitative overview analysis to find possible combinations of passive cooling methods for hot and humid climates. Finally, a feasible combination of passive cooling methods, considering traditional knowledge, that was focused on this study was proposed.

2.2. Methodology

2.2.1. Outline of the bibliometric analysis

Fig. 2.1 presents the research flow for sampling and screening the publications, which is the first step in the bibliometric analysis. First, the Web of Science (WoS) and Scopus engines were used to find the target publications. These citation indexing platforms are regarded as the largest databases for academic journals and conference proceedings in various

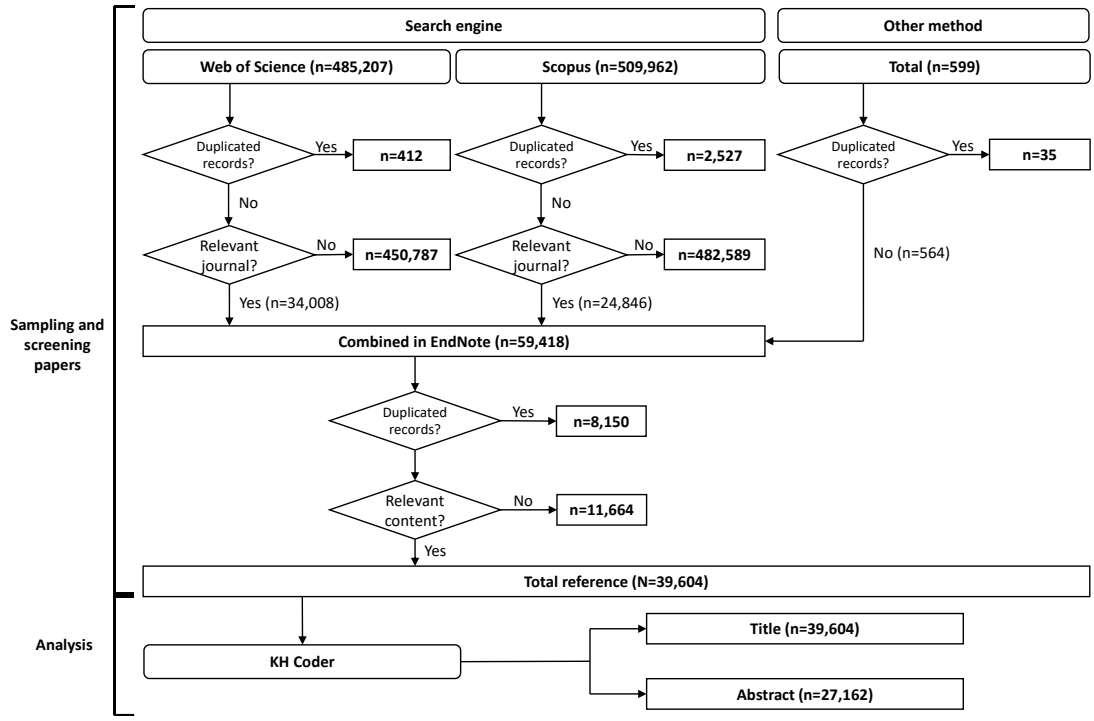

Fig. 2.1. Research flow for sampling and screening the publications.

academic disciplines. Martín-Martín et al. [2.17, 2.18] compared Google Scholar, Web of Science, and Scopus to determine the influence of publication coverage on the bibliometric analysis. Although Google Scholar had 1.5–1.8 times more publications than WoS and Scopus in the engineering and computer science fields, more than 60% of the unique publications in Google Scholar comprise dissertations, book chapters, and informally-published papers [2.17–2.19]. Thus, Scopus and WoS were selected as the suitable search engines for obtaining reliable publications. The publications sampled from the two engines were then screened and organized using EndNote (Clarivate, USA), a commercial reference management software. After screening the publications, KH Coder (Higuchi, Japan), an open-source software for bibliometric analysis, was used for text mining the titles and abstracts of the screened papers. To provide a comprehensive overview of passive cooling methods, the title of the publications was used as the target because using a large number of words would make the analysis difficult if the text mining includes the whole article. Moreover, the title often represents an overview of the publication. To find potential combinations of passive cooling methods in detail, the abstracts of the sampled and screened papers were subjected to text mining.

Fig. 2.2 shows the constructed bibliometric analysis method, which corresponds to the analysis of the title and abstract shown in Fig. 2.1. First, text mining was performed on the titles of the sampled publications to provide a comprehensive overview of passive cooling

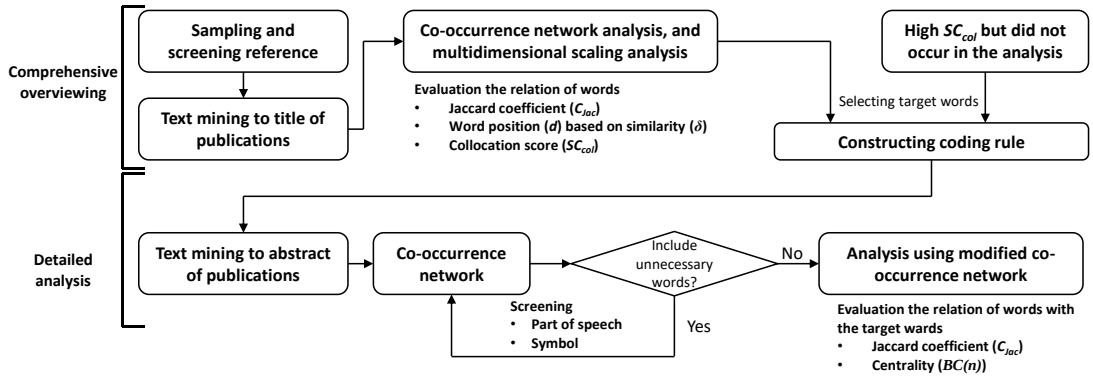

Fig. 2.2. The constructed bibliometric analysis method using text mining.

methods. Based on the co-occurrence network and multidimensional scaling analyses, the relationships between the words were obtained and coding rules were constructed to set the target compound words for the text mining of the abstracts of the sampled publications. Previous studies have used existing categories such as the author name, year, and journal name in search engines to quantitatively evaluate the publications [2.9, 2.16]. Meanwhile, the advantage of the methods constructed in our study is that they can arrange the effective categories using coding rules that respond to recent increases in publications, and can quantitatively handle the large number of the publications while reducing the potential bias in selecting publications. Using coding rules, the text mining of the abstracts of the sampled publications (detailed analysis is shown in Fig. 2.2) was performed to discuss the possible combinations of passive cooling methods.

2.2.2. Sampling and screening papers

The papers were sampled and screened based on the systematic review of the guidelines proposed by Pullin and Stewart [2.20] (Fig. 2.1). Three categories of words (as listed in Table 2.1), which include possible contextual search words, were set using the Boolean search formula, OR and AND, to avoid missing relevant papers. The words commonly used in the previous comprehensive literature reviews on passive cooling methods were used to create the categories. Categories 1, 2, and 3 represent the architectural objects, technologies, methods, climates, and regions, respectively. Miranda et al. [2.9] reported that creating categories consisting of a search formula is effective for properly collecting publications in the target research field. The search formula consisted of terms from each category to screen the publications on passive cooling methods for hot and humid climates. In the Scopus engine, the maximum number of exports was up to 20,000 publications in one search result; thus, the papers were exported separately for each year. Using the above-

Table 2.1. Keywords of the search formula for the sampling publications.

Keywords of the search formula (Field Topic)	
#1 Architectural object	apartment* OR architect* OR buil* OR dwelling* OR home* OR hous* OR indoor* OR office* OR residen* OR room*
#2 Technology and method	air OR bioclimat* OR climat* OR cool* OR evaporat* OR green OR heat* OR natural* OR passive* OR PCM OR radia* OR shad* OR simulation OR solar OR stor* OR sustainab* OR system* OR technolog* OR thermal OR tradition* OR ventilat* OR vernacular
#3 Climate and region	"hot and humid" OR "hot climat*" OR "hot dry" OR "hot humid" OR "humid climat*" OR "South East Asia" OR "Southeast Asia" OR "Sub tropic" OR "Subtropical climate" OR area* OR subtropics* OR summer OR thermal OR tropic*
Search formula used in the search engines	#1 AND #2 AND #3

*: Unlimited flection, " ": Phrase search

mentioned methods, 485,207 and 509,962 publications from 1970-2022 (until March) were exported from the Web of Science and Scopus, respectively. In addition to the publications from Web of Science and Scopus, publications referring to papers written in the local language and excluded from the two search engines were manually added to the analysis (n=599). Although the search formula for passive cooling methods was developed, ineligible research fields such as foods and animals were included in the outputted publications. The exported papers were screened properly by duplication and the relevance of journal names based on preferred reporting items for systematic reviews and meta-analysis (PRISMA) guidelines [2.21]. A total of 936,350 publications were removed, and 59,418 publications were combined for use in EndNote. In EndNote, the title, abstract, and keywords were checked, and 11,664 publications were removed for lacking relevancy. Overlapping documents between Web of Science and Scopus were also eliminated (n=8,150) to avoid redundancy. Finally, 39,604 publications were selected as target publications for bibliometric analysis.

2.2.3. Quantitative evaluation of the papers

To understand the comprehensive overview of passive cooling methods, the top 200 most frequent nouns, proper nouns, adjectives, and verbs were extracted from the sampled publications using the text-mining method (Fig. 2.2). Based on these words, their relationships were quantitatively evaluated using the Jaccard coefficient in the analysis of the co-occurrence network. The Jaccard coefficient (C_{Jac}) was calculated as follows (Eq. 2.1):

$$C_{Jac} = \frac{A \cap B}{A \cup B} = \frac{A \cap B}{A + B - A \cap B} \tag{2.1}$$

A high C_{Jac} value indicates that the connected words appear frequently in the same document. In addition to the co-occurrence network analysis, a multidimensional scaling analysis using Kruskal's algorithm [2.22, 2.23] was applied to provide the comprehensive overview of the passive cooling methods. The following relationship (Eq. 2.2) between the similarity of the words (δ) and distance between the words (d) must be satisfied by Kruskal's algorithm to be able to determine the position of words in the multidimensional space:

$$\delta_{ij} > \delta_{rs} \rightarrow d_{ij} \leq d_{rs} \tag{2.2}$$

Although the position of words can be determined based on the monotonic-decreasing relationship between the similarity of the words and the distance between them, the position of words does not always satisfy the monotonic-decreasing relationship due to the relationship between other words. In the multidimensional scaling map, incompatibility stress (S) is used to evaluate the satisfaction of the monotonic relationship. In this study, 1000 iterations were performed using Kruskal's algorithm to minimize the incompatibility stress (S) when determining the position of words, which is expressed by Eq. 2.3:

$$S = \sqrt{\frac{\sum_{i=1}^{n-1}\sum_{j=2}^{n}(d_{ij} - \widehat{d_{ij}})^2}{\sum_{i=1}^{n-1}\sum_{j=2}^{n} d_{ij}^2}} \tag{2.3}$$

Based on the results of the co-occurrence network and multidimensional scaling analyses, a coding rule was constructed to find possible combinations of the passive cooling methods. The constructed coding rule consists of two or more words (such as natural ventilation and night ventilation) because it was difficult to represent passive cooling methods using a single term (such as ventilation). The collocation score (SC_{Col}) proposed by Nakagawa et al. [2.24] was used to determine the compound words concerning passive cooling methods, which were frequently used. The collocation score (SC_{Col}) was calculated using the frequency of the target compound word ($f(cw)$) and the frequency of the concatenated words before (fl) and after (fr) each word (w_i) of the target compound word (cw) (Eq. 2.4):

$$SC_{Col} = f(cw) \times \left(\prod_{i=1}^{k}(fl(w_i) + 1)(fr(w_i) + 1)\right)^{\frac{1}{2k}} \tag{2.4}$$

$$cw = w_1, w_2, \cdots, w_k$$

Using 15 coding rules (see section 2.3.2) that had a high collocation score (SC_{Col}) and were based on the words in the co-occurrence network and multidimensional scaling map, the text

mining was applied to the titles and abstracts of the publications. Each coding rule consisted of several compound words.

In the following analysis, the co-occurrence network was expressed by Jaccard coefficient (C_{Jac}) and centrality of the target compound words. The betweenness centrality (*BC(n)*) illustrates the extent to which a target node (*n*) is between others, and is expressed as follows (Eq. 2.5) [2.25]:

$$BC(n) = \sum_{s=1}^{N} \sum_{g=1}^{s-1} \frac{P_{n(s,g)}}{P_{(s,g)}} \quad (2.5)$$

where *N* is the total number of nodes, $P_{(s,g)}$ is the shortest path from *s* to *g*, and $P_{n(s,g)}$ is the shortest path from *s* to *g* via *n*. 75 words with the highest C_{Jac} were extracted from the top of the target compound words. In previous studies, a total of 75 words were determined for the co-occurrence network to identify clear co-occurrence relationships [2.26, 2.27]. Based on the co-occurrence relationships between the 75 words and *BC(n)*, the co-occurrence networks, including the target compound word, are presented.

2.3. Results

2.3.1. Comprehensive overview of the passive cooling methods

Fig. 2.3 shows the co-occurrence network with the C_{Jac} and multidimensional scaling map for words appearing in the titles of papers for the comprehensive overview of the passive cooling methods. The words with a C_{Jac} of more than 0.08 appeared in the co-occurrence network. *Building* was the most commonly used, with the frequency of 10,389 in 39,604 references, followed by *thermal* with the frequency of 9,352. The C_{Jac} between *thermal* and *comfort* was 0.23. The high frequency of *thermal* and C_{Jac} of *thermal_comfort* imply that studies on thermal comfort have been frequently conducted. *Phase_change* had the highest C_{Jac} of 0.59 among the top 200 words, and both words were strongly connected with *material*, with the C_{Jac} of 0.31 and 0.37 for *change_material* and *phase_material*, respectively. Phase change material (PCM) had a relationship through *heat_storage* and *thermal_storage*, indicating that PCM have been frequently studied owing to their thermal storage effect. In the multidimensional map, *PCM* and *phase change material* were placed near *envelope*, *wall*, and *roof*. *Natural_ventilation* (C_{Jac}=0.23), *wall_insulation* (C_{Jac}=0.09), and *green_roof* (C_{Jac}=0.17) were passive cooling strategies that appeared in the co-occurrence network. In particular, *ventilation* was located near *comfort*, *hot*, and *climate* in the multidimensional scaling map. Natural ventilation can be regarded as a passive cooling strategy expected improving thermal comfort in hot climates. *Occupant_behavior* appeared in the co-occurrence network for

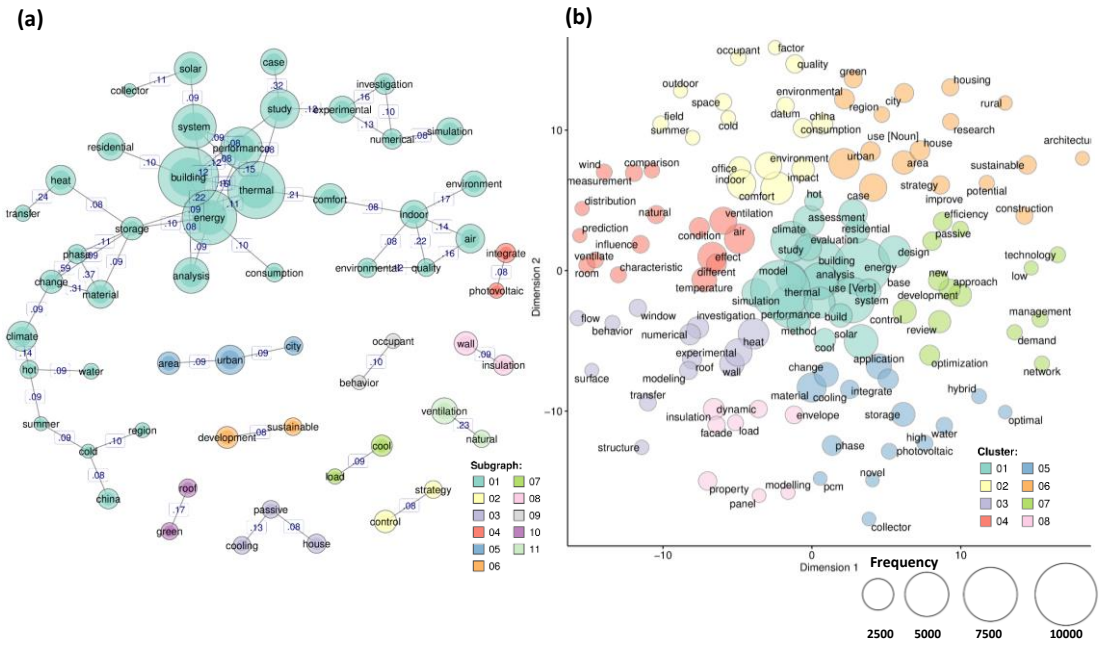

Fig. 2.3. (a) Co-occurrence network and (b) multidimensional scaling map for words in the title of papers.

passive cooling methods, with C_{Jac} of 0.10. Because *window*, *ventilate*, and *room* were positioned near *behavior*, previous studies may have been focused mainly on the window-opening behavior in ventilated rooms. The co-occurrence network and multidimensional scaling analyses can be used to clarify the commonly-studied passive cooling strategies and analyze the purposes and applications of previous studies.

2.3.2. Constructing coding rules

Using the titles of the 39,604 references, the collocation score (SC_{Col}) of 68,127 compound words was calculated. Based on the words in the co-occurrence network and multidimensional scaling maps, coding rules, which were regarded as having relatively high SC_{Col}, were constructed (Table 2.2). *Thermal comfort* had the highest SC_{Col} of 2,676,805 among the 68,127 compound words because the frequencies of *thermal* and *comfort* were 9,352 and 2,737, respectively. The effect of passive cooling methods has been frequently evaluated in terms of thermal comfort [2.28]. Thus, the SC_{Col} of *thermal comfort* was high. Regarding passive cooling methods, **thermal energy storage* (* indicates category), including *thermal storage* (SC_{Col}= 149,724), *heat storage* (SC_{Col}= 14,497), and *thermal energy storage* (SC_{Col}= 768,985), had the fifth-highest SC_{Col} in the high-coding category. In the co-occurrence

Table 2.2. Coding rules of passive cooling methods and their collocation scores (SC_{Col}).

*cool roof cool+roof (1,898) OR cool+roofs (2,490)
*evaporative cooling evaporative+cooling (12,489)
*green roof green+roof (16,198) OR green+roofs (12,071)
*green wall green+wall (900) OR green+walls (4,459) OR greenwall
*natural ventilation natural+ventilation (152,725)
*night ventilation night+ventilation (5,831)
*occupant behavior occupant+behavior (4,108)
*phase change material phase+change+material (99,009) OR phase+change+materials (98,214) OR pcm
*radiant cooling radiant+cooling (5,153) OR radiative cooling (1,866)
*solar shading solar+shading (3,097)
*thermal behavior thermal+behavior (92,822) OR thermal+behaviour (61,084)
*thermal comfort thermal+comfort (2,676,805)
*thermal insulation thermal+insulation (221,109)
*thermal storage thermal+storage (149,724) OR heat+storage (14,497) OR thermal+energy+storage (768,985)
*tropical climate tropical+climate (28,031) OR hot+humid (4,866)

*: Classification, +: Collocation

network, the word *storage* was connected to *phase_change_material*, which has a relatively high latent heat storage. The collocation scores of *phase change material* and *phase change materials* were 99,009 and 98,214, respectively. *Natural ventilation* (SC_{Col}= 152,725) and *green roof* (SC_{Col}= 16,198), which appeared in the co-occurrence network owing to the high C_{Jac}, also appeared in the top 200 compound words. If words appear in the co-occurrence network owing to a high C_{Jac}, the SC_{Col} tends to be high. The high C_{Jac} can be a criterion for making a suitable coding rule; thus, a C_{Jac} of more than 0.08 was used in this study.

**thermal insulation*, **green wall*, **cool roof*, and **night ventilation* were added to the coding rules as the derivative words for the above mentioned compound words. Although

wall and *insulation* were connected to each other, with the C_{Jac} of 0.08, *thermal insulation*, whose SC_{Col} was the twelfth highest (SC_{Col}=221,190) among the 68,127 compound words, was more frequently used compound word. Therefore, *thermal insulation* was added to the coding rule instead of *wall insulation*. *Green roof* was shown in the co-occurrence network, and *roof* was positioned near *wall* in the multidimensional scaling map; thus, the *green wall* was selected as a coding rule for further analysis. Among the 15 coding rules, cool roof had a relatively low SC_{Col}, with the maximum SC_{Col} of 2,490 for **cool roof*. Nevertheless, it was in the top 2.2% of compound words. Therefore, cool roofs can be regarded as representative passive cooling methods.

**evaporative cooling* and **radiant cooling* did not appear in both the co-occurrence network and multidimensional scaling maps. Both passive cooling methods considered materials, structures, and installation positions [2.28–2.32, 2.33–2.35]; thus, it is difficult to be connected with specific words in the co-occurrence network. Interestingly, the words *radiant* and *evaporative* were out of the 200 most frequently-used words. Nevertheless, *evaporative cooling* and *radiant cooling* had relatively high SC_{Col} values of 12,489 and 5,153, respectively. As discussed above, it is difficult for a single term to represent passive cooling methods. Therefore, *evaporative* and *radiant* were employed as compound terms using two or more words rather than a single term because neither word appeared in the co-occurrence network and multidimensional scaling maps despite the relatively high SC_{Col}. Therefore, **evaporative cooling* and **radiative cooling* were added to the coding rules. To construct effective coding rules based on the quantitative literature review that can represent passive cooling methods, referring the collocation score (SC_{Col}) is recommended as well as Jaccard coefficient (C_{Jac}) in the co-occurrence network and the position of words in the multidimensional scaling map. The 15 coding rules listed in Table 2 were applied for the detailed analysis.

2.3.3. Trends in passive cooling methods

In the following sections, the list of the publications used for creating the co-occurrence network are referred in the discussion of features of the respective passive cooling applications. Fig. 2.4a shows the number of publications in each year from 1970 to 2021 using keywords from the search formula. Here, the trend in the sampled publications was compared with the number of publications registered in the "Construction & Building technology" category, which includes heating and air conditioning, energy system, and indoor air quality research as the referential data in the Web of Science (WoS) database. The number of referential publications on Construction & Building technology in the WoS increased by 624% between 1990 and 2020. The ratio of the number of sampled publications to that of the referential publications ranged from 2.8–7.3% from 1991–2000, and increased to 8.1–13.8%

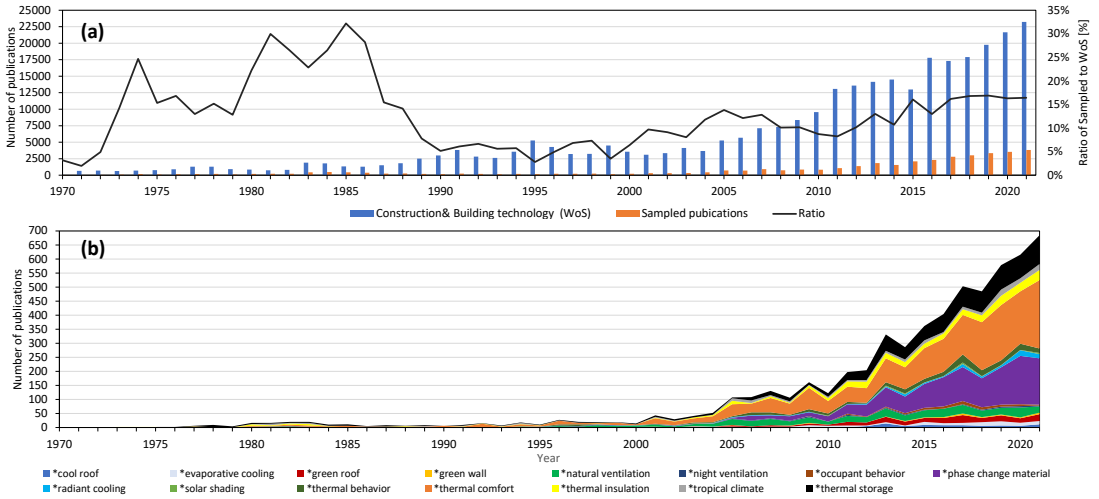

Fig. 2.4. Annual number of publications in: (a) the Construction & Building technology category in Web of Science (WoS) and the sampled publications with the ratio of the sampled publication in WoS, and (b) under the 15 coding rules from 1970 to 2021.

and 8.2–16.9% from 2001-2010 and 2011-2020, respectively. Cañas-Guerrero et al. [2.16] found the growth in words related to the indoor environment and energy efficiency such as simulations, temperature, energy, environment, and thermal comfort from 2006–2011. This tendency can affect the recent increase in the number of publications on passive cooling methods, which improve the indoor thermal environment and reduce building energy consumption.

Fig. 2.4b presents the number of publications between 1970 and 2021 containing the compound words in their title based on the 15 coding rules. The publications obtained under the 15 coding rules accounted for 1.5–9.8% of the sampled publications between 1970-1999 (Table 2.3). This rises to 11.2–17.2% from 2000-2020 mainly owing to the rapid increase in the publications related to phase change material (PCM). The number of publications on PCM increased by 8150% between 2002 and 2021. Owing to its light weight and high energy density, PCM have been installed on the wall [2.36–2.38], roof [2.39], and ceiling [2.40] of buildings in hot and humid climate regions, where the diurnal temperature range is less than 10 °C. Souayfane et al. [2.41] found that the required PCM ambient temperature range to employ its cooling effect is less than 5 °C. The wide applicability of PCM in buildings may have contributed to this increasing occurrence in recent studies.

Among the 15 coding rules, studies on thermal comfort were most frequently conducted from 1990-2022 (March). The publications on thermal comfort account for 3.0–5.9% of the sampled publications. The purpose of the previous studies on thermal comfort can be divided into two large categories: developing the thermal comfort ranges of the occupants

Table 2.3. Number of publications on passive cooling methods for each period.

	1970~ 1974	1975~ 1979	1980~ 1984	1985~ 1989	1990~ 1994	1995~ 1999	2000~ 2004	2005~ 2009	2010~ 2014	2015~ 2019	2020~ 2022*
Sampled publications	332	748	1,540	1,476	925	971	1,598	3,918	6,681	13,537	7,878
*cool roof	0	0	0	0	0	0	0	2	26	38	17
*evaporative cooling	0	0	2	0	2	2	11	17	20	54	24
*green roof	0	0	0	0	0	1	2	21	61	97	44
*green wall	0	0	0	0	0	0	0	4	3	17	9
*natural ventilation	0	1	7	2	2	20	32	97	100	132	61
*night ventilation	0	0	1	0	0	8	1	13	10	12	8
*occupant behavior	0	0	0	0	0	0	0	1	14	42	10
*phase change material	0	1	2	0	0	0	4	59	222	546	363
*radiant cooling	0	0	0	1	0	3	3	10	17	31	40
*solar shading	0	0	0	0	1	0	2	0	8	10	5
*thermal behavior	1	1	6	4	3	10	11	34	45	95	41
*thermal comfort	1	3	15	12	28	35	71	241	313	736	467
*thermal insulation	3	2	17	2	4	2	11	32	91	112	71
*thermal storage	0	15	19	14	8	11	25	52	178	351	200
*tropical climate	0	0	13	3	7	3	6	29	32	58	41

*until Mar 2022

using thermal comfort indices such as the operative temperature (OT), predicted mean vote (PMV), and standard effective temperature (SET*) [2.42–2.44]; and evaluating the cooling effect of each method and technique in terms of the indices [2.45–2.48]. The broad scope of the research on thermal comfort has led to an increase in the publications.

Natural ventilation is one of the bases of passive cooling. From 1995-2009, the number of papers with natural ventilation in their title was the second largest among the ones analyzed under the 15 coding rules. Because the number of publications on natural ventilation has steadily increased since the 1980s, natural ventilation can be regarded as a common passive cooling method. Previous studies have shown that natural ventilation can be combined with building elements such as windows, wind catchers, balconies, and wing walls, as well as other cooling methods such as evaporative cooling and radiant cooling [2.49–2.51].

Fig. 2.5 depicts the co-occurrence network that connects each decade to clarify the trend in the research on passive cooling methods, considering all the sampled publications (N=39,604). Construction, materials, and structures, which are regarded as the fundamental elements of architecture, were found in the 1970s and 1980s. Meanwhile, the term material was also obtained in the 2000s and 2020s. Cañas-Guerrero et al. [2.16] reported that materials and structures such as cement, steel, composite, and fiber stood out and continued to be important subjects because they were related to the energy, thermal comfort, and ventilation of buildings. Moreover, the studies on PCM have rapidly increased since the 2000s. Consequently, the PCM was found in the 2010s and 2020s. Materials may play an important role in passive cooling methods throughout the whole period. Wind, natural ventilation, ventilate, and ventilation, which are associated with ventilation, were linked in the 1970s and 1990s-2020s. The number of publications with natural ventilation in their title accounted for 4.4% of the publications obtained in the 2020s under the 15 coding rules (Table 2.3). Nevertheless, ventilation is still frequently investigated.

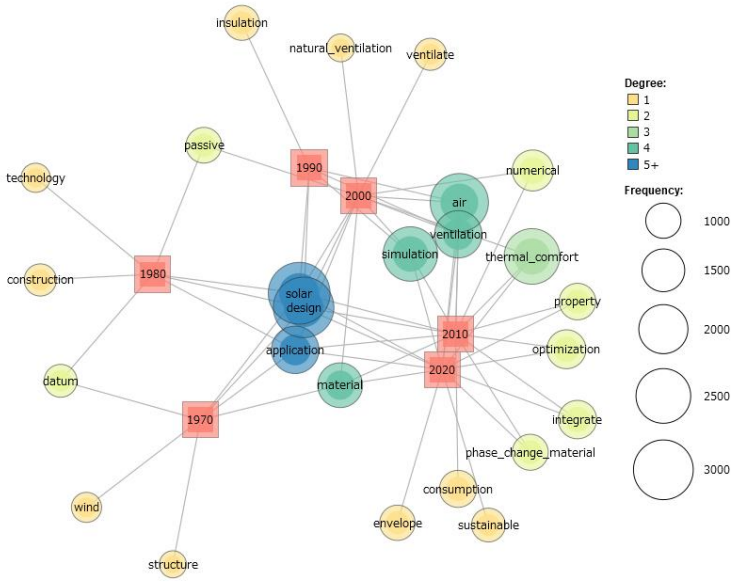

Fig. 2.5. Co-occurrence network for each decade (※2020s including the publications from 2020 to Mar 2022).

Regarding the tools used for evaluating passive cooling methods, the word numerical was obtained in the 2000s and 2010s in the co-occurrence network. Computational fluid dynamics (CFD) was first introduced in the ventilation industry in the 1970s [2.52]. In 1980, a numerical calculation of the flow related to ventilation over an aerofoil took half an hour with a cost of 1000 USD [2.53]. Nowadays, the calculation time and cost are minimal. Regarding building energy simulation programs, DOE-2, BLAST and ESP-r were found in the 1970s [2.54]. EnergyPlus, which combines the advantages of BLAST and DOE-2, was developed in 2001 [2.55]. Strachan et al. [2.56] reported that errors in the thermal load calculated by simulation programs, including ESP-r, were ±25% in daily values in the 1970s. Approximately 30 years later, Fumo et al. [2.57] reported that the error in calculating the energy consumption was mostly less than 10% using the EnergyPlus benchmark models. Owing to the improvement and dissemination of computers, many researchers can easily conduct numerical simulations; thus, the number of studies using numerical simulations has increased rapidly since the 2000s. Optimization has been in use since the 2010s. Gassar et al. [2.58] conducted a comprehensive literature review on optimization studies for use in building fields. They excluded studies published before 2000 because the amount of literature on building optimization is not significant [2.58]. Previously, optimization was performed based on only one objective, which was used to determine the optimal solution for maximizing or minimizing the objective function [2.59]. However, multi-objective optimization problems need to be solved using real-world designs [2.60]. The advantage of numerical simulation is

the investigation of several parameters under a limited time and cost owing to its improved computing capacity. For these reasons, multi-objective research, such as evaluating the trade-off relationship between thermal and daylighting environments for shading devices and windows [2.61, 2.62], was frequently conducted in the 2010s and the 2020s. The prevalence of reliable numerical simulations with a reduced time and cost could be the cause for the increase in the number of sampled publications since the 2000s.

Overall, the text-mining method for the titles of papers and co-occurrence networks can be effective in clarifying the trends in the studies on passive cooling methods. In particular, the 15 coding rules can be used as a representative research topic on passive cooling methods because the co-occurrence network for each decade considered all the sampled publications (N=39,604). Most words appearing in the co-occurrence network were related to the 15 coding rules because of their similarities. Although the number of sampled publications has dramatically increased since the 2000s, the coding rules can capture the recent rapid increase and clarify the research trend based on a large number of publications.

2.3.4. Co-occurrence network analysis based on the coding rules

Using the 15 coding rules, a co-occurrence network analysis, which refers to co-occurrence relationship, was constructed on the abstracts to find the purposes of application as well as the strengths and weakness of each passive cooling method. In particular, the potential combination of passive cooling methods for hot and humid climates were uncovered, including rapid in the number of publications. Because the abstracts of the publications were the objects of text mining, unnecessary terms based on parts of speech were screened (Fig. 2.2).

2.3.4.1. Natural ventilation, tropical climate, thermal comfort, and occupant behavior

Figs. 2.6 and 2.7 present the co-occurrence network of natural ventilation, tropical climate, thermal comfort, and occupant behavior with the minimum spanning tree, which minimizes the length of the edges of the tree. In the co-occurrence network of the tropical climate, *passive_natural_ventilation* and *comfort*, which had relatively high centrality and frequency, were observed. Similarly, *natural_ventilation* was linked to *thermal_comfort*, with C_{Jac} of 0.66, in the co- occurrence network of natural ventilation. No words related to energy consumption were found. Sakiyama et al. [2.63] reported that 43% of the reviewed papers on naturally ventilated buildings are in hot-humid, tropical, and subtropical climates, and

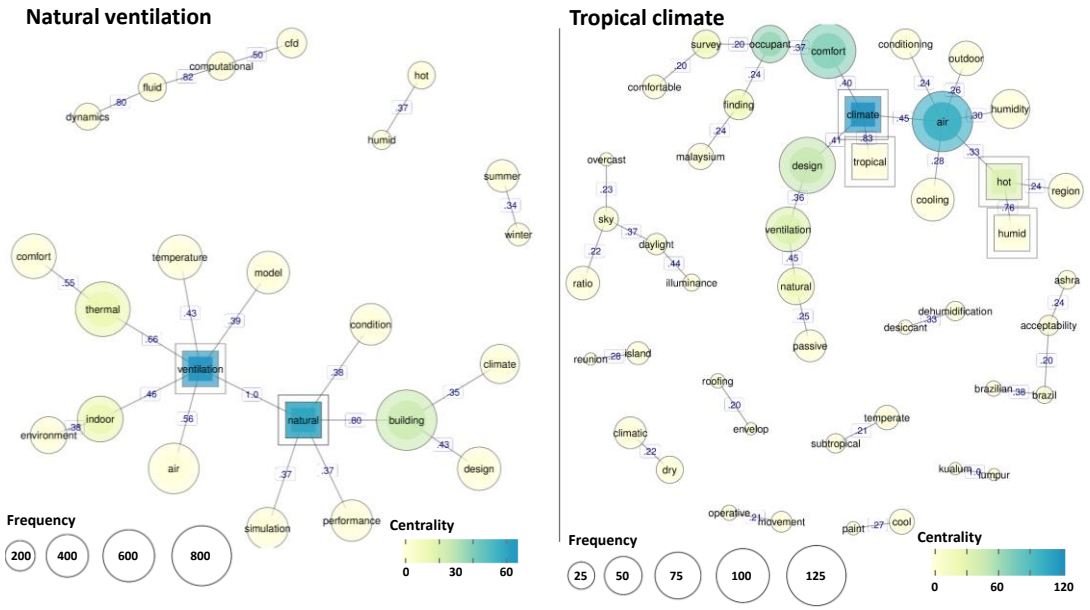

Fig. 2.6. Co-occurrence network of natural ventilation and tropical climate.

concluded that thermal comfort is a vital aspect of natural ventilation performance in their comprehensive literature review of natural ventilation. Previous studies on natural ventilation focused on improving thermal comfort rather than reducing the energy consumption of buildings. In general, the ratios of the heat loss from the human body in indoor spaces is approximately 50% through radiation, 30% through convection, and the rest through evaporation [2.64–2.66]. Evaporative heat loss from the human body accounts for more than 50% of the total heat loss in a warm environment, with a relative humidity of approximately 60% [2.67, 2.68]. Previous studies showed that the convective heat transfer coefficient of the human body, which affects the evaporative heat transfer coefficient as well, increases significantly when the airspeed exceeds 0.3 m/s [2.69, 2.70]. Under hot and humid conditions in naturally ventilated buildings in Indonesia, the results of a questionnaire survey indicated that the occupants generally prefer high wind speeds [2.71]. When the operative temperature was 30 °C, the minimum preferred wind speed was 0.9 m/s in a hot-humid climate [2.72]. Passive cooling methods that employ natural ventilation under hot and humid conditions these criteria to improve thermal comfort. The combination of natural ventilation with other passive cooling methods, such as roof covers and ceiling insulation [2.48], increases thermal comfort. Accordingly, improving the thermal comfort contributes to a reduction in the energy consumption. The C_{Jac} of *comfort_energy* and *energy_consumption* were 0.58 and 0.43, respectively.

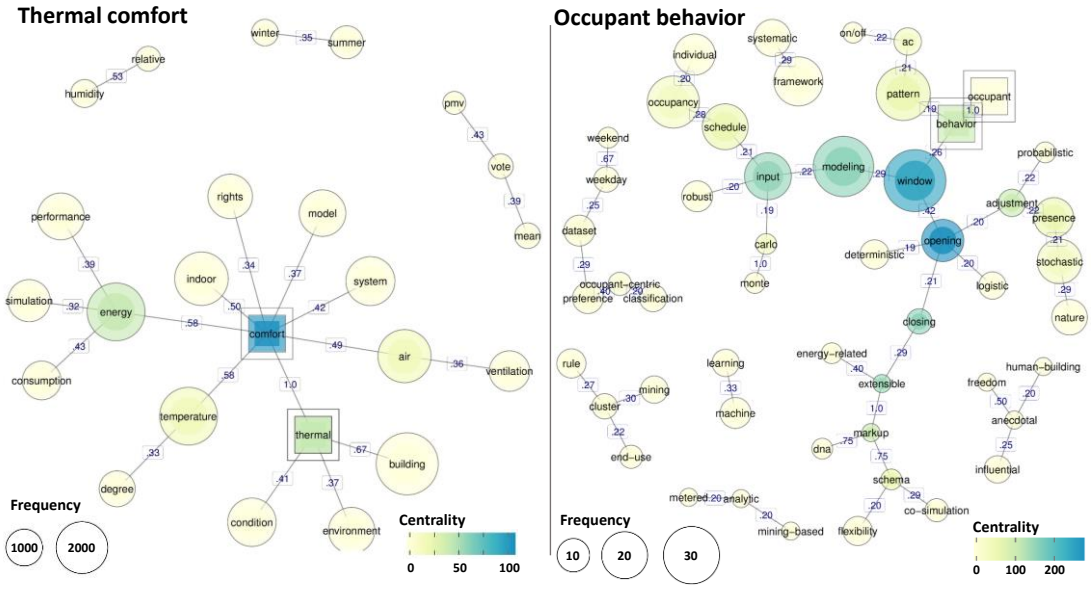

Fig. 2.7. Co-occurrence network of thermal comfort and occupant behavior.

In the co-occurrence network of the occupant behavior, *behavior_window_opening_closing*, which is related to natural ventilation, had a higher centrality than *behavior_pattern_ac_on/off*, which is related to energy consumption. This supports the above-mentioned implication for the preference of thermal comfort in natural ventilation studies. Nevertheless, window-opening patterns in hot and humid climates are affected by the household size, age of the respondent, household income, and concerns about insects more than the thermal sensation of the occupants [2.73].

2.3.4.2. Thermal energy storage, phase change materials, thermal behavior, night ventilation, and radiant cooling

Figs. 2.8 and 2.9 depict the co-occurrence network of thermal energy storage, phase change material, thermal behavior, night ventilation, and radiant cooling with the minimum spanning tree. In the co-occurrence network of thermal energy storage, *material_phase_change* and *pcm*, whose frequencies were 587–801 and 1,277–5,440 in the conditional and unconditional occurrences in the network, respectively, are shown. The conditional refers to only the co-occurrence, and unconditional indicates all occurrences in the detailed analysis. Previous studies on thermal energy storage have mainly focused on PCM, which is a latent heat storage material, and there has been a rapid increase in research since

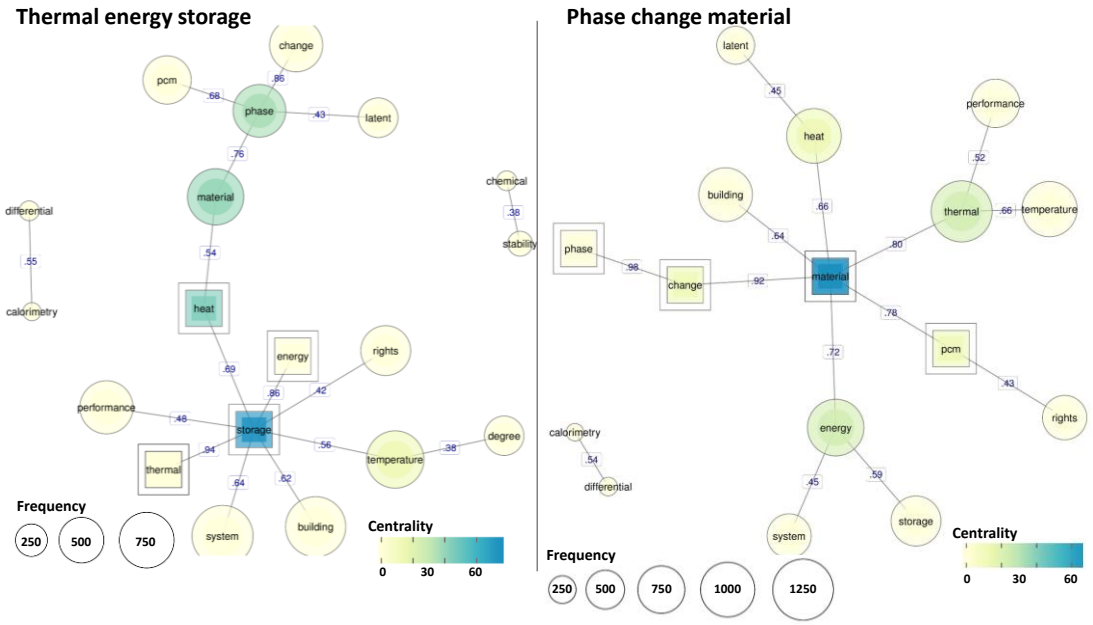

Fig. 2.8. Co-occurrence network of thermal energy storage and phase change material.

the 2010s. Moreover, sensible heat storage materials such as concrete have not been frequently investigated, although thermal energy storage has been investigated since the 1970s. Devax et al. [2.74] reported that a latent heat thermal storage material, i.e., PCM, stored and released heat per unit volume 5–14 times as much as a sensible heat thermal storage material such as concrete for building applications. Therefore, the PCM is a suitable material for thermal storage through night ventilation in hot and humid climate regions, where the diurnal temperature range tends to be small.

Material_phase_change and *pcm* appeared in the co-occurrence network of thermal behavior. Because of the complex phenomena in the phase changes of the PCMs, previous studies have investigated the unique thermal behavior of PCM (paraffin) during phase-change processes. Liu et al. [2.75] found that the melting time of PCMs (paraffin) exposed to a fixed temperature was shorter than that of employing a fluctuating inflow temperature, although the average exposure temperatures for both cases were the same. Iten et al. [2.76] reported that the latent heat of PCMs (paraffin) was underestimated under a heating rate of 10 °C/min, compared to the slower heating rate of 0.2 °C/min in differential scanning calorimetry (DSC) testing. The *differential_calorimetry*, which is a common method for measuring the thermal properties of PCM, appeared in the co-occurrence networks of the thermal energy storage and phase change material. Although PCMs have been employed in radiant cooling systems for buildings in hot and humid climates, such as ceilings [2.77], by lowering the surface

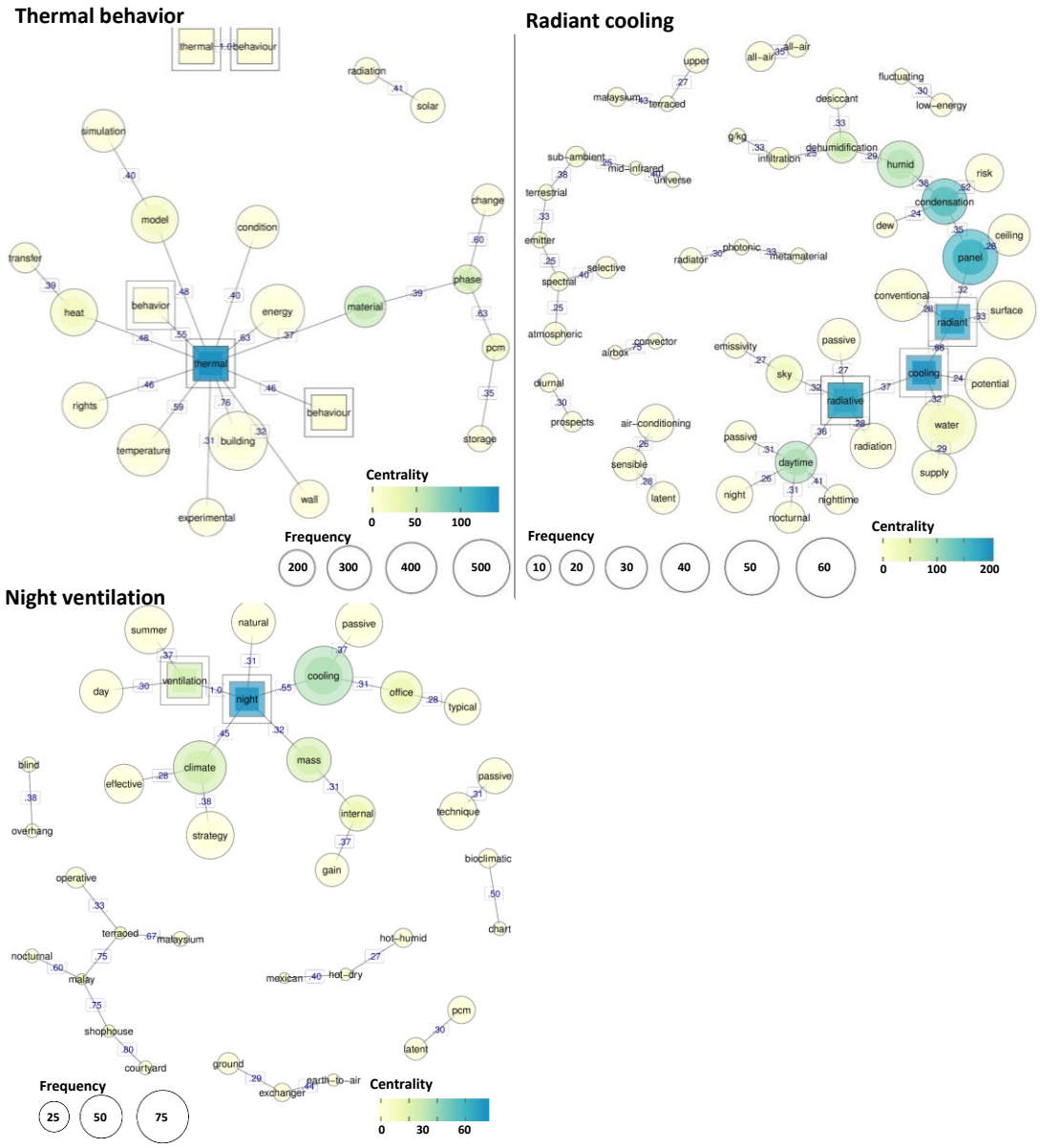

Fig. 2.9. Co-occurrence network of thermal behavior, radiant cooling, and night ventilation.

temperature of the building surface, *PCM* was not observed in the co-occurrence network in radiant cooling.

Condensation was frequently observed in the co-occurrence network, with the frequency of 36 conditional occurrences. When active radiant cooling systems employing chilled water with the supply temperature of 17–22 °C are applied to buildings in hot and

humid climates, the condensation that forms on the panels due to the high humidity, which has a C_{Jac} of 0.35 in the co-occurrence network, can be a problem [2.78, 2.79]. The annual average dew point temperature in the hot and humid climate of Jakarta, Indonesia was 25.0 ℃ [2.80]; thus, the active radiant cooling system had a high chance of suffering from condensation.

For night ventilation, *overhung*, *blind*, and *PCM* were observed in the co-occurrence network. Toe and Kubota [2.81] predicted the cooling effect of passive cooling methods for Malaysian terraced houses and recommended the combination of night ventilation with the roof and ceiling insulations, and continuous low-roof eaves at approximately the window height level (650–750 mm depth), to increase the thermal comfort period. Al-Absi et al. [2.36–2.38] used PCM to increase the thermal storage of Malaysian apartments, thus improving the cooling effect through night ventilation in hot and humid climates. Ran and Tang [2.82] proposed the use of a combination of a green roof and night ventilation for controlling the indoor air temperature in hot and humid regions, which can reduce the temperatures by up to 2.3 °C compared with the building's combined night ventilation and walls insulation. Although the cooling potential of night ventilation in hot and humid climates was considered low compared with that in other climatic regions [2.83], thermal comfort can be improved by combining night ventilation with other passive cooling methods.

2.4. Discussion

2.4.1. Evaluation of the constructed bibliometric analysis methods

Miranda et al. [2.9] reported that the largest sample size of reviewed research papers on passive cooling technology contains a maximum number of 2,859 samples. Nevertheless, they referred to publications written by authors who published a large number of publications only and concluded that the exclusion of a substantial number of other studies was a limitation of their study [2.9]. Cañas-Guerrero et al. [2.16] classified the publications on Construction & Building technology in the WoS based on the existing categories, such as research institutes and journals, to reduce the bias in selecting papers. However, this method is unable to analyze a specific topic because of limitations in the categorization functions of the WoS [2.16]. In this study, passive cooling was selected as the target topic, and the use of the coding rules, which were composed of the compound words, enabled the limitations in previous studies to be overcome in this analysis.

From the titles of the sampled publications (N=39,604), 68,127 compound words were detected in the analysis. Subsequently, 26 compound words were selected based on the C_{Jac}, that is, the relationship between the position (d) and similarity (δ) of each word, and the collocation score (SC_{Col}), to create the 15 coding rules. Nakagawa et al. [2.24] indicated that

it is difficult to express technical terms using a single term. In this study, we found that some words, such as evaporative and radiant, were employed as compound words rather than single terms. Therefore, calculating SC_{Col}, which evaluates the importance of compound words, is recommended for constructing effective coding rules. Based on the results of SC_{Col}, each coding rule needs to include compound words with a minimum SC_{Col} of approximately more than 2,500 to construct effective coding rules. 15 coding rules were employed 26 out of the 6,8127 compound words that accounted for approximately 15% (n=5,961) of the sampled publications (N=39,604) between 1970–2022. Compared to the number of references in previous literature reviews [2.3–2.9], the number of the sampled publications based on the coding rules was much larger, and the analysis was more comprehensive. Constructing coding rules based on quantitative data, such as C_{Jac} and SC_{Col}, can reduce the bias when selecting publications and efficiently analyzing the commonly-studied passive cooling methods, while allowing the consideration of the research trends in a large number of publications.

2.4.2. Potential combinations of passive cooling methods for hot and humid climate regions

The results of the detailed analysis using the coding rule and the further reviews of the publications involved in the co-occurrence networks indicate the detailed features of the respective passive cooling applications. The above results help find potential combinations of passive cooling methods for hot and humid climate regions. For example, in a previous study, a strong improvement in the thermal comfort was reported when natural ventilation was applied as comfort ventilation [2.69, 2.70]. Correspondingly, our results show that the C_{Jac} of *natural_ventilation_thermal_comfort* is more than 0.5 in the co-occurrence network of natural ventilation. Nevertheless, opening windows for natural ventilation during the daytime often increases the heat gain in the tropics. Several previous studies have proven that roof cover and ceiling insulation [2.47, 2.48] which reduce the additional heat gain from solar radiation were better to be combined with natural ventilation to reduce the total heat gain of buildings as much as possible. On the other hand, previous studies [2.84] have argued that although external shading devices such as louvers, shutters, and blinds decrease the heat gain from solar radiation, they are not recommended for naturally ventilated buildings due to the wind blockage effect.

Meanwhile, in the combination with night ventilation, the thermal storage effect has been frequently investigated in previous studies. In the present analysis, *overhang* and *blind* appeared in the co-occurrence network of night ventilation, suggesting that the reduction in solar heat gain using these shading devices can be effective in maintaining the coolness obtained through night ventilation during the daytime. Similarly, in previous studies, green roofs and wall insulation were combined with night ventilation to eliminate the heat gain in

indoor spaces [2.82]. Meanwhile, the high occurrence of the words related to PCM in the night ventilation and thermal energy storage co-occurrence networks indicates that there is a high potential for the use of latent heat thermal storage systems employing PCMs to increase the thermal storage effect through night ventilation in hot and humid climates. Considering the recent drastic increase in the number of publications on PCMs, this combination is expected to be investigated further in future studies.

2.4.2.1. Combination of natural ventilation with PCM

Natural ventilation is regarded as a common passive cooling method that improves thermal comfort in hot and humid climates because the number of publications on natural ventilation has stably increased since 1980s. Meanwhile, the number of publications on PCM has been rapidly increased by 8150% between 2002 and 2021. Nevertheless, few study investigated the combination of natural ventilation with PCM, and thus the combination was not seen in the co-occurrence networks of natural ventilation and PCM respectively. This is because natural ventilation during daytime reduces the thermal storage effect and increases the heat gain. Existing studies of PCM were conducted under closed window condition during daytime to maintain thermal storage effect [2.36–2.40], although night ventilation was applied in some studies.

As discussed, passive cooling methods are often constructed based on traditional knowledge and experience [2.1]. In hot and humid climate of Asia, colonial architecture was established between 17th and 19th century [2.85, 2.86]. For example, the Dutch colonial buildings in Indonesia in the early period were mimic to those in the home country [2.87]. Meanwhile, as time proceeded, the Dutch colonial buildings gradually adapted to the hot and humid climates that employed larger windows area to allow natural ventilation (Fig. 2.10) [2.87, 2.88]. Interestingly, the indoor air temperature profiles measured in the field measurement were not significantly different among three ventilation conditions, i.e., full-day,

Fig. 2.10. Dutch colonial building.

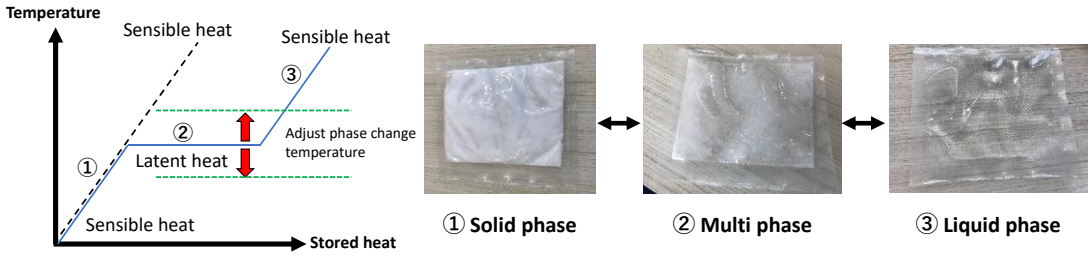

Fig. 2.11. Characteristics of PCM.

day, and night, because of wide corridor space, large windows, and thick walls (350–400 mm). The indoor air in the Dutch colonial building maintained lower temperature than the corresponding outdoors [2.86]. Alfata [2.86] firstly recommended high thermal mass (more than 2,600 kg/m^2) and comfort ventilation, although structural load needs to be considered if it is applied to the modern houses. The light weight and high energy density is the advantage of PCM compared to sensible heat storage materials. These imply that the natural ventilation during the daytime, i.e., comfort ventilation can be compatible with the thermal storage effect using PCM.

2.4.2.2. Application of PCM in buildings

The PCM can conserve a relatively higher amount energy in small temperature range than sensible heat storage materials, and thus it can be a suitable for hot and humid climate

Table 2. 4. Comparison of three types of PCMs.

Classification	Advantage	Disadvantage
Organic PCM	1.Availability in a large temperature range 2.High latent heat in phase change 3.No supercooling 4.Chemically stable and recyclable 5.Good compatibility with other materials	1. Low thermal conductivity 2. Relatively large volume change 3. Flammability
Inorganic PCM	1. High thermal conductivity 2. Low volume change 3. Availability in low cost	1. Supercooling 2. Corrosion
Eutectics	1. Sharp melting temperature 2. High volumetric thermal storage density	Lack of currently available test data of thermos-physical properties

regions, where diurnal temperature range tends to small (Fig. 2.11). In 1983, Abhat [2.89] first wrote a review on the low temperature latent heat storage system. Following, several reviews on the PCM and the building applications have been carried out. Based on the reviews, Zhou et al. [2.90] classified PCMs an summarized characteristics of them, as listed in Table 2.4; PCM can be divided into three group, i.e., organic, inorganic, and eutectics. Wide availability for phase change temperature, no super cooling, high latent heat capacity of organic PCM is suitable features for hot and humid climate regions, although it is flammable. Moreover, Shukla et al. [2.91] conducted thermal cycling test for organic and inorganic PCMs and the organic PCM tended to have better thermal stabilities than inorganic PCMs.

Regarding the installation methods of PCM in buildings, three types of the method were proposed by Hawes et al. [2.92]. First, liquid or powdered PCMs are directly added to building materials. This method does not need extra equipment but leakage and incompatible with construction material may be the biggest problems. Second, building components, such as gypsum, brick or concrete, are immersed in melted PCMs and they absorb PCMs into their internal pores. However, some researchers indicated this method cause a leakage problem which may not be suitable for long-term use. Third, encapsulation, i.e., macroencapsulation and macroencapsulation, can solve the leakage problem. The macroencapsulation is a method that PCM particles are enclosed in a thin high molecular weight polymeric film and microencapsulated PCM was mixed in gypsum and concrete. Meanwhile, in case of macroencapsulation, PCMs are packed into a container, such as tubes, spheres and panels. In particular, macroencapsulated PCM is easy to install building. Nevertheless, the encapsulation of PCMs need to consider thermal conductivity to ensure phase changes. The thickness of PCMs and cooling methods for PCMs during nighttime will be discussed in the following chapters (Chapters 5 and 6).

2.5. Proposal of floor cooling systems using PCMs

Fig. 2.12 shows the basic concept of the proposed floor cooling system for naturally ventilated buildings. The main idea is to utilize the thermal storage effect of a floor structure by attaching macroencapsulated PCMs to the backside of floor panels and employing forced ventilation for the underfloor space to cool the floor structure with PCMs at night. As discussed before, the application of PCMs to buildings can be a feasible cooling strategy for hot and humid climates. First, a relatively constant nocturnal temperature, attributed to the narrow annual temperature range, ensures solidification throughout the year. Therefore, PCM can be utilized year-round, unlike other climate regions, where PCM function in a specific season [2.93]. Second, in some countries, including Indonesia, typical modern apartments are often constructed of materials with relatively low thermal mass, such as aerated lightweight concrete panels of approximately 430–800 kg/m3, compared to a normal concrete of 2400 kg/m3 [2.94].

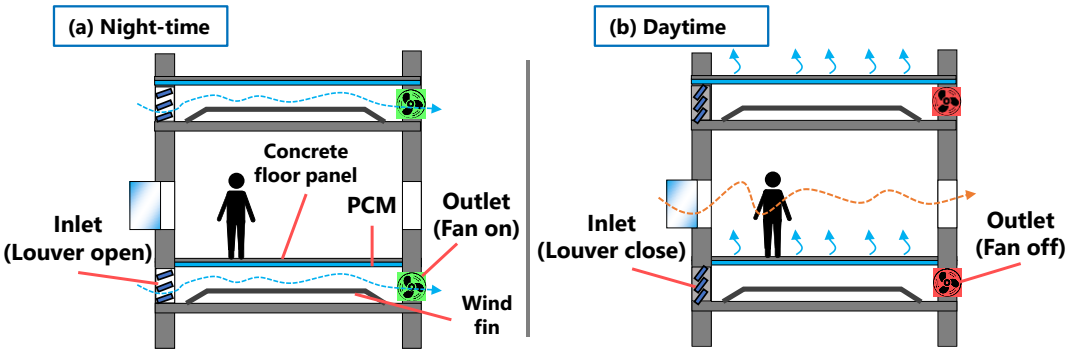

Fig. 2.12. Concept of the proposed floor cooling system using PCM during (a) nighttime and (b) daytime.

Nevertheless, the nocturnal wind condition in the tropical region is calm most of the time, which is disadvantageous for adopting free cooling to buildings. If cool nocturnal air does not enter a room effectively, the solidification time of the PCMs will be limited [2.95]. Moreover, the low thermal conductivities of PCMs may prolong the solidification time [2.90]. To address these limitations, we adopted forced ventilation for the heat dissipation in the underfloor space with the assistance of exhaust fans that is regarded as free cooling [2.95, 2.96]. Previous study classified the free cooling as a passive cooling method according to the natural source from where the cooling energy is derived [2.96]. As shown in Fig. 2.12, windows are designated at the inlets of the underfloor space, whereas exhaust fans are installed at the outlets. The exhaust fans contributed to inducing cool nocturnal outdoor air to the ventilation space continuously, regardless of the outdoor wind conditions. Moreover, PCMs can solidify quickly at higher air velocities near PCMs [2.3, 2.95, 2.97]. In the proposed system, a contraction panel (i.e., wind fin) was installed in the underfloor space to accelerate the convective heat transfer by narrowing the ventilation space, that is, the underfloor space.

The exhaust fans are turned on during the nighttime, while the louver windows are opened (Fig. 2.12a). Although the occupants in Indonesia tend to close windows during nighttime because of the security [2.73], the forced ventilation for the underfloor space effectively dissipate the heat from the PCMs. Meanwhile, the exhaust fans are turned off during the daytime, and the louver windows are closed (Fig. 2.12b). Windows tend to be opened during daytime based on a typical window-opening pattern in the tropics [2.73]. In the tropics, the diurnal outdoor temperature usually exceeds 30 °C, and the PCM melts with an increase in temperature. When the PCM melts, the PCM absorbs the surrounding heat. Therefore, the proposed system is expected to provide a cooling effect to the living space through radiation even when the room windows are opened for comfort ventilation because latent heat thermal storage (PCM) is likely to maintain a relatively constant temperature during the melting periods. Moreover, people tend to stay directly on the floor structure, frequently

constructed of ceramic tiles, in bare feet in tropics [2.98, 2.99]. Installing PCM on the floor is expected to feel the coolness when occupants contact with floor surface.

In the following chapter, window design for ventilative cooling (Chapter 3), cooling methods of the PCMs (Chapters 4 and 5), application of the PCM (Chapters 4 and 6), and window-opening control for the combination of natural ventilation and thermal storage effect of the PCMs (Chapter 7) will be discussed.

Chapter 3

Optimum window design for ventilative cooling with radiant floor cooling systems

Abstract

The combination of ventilative cooling and thermal storage effect is a feasible approach for improving the cooling performance of buildings, thus achieving better thermal comfort of occupants in hot and humid climates. As discussed in Chapter 2, the novel radiant floor cooling system using phase change materials (PCMs) for hot and humid climates was proposed. Chapter 3 aims to determine the window design that optimizes indoor air flow pattern to provide ventilative cooling, while maintaining theproposed floor cooling system during daytime. Chapter 3 analyzed several window types through a field measurement using an experimental building in Tangerang, Indonesia. The performance of the windows was analyzed with an air flow pattern and was assessed in convective heat transfers on the floors and by the standard effective temperature (SET*) at the center of the room. The results showed that the horizontal pivot windows led to air inflows to the occupied level (FL+1.1 m) regardless of the outdoor wind conditions. The heat transfer coefficient on the floor was reduced by approximately 1.5 W/m^2K compared with that of the simple opening. Nevertheless, the increase in thermal storage owing to the PCM had a greater effect on the retention of the floor cooling effect compared with the effect of the window type. Consequently, the SET* was reduced by approximately 0.8 ℃ during the daytime, showing that the proposed window design with the radiant floor cooling system achieved better thermal comfort in a hot and humid climate. Particularly, the horizontal pivot windows contributed to thermal comfort mainly because of the ventilative cooling effect.

Keywords
Window design, Indoor air flow pattern, Convective heat transfer coefficient.

3.1. Introduction

Under hot and humid conditions, window-opening during daytime would often result in the increase in the indoor temperature, although the indoor air flow will be improved. Ventilative cooling involves cooling the occupants directly through sweat evaporation and convective heat transfer, which is considered to be a traditional ventilation strategy as a comfort ventilation in the tropics [3.1]. Recent studies have shown that even in modern houses across tropical Southeast Asia, most occupants tend to open their living room windows during the daytime to allow for comfort ventilation because AC is mainly installed in their bedrooms for use at night [3.2–3.4]. Therefore, enhancing the comfort ventilation is important to improve thermal comfort through the sweat evaporation and convective heat transfer.

In hot and humid climate, the ratio of the heat loss from the human body in indoor space sometimes reaches approximately 50% [3.5, 3.6]. Ogawa [3.7] reported that upper body, such as face, chest, back, and waist, tends to sweat a lot, compared with other body parts, in hot condition. According to ASHRAE Standard 55 [3.8], the height of abdomen and head is 0.6 m and 1.1 m for a seated position, and 1.1 m and 1.7 m for a standing position, respectively. Consequently, in general, the thermal comfort is often evaluated between 0.6 m and 1.7 m above the floor which is defined as an occupied level. Controlling indoor air flow vertically toward the upper bodies of occupants can be effective to enhance the comfort ventilation.

However, in the tropics, where the outdoor temperature is often higher than indoors during daytime, if a building is naturally ventilated during daytime, the inflow of hot outdoor air would increase not only indoor air temperature but also release the thermal storage effect of the building structure [3.9]. Moreover, a higher wind speed for ventilative cooling may increase the convective heat transfer near the floor surface unintentionally during the daytime and thus accelerate the heat accumulation of the building structure. Hence, it is particularly important to determine an optimum window design to maximize the cooling effect of comfort ventilation without diminishing the thermal storage effect.

The influence of an opening design on ventilation performance and indoor air flow pattern was often investigated in previous studies. Shetabivash [3.10] investigated the influence of opening position and shape on cross ventilation, and ventilation performance was evaluated in terms of flow rate and flow circulation. Liu and Lee [3.11] studied the influence of window types on flow rate in residential building. Gao and Lee [3.12] clarified the influence of opening configurations on mean air age. Tantasavasdi et al. [3.13] proposed effective opening configurations to improve thermal comfort through comfort ventilation in the hot and

Fig. 3.1. Experimental building in Tangerang, Indonesia

humid climate of Thailand. Although opening configurations, shape, and window types have been frequently studied to improve natural ventilation performance, such as flow rate, few studies evaluated the vertical indoor air flow pattern by focusing window types and its pane to improve comfort ventilation, while maintaining thermal storage effect.

3.1.1. Objective

Chapter 3 aims to determine a window design for the living room to achieve the diurnal thermal comfort of occupants with ventilative cooling in the hot and humid climate, while maintaining the thermal storage effect through the novel floor cooling system using phase change materials (PCMs) which proposed in Chapter 2. For ventilative cooling, Chapter 3 determines a window system that vertically controls the indoor air flow to increase the wind speeds at the occupied level while reducing the air velocity near the floor surface during the daytime. For the floor cooling system, this chapter attempts to reinforce the thermal storage effect during daytime, by using PCM with a high latent heat thermal storage. Thermal performance of various window designs for ventilative cooling and radiant floor cooling systems is evaluated based on the results of a field measurement conducted in a full-scale experimental building in Tangerang, Indonesia.

3.2. Methodology

3.2.1. Experimental building

A field measurement was conducted in Tangerang, Indonesia (6.22°S, 106.57°E). The experimental building has two identical rooms (Rooms A and B), and both rooms have the same side of 4.98 m × 5.15 m, with a floor to ceiling height of 3 m, representing a typical living room of Indonesian high-rise apartments (Fig. 3.1). The experimental building is constructed of aerated lightweight concrete (ALC) walls and a concrete structure, which also represents a typical construction of high-rise apartments, as explained before. The thickness of external wall is 140 mm, comprising the ALC panel of 100 mm, plaster of 40 mm, and GRC board of 6 mm. Only the external wall facing the east and west was installed with glass wool thermal insulation boards of 50 mm to eliminate the thermal influences from the outdoors. The original floor is composed of a steeled deck slab and reinforced concrete slab of 125 mm thick. To exclude the influence from the ground, the original floor was lifted up by 2.4 m from the ground. For the roofs, zincalume panels (0.4 mm thick) are laid on the steel frame. GRC boards (10 mm thick) were adopted for the ceiling with steel frames. As shown in Fig. 3.1, each of the rooms has adjustable panels on the center of northern (front) and southern (rear) external walls to carry out measurements with various windows. The position, size, and type of windows can be changed within the adjustable panels of 2.4 m × 5.0 m.

In both Rooms A and B, the concrete floor panels (500 mm × 500 mm × 30 mm) were laid 500 mm above the original floor (Fig. 3.2a-c). The back side of the floor panel is divided into four sections. The PCM (paraffin) was packed into an aluminum package of 210 mm ×

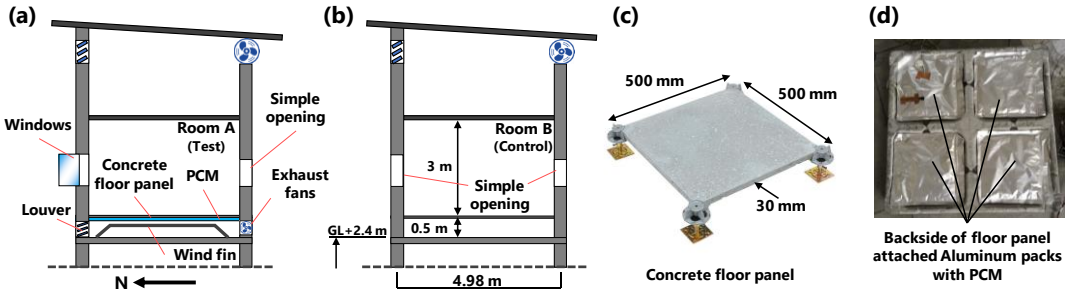

Fig. 3.2. Description of experimental building: (a) Section of Room A, (b) Section of Room B, (c) Detail of concrete floor panel, and (d) Photo of PCM.

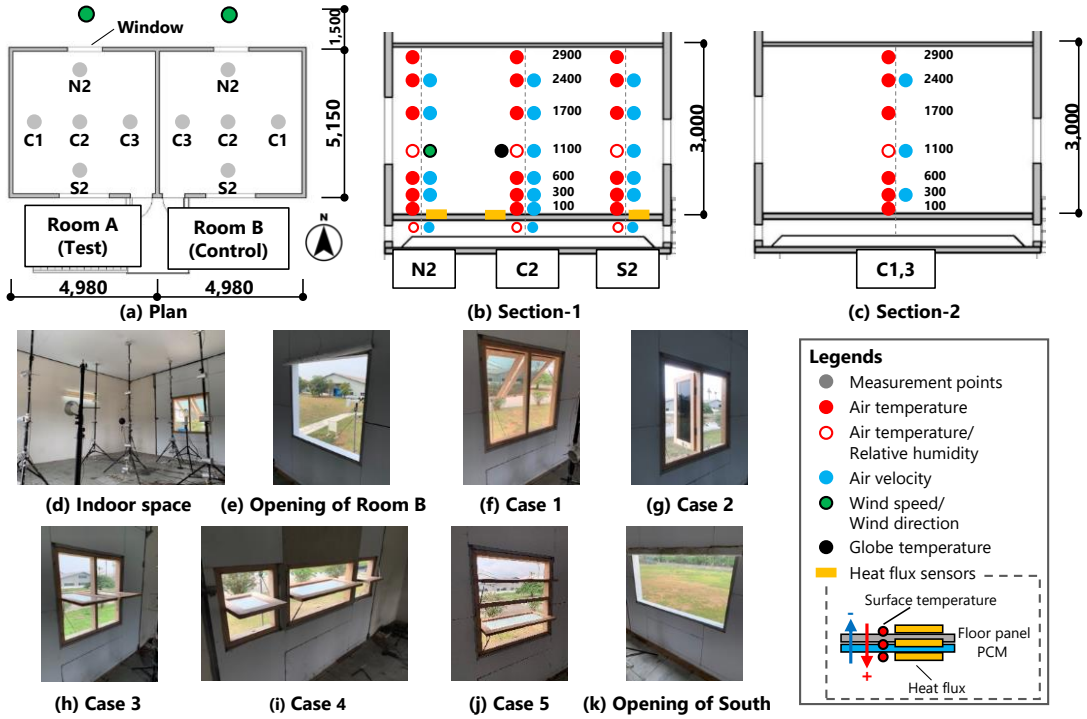

Fig. 3.3. (a) Layout of experimental units, (b, c) sensor/measurement setting, (d) weather station, (e) outside view of the experimental building, (f) indoor measurement setting, (g) opening (inlet) in Room B, (h) opening (outlet) in Room A and B, and (i-m) opening (inlet) in Room A for each case.

210 mm, and 16 aluminum packages per square meter (2.54 kg/m^2) were attached on the back side of the temporal floor panels using an epoxy adhesive (Fig. 3.2d). Table 3.1 summarizes the thermal properties of the PCM used in this measurement. The thermal properties of the PCMs were measured by differential scanning calorimetry (DSC). The phase change temperature of the PCM was set to 28–29 ℃ [3.14]. The solidification temperature range was 1–2 ℃ lower than the melting temperature range due to the supercooling, which is one of the main features of the PCM. Room A was used as a test room. Thus, the PCMs were installed only in Room A. Although three exhaust fans (south) and louver windows (north) were installed in the underfloor space of Room B as well, we completely closed them throughout the measurement period. Therefore, there was no influence from the underfloor cooling system for Room B. The exhaust capacity of the fans was 0.95 m^3/s. In addition, the wind fin was installed inside the underfloor space for Room A to further increase the air velocity near the PCMs. In contrast, Room B was set as the control room without installing the radiant floor cooling system using a PCM.

Table 3.1. PCM properties.

Parameter	Description	
Type of material	Paraffin	
Melting temperature range	29–30 (main peak: 29)	[℃]
Solidification temperature range	27–28 (main peak: 28)	[℃]
Latent heat capacity (at 25 ℃)	220	[kJ/kg]
Specific heat capacity	2	[kJ/kg·K]
Density of solid (at 25 ℃)	870	[kg/m^3]
Density of liquid (at 25 ℃)	790	[kg/m^3]
Heat conductivity (both phases)	0.2	[W/m·K]
Installed amount	2.54	[kg/m^2]

3.2.2. Experimental design

A field measurement was carried out to determine an effective window system under natural ventilation conditions. The measurement was conducted from November 15, 2019 to January 23, 2020. Data were collected over a span of five periods, and 2–3 continuous sunny days were selected from each period to evaluate air flow patterns and the resultant thermal comfort. On the north (front) side of the building, which is the prevailing wind direction, different window systems were installed for the two rooms. Here, we compared several types of windows (Room A) with the simple opening (Room B) to evaluate the indoor air flow pattern, standard effective temperature (SET*) at the center of rooms (FL+1.1 m), and the convective heat transfer on the floor. As listed in Table 3.2, five different types of windows were chosen for the measurement cases. Room A, which changed the window types as the test room, was equipped with a radiant floor cooling system to improve the indoor thermal environment by the combination of structural cooling and ventilative cooling. The floor cooling system was operated by opening the louver windows of the underfloor space throughout the day and turning on the exhaust fans at night. Meanwhile, Room B was set to

Table 3.2. Case design of the field measurement.

Case	Room A (Test room)		Room B (Control room)	
	Window type	Opening size [mm]	Window type	Opening size [mm]
Case 1	Top-hung (45°)	1200 × 1200	Simple opening	1200 × 1200
Case 2	Casement (90°)	1200 × 1200	Simple opening	1200 × 1200
Case 3	Horizontal pivot (90°) with pane height of 1200 mm	1200 × 1200	Simple opening	1200 × 1200
Case 4	Horizontal pivot (90°)	2400 × 600	Simple opening	2400 × 600
Case 5	Horizontal pivot (90°) with pane height of 600 mm	1200 × 1200	Simple opening	1200 × 1200

Table 3.3. Description of measurement instruments.

Measured variables	Instrument model	Accuracy
Indoor measurement		
Air temperature and relative humidity	T&D TR-72nw-S	±0.3 ℃, ±2.5%RH at 10–85% RH, ±3.5%RH at 0–10 and 85–95%RH
Air and surface temperature	Thermocouple type-T, φ0.35 mm	±0.1%+0.5 ℃ plus ±0.5 ℃ for cold junction compensation
Air velocity	Kanomax 6332D with Probe 9065-3	±0.15 m/s at 0.1–4.99 m/s
Wind speed and direction	Young CYG-81000	±0.05 m/s and ±2°
Globe temperature	PGT-01	±0.15 ℃
Heat flux	Prede PHF-100	±0.05
Outdoor measurement (weather station)		
Air temperature and relative humidity	Onset, S-THB-M002	±0.2 ℃, ±2.5% (10–90%RH)
Wind speed and direction	Onset, S-WSET-B	±0.5 m/s, ±5°
Global horizontal solar radiation	Onset, S-LIB-M003	±10 W/m^2 or ±5%
Rainfall	Onset, S-RGB-M002	±1% (<20 mm/h)
Barometric pressure	Onset, S-BPB-CM50	±3 mbar
Outdoor measurement (front of the northern external wall)		
Wind speed and direction (Room A)	Young CYG-86000	±0.1 m/s, ±2°
Wind speed and direction (Room B)	Young CYG-05103	±0.3 m/s, ±3°

be the control room with a simple opening (1200 mm × 1200 mm) on the north side of the wall throughout the field measurement (Fig. 3.3e).

In Case 1, Room A was installed with top hung window with a 45° opening angle, which is commonly used for apartments in Indonesia (Fig. 3.3f). In Case 2, a casement window (90°) was employed, assuming that the window panes will act as a wind catcher that induces crosswind to the room (Fig. 3.3g). Prianto and Depecker [3.15] reported that the horizontal louver with and opening angle of 90° brought 4.8–5.6 times higher air velocity to the occupied level than that with others angle, including 30°, 45°, and 60°. In Cases 3–5, this study focusses on the horizontal pivot windows of various aspect ratios with an opening angle of 90°. The horizontal pivot windows in Cases 3 and 5 had the same opening ratio of 1200 mm × 1200 mm, that is, square type, but the size of window panes was different as shown in Fig 3.3h and 3j. The window in Case 3 consisted of two long vertical panes with a height of 1200 mm, whereas the window in Case 5 was divided horizontally into two short window panes with a

height of 600 mm each. In Case 4, the horizontal pivot window with a different opening ratio of 2400 mm × 600 mm, i.e. horizontally wide window, was applied (Fig. 3.3i). The opening area in all cases was set to be 1.44 m^2.

3.2.3. Data collection

As shown in Fig. 3.3, parameters were measured at the five horizontal points. Detailed measurements of physical thermal comfort variables including air temperature, relative humidity, air velocity, and globe temperature were measured at the center of each room at 1.1 m above the floor. Air temperatures were measured vertically at 0.1 m, 0.3 m, 0.6 m, 1.1 m, 1.7 m, 2.4 m, 2.9 m above the floor based on the guideline of architectural institute of Japan (AIJ) [3.16]. In addition to the vertical distribution of air temperature, air velocity also measured at also measured at 0.3 m, 0.6 m, 1.1 m, 1.7 m, 2.4 m (plus 0.1 m only at the center of the room) above the floor simultaneously to investigate the indoor air flow pattern. In front of the northern wall of the experimental building, as shown in Fig. 3.3, two-dimensional anemometers were installed to distinguish direction of incoming flow. After inflow passed opening, three-dimensional sonic anemometer detected the air velocity and elevation angle of the inflow to investigate indoor air flow pattern. For the evaluation of the thermal storage effect, surface temperature and heat flux of the concrete floor panel and PCM were measured mainly at the center. During the measurement, the outdoor weather condition was recorded with a weather station that was placed in an open space approximately 10 m away from the building. All measurements were logged automatically at two-minute intervals. Table 3.3 presents the measurement instruments used during the field measurement.

Before analyzing indoor thermal environment, some variables such as mean radiant temperature were calculated using equation in order to make the data processing consistent throughout this thesis. Mean radiant temperature is defined as the uniform temperature of an imaginary enclosure in which radiant heat transfer from the human body equals the radiant heat transfer in the actual non-uniform enclosure [3.17]. The mean radiant temperature is calculated based on the globe temperature, which is in case of the natural convection is expressed by the following equation [3.18].

$$T_r = \left[(T_g + 273)^4 + \frac{1.1\times10^8\times v^{0.6}}{\varepsilon_g \times D^{0.4}}(T_g - T_a)\right]^{1/4} - 273 \qquad (1)$$

where T_r is the mean radiant temperature [℃], T_g is the globe temperature [℃], v is the wind speed (measured at the level of the globe) [m/s], ε_g is the emissivity of the black globe [-] and D is the diameter of the globe [m]. The emissivity of the black globe is taken as 0.98 in all the calculation in this thesis.

3.3. Results

3.3.1. Outdoor weather conditions

The recent weather data (2005-2019) at the nearest weather station (Tangerang) indicate that the monthly mean outdoor air temperature during the daytime ranged from 28.5–30.7 °C, while that at night ranged from 25.5–26.4 °C [3.19]. Meanwhile, the average wind speeds ranges from 2.6–3.4 m/s. Fig. 3.4. shows the outdoor weather conditions with the

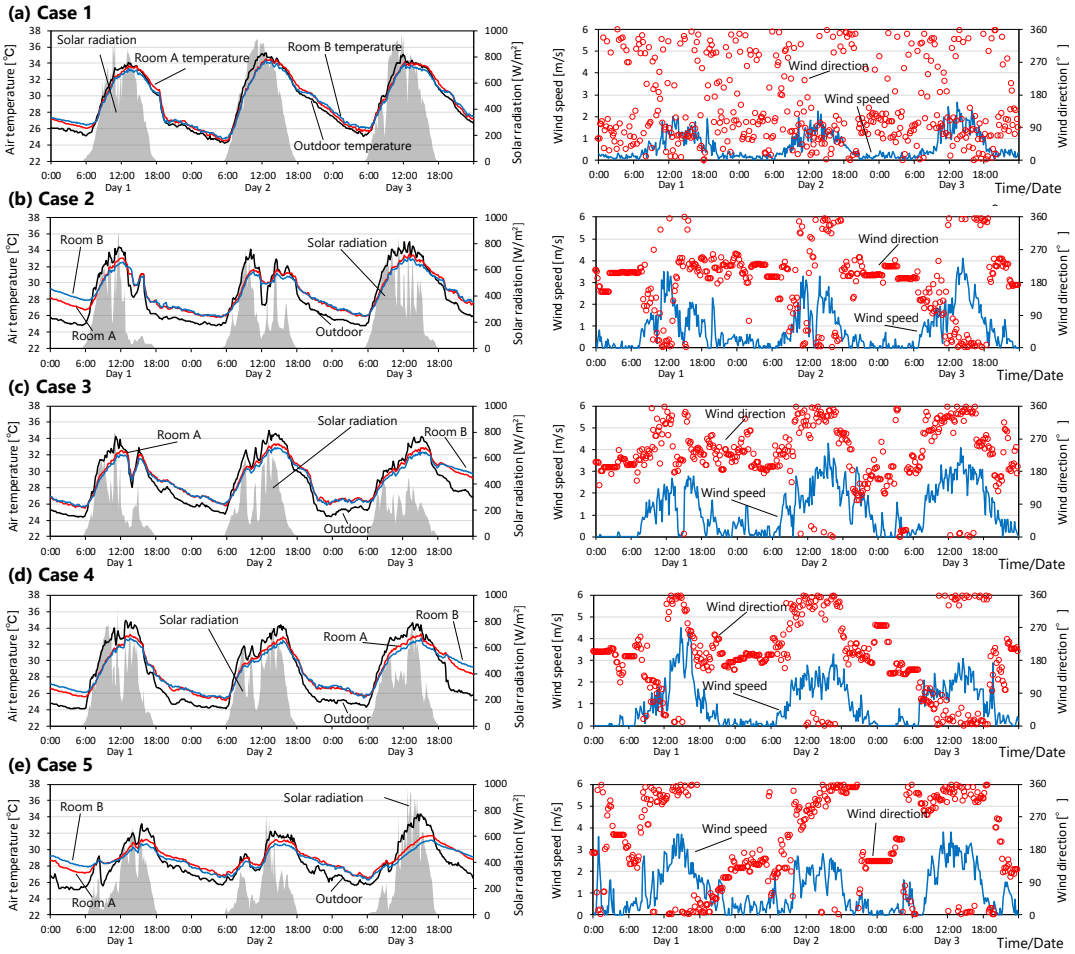

Fig. 3.4. Temporal variation of the measured air temperature in the experimental building and the corresponding outdoor conditions in Case (a) Case 1; (b) Case 2; (c) Case 3; (d) Case 4; (5) Case 5.

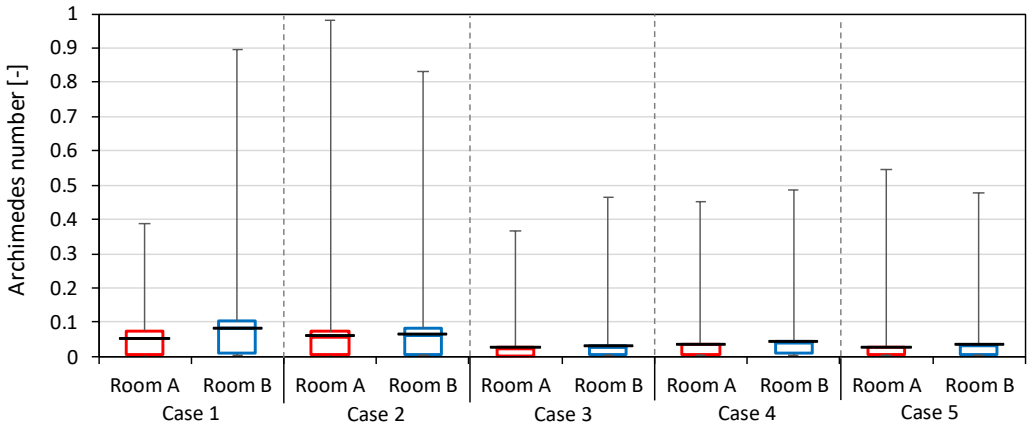

Fig. 3.5. Comparison on Archimedes number in Cases 1–5.

corresponding indoor air temperature in Rooms A and B during the field measurement. The outdoor air temperature ranged from 24.1–35.3 ℃ with the diurnal and nocturnal averages of 29.5–31.7 ℃ and 25.4–26.9 ℃, respectively. Since the field measurement was carried out from the beginning to the middle of the rainy season, solar radiation in most cases was uneven. Moreover, the air temperature in Case 5, which was card out in the middle of rainy season, was relatively lower with a diurnal average of 29.5 ℃, compared with the other cases. The main direction of prevailing wind was from north and south during the daytime and nighttime respectively. The average outdoor wind speeds at the weather station, which was placed in the open space approximately 10 m away from the buildings were 1.0 m/s (Case 1), 1.5 m/s (Case 2), 1.9 m/s (Case 3), 1.6 m/s (Case 4), and 1.6 m/s (Case 5), respectively, during the daytime. In general, the measured outdoor wind speeds in Case 1 were slightly lower than the other cases. The inflow coming from the north (±45°) measured in the front of the north external wall, with a distance of 1.5 m, was used for the following analysis of the air flow patterns. The inflow velocities at the corresponding measurement point were 0.6 m/s (Case 1), 0.5 m/s (Case 2), 0.6 m/s (Case 3), 0.5 m/s (Case 4), and 0.5 m/s (Case 5). This implies that the inflow conditions for the indoor airflow pattern analysis were almost the same in Cases 1–5.

As mentioned above, Room A was equipped with the floor cooling system using the PCMs. However, air temperature followed corresponding outdoor temperature due to large ventilation rate. During the daytime, the air temperatures in Room A and Room B measured at the center of room were 29.4–31.4 ℃ and 29.1–31.2 ℃, respectively. In Indonesia, the national standard SNI 6390:2011 recommends an indoor air temperature at 25.5 ℃ [3.20]. The indoor thermal environment, based on air temperature, in the experimental building was very hot, compared with the recommended air temperature. In the following section, indoor thermal environment was evaluated comprehensively, i.e., effect of radiation and ventilative cooling.

For evaluation on the ventilation performance, naturally ventilated buildings concern two types of ventilation, i.e., the buoyancy-driven ventilation and wind-driven ventilation, and the buoyancy-driven ventilation affects indoor air flow pattern as well as the wind-driven ventilation. Thus, it is important to examine this possibility under current measurement condition for each case [3.21]. Archimedes (Ar) number is the dimensionless index describing the flow field characteristics and it is defined as a ratio of external forces to internal viscous form. The Ar number during the measurement period was calculated using following equations (Eq. 3.2, 3.3) [3.22].

$$Ar = \frac{g\beta h\Delta T}{v^2} \tag{3.2}$$

$$\Delta T = T_{FL+1,100} - T_{out} \tag{3.3}$$

where Ar is the Archimedes number [-], g is the gravitational force, β is the thermal expansion coefficient [1/K], ΔT is the temperature difference [℃], v is the wind speed of the external flow [m/s], $T_{FL+1,100}$ is the indoor air temperature measured at 1.1 m above the floor [℃], T_{out} outdoor air temperature [℃]

The calculated Ar number during the daytime ranged from 0.0008 to 0.98 with the average of 0.05–0.08 (Case 1), 0.06 (Case 2), 0.02–0.03 (Case 3), 0.03–0.04 (Case 4), and 0.03 (Case 5) (Fig. 3.5). Because the Ar numbers were much less than one for each room in Cases 1-5, natural convection due to the buoyancy force was much smaller than forced convection through the wind force. In this measurement, the airflow inside and wind flow outside the experimental building was wind dominant, and the influence of buoyancy force on the indoor air flow pattern can be ignored.

3.3.2. Indoor air flow pattern

Fig. 3.6 presents the frequency of inflow elevation angle measured immediately inside the windows (N2), while Fig. 3.7 shows the vertical distribution of average air velocity at the windward side (N2), the middle of the room (C2), and the leeward side (S2) respectively. As shown in the results from Room B (control), the air flow through the simple opening mostly went downward, accounting for approximately 54–61% of the total time, because when the wind reaches the outer wall, it diverges from a stagnation point [3.23]. The highest air velocity in Room B was observed at FL+0.1 m at the middle of the room (C2). Although the outdoor wind conditions were different in each case, the indoor air flow patterns were mostly similar in Room B.

In Room A (test) by contrast, it is apparent that the indoor air flow patterns varied, depending on the window type (Figs. 3.6 and 3.7). In Case 1, the top-hung window led to air flow towards the upper space of the room, and 73% of the inflow passed straight or upward.

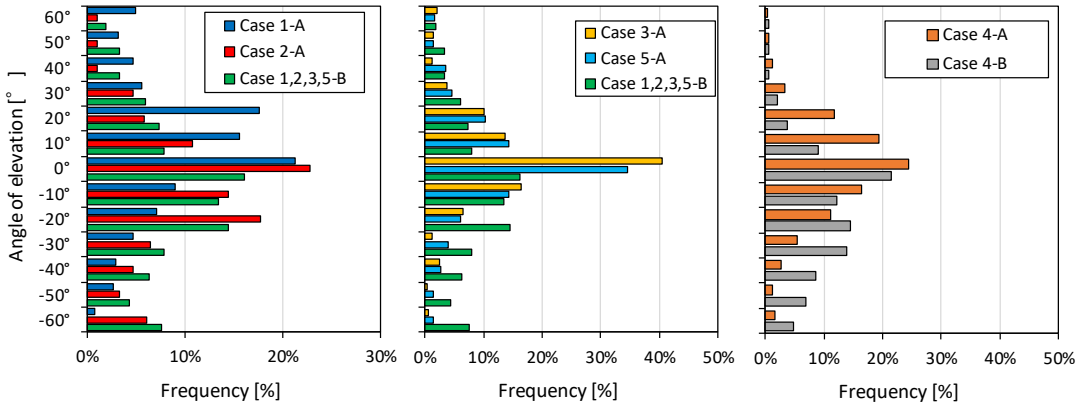

Fig. 3.6. Frequency of inflow elevation angle measured at windward side of FL+1.1 m.

Owing to the small effective opening area, Room A generally obtained low air velocity, although some influences of the window types on the air flow pattern can be observed. The highest air velocity at the middle of Room A (C2) was measured at FL+2.4 with an air velocity of 0.4 m/s, although that in Room B as observed near the floor at the same position. In Case 2 (casement), the frequency distributions of the inflow elevation angle for both Rooms A and B were similar, but the vertical air flow distributions were slightly different. In both rooms, approximately 50% of the inflows went downward and the highest air velocity was recorded in the middle of the rooms at FL+0.1 m. When the outdoor wind speed was more than 0.8 m/s, the air velocity at FL+0.1 m in Room A was approximately 0.3 m/s higher than that in Room B. It is presumed that a casement window created horizontal air flows.

In Cases 3–5, the horizontal pivot windows brought air velocities 1.7–2.6 times higher to the occupied level (FL+1.1 m) than to the space near the floor surface (FL+0.3 m) at the middle of the room, regardless of the inflow direction with air velocities of 0.6–0.9 m/s (FL+1.1 m) and 0.3–0.4 m/s (FL+0.3 m), respectively. These results indicate that the horizontal pivot windows could provide relatively high air velocities to the occupied level while maintaining relatively lower air velocity near the floor, showing the potential of reducing the convective heat transfer on the floor during the daytime. This implies that a horizontal pivot window may contribute to the improvement of thermal comfort at the occupied level, while retaining a certain degree of the thermal storage effect.

As mentioned above, the field measurement involved three types of the horizontal pivot windows. The height of the window pane was 1,200 mm in Case 3, while, that of Case 5 was 600 mm with a change in the position of the rotation axes. The results of a CFD simulation in a previous study showed that the horizontal louver (90° opening angle) with a depth of 1,440 mm induced 1.5 times more air flow than that with a depth of 480 mm [3.24].

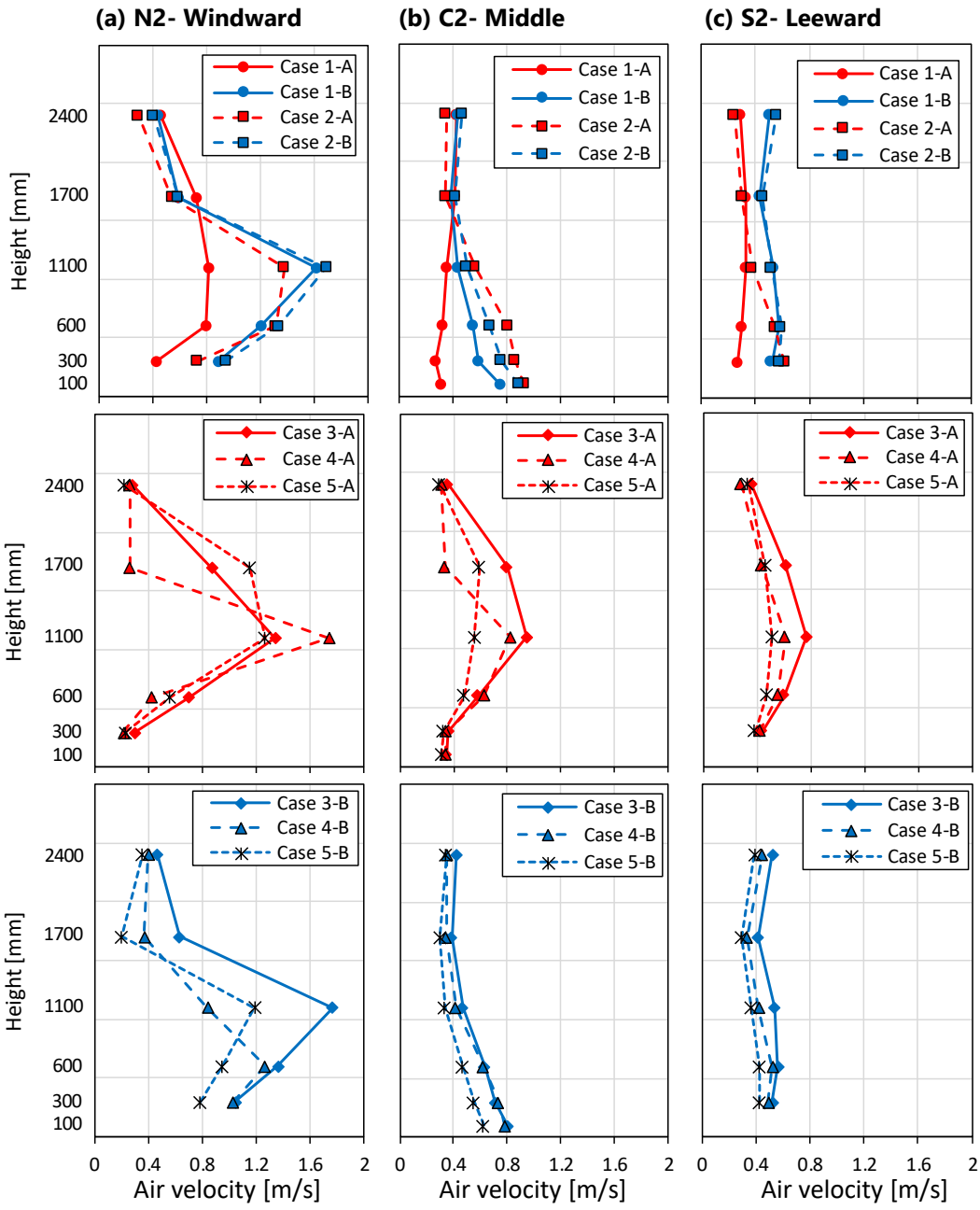

Fig. 3.7. Vertical distribution of air velocity at (a) windward side; (b) middle; (c) leeward side in Room A and Room B.

Similarly, Case 3 (1,200 mm) generally obtained higher air velocities than those in Case 5 (600 mm). Although the air velocities at the occupied level (FL+1.1 m) at the windward side

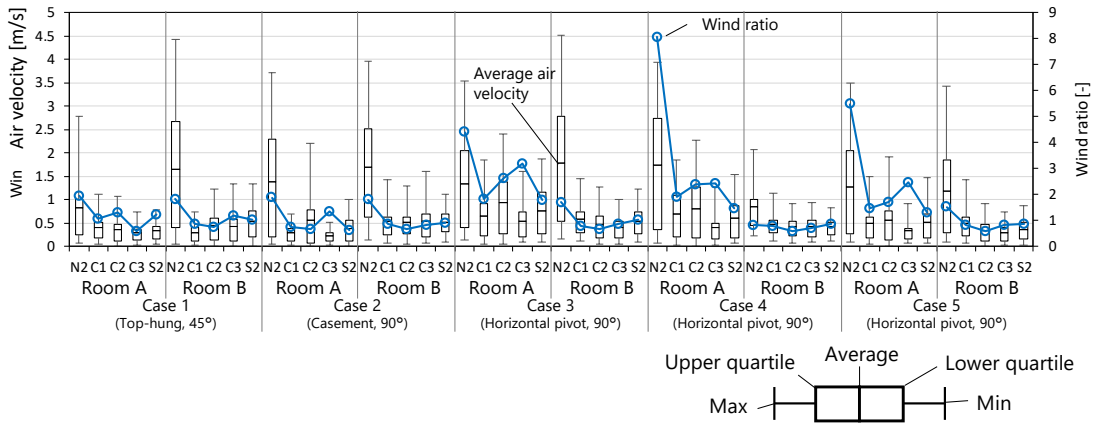

Fig. 3.8. Wind speed at the occupied level (FL+1.1 m) and wind ratio at each measurement points (N2, C1, C2, C3, S2).

(N2) were similar between Case 3 (1.4 m/s) and Case 5 (1.3 m/s), those at the middle of the room (C2) were 0.9 m/s and 0.6 m/s respectively. In particular, in Case 3, approximately 40% of the inflows went straight, and relatively strong air flows reached the occupied level until the leeward side (S2) with an air velocity of 0.8 m/s. As such, the length of the window pane could affect the indoor air flow pattern due to the Coandă effect. Since Cases 4 and 5 adopted shorter lengths of window pane, the percentage of the straightforward inflows was lesser than Case 3, about 24–34%. As depicted in Fig. 3.7, the wide horizontal pivot window in Case 4 obtained relatively lower air velocities not only near the floor surfaces, but also at the upper level, mainly because the height of the window pane was reduced to 600 mm.

Fig. 3.8 depicts the horizontal distributions of wind speeds and wind ratios, showing the ratios of the measured air velocities at the occupied level (FL+1.1 m) to those near the floor surface (FL+0.3 m/s). As the top-hung window (Case 1) and the horizontal pivot windows (Cases 3–5) mainly control the vertical air flow patterns, there was no significant differences in the horizontal distributions for each case. The casement window with a 90° opening angle (Case 2) generally let the wind flow horizontally straight. Comparing Room A with B in Case 2, the wind speeds in the middle of Room A (C2) were higher than those in Room B, whereas the other measurement points, that is, C1 and C3, recorded relatively lower wind speeds in Room A. This indicates that the casement window helped change the horizontal inflow angle.

Cases 4 and 5 employed the same window type with the same length of window pane, i.e. horizontal pivot with a window of 600 mm, but its aspect ratio was different: 4:1 for Case 4 and 1:1 for Case 5. As described above, the average outdoor wind speed in Case 4 was the same as that in Case 5, but the air velocities at the occupied level (FL+1.1 m) in Case 4 were

on average 0.1–0.5 m/s higher than those in Case 5. The wide horizontal pivot window was found to be more effective in supplying air flows to the occupied level, while lowering air velocities near the floor surfaces, compared with the square horizontal pivot window.

3.3.3. Heat transfer coefficient on floor

As discussed above, the daytime ventilation can diminish the nocturnal cooling storage due to the daytime heating effect. Therefore, the heat transfer which influences the retention of structural cooling effect was analyzed. Following equations (Eq. 3.4 and 3.5) are the calculation of the heat transfer coefficient using the surface temperature on the floor, the air temperature near the floor surface, and the heat flux on the floor. When the temperature difference between the floor surface temperature and the air temperature was small or the errors caused by response delay of sensors was observed, the calculated heat transfer coefficients were removed from the results because these values overestimate the heat transfer coefficient [3.25, 3.26]. To compare the experimentally measured values with the values using the results of the air velocities, the heat transfer coefficient was estimated using the Jürges equation (Eq. 3.6 and 3.7).

$$\alpha = \frac{q}{\Delta T} \tag{3.4}$$

$$\Delta T = T_s - T_a \tag{3.5}$$

Table 3. 4. Estimated and measured heat transfer coefficients.

	Estimated values		Measured values	
	Range [W/m^{2}K]	Average [W/m^{2}K]	Range [W/m^{2}K]	Average [W/m^{2}K]
Case 1				
Room A	10.7–12.4	11.3	4.2–19.1	9.5
Room B	10.7–15.1	12.0	2.4–21.3	9.4
Case 2				
Room A	10.7–16.2	12.0	4.1–22.3	9.8
Room B	10.7–13.9	11.5	5.5–21.7	10.3
Case 3				
Room A	10.8–12.6	11.4	4.0–18.8	9.5
Room B	10.8–14.6	11.7	5.5–26.8	11.0
Case 4				
Room A	10.8–12.6	11.4	3.3–21.0	9.7
Room B	10.7–14.5	11.8	5.1–24.1	10.4
Case 5				
Room A	10.8–12.6	11.3	4.0–23.7	11.0
Room B	10.9–14.5	11.9	5.2–24.1	11.2

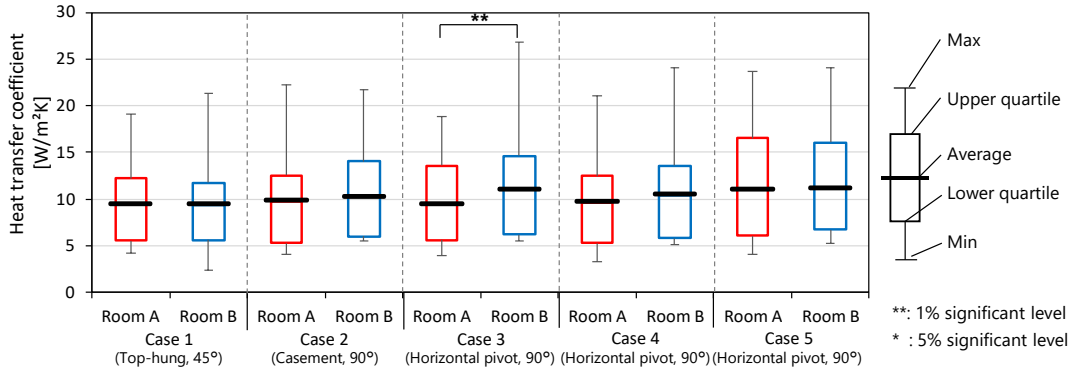

Fig. 3.9. Comparison of heat transfer coefficient in Room A (test) and Room B (control).

$$h_c = 5.6 + 3.9v \qquad (v \leq 4.9 \text{ m/s}) \qquad (3.6)$$

$$h_c = 7.2v^{0.78} \qquad (v > 4.9 \text{ m/s}) \qquad (3.7)$$

where $\boldsymbol{\alpha}$ is the heat transfer coefficient [W/m^{2}K], q is the heat flux [W/m^2], ΔT is the temperature difference between T_s is the surface temperature on floor and T_a is the air temperature. measured at FL+0.1 m [°C], h_c is the convective heat transfer [W/m^{2}K], v is the air velocity near the floor surface [m/s].

Firstly, the validation on the measured heat transfer coefficients were conducted based on literature reviews. Regarding convective heat transfer, there are three convection modes, i.e., natural convection, forced convection, and mixed convection. In general, under naturally ventilated condition, the convective heat transfer is regarded as the mixed convective heat transfer with the convective heat transfer coefficients of approximately 5–20 W/m^{2}K [3.26–3.28]. The radiant heat transfer coefficients for a cooled radiant floor often adopts 4.9–5.5 W/m^{2}K [3.29, 3.30]. The heat transfer coefficients were estimated using the Jürges equation with a radiant heat transfer coefficient of 5.0 W/m^{2}K [3.31]. The resultant heat transfer coefficients were averaged at 11.3–12.0 W/m^{2}K for Room A and 11.5–12.0 W/m^{2}K for Room B (Table 3.4). Meanwhile, as shown in Fig. 3.9, the heat transfer coefficients were

measured at 2.4–26.8 W/m^{2}K in this measurement, with average values of 9.5–11.0 W/m^{2}K (Room A) and 9.4–11.2 W/m^{2}K (Room B). The average measured heat transfer coefficients were slightly lower than the average estimated values. Although the measured heat transfer coefficients were reflected by the air velocities near the floor, turbulence and direction of heat flux can be possible causes of the above-mentioned inconsistencies with the estimated values.

As illustrated in Fig. 3.9, the heat transfer coefficients in Room A (test)obtained relatively lower than those in Room B (control), owing to the lower air velocities near the floor, especially in Case 3. In Case 1(Top-hung, 45°), the maximum heat transfer coefficient in

Room B (Simple opening) was 2.2 W/ m^2K higher than that in Room A (Top-hung), nevertheless the average heat transfer coefficient was similar in both rooms (around 9.4 W/m^2K). Meanwhile, in Case 2 (Casement, 90°), the maximum heat transfer coefficient in Room A was higher than that in Room B even though average heat transfer coefficient in Room A was lower than that in Room B. This is because the analysis of the heat transfer coefficient considered both inflows from the north and south, and the inflow of simple opening on south side influenced the results of the heat transfer coefficient. However, in the afternoon, when the wind speed was relatively strong, the prevailing wind direction was mainly from the north. Therefore, the maximum heat transfer coefficient was affected by those wind condition.

In Cases 3–5, Room A was equipped with the horizontal pivot window with 90° opening angle. In Case 3 (square, 1,200 mm), the average heat transfer coefficients were 9.5 W/m^2K (Room A) and 11.0 W/m^2K (Room B). Moreover, the difference of the maximum heat transfer coefficient between in Room A and in Room B was up to 8.0 W/m^2K. Regarding the aspect ratio, in Case 4, the wide horizontal pivot window (aspect ratio of 4:1) worked to reduce the heat transfer coefficient as well. The average heat transfer coefficient in Room A was 0.8 W/m^2K lower than that in Room B. Lowering the air velocity near the floor surface affected the reduction of the heat transfer coefficient. Nevertheless, in Case 5, the average heat transfer coefficient in Room A was almost the same as that of Room B. As depicted in Fig. 3.7, the air velocities near the floor in Case 5 were generally lower than those in the other cases. However, lager heat transfer coefficients were recorded in Rooms A and B in Case 5 compared with the other cases. This is probably because the relatively small temperature differences between the air temperature at FL+0.1 m and floor surface temperature in Case 5 increased the values [3.26]. The results indicate that the horizontal pivot window in particular the square type with long window panes or wide types, can reduce the convective heat transfer on the floor, and it may influence the retention of structural cooling effect of the proposed system during the daytime.

3.3.4. Floor surface temperature

Radiant cooling is useful for improving the thermal comfort of occupants even with relatively small temperature differences between the room temperature and surface temperature [3.32]. Fig. 3.10 illustrates the temperature differences between the air temperature and the floor surface temperature in Rooms A (test room) and B (control room) for Cases 1–5. The temporal average floor surface temperatures in Rooms A and B were 0.8–1.7 ℃ and 0.1–0.8 ℃ lower than the air temperatures (FL+1.1 m) measured in the middle of the room during the daytime. Owing to the increased thermal mass by the PCMs and the forced ventilation to the underfloor space during the nighttime, the durations of thermal storage effect (when the surface temperatures were lower than the ambient temperature) in Room A was

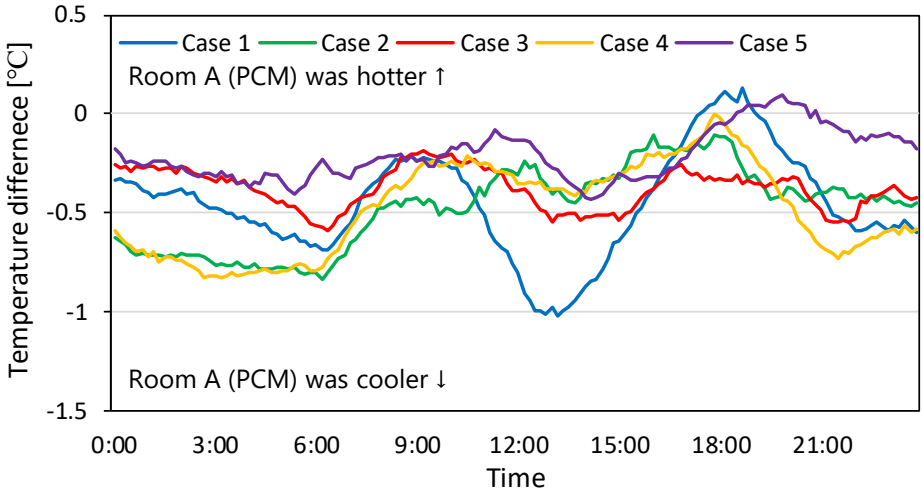

Fig. 3.10. Floor surface temperature difference between Rooms A and B.

approximately two hours longer than that in Room B. In Case 1, the temperature difference was up to 2.7 ℃. In Cases 3 and 5, a sudden variation in the temperature difference was caused by a light shower. During the periods, the air temperature dropped by up to 3.2 ℃ in an hour, although the corresponding surface temperature was almost constant due to thermal inertia. Meanwhile, in the case of sunny periods with high indoor air temperatures, the temperature difference varied within a range of 1–2 ℃. The floor cooling system maintained a cooler floor surface temperature than the corresponding air temperature for most of the afternoon period.

Fig. 3.11presents the surface temperature differences between Rooms A and B. The floor surface in Room A was cooler than that in Room B during most of the measurement period, with daytime average differences of 0.24–0.51 ℃, due to the increased thermal storage of the floor structure and the forced ventilation of the underfloor space at night. In the peak temperature hours (12:00–15:00), when the temperature of the PCMs reached 29 ℃, the

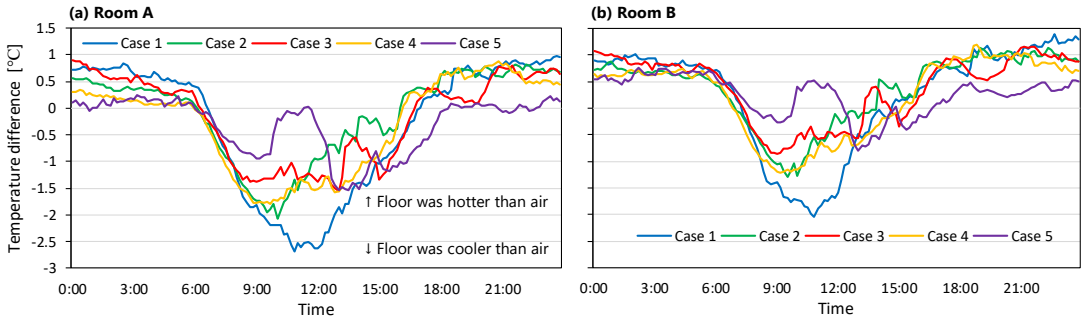

Fig. 3.11. Temporal variation in temperature difference between FL+1.1 m and floor surface in Room A (test room) and Room B (control room).

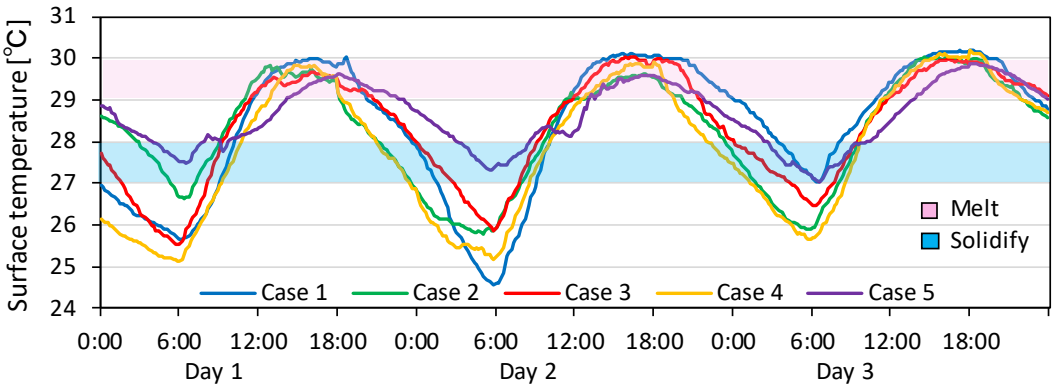

Fig. 3.12. Temporal variation of the surface temperature of the lower side of the PCM pack for each case (Cases 1-5).

temperature differences tended to be larger than those in the morning (9:00–12:00) and the late afternoon (15:00–18:00) because of the latent hear thermal storage of the PCMs. Fig. 3.12 shows the surface temperatures of the bottom side of the PCMs for each case. Between 12:00 and 15:00, the surface temperature variation of the PCMs was gentle within the melting temperature range; therefore, the floor surface temperature in Room A was reduced by up to 1.0 ℃ due to the large latent heat storage. When the exhaust fans were on (18:00), the temperature difference of the floor surface rapidly became larger despite the increased thermal storage in Room A. During the nighttime, the floor surface temperatures in Room A were still 0.2–0.6 ℃ lower than those in Room B. This result implies that the exhaust fans contributed to heat dissipation from the floor structure and enhanced the thermal storage effect. As shown in Fig. 3.12, the surface temperatures of the PCMs dropped further than the solidification temperature range (27–28 ℃) after midnight, indicating that the PCM solidification was completed under the given weather conditions.

Although the lowered air velocities near the floor surface affected the reduction of the convective heat transfer particularly in the case of the horizontal pivot windows (Case 3), the influence of the lowered convective heat transfer on the differences in surface temperature between the cases cannot be seen clearly. For instance, the floor surface temperature reduction in Case 3 was 0.1 ℃ lower than that in Case 1 (top-hung window). In general, the temperature of objects with little thermal mass, for example, leaves, is dominantly influenced by air velocities near the surface [3.33]. This implies that the thermal storage effect was influenced more by its thermal mass and the cooling strategy for the floor structure with the PCMs (e.g., exhaust fans) at night, than by the convective heat transfer.

3.3.5. Evaluation of indoor thermal comfort at the occupied level

The influence of the window types on the indoor thermal comfort was evaluated using the operative temperature (OT) and standard effective temperature (SET*) in the middle of the rooms at 1.1 m height above the floor. The data from the field measurement was used in the thermal comfort. The OT express the uniform temperature of an imaginary black globe enclosure in which an occupant would exchange the same amount of heat by radiation plus convection as in the actual non-uniform environment [3.8]. The OT was calculated based on the air temperature, mean radiant temperature and air velocity, using the following formula (Eq. 3.8) [3.18].

$$T_{op} = \frac{T_a\sqrt{10v}+T_r}{1+\sqrt{10v}} \tag{3.8}$$

where T_{op} is the operative temperature [°C], T_a is the air temperature [°C], v is the air velocity [m/s], and T_r is the mean radiant temperature [°C].

The SET* is defined as the equivalent air temperature of an isothermal environment at 50% of relative humidity in which a subject, wearing clothing standardized for the activity concerned, has the same heat stress and thermoregulatory strain as in the actual environment [3.8]. Based on the ANSI/ASHRAE Standard 55-2020, the SET* was calculated [3.8]. In calculating SET*, the metabolic rate was assumed to be 1.0 met, which indicates seated position. Meanwhile, clothing insulation was estimated to be 0.5 clo, which express typical clothing worm when the outdoor condition is warm [3.34]. The convective, evaporative, and radiant heat transfer coefficients of 3.0–12.8 W/m^{2}K, 49.5–211 W/m^{2}kPa, and 4.4–4.8 W/m^{2}K, respectively, were used to calculate SET*.

The following equations give quantitative information on calculating heat exchange between people and the environment. In the heat balance equations, mathematical statements for various terms of the heat exchange clarify the influence of factors on thermal comfort. Fundamental heat transfer theory is used to describe the various mechanism of sensible and latent heat exchange, and empirical expressions are used to determine the values of coefficients describing these rates of the heat exchange. The heat losses from a human body were calculated as follows [3.34–3.36].

$$M = C + R + E + R_{es} + \Delta S \tag{3.9}$$

$$C = h_c(T_{sk} - T_a)F_{cl}f_{cl} \tag{3.10}$$

$$R = h_r(T_{sk} - T_r)F_{cl}f_{cl} \tag{3.11}$$

$$E = LRwh_cF_{pcl}f_{cl}(p_{ssk} - p_a) \tag{3.12}$$

$$R_{es} = 0.0014M(35 - T_a) + 0.0173M(5.624 - p_a) \tag{3.13}$$

$$f_{cl} = 1 + 0.31I_{cl} \tag{3.14}$$

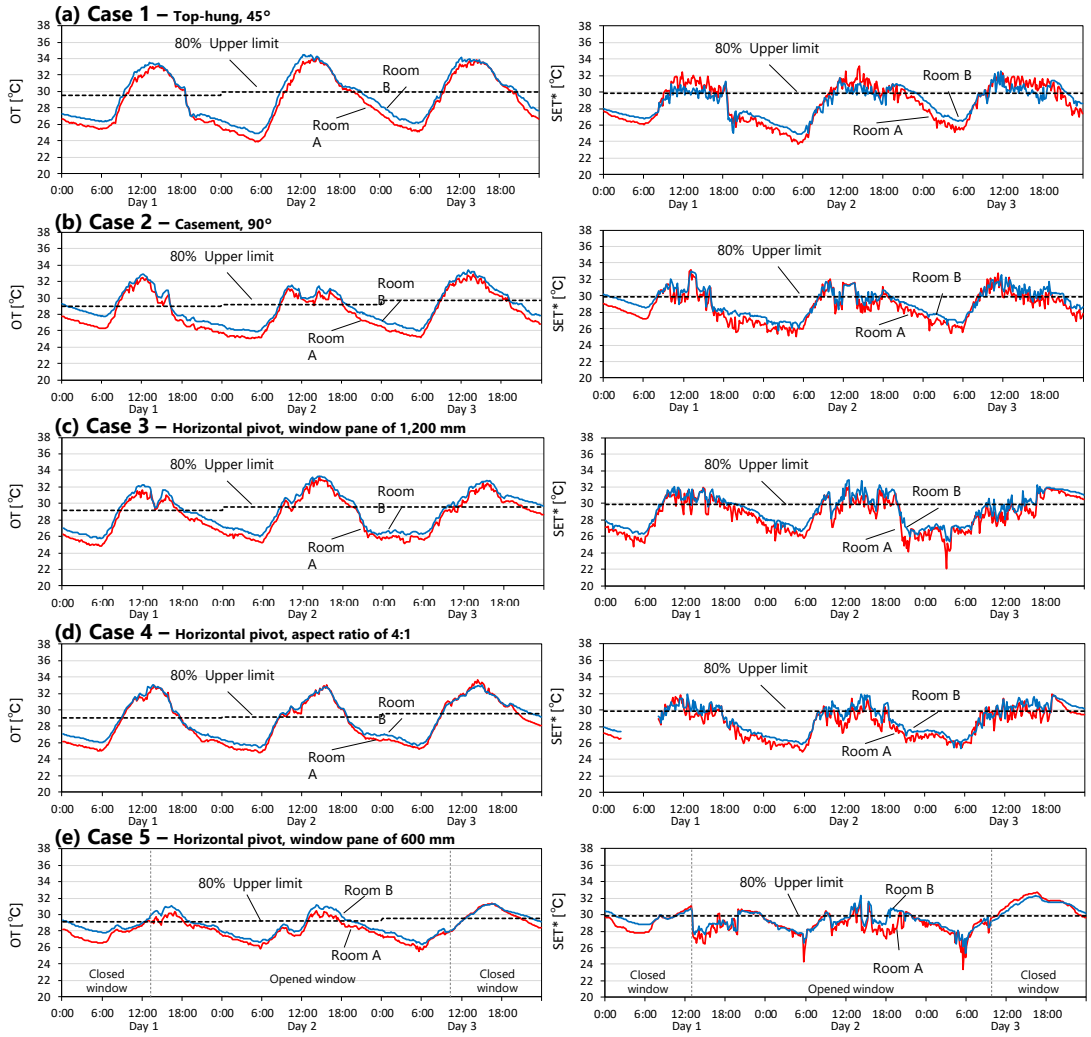

Fig. 3.13. Temporal variation of OT and SET* in (a) Case 1; (b) Case 2; (c) Case 3; (d) Case 4; (e) Case 5 with the upper comfort limit.

$$F_{cl} = \frac{1}{1+0.155I_{cl}(h_c+h_r)f_{cl}} \tag{3.15}$$

$$F_{pcl} = \frac{1}{1+\frac{0.155I_{cl}}{0.34h_cf_{cl}}} \tag{3.16}$$

where M is metabolic rate [W/m^2], C is convective heat loss [W/m^2], R is radiant heat loss [W/m^2], E is evaporative heat loss [W/m^2], R_{es} is Total heat loss by respiration [W/m^2], ΔS is heat storage at a given moment [W/m^2], h_c is convective heat transfer coefficient [W/m^{2}K], h_r is radiant heat transfer coefficient [W/m^{2}K], F_{cl} is Intrinsic clothing thermal efficiency [-], f_{cl}

Table 3. 5. Evaluation of the OT and SET* during the daytime.

	OT [°C]	Thermal comfort period [%]	SET* [°C]	Thermal comfort period [%]
Case 1				
Room A	30.7–31.4	26–28	29.7–30.3	26–40
Room B	30.9–31.6	25–28	29.2–29.8	40–64
Case 2				
Room A	29.8–30.9	22–32	29.6–30.0	39–61
Room B	29.9–31.0	22–31	29.9–30.3	22–42
Case 3				
Room A	29.9–30.7	24–31	29.6–29.9	38–85
Room B	30.1–30.9	19–29	29.5–30.4	22–63
Case 4				
Room A	30.2–30.8	22–28	28.9–29.9	64–78
Room B	30.2–30.6	22–28	29.6–30.2	39–47
Case 5				
Room A	29.0–29.1	54–56	29.0	71–79
Room B	29.1–29.3	53–56	29.3–29.5	76

is clothing area factor [-], F_{pcl} is permeation efficiency of clothing [-], LR is Lewis ratio (16.5) [kPa/K], w is skin wittedness [-], p_{ssk} is saturated vapor pressure at a skin temperature [kPa], p_a is water vapor pressure [kPa], T_a is air temperature [°C], T_r is mean radiant temperature [°C], T_{sk} is skin temperature [°C], I_{cl} is clothing insulation [clo].

According to the ASHRAE standard [3.8], a thermal environment can be considered as an acceptable condition if more than 80% of occupants feel it acceptable. For the evaluation on the OT, the comfortable ranges were evaluated on the basis of an adaptive comfort equation (ACE) for naturally ventilated buildings in the hot and humid climates. Toe and Kubota [3.37] determined the ACE based on the statistical meta-analysis of the ASHRAE RP-884 database. The suggested ACE for naturally ventilated buildings was proven to have a coefficient of determination of 0.6, which is more than twice the existing standards. The 80% of the upper comfortable OT limit was calculated using the following equation (Eqs. 3.17 and 3.18). The resulting limit ranged from 28.9–30.0 °C.

$$T_{neutop} = 0.57T_{outdm} + 13.8 \tag{3.17}$$

$$T_{upper} = T_{neutop} - 0.7 \tag{3.18}$$

where T_{nuetop} is the neutral operative temperature [°C], T_{outdm} is the daily mean outdoor air temperature [°C], i.e. the 24-hour arithmetic mean for the day in question, and T_{upper} is upper comfort operative temperature [°C].

Regarding the acceptable condition on the SET*, in general, the 80% acceptavle upper limit on the warm side of thermal sensation vote (TSV) is 0.85 [3.38]. A following equation (Eq. 3.19) presents the correlation between the TSV and the SET* for naturally ventilated buildings in the hot and humid climates [3.39]. Upper comfort SET* limit was set to be 29.9 ℃.

$$\text{TSV} = 0.195SET^{*} - 4.97 \quad (3.19)$$

Fig. 3.13 shows temporal variation of the OT and SET*, calculated using the measured data at 1.1 m above the floor in the center of the rooms, with above mentioned upper comfort limit. The OT in Room A was 0–0.4 ℃ lower than that in Room B during the daytime for Cases 1–4 because the corresponding floor surface temperature in Room A was 0.3–0.5 ℃ lower than that in Room B. The floor cooling system using the PCMs contributed to lowering the floor surface temperature, and thus reduced the OT in Room A, compared with that in Room B. However, the acceptable thermal comfort period, based on the measured OT, was only 22–32% of the day because the maximum outdoor temperature often exceeded 34 ℃. It implies that it is difficult to satisfy the thermal comfort by employing the structural cooling effect alone. Meanwhile, in the daytime of Case 5, the mean daytime outdoor temperature ranged from 29.4–29.5 ℃ which was around 1.5 ℃ lower than that in the other cases. That temperature was insufficient to let the PCMs melt. Consequently, the difference of the floor surface temperature was slight, and the improvement of the OT could not be observed. In the daytime of Case 5, more than half period of the daytime could meet the acceptable range. Since the difference of the OT reduction effect was mainly from the effect of the floor cooling system, it can be said that the influence on the window system improving OT was small.

In contrast with the OT, the window type strongly affected the improvement of the SET*. As shown in Fig. 3.13, the temporal variation of the SET* depended on the window types. In Case 1 (top-hung, 45°), the SET* in Room A was 0.5–0.7 ℃ higher than that in Room B (simple opening). This is because the corresponding air temperature in Room A was 0.3 ℃ higher than in Room B, whereas Room A received 0.1–0.2 m/s lower air velocities compared with Room B due to the smaller effective opening area. Consequently, in Case 1 the thermal comfort period (i.e. SET* was less than 29.9 ℃) ranged only between 26–40% of the daytime in Room A (Table 3.5). In Case 2 (casement, 90°), as described before, the air velocities at the middle of Room A were 0.1–0.2 m/s higher than those of Room B. As a result, the diurnal SET* in Room A was reduced by 0.3–0.6 ℃, compared with Room B.

As shown in Fig. 3.7, the horizontal pivot windows (Cases 3–5) provided preferable indoor air flow patterns. This chapter analyzed the thermal components in the SET* calculation in detain and found that in Cases 3–5, the daytime average evaporative and convective heat losses from the human body in Room A were higher than those in Room B with respective values of 0.1–9.0 W/m^2 and 0.2–3.8 W/m^2, owing to the higher air velocities at the occupied level. Meanwhile, the radiant floor cooling system contributed to the increase

in the radiant heat loss from the human body with a diurnal average of 2.6–4.2 W/m^2 in Cases 3–5. Consequently, in the daytime of Case 3 (window pane of 1,200 mm), the diurnal average SET* in Room A was 0.5–0.8 ℃ lower than Room B (simple opening), and the thermal comfort period in Room A extended more than half of the daytime (Fig. 3.13 and Table 3.5). In particular, on the third day of Case 3, the thermal comfort period in Room A was very high, which was 85% of the day, mostly because of the high outdoor wind speeds (2.3 m/s on average), while the corresponding period in Room B was 39%. This implies that thermal comfort is improved largely due to the increased air velocities at the occupied level. In Case 4 (aspect ratio of 4:1), the daytime SET* in Room A was 0.3–0.8 ℃ lower than Room B, and the thermal comfort period in Room A and B was 64–78% and 39–47% of the day, respectively. Comparing Room A with B in Case 5 (window pane of 600 mm), the reduction of the SET* was by 0.3–0.4 ℃ during daytime. Because Case 5 measured lower diurnal outdoor air temperature (29.5 ℃ on average), the thermal comfort period was more than 70% of the daytime in both rooms.

3.4. Discussion

3.4.1. Thermal comfort evaluation

In a previous study on night ventilation with the PCM in Iran, the wall surface temperature was 0.5–0.6 ℃ lower than the room temperature during the daytime, bringing the improvement of thermal comfort through radiation [3.40]. During the field measurement in this study, the floor surface temperature in Room A (test) was 0.8–1.7 ℃ lower than the corresponding room temperature (Fig. 3.10). This implies that the proposed floor cooling system has a positive impact on thermal comfort even under the daytime ventilation conditions.

In Indonesia, the results of a questionnaire survey showed that occupants generally prefer a higher air velocity [3.41]. Cândido et al. [3.42] determined the minimum preferred wind speed in a hot-humid climate, which was 0.9 m/s for an operative temperature of 30 ℃. The outdoor wind speeds, which were recorded at 10 m above the ground in this study, were approximately 1–2 m/s lower than those observed at the official weather station. Nevertheless, the measured wind speeds at the middle of Room A (FL+1.1 m) in Case 3 (i.e., horizontal pivot window) were 0.9 m/s on average, satisfying the above-mentioned criterion (Fig. 3.7). A horizontal pivot window especially with a long window pane, is found to induce sufficient air flows to the occupied level. As discussed above, the inflow elevation angle for a building is preliminarily determined by the positions of the stagnation point and opening. Nevertheless, a horizontal pivot window can lead to the straight inflow of air, regardless of the inflow elevation angle.

A top-hung window is commonly used for urban houses, for example, in Australia and Indonesia. In the temperate climate of Australia, it was reported that a small angle of the top-hung window can be effective for achieving thermal comfort by reducing the influence of outdoor air [3.43]. However, in the tropical climate of Indonesia, it is difficult to achieve the required thermal comfort without utilizing sweat evaporation assisted by a sufficient air flow. Even though the highest surface temperature reduction was observed in Case 1 (top-hung), positively affecting the thermal comfort, the thermal comfort period in Room A was 14–31% shorter than that in Room B (simple opening). In this case, a top-hug window may diminish the cooling effect through ventilative cooling. On the contrary, in Case 3 (i.e. horizontal pivot window), the thermal comfort period in Room A was 15–22% longer than that in Room B during the daytime. Under hot and humid conditions, adequate air movements can compensate for the increased air temperature and humidity [3.44]. Consequently, the horizontal pivot window is found to be a better option than the top-hung window for ventilative cooling in the tropics.

In Case 3 (horizontal pivot window), the thermal comfort period was increased up to 85% when the outdoor wind speed was satisfactory, which was approximately 2.3 m/s. In a previous study in the tropical humid regions, the horizontal pivot window (45°) achieved thermally neutral conditions when the outdoor wind speed was 2.4 m/s [3.45]. To achieve thermal comfort by ventilative cooling through the horizontal pivot window, outdoor wind speeds more than 2.0 m/s may be required. Meanwhile, Case 4 recorded a higher diurnal mean outdoor temperature than the recent weather data, which was 31.3 ℃. However, the thermal comfort period in Case 4 reached approximately 70%. The weather data at the nearest official station show that the diurnal mean outdoor temperature ranges from 8.5–30.7 ℃ with an average wind speed of 2.62–3.38 m/s [3.19]. The field measurement was conducted at the higher temperature (29.5–31.7 ℃) than the weather data at the nearest station. Moreover, compared with the weather data in other major cities of Indonesia, the air temperature at the nearest weather station tends to be higher. These implies that indoor thermal comfort can be achieved for most of the daytime even under natural ventilation conditions in the radiant floor cooling system with the horizontal pivot windows.

3.4.2. Limitation

As indicated in Fig. 3.12, the difference in the floor surface temperatures between Room A (with PCM) and B (no PCM) in Cases 5 was 0.1–0.3 ℃ smaller than in the other cases. This is primarily because the average diurnal outdoor air temperature of 29.5 ℃ did not exceed the melting temperature range of 29–30 ℃. The long-term weather data at the nearest station indicated that the diurnal outdoor temperature ranged from 28.5–29.9 ℃ during the rainy season [3.19]. This means that the melting temperature set in this measurement was not

suitable for the rainy season, although it is preferable for the weather conditions during the dry season. The subtle outdoor temperature change can affect the thermal storage effect of the PCMs. Therefore, the annual performance of the PCMs would be investigated in Chapter 6. Meanwhile, the nocturnal outdoor air temperatures were relatively stable (i.e., 25.5–26.4 ℃) throughout the year, as discussed above. On the first day of Case 1, the outdoor temperature was 26.4 ℃, which was the same as the upper value of the recently averaged nocturnal outdoor temperature, and the PCM completely solidified. Based on this result, the solidification temperature may be appropriate.

Although the phase states of the PCMs were evaluated in terms of the PCM temperature, the heat balance analysis of the PCMs was absent. To clarify the relationship between the thermal storage effect and temperature field, it may be necessary to analyze how much the PCMs stored and released the heat quantitatively. The heat balance of the PCMs would be investigated in Chapters 4 and 5.

3.5. Summary

A field measurement was conducted to determine the effective window design for ventilative cooling with a floor cooling system in the hot and humid climate of Indonesia. To achieve thermal comfort of the occupants, while maintaining the thermal storage effect in the daytime, several window systems, in particular three types of the horizontal pivot windows were evaluated based on the measurements using the experimental building. In the proposed system, the PCMs increased thermal mass of the floor structure, while the ventilation fans enhanced the nocturnal cooling effect through night ventilation. Consequently, the floor surface temperature in the room with the floor cooling system was 0.3–0.5 ℃ lower than that without it. Regarding the indoor air flow patterns, the horizontal pivot windows brought air velocities 1.7–2.6 times higher to the occupied level (FL+1.1 m) than to the space near the floor surface (FL+0.3 m) in the middle of the room. Moreover, the horizontal pivot window with a long window pane (Case 3) brought relatively strong air flows to the occupied level even until the leeward side. As for the aspect ratio, the wide horizontal pivot window (Case 4) obtained 0.1–0.5 m/s higher air velocities at the occupied level than the square horizontal pivot window (Case 5), even when the outdoor wind speed was almost the same. Further analysis of indoor thermal comfort showed that the horizontal pivot window with a long window pane of 1,200 mm (Case 3) and the radiant floor cooling system reduced the average diurnal SET* by up to 0.8 ℃ at the middle of the room, in comparison with the simple opening without the cooling system. In this case, the average heat transfer coefficient was reduced by 1.5 W/m^2K. The horizontal pivot windows were able to improve thermal comfort that is lowering the SET* at the occupied level and preventing the heat transfer coefficient on the floor from increasing, in a naturally ventilated building of the tropics. However, the reduced convective heat transfer

coefficient did not strongly influence the retention of the thermal storage effect in the high thermal mass floor. If the floor structure stores the “coolness” sufficiently through night ventilation, then the increased thermal mass by the PCMs could maintain a low surface temperature on the floor during daytime, regardless of the window type. The results of this chapter suggest that the most essential point of window design in the proposed system is not to reduce the air flow near the floor structure, but to improve the ventilative cooling at the occupied level.

Chapter 4

Field measurement of thermal storage effect of phase change materials

Abstract

Chapter 4 aims to clarify the measures to ensure the thermal storage effect of the proposed system during daytime for a naturally ventilated room within a relatively narrow diurnal temperature range, mainly focusing on the heat balance of the PCMs. Another field measurement was conducted to analyze the relationship between the indoor vertical air temperature distributions and heat flows of the proposed system using an experimental building in Tangerang, Indonesia, as with Chapter 3. The results confirmed that the thermal storage of the PCMs and the cooling strategy for the floor structure at night strongly contributed to maintaining a low floor surface temperature during the subsequent daytime. Calm wind conditions and warm nocturnal ambient temperature, which was 0.7–3.2 ℃ lower than the set-point solidifying temperature and are common in the tropics, prevented the PCMs from solidifying in case of natural ventilation for the underfloor space. In contrast, forced ventilation for the underfloor space attaching the PCMs was effective in ensuring sufficient solidification. Furthermore, 95% of the thermal storage capacity of the PCMs might be utilized when the ambient temperature was 2–3 ℃ higher than the set-point melting temperature during the daytime. The phase change temperature for PCMs can be determined based on the average ambient temperature, whereas a relatively wide diurnal ambient temperature range at least 4.7 ℃, was required to ensure the latent heat thermal storage effect caused by the supercooling.

Key words
Thermal storage effect, Field measurement, Temperature distribution, Heat flux.

4.1. Introduction

As shown in Chapter 2, recently, phase change materials (PCMs) have been widely used in buildings owing to their high energy density and thermal storage capacities in a constant temperature phase change process [4.1]. Latent heat thermal storage can be used within a relatively narrow temperature range [4.2]. For example, Wonorahardjo et al. [4.3] conducted a field measurement in Indonesia and results showed that the indoor temperature using a passive air conditioner employing PCMs was 0.2 ℃ lower than that using sensible heat storage materials.

The reduction of the peak daytime indoor temperature is typically required in the tropics [4.4]. Hence, it is important to sufficiently complete the phase changes of PCMs within a day to maximize the thermal storage effects for cooling. As shown, thermal storage effects using PCMs have been observed even in hot and humid climates where the diurnal temperature range is relatively narrow (e.g., approximately 6.3 ℃ in Malaysia) if the solidification process of the PCMs during the previous nights was completed [4.5]. Nevertheless, it is still uncertain how the thermal storage effects can be maximized by optimizing the thermal properties of PCMs and cooling methods during nighttime, especially in naturally ventilated buildings under the conditions of such narrow diurnal temperature ranges. Most of the existing studies on the application of PCMs for buildings mainly focused on the resultant reductions in indoor temperature and cooling loads [4.5–4.8]. However, few studies have analyzed the phase state of PCMs and the resulting amounts of heat stored and released by the PCMs, that is, heat balance, although these analyses are required to determine the optimum settings for PCMs as well as the entire cooling system. Previous studies investigated the influence of inlet airflow temperature [4.9, 4.10] and airflow rate [4.9–4.11] on air-PCM heat transfer and the duration of the melting process of the PCM under warm-hot conditions (more than 25 ℃). In most of these studies, the inlet temperature and flow rate were set to a constant value, which were different from the conditions in the natural environment, and few studies analyzed the influential factors under transitional conditions. The radiant floor cooling system using PCMs with night ventilation was proposed in Chapter 2, and the relationship between the heat transfer coefficient on the floor and the cooling effect was investigated in Chapter 3. Although the results in Chapter 3 implied that the thermal storage effect was influenced more by thermal storage and the cooling method for the floor structure with the PCMs at night than by the convective heat transfer, the quantitative evaluation of the thermal storage of PCM, i.e., heat balance, was absent.

4.1.1. Objective

The annual outdoor temperature ranges are often very narrow in hot-humid tropical climates, for example, approximately 1.7 ℃ in Jakarta. This implies that if optimum settings are adopted for the cooling system in the hot-humid tropics, there is a high possibility of obtaining a high cooling effect stably throughout the year, even under naturally ventilated conditions. Chapter 4 aims to clarify the measures to ensure the thermal storage effect of the proposed system during daytime for a naturally ventilated room in the hot and humid climate of Indonesia, focusing especially on the heat balance of the PCMs and cooling strategies during nighttime. The cooling effect of the proposed system under closed/open window conditions and different ventilation conditions of the underfloor space was evaluated based on the results of a field measurement conducted in the full-scale experimental building in Tangerang, Indonesia, as with Chapter 3. The field measurement was conducted to analyze the relationship between the indoor vertical temperature distributions and heat flows of the proposed system. This study also analyzed the relationship between the phase change state of the PCMs and the amount of the heat stored and released by the PCMs, that is, heat balance, to clarify the influence of the thermal storage of the PCMs on the overall cooling effect of the proposed system. Finally, the factors influencing thermal storage were investigated.

4.2. Methodology

4.2.1. Experimental design

A field measurement was conducted from March 6 to May 25, 2019, to analyze the thermal storage effect of the proposed cooling system. The case design of the field

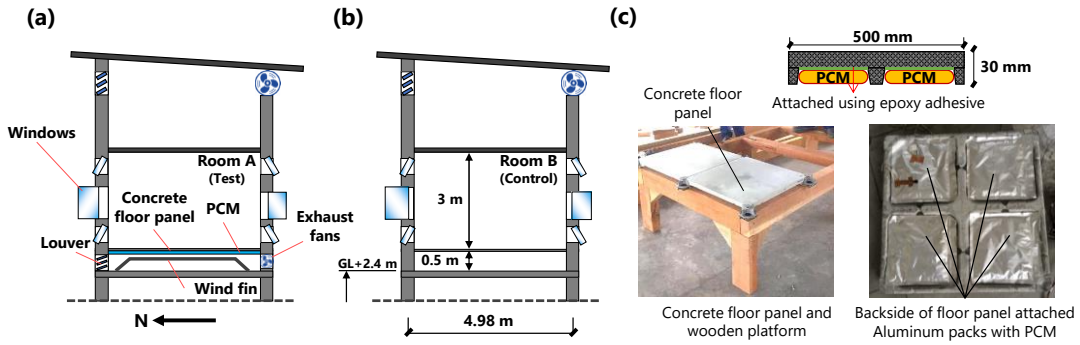

Fig. 4.1. Description of experimental building: (a) Section of Room A, (b) Section of Room B, (c) Details of the concrete floor panel and PCM packs.

Table 4.1. Case setting.

Case	Operating device	Room A (test) Day	Room A (test) Night	Room B (control) Day & Night	Description
Case 1	Room windows Louvers Fans	Close Open Off	Close Open Off	Close - -	Room window: No ventilation Underfloor space: Natural ventilation
Case 2	Room windows Louvers Fans	Close Open Off	Close Open On	Close - -	Room window: No ventilation Underfloor space: Forced ventilation
Case 3	Room windows Louvers Fans	Open Open Off	Open Open Off	Open - -	Room window: Full-day ventilation Underfloor space: Natural ventilation
Case 4	Room windows Louvers Fans	Open Open Off	Open Open On	Open - -	Room window: Full-day ventilation Underfloor space: Forced ventilation
Case 5	Room windows Louvers Fans	Open Close Off	Open Open On	Open - -	Room window: Full-day ventilation Underfloor space: Forced ventilation

measurement is listed in Table 4.1. For the evaluation, consecutive sunny days were chosen from each case. As shown in Fig. 4.1, we compared Room A (test) with B (control) to evaluate the thermal storage effect of the proposed system under different operating conditions. In particular, this chapter analyzed the factor affecting the indoor temperature fields and the thermal storage effects of the proposed cooling system. As a result, the thermal storage effect of the PCMs can be calculated using the following formula (Eq. 4.1).

$$TS = \int \{H_{lower}(t) - H_{upper}(t)\} dt \quad (4.1)$$

where TS is the thermal storage [kJ/m^2], H_{lower} is the heat flux of the lower side of the PCM [W/m^2], and H_{upper} is the heat flux of the upper side of the PCM [W/m^2].

In Case 1, natural ventilation was employed in the underfloor space (Table 4.1). The louver windows (inlet) for the underfloor space were opened, and the exhaust fans (outlet) were turned off throughout the day. In Case 2, the exhaust fans were turned on at night (18:00–7:00), and thus the PCMs were cooled with the assistance of forced ventilation in the underfloor space. In both cases, the room windows were closed for an entire day, that is, no ventilation condition, to reduce the influence of outdoor air on the indoor temperature fields. In contrast, the subsequent cases (Cases 3–5) were carried out under the full-day ventilation condition with opening room windows during the day and night. In Cases 3 and 4, the operational conditions of the louver windows and exhaust fans were the same as those in Cases 1 and 2, respectively. Case 5 is considered to be the optimum operation condition of the proposed cooling system, where the louver windows were opened, and exhaust fans were turned on only at night. The exhaust fans were turned on and off automatically, whereas the louver windows were opened and closed manually.

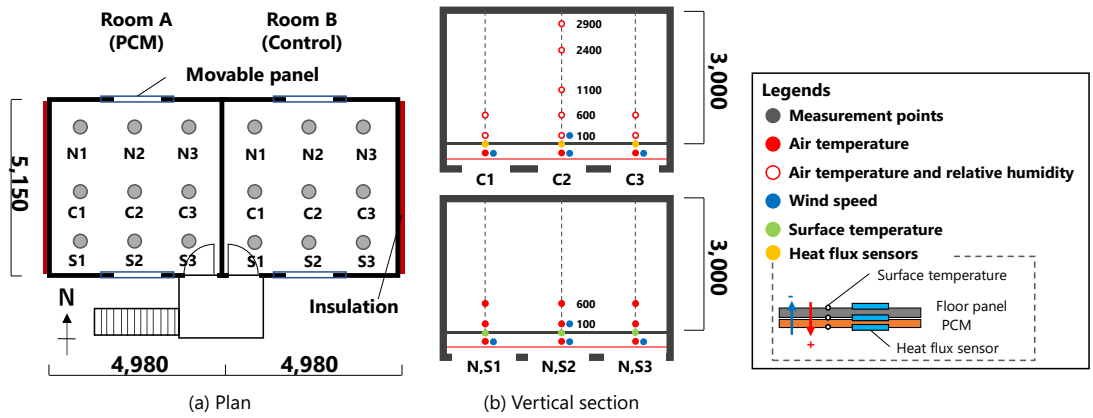

Fig. 4.2. Layout of experimental units and sensor/measurement setting in (a) Plan and (b) Section.

4.2.2. Data collection

The details of the equipment used in the experiments are listed in Table 4.2. The parameters in the outdoor space and both rooms were measured simultaneously every 10 min. During the experiment, the outdoor weather conditions were recorded at a weather station that was placed in an open space approximately 10 m away from the experimental building. As shown in Fig. 4.2, the air temperature and floor surface temperature were measured at nine horizontal points (3×3 points). To evaluate the thermal storage effect, the surface temperature and heat flux of the concrete floor panels and PCMs were measured at three points (C1–C3). To clarify the influences of the thermal storage on the indoor temperature fields, the vertical distribution of air temperature was measured at 0.1 m, 0.6 m, 1.1 m, 2.4 m, and 2.9 m from the floor surface at the center of the rooms (C2). All sensors measuring air temperature and

Table 4.2. Sensors for the measurement.

Measured variables	Instrument model	Accuracy
Indoor measurement		
Air temperature and relative humidity	TR-72nw-S (T&D Corporation, Japan)	±0.3 ℃, ±2.5% (30-80%RH)
Air and Surface temperature	Thermocouple type-T φ0.35 mm	±0.1%+0.5 ℃ plus ±0.5 ℃ for cold junction compensation
Wind speed	6332D with probe 9065-3 (KANOMAX, Japan)	±0.15 m/s (0.1-4.99 m/s)
Heat flux	PHF-100 (Prede, Japan)	±0.05%
Outdoor measurement (Weather station)		
Air temperature and relative humidity	S-THB-M002 (Onset Computer Corporation, USA)	±0.2 ℃, ±2.5% (10-90%RH)
Wind speed and direction	S-WSET-B (Onset Computer Corporation, USA)	±0.5 m/s, ±5°
Global horizontal solar radiation	S-LIB-M003 (Onset Computer Corporation, USA)	±10 W/m^2 or ±5%
Rainfall	S-RGB-M002 (Onset Computer Corporation, USA)	±1% (<20 mm/h)
Barometric pressure	S-BPB-CM50 (Onset Computer Corporation, USA)	±3.0 mbar
Data logger	HOBO RX300 (Onset Computer Corporation, USA)	

relative humidity were validated in advance of the experiment by comparing with an Assman psychrometer.

4.3. Results

4.3.1. Outdoor weather condition and indoor air temperature.

The recent weather observation data (2005–2019) at the nearest official station (Tangerang) have shown weather conditions similar to those of other coastal cities of Java Island, with with monthly diurnal and nocturnal averages of 28.5–30.7 °C and 25.5–26.4 °C, respectively [4.12]. Although there are two seasons in Indonesia, i.e., rainy season and dry season, the seasonal temperature variation is relatively small. Fig. 4.3 shows the outdoor weather conditions with the corresponding indoor air temperature measured at the center of Rooms A and B (FL+1.1 m, C2) during the field experiment. The outdoor temperature range was 24.0–35.3 °C with diurnal (7:00~18:0) and nocturnal (18:00~7:00) averages of 28.1–31.9 °C and 24.8–27.3 °C, respectively. The data were averaged every single day and night. Although the daytime temperatures on April 20 and May 1 with diurnal averages of 28.9 °C and 28.1 °C, respectively, were slightly lower than the other cases, there was no precipitation, and the maximum temperatures exceeded 32 °C. The wind conditions were similar among Cases 3–5, which were conducted under full-day ventilation conditions. The prevailing wind direction was north in the afternoon due to the sea breeze, whereas it was south at night. The average outdoor wind speeds measured at the weather station were 1.4–1.9 m/s and 0.3–0.5 m/s during the daytime and the nighttime, respectively, in Cases 3–5.

For indoor temperature (Fig. 4.3), when the PCMs in the underfloor space of Room A were cooled by the natural ventilation (Cases 1 and 3), the cooling effect of the proposed system cannot be seen at the center of the rooms (FL+1.1 m, C2). The average diurnal temperatures at the center of Rooms A and B were measured at 29.0–30.5 °C and 28.8–30.4 °C, respectively, during the daytime. In contrast, when the PCMs were cooled by the forced ventilation (Cases 2, 4 and 5), a temperature reduction was observed for most of the period.

Table 4.3. Room air temperature in Rooms A and B.

Case	Daytime			Nighttime		
	Room A	Room B	Reduction	Room A	Room B	Reduction
Case 1	29.0–30.4 °C	28.8–30.4 °C	(-0.2)–0.0 °C	28.6–28.8 °C	28.6–29.1 °C	(-0.1)–0.3 °C
Case 2	28.1–29.9 °C	28.5–30.5 °C	0.4–0.6 °C	27.3–28.7 °C	27.9–29.5 °C	0.6–0.8 °C
Case 3	30.4–30.5 °C	30.3–30.4 °C	(-0.1)–0.0 °C	28.5–29.0 °C	28.5–29.1 °C	0.0–0.1 °C
Case 4	29.1–30.0 °C	29.4–30.3 °C	0.3 °C	27.1–27.6 °C	28.1–28.3 °C	0.5–1.0 °C
Case 5	29.9–30.7 °C	30.2–31.2 °C	0.4–0.5 °C	27.4–27.9 °C	28.4–29.1 °C	0.1–1.2 °C

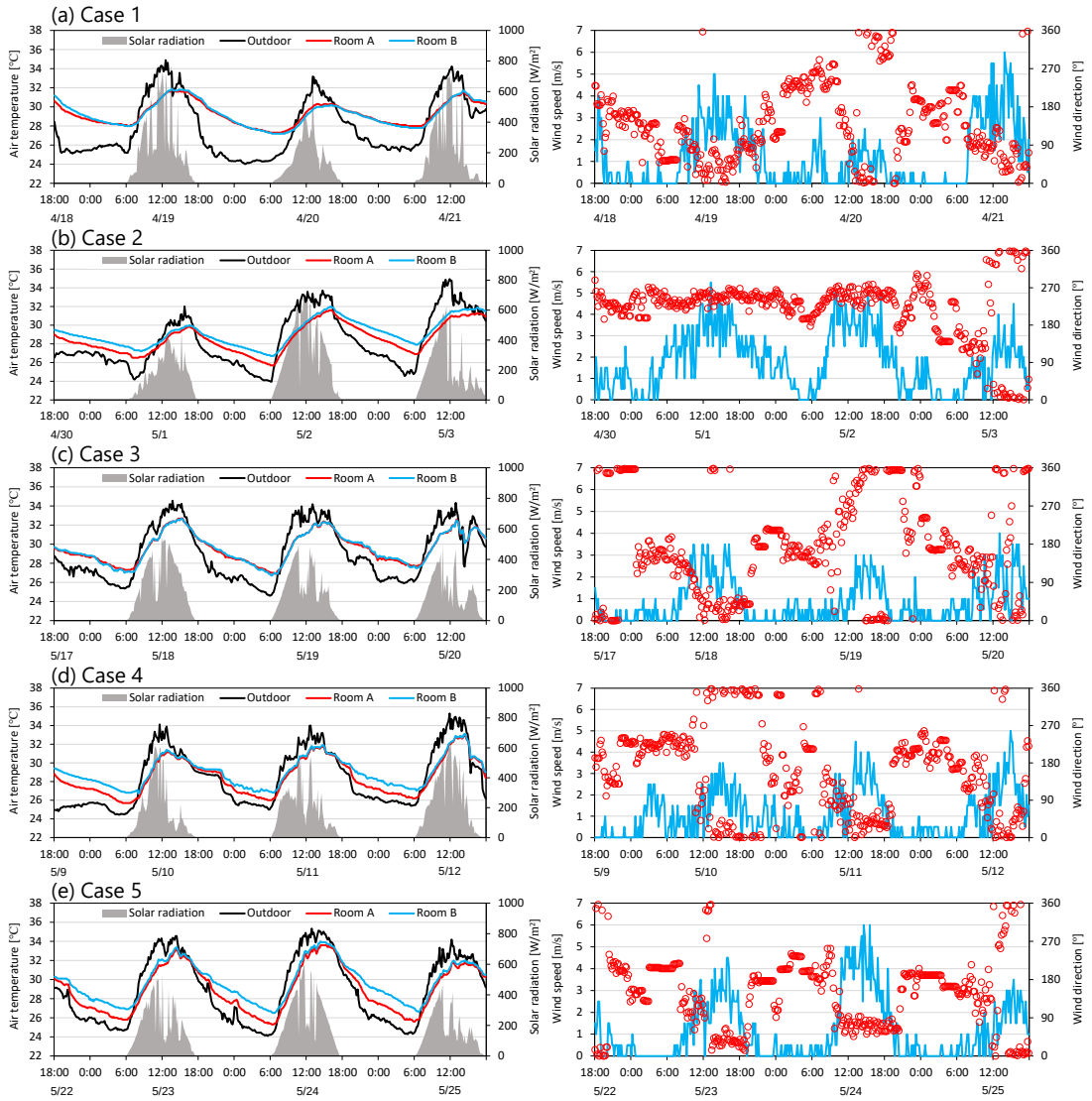

Fig. 4.3. Temporal variations of outdoor weather conditions and corresponding air temperature in the experimental building in (a) Case 1, (b) Case 2, (c) Case 3, (d) Case 4, and (e) Case 5.

The nighttime air temperature in Room A was 0.5–1.2 °C lower than that in Room B. This is primary because, in Room A, the floor temperatures were reduced further by the cooled underfloor space with the assistance of forced ventilation, in addition to the thermal storage effect.

In Case 2, the average diurnal temperature at FL+1.1 m in Room A was lower than Room B, primarily due to the latent heat thermal storage of the PCMs. Similarly, in Cases 4 and 5, although the room windows were opened, the corresponding temperature difference

was 0.2–0.5 ℃ during the daytime. This implies that if an appropriate amount of PCMs is installed in the proposed floor cooling system and sufficient thermal storage during nighttime, air temperature reduction is possible during daytime, even under the window-opening conditions.

4.3.2. Vertical temperature distribution and heat flux

Figs. 4.4 and 4.5 show the vertical distribution of temperatures, including air, floor, and PCM, and the heat flux on the floor surface at the center of Room A (C2) during the nighttime and daytime with the corresponding temperatures of Room B and the outdoor temperatures (T_{out_time}) on a representative day for each case. The representative day was chosen because the average nocturnal temperatures were almost identical to the recent weather data at the nearest official weather station, which was 25.7–26.9 ℃ among all cases. Meanwhile, the diurnal outdoor temperature during the measurement period was 31.0–31.6 ℃, which was slightly higher than that measured at the nearest official station.

In the most nighttime of Cases 1 and 3 (natural ventilation for the underfloor space), the air temperature difference between Rooms A and B was less than 0.2 ℃ at the most measurement points (FL+0.1–2.9m). Although Room A was equipped with the floor cooling system, the heat flux on the top of the floor surface (Fs) was 4.0–11.3 and 2.4–8.9 W/m^2 in Rooms A and B, respectively. In case of the natural ventilation for the underfloor space, the influence of the proposed system on the indoor temperature field was small. In Case 3, the heat flux on the floor surface in Room A was 1.3 times as large as that in Case 1, when the room window was opened (Case 3), because the cool nocturnal air entered the lower part of the room (Fig. 4.4c). Lee et al. [4.13] reported that the thermal storage changed about 1.5 times depending on the temperature condition near the PCMs. Although the room temperature contributed to increasing heat flux in this study, the heat dissipation was insufficient to cause the phase change, and thus the cooling effect of the proposed system could not be observed during the daytime (Fig. 4.5c). Because the PCMs of the proposed system is attached to the backside of the floor panel, the heat flux on the floor surface may not strongly affect the thermal storage of the PCMs. Meanwhile, the air temperature in the underfloor space remained 2.5–3.9 ℃ higher than the outdoor temperature due to the small ventilation rate, and the average air temperature was only 0.1–0.6 ℃ lower than the average surface temperature of the backside of the floor panel, i.e., PCM surface temperature in Cases 1 and 3. As a result of that, the heat flux on the backside was 3.7–7.1 W/m^2 and smaller than that on the floor surface. The heat flux on the backside of the floor panel was also so deficient that the phase change of the PCM occur.

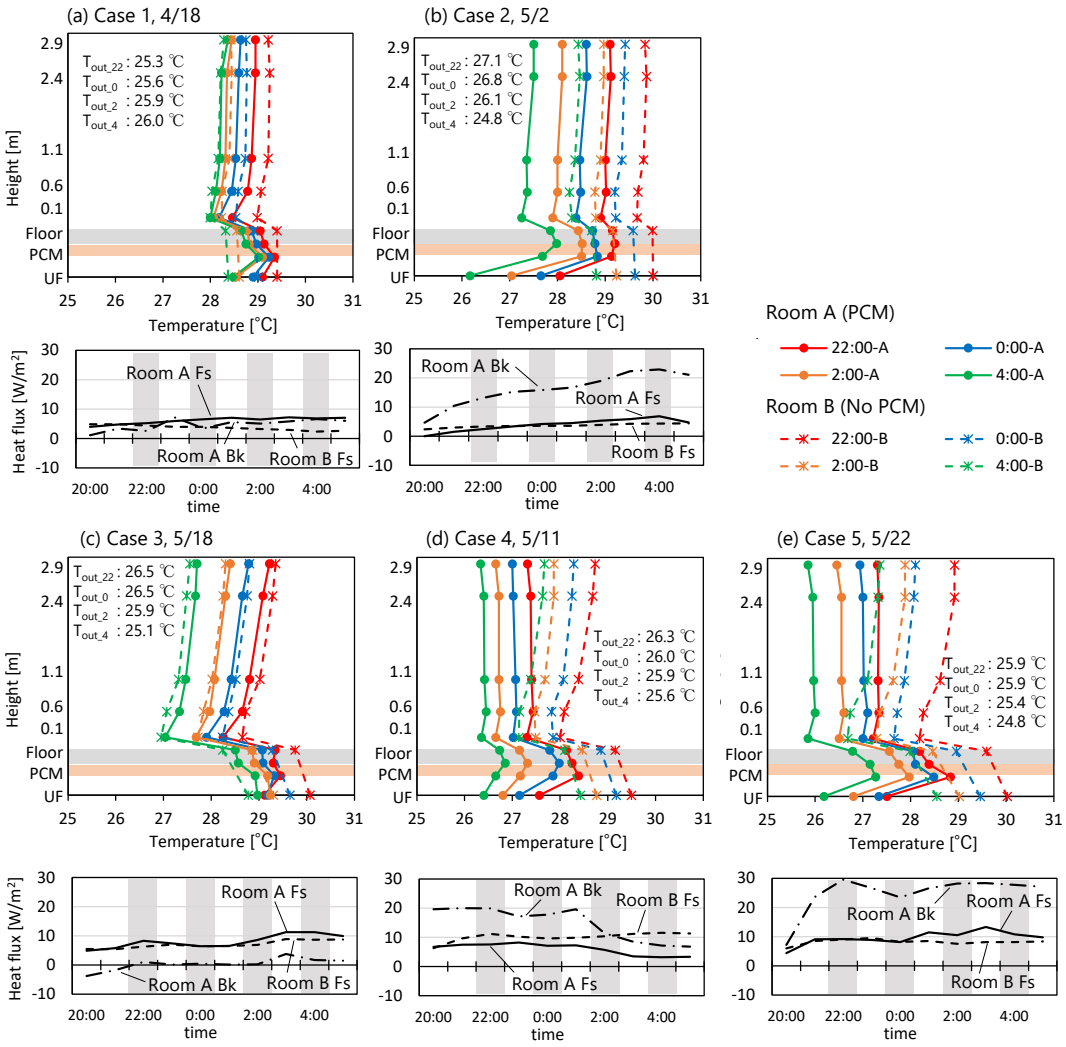

Fig. 4.4. Vertical temperature distribution and heat flux on the floor surface in Rooms A and B during nighttime; (a) Case 1, Apr. 18; (b) Case 2, May 2; (c) Case 3, May 18; (d) Case 4, May 11; (e) Case 5, May 22.

Unlike Cases 1 and 3, the increase in the heat flux on the backside of the floor panel was observed in Cases 2, 4 and 5 due to the forced ventilation by the exhaust fans. In Case 2, the heat flux on the floor surface was 0–6.8 W/m^2 and 2.4–4.4 W/m^2 in Rooms A and B, respectively. The heat flux on the floor surface in Case 2 was similar to that in Cases 1 and 3. As the floor surface temperature in Room A decreased, the room temperature became lower. Therefore, the heat flux on the floor did not increase. In contrast, the heat flux on the backside of the floor panel was 4.6–22.9 W/m^2 in Room A. Owing to the continuous ventilation for the underfloor space during the nighttime, the cool nocturnal air entered the underfloor space and

the temperature difference between the air and PCM surface was 0.5–1.5 ℃. Moreover, the air velocity at the C2 was 1.0–1.3 m/s during the nighttime. The increased temperature difference and air velocity near the PCM surface strongly contributed to the increase in the heat flux on the backside of the floor panel.

The heat flux in Cases 4 and 5 showed similar tendency. The heat flux on the floor surface in Cases 4 and 5 was 1.6–2.5 times as large as that in Case 2, nevertheless the heat flux on the floor surface was not strongly contributed to the heat dissipation from the floor structure. Meanwhile, because of the exhaust fans, the heat flux on the backside of the floor panel in Cases 4 and 5 was 6.8–20.0 W/m^2 and 7.2–29.6 W/m^2, respectively. For the vertical temperature distribution in Cases 2, 4 and 5, the temperature reduction was observed at all measurement, nevertheless the shape of the vertical temperature distribution was different. In Case 2 (closing room windows), the indoor temperature tended to be uniform. The air temperature was 27.3–28.9 ℃ (FL+0.1 m) and 27.5–29.1 ℃ (FL+2.9 m). Kobayashi [4.14] indicated that the temperature gradient was small when the circulating airflow was weak and the direction of heat flux on the floor was upward. In this study, closing window and higher floor surface temperature might influence the shape of the vertical temperature distribution in Case 2. When the room windows were opened, the temperature reduction became larger compared to Case 2. In Case 2, the temperature reduction was 0.7 (FL+2.9 m) –1.1 ℃ (FL+0.1 m), meanwhile that was 0.7 (FL+0.1 m) –1.6 ℃ (FL+2.9 m) in Cases 4 and 5. The larger temperature reduction was observed at the upper part of the room because of the difference of shape of the vertical temperature distribution. Although the air temperature in Room B increased as the increase in the floor level, the air temperature in Room A (Cases 4 and 5) was almost the same regardless of the floor level. In Room B, the cool outdoor air entered the room and accumulated at the lower part of the room. Meanwhile, the outdoor air may not accumulate at the lower part of Room A because the air which was cooled by the proposed floor cooling system had already accumulated at the lower part of the room.

The heat dissipation during the nighttime strongly affected the cooling effect during the daytime. When the underfloor space was naturally ventilated at night (Cases 1 and 3), as the outdoor temperature increased, temperature reductions compared with Room B were observed near the floor in Room A (Fig. 4.5 a,c). In Case 1, the temperatures in Room A were almost identical to those in Room B at all measurement points in the morning (10:00). Meanwhile, in the afternoon (14:00 and 16:00), the temperatures at FL+0.1 m and floor surface temperature (FL+0 m) in Room A were 0.4 °C and 0.5 °C lower than Room B because the proposed system (Room A) absorbed the heat by 1.6–2.0 times that of the concrete floor panel alone (Room B). When the PCMs in the underfloor space was cooled by the natural ventilation, the temperature reduction was observed only at the lower part of the room (Room A) because of the small heat absorption of 4.1–7.2 W/m^2. The small heat absorption of the proposed system did not affect the temperature reduction in the upper parts of the room, especially when the room windows were opened in Case (Fig. 4.5c). Although the heat absorptions in Room A

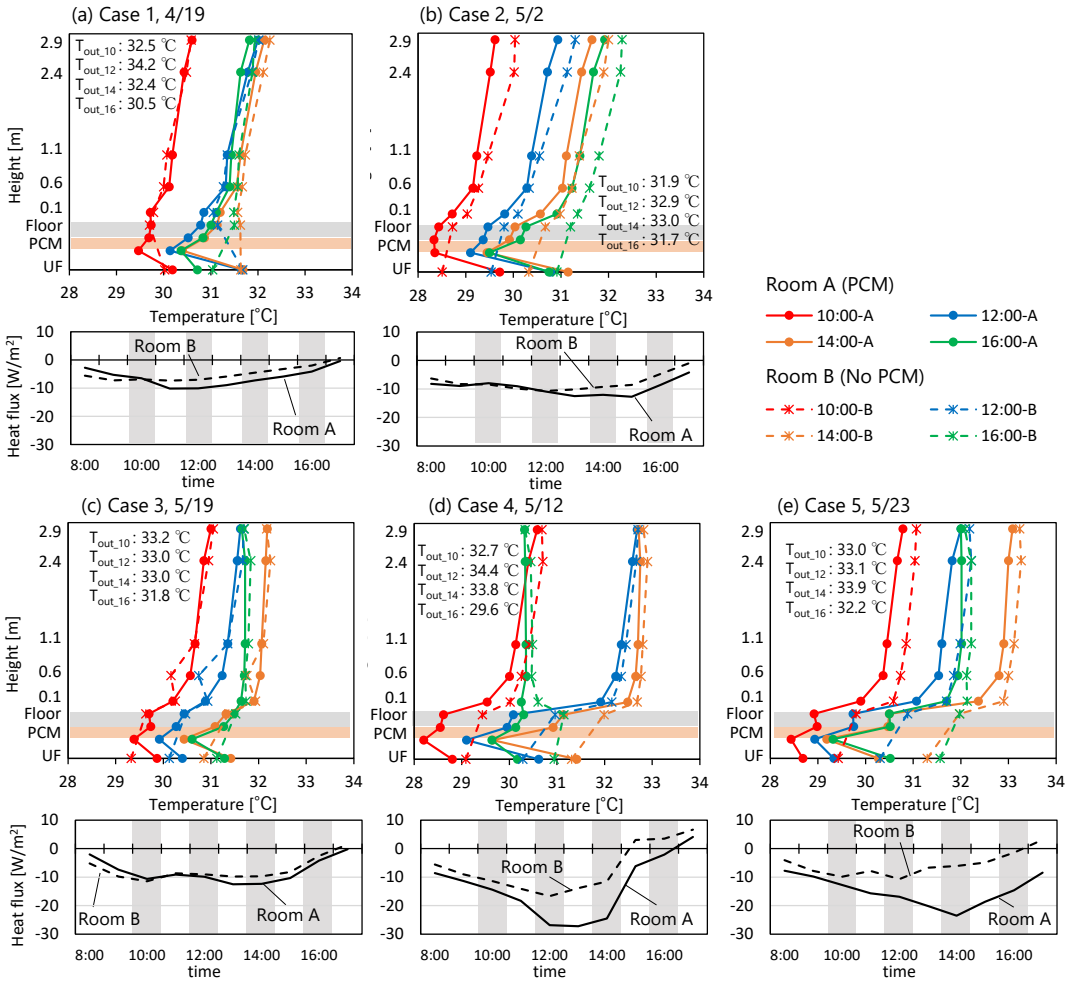

Fig. 4.5. Vertical temperature distribution and heat flux on the floor surface in Rooms A and B during daytime; (a) Case 1, Apr. 19; (b) Case 2, May 2; (c) Case 3, May 19; (d) Case 4, May 12; (e) Case 5, May 24.

were 1.7 W/m^2 and 2.6 W/m^2 higher than those in Room B at 14:00 and 16:00 in Case 3, a clear temperature reduction was not seen in Room A even near the floor surface. The corresponding air velocities at FL+0.1 m ($V_{0.1}$) in Room A were 0.24 m/s (14:00) and 0.34 m/s (16:00), respectively. It is presumed that the air flow dissipated the temperature reduction near the floor surface.

When the forced ventilation was applied to the underfloor space at night, and the room windows were closed throughout the day (Case 2), an apparent temperature reduction was observed at all measurement points for an entire day (Fig. 4.5b). At 10:00, the temperature reduction were 0.1 °C (FL+2.9 m) –0.5 °C (FL+0 m). Owing to the closed window condition,

a considerable temperature reduction during the nighttime was maintained in the morning. Meanwhile, in Case 2, the thermal storage of the PCMs contributed to the temperature reduction in the afternoon. The temperature reductions were 0.4 °C (FL+2.9 m) –0.9 °C (FL+0 m) at 16:00. The heat absorption in Room A was 3.8 W/m^2 higher than that in Room B at 16:00 in Case 2. This indicates that under the no ventilation condition, that is, Case 2, when the PCMs sufficiently dissipated the heat with the assistance of the forced ventilation during the nighttime, the thermal storage effect reached the upper part of the room.

The room windows were fully opened in Case 4. Although the heat absorption of the proposed system was up to 27.2 W/m^2 in Case 4, the air temperature in Rooms A and B was almost constant above FL+0.1 m in the afternoon, with the temperature differences between FL+0.1 m and FL+2.9 m Room A at 0.1–0.2 °C (Fig. 4.5d). In Room A, the $V_{0.1}$ at 14:00 was relatively high (0.48 m/s); thus, the air near the floor surface mixed well with that of the upper parts. Meanwhile, in Case 5, the $V_{0.1}$ in Room A was less than 0.2 m/s for a whole day despite the same full-day ventilation condition, and thus the temperature difference between FL+0.1 m and FL+2.9 m increased to 0.7 °C at 14:00 when the extensive heat absorption was observed (23.5 W/m^2) (Fig. 4.5e). In particular, the temperature gradient from FL+0.1–0.6 m was 0.9 °C/m even under the full-day ventilation condition. Nevertheless, the air temperature in Room A at all measurement points at 14:00 were still 0.2 °C (FL+2.9 m)–1.5 °C (FL+0 m) lower than those in Room B.

As shown in Fig. 4.5, overall, the temperature ranges of the PCMs in the afternoon are generally much narrower than those of the corresponding ambient air temperatures. In particular, in Cases 2, 4 and 5, the PCM temperatures maintained relatively low values (less than 30 °C), primarily because of the assistance of the forced ventilation. For example, in Case 3, the difference in heat absorption between Rooms A and B was only 0.5–2.8 W/m^2 because the PCMs did not solidify the previous night. On the other hand, in Cases 4 and 5, the PCMs reached the melting temperature range between 12:00 and 16:00, and thus the heat absorption in Room A became 5.6–17.5 W/m^2 higher than that in Room B. As a result, the floor surface temperature in Room A was reduced by 0.7–1.6 °C, compared with Room B. Particularly in Cases 4 and 5, the proposed system increased the heat absorption in the afternoon owing to the latent heat thermal storage and contributed to the room air temperature reduction at both the lower and upper parts of the room even when the room windows were opened.

4.3.3. Influential factor of vertical temperature distribution

Based on the results of the vertical temperature distribution, the factors influencing indoor temperature fields during the daytime were investigated. The temperature differences were analyzed in four different layers, i.e., FL+0.1–0.6 m, FL+0.6–1.1 m, FL+1.1–2.4 m, and FL+2.4–2.9 m, respectively. The diurnal hourly averaged data were used in the analysis. In

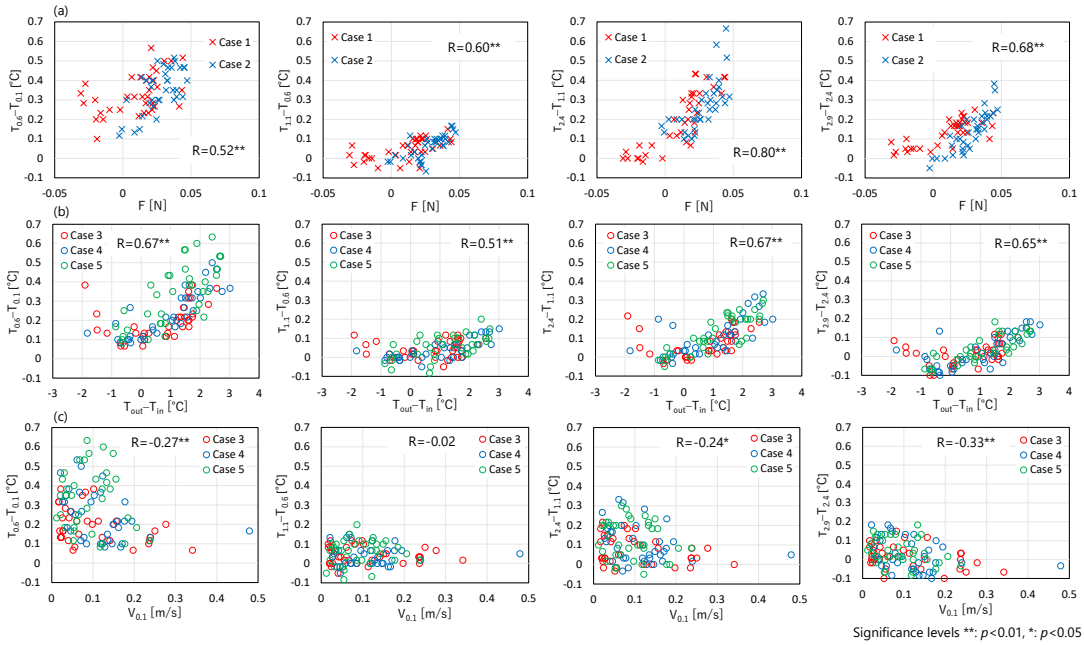

Fig. 4.6. Correlation between air temperature difference of each layer ($T_{higher\ height}$-$T_{lower\ height}$) and (a) buoyancy force (F), (b) outdoor-indoor temperature difference (T_{out}–T_{in}), (c) wind speed at FL+0.1 m ($V_{0.1}$) in Room A during daytime.

Cases 1 and 2, the buoyancy force can be a dominant factor affecting the vertical temperature distribution because the room windows were closed. The buoyancy force (F) in Room A was the calculated using the Boussinesq approximation (Eq. 4.2):

$$F = -\rho_0 g \beta (T_s - T_0) \tag{4.2}$$

where F is the buoyancy force [N], ρ_0 is the density of the reference temperature [kg/m^3], g is the acceleration due to gravity [m/s^2], β is the coefficient of thermal expansion of the fluid [1/K], T_s is the floor surface temperature [K], and T_0 is the reference temperature [K].

Fig. 4.6a shows the correlation between air temperature difference in each layer ($T_{higher\ height}$-$T_{lower\ height}$) and the buoyancy force (F) in Room A during Cases 1 and 2 (no ventilation). The temperature differences show proportional relationships to the buoyancy force at all layers, with a correlation coefficient of 0.52–0.80. A strong relationship (R>0.7) was not obtained for all the cases because the buoyancy force by the walls also influenced the indoor temperature distributions. Under the open-window conditions, such as Cases 3–5, the outdoor condition directly influenced the indoor thermal environment. Fig. 4.6b shows the correlation between the air temperature difference of each layer and the outdoor-indoor temperature difference (T_{out}-T_{in}) in Cases 3–5. T_{out}-T_{in} was proportional to the air temperature differences of each layer, with a moderate correlation of 0.5–0.7. This is primarily because the

smaller ventilation rates, attributed to the relatively lower outdoor wind speeds, prevented indoor air from mixing. Fig. 4.6c presents the correlation between the air temperature difference of each layer and $V_{0.1}$ in Cases 3–5. The correlations with $V_{0.1}$ showed weak or no correlation, less than 0.33, because the indoor flow was turbulent, and one measuring point was difficult to represent in the overall indoor flow patterns. Nevertheless, it should be noted that a large temperature difference was not observed below FL+0.6 m when $V_{0.1}$ was more than 0.2 m/s, as discussed in Section 4.3.2.

4.3.4. Phase state of PCM and floor surface temperature reduction

Fig. 4.7 shows the surface temperatures of the PCMs for each case. Moreover, Fig. 4.8 shows the relation between the heat flux and the surface temperature of the lower side of the PCM. When the underfloor space was naturally ventilated to cool the PCMs (Cases 1 and 3), the surface temperature ranges of the PCMs were 28.1–30.8 ℃ with liner relationships with the heat flux (Fig. 4.8a, c). This result implies that phase change states of the PCMs were regarded as a liquid state in most periods in Cases 1 and 3, and the sensible heat mainly contributed to the heat flux because the above-mentioned PCM temperatures were not necessarily lower than the solidification temperature range of 27–28 °C. Although the outdoor temperature dropped to 24.0–25.9 ℃ in these cases, natural ventilation was insufficient to cool the PCMs because nocturnal outdoor wind speed was very low, i.e., 0.1–0.8 m/s in Case 1 and 0.2–0.3 m/s in Case 3, respectively. The resultant average air velocity in the underfloor space was less than 0.1 m/s at night. Meanwhile, in Cases 2, 4, and 5, the heat flux of the PCM reached the peal levels at the solidification temperature ranges, resulting in non-liner

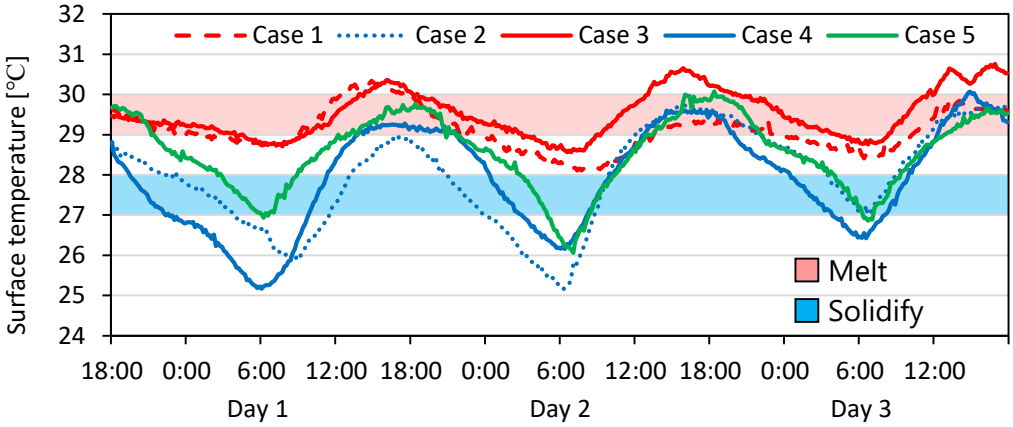

Fig. 4.7. Temporal variation of the surface temperature on the lower side of the PCM pack for each case (Cases 1-5).

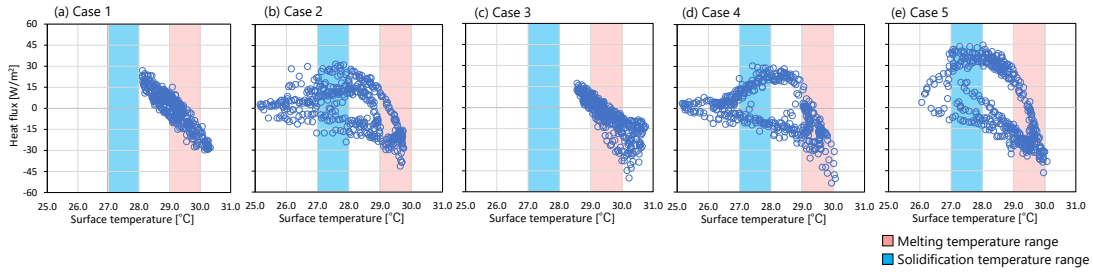

Fig. 4.8. Relationship between the heat flux and the surface temperature on the lower side of the PCM pack in (a) Case 1, (b) Case 2, (c) Case 3, (d) Case 4 and (e) Case 5.

relationships, i.e., hysteresis, caused by influences of the latent heat (Fig. 4.8b, d, e). In the morning, the surface temperature of the PCM dropped to 25.2–26.9 °C, which was likely to be lower than the solidification temperature range of 27–28 °C. On the other hand, the forced ventilation for the underfloor space was very effective in cooling the PCM with air velocity of 0.91–0.98 m/s, regardless of the calm wind conditions. Thus, the PCMs appeared to be in a solid-state in these cases.

Fig. 4.9 shows the reduction in the floor surface temperature in Room A compared with Room B. The floor surface temperature reduction was averaged for the nine horizontal measurement points. Furthermore, Fig. 4.10 presents the temporal variations of the PCM surface temperature with the corresponding integrated thermal storage of the PCMs. In Cases 1 and 3, the floor surface temperatures in Room A were cooler than those in Room B for barely 58% of the daytime, with a floor surface temperature reduction of 0.1–0.2 °C (Fig. 4.9). The phase state of the PCMs was presumed to be in the liquid state for most of the period. In fact, the diurnal range of the PCM temperature was found to be only 1.3–2.1 °C (see Fig. 4.7). As

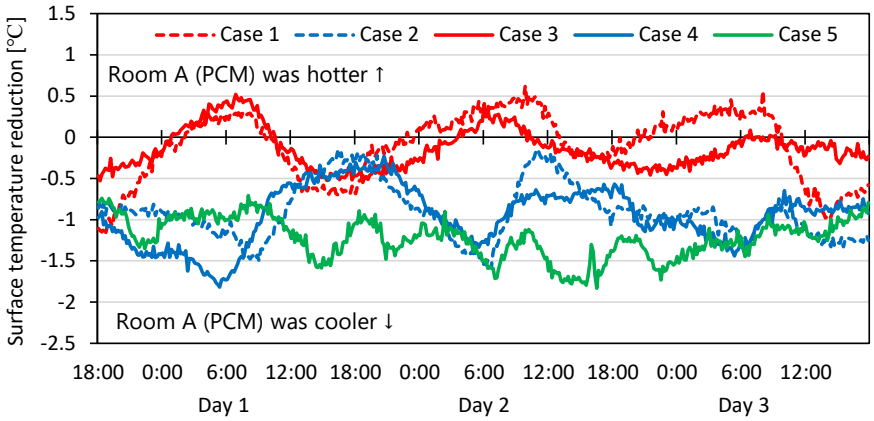

Fig. 4.9. Floor surface temperature reduction in Room A compared with Room B.

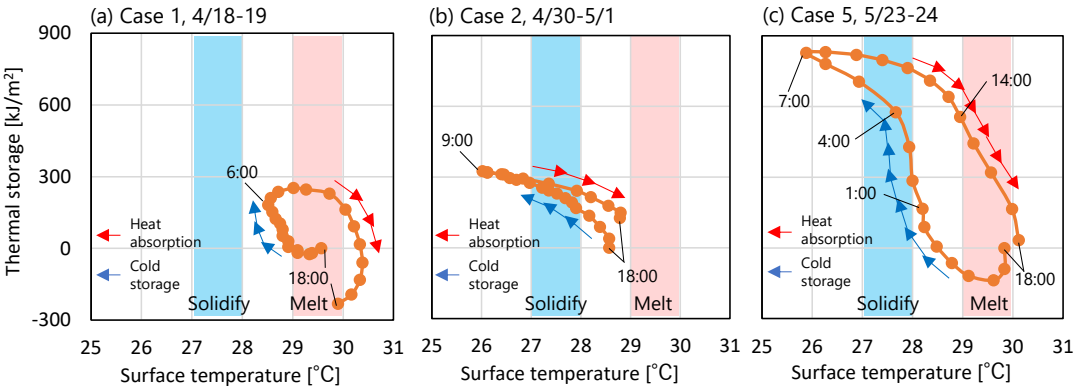

Fig. 4.10. Temporal variation of surface temperature of the lower side of the PCM pack and thermal storage of the PCM (a) Case 1, Apr. 18-19; (b) Case 2, Apr 30-May 1; (c) Case 5, 5/23-24.

shown in Fig. 4.10a, the variation in the thermal storage was small because the phase change of the PCMs did not occur. Therefore, the sensible heat thermal storage with a small temperature fluctuation of the PCMs hardly affected the floor surface temperature reduction.

In Case 2, the PCM solidified on day 1 (April); nevertheless, the PCM did not reach the melting temperature during the daytime on the following day because of the relatively lower outdoor temperature (28.1 °C on diurnal average); thus, the latent heat thermal storage was not sufficient (Fig 4.10b). On day 1 (April 30), the heat dissipation accelerated by the forced ventilation reduced the surface temperature by 1.2 °C in the morning, whereas the floor surface temperature reduction was approximately 0.4 °C in the afternoon. Meanwhile, when the PCMs reached the melting temperature range in the afternoon, the floor surface temperature in Room A was 0.6–1.2 °C than that in Room B, indicating the latent heat thermal storage effect. In Case 4, the average floor surface temperature reduction was 0.8–0.9 °C during the daytime.

In Case 5, the minimum PCM temperature in the morning was higher than that in Cases 2 and 4 (see Fig. 4.7). However, the diurnal mean floor surface temperature reduction in Case 5 was 0.4 °C higher than those in Cases 2 and 4 (Fig. 4.9). This is primarily because more latent heat thermal storage was utilized in Case 5 than in the other cases. On day 2 (May 24), which was the hottest outdoor condition during the entire experimental period (31.9 °C on diurnal average), the floor surface temperature reduction was higher than that on the other days, with an average of 1.5 °C. The maximum PCM temperature reached 30.1 °C (see Fig. 4.7), which was almost the same value as the upper melting temperature range showing that the latent heat thermal storage of the PCMs seemed to be fully utilized. As shown in Fig. 4.10c, the thermal storage decreased sharply between 14:00 and 18:00, whereas the thermal storage increased by 487 kJ/m^2 with a small PCM temperature difference during the solidification period between 1:00 and 4:00. Although the surface temperature of the PCM decreased by

1.1 ℃ between 5:00 and 7:00, the variation in the thermal storage was small compared with that at the phase change period. Because the influence of latent heat of the PCMs is much larger than that of sensible heat, the minimum PCM temperature in the morning did not strongly influence the floor surface temperature reduction.

Comparing Cases 4 and 5 (opened room windows) with Case 2 (closed room windows), the floor surface temperature was reduced by 0.8–1.5 ℃ (Cases 4 and 5) and 0.7–1.1 ℃ (Case 2) during the daytime on average. This indicates that although the window-opening conditions affected the indoor temperature fields, as discussed above, they might not strongly affect the floor surface temperature reduction. This is primarily because the effect of the thermal storage and heat dissipation from the PCMs during nighttime can be a dominant factor in floor surface temperature reduction during daytime.

4.3.5. Evaluation of thermal storage effect

Fig. 4.11 shows the average thermal storage of the PCMs with the maximum and minimum PCM surface temperatures during the daytime (D) and nighttime (N), respectively. The thermal storage capacity of the PCMs was estimated to be approximately 1,100 kJ/m^2 based on the volume of the aluminum package containing the PCM. However, the measured values sometimes exceeded the estimated value because the thickness of the PCM package became uneven. In Cases 1 and 3, where the underfloor space was naturally ventilated, the PCM surface temperature indicated that its phase state was in the liquid state, and the PCMs did not sufficiently dissipate and absorb the heat. As shown, the thermal storage (positive side) was less than 400 kJ/m^2 in most of the period in Cases 1 and 3, which was only 12–36% of the estimated capacity. In contrast, the thermal storage of the PCMs in Cases 3 and 4 was larger than that in Cases 1 and 3 owing to the forced ventilation in the underfloor space. Consequently,

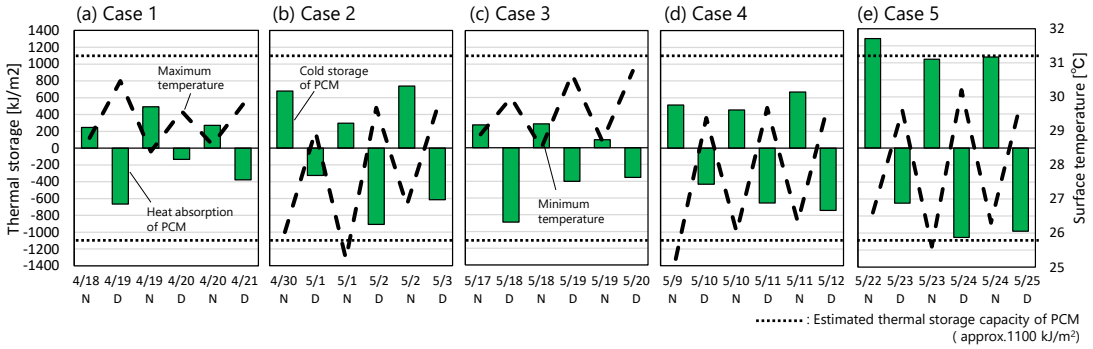

Fig. 4.11. Average thermal storage of PCM with PCM temperature for each case (Cases 1–5), N: nighttime, D: Daytime.

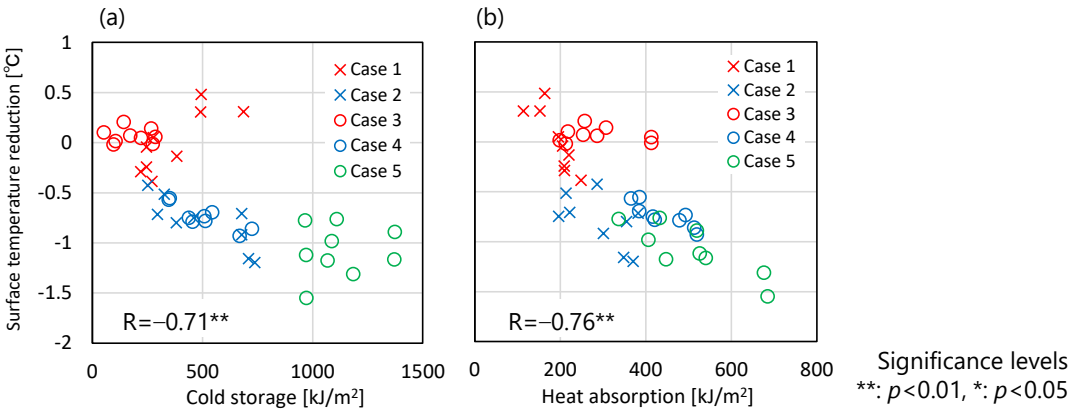

Fig. 4.12. Correlation between the surface temperature reduction measured at C1–3 and (a) thermal storage of the PCM during nighttime and (b) heat absorption on the floor surface during daytime.

the heat absorption ranged from 454–909 kJ/m^2, except on May 1. On May 1 (day 1 of Case 2), the PCM surface temperature did not reach the melting temperature range, therefore, the heat absorption was 326 kJ/m^2, and the PCMs did not dissipate the heat in the following night. In Case 5, the largest thermal storage among the five cases resulted in the largest heat absorption. The thermal storage ranged from 1,042–1,284 kJ/m^2 (95–117% of the estimated capacity) at night. During the daytime, the heat absorption of the PCMs was 649–1,050 kJ/m^2. Therefore, approximately 59–95% of the thermal storage may be employed for the heat absorption during the daytime in Case 5. Overall, the larger thermal storage contributed to increasing the heat absorption on the following day.

Fig. 4.12a presents the correlation between the diurnal floor surface temperature reduction in Room A compared with Room B and the thermal storage of the PCMs in the previous nights. As expected, as the PCMs dissipated more heat, the floor surface temperature reduction increased in the following day. In Cases 1 and 3, the thermal storage was less than 400 kJ/m^2 during most of the period. On the other hand, in Case 5, the floor surface temperature reduction was larger than in Cases 2 and 4 because the PCMs dissipated more heat than the other cases with the thermal storage of 966–1,373 kJ/m^2. Although the thermal storage was influenced by the weather conditions and phase state of the PCMs, there was the strong proportionate correlation (R=-0.71) with the floor surface temperature reduction.

Fig. 4.12b shows the correlation between the diurnal floor surface temperature reduction and the heat absorption on the floor surface in Room A. As the heat absorption on the floor surface increased, the diurnal floor surface temperature reduction increased, with a correlation coefficient (R) of -0.76. In Cases 1 and 3, the heat absorption on the floor was less than 300 kJ/m^2 during most of the period. Meanwhile in Cases 4 and 5, the heat absorption on the floor increased to 337–685 kJ/m^2 because the PCMs sufficiently dissipate the heat with the

assistance of the forced ventilation. Therefore, the floor surface temperature reduction in Cases 4 and 5 was higher than in Cases 1 and 3. Approximately 49–73% of the thermal storage in the PCM was transferred to the floor structure. The rest is considered to transfer to the underfloor space. The ratio of the heat absorbed from the underfloor space in Case 5 was 5–15% lower than that in Cases 2 and 4 because closing louvers and turning of the fans suppressed the increase in the air temperature in the underfloor space. In summary, forced ventilation for the underfloor space increased the thermal storage of the PCMs at night. During the daytime, closing the louver and turning off the fans can be effective to increase the heat absorption of the floor.

4.4. Discussion

4.4.1. Influence of temperature and air velocity on thermal storage effect

As analyzed above, the heat absorption on the floor affected the temperature reduction. To improve the thermal storage effect, the influential factors of the heat absorption are discussed. Fig. 4.13a shows the influence of the temperature difference between FL+0.1 m and the floor surface ($T_{0.1}$–T_{floor}), $V_{0.1}$, and indoor air temperature (T_{in}) on the heat absorption during daytime in Room A. Fig. 4.13b shows the influence of $V_{0.1}$, T_{out}–T_{in} and buoyancy force (F) on $T_{0.1}$–T_{floor}. $T_{0.1}$–T_{floor} was found to have a strong correlation (R=0.93) with heat absorption. In the tropics, the diurnal outdoor temperature usually exceeds 30 °C. Therefore, minimizing ventilation with hot outdoor air can reduce the indoor air temperature during the daytime [4.15]. As shown in Fig. 4.3, the maximum T_{in} in Case 2 (no ventilation) was 1.2–2.0 °C lower than in Cases 4 and 5 (full-day ventilation). Although the increase in $T_{0.1}$–T_{floor} increased F, the cooler T_{in} in Case 3 contributed to maintaining $T_{0.1}$–T_{floor} to be less than 1 °C throughout the measurement period (Fig. 4.13b). Consequently, the hourly heat absorption on the floor was less than 15 kJ/m^2 in Case 2 (Fig. 4.13a).

Even under the full-day ventilation condition (Case 5), when $V_{0.1}$ was less than 0.2 m/s, the temperature gradient of 0.9 °C/m was observed at the lower part of Room A (Fig. 4.5e). The previous study on indoor thermal conditions of the courtyard houses with a high thermal mass in the hot-humid climate of Malaysia showed that the air temperature in the courtyard and the adjacent living hall maintained relatively low values when the indoor air flow was less than 0.2 m/s [4.16]. If the PCMs sufficiently dissipate the heat during nighttime and air velocity bear the floor surface is low (i.e., less than 0.2 m/s), the cool air will accumulate at the lower part of the room. However, $V_{0.1}$ influenced the floor surface

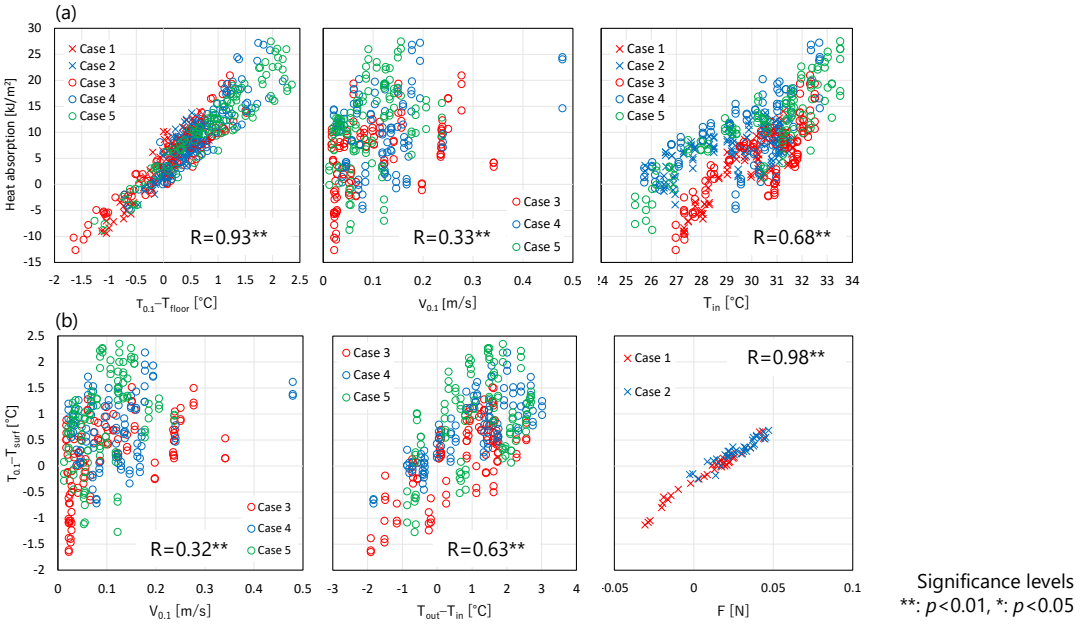

Fig. 4.13. Correlation between (a) hourly heat absorption and $T_{0.1}$–T_{floor}, $V_{0.1}$, T_{in}, (b) $T_{0.1}$–T_{floor} and $V_{0.1}$, T_{out}–T_{in}, F during daytime in Room A

temperature (T_{floor}) less because the PCM maintained a relatively constant temperature through melting (Fig. 4.13b).

Iten et al [4.10] reported that the cooling effect diminished dramatically after the phase change process. This implies that the thermal storage effect of the floor was influenced more by the phase change of the PCMs than by convective heat transfer unless the PCMs melted completely. This result was consistent with that of Chapter 3 obtained through the different analysis. When T_{out}–T_{in} was large, $T_{0.1}$–T_{floor} became larger, and thus the proposed system absorbed more heat. T_{out}–T_{in} tended to be larger in a building with a high thermal mass during the peak temperature period [4.15]. Lee et al [4.13] reported that the thermal storage tended to change approximately 1.5 times depending on outdoor air temperature in the case of natural ventilation. Similarly, in this study, the influence of the outdoor temperature on heat absorption might be large.

As shown in Fig. 4.4, the heat flux on the lower side of the PCM pack was much larger than the floor surface. The outdoor temperature during the nighttime and air velocity in the underfloor space may influence the thermal storage of the PCMs during the nighttime. Fig. 4.14a shows the correlation between the thermal storage of the PCMs during the nighttime and air velocity bear the PCMs (left) and mean nocturnal outdoor temperature (right) in case of the natural ventilation (Cases 1 and 3). Although the air velocity near the PCM when the exhaust fans were off was very weak, that is less than 0.1 m/s, the PCMs dissipated more heat as the

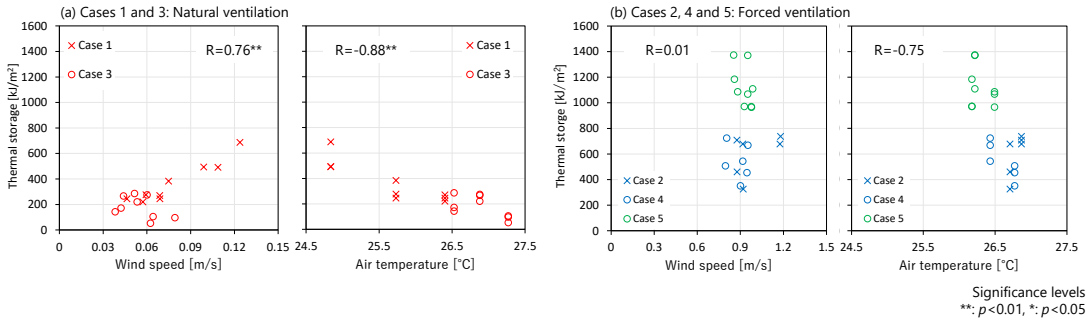

Fig. 4.14. Correlation between the thermal storage of PCM and wind speed/ mean outdoor temperature during the nighttime in case of (a) natural ventilation and (b) forced ventilation

air velocity hear the CPMs increased because the increase in the air velocity affected the convective heat transfer. The outdoor temperature influenced the thermal storage with a strong correlation (R=-0.88). This result consistent with the previous study of the PCM in naturally ventilated house. Fig. 4.14b shows the correlation in case of the forced ventilation (Cases 2, 4 and 5). When the underfloor space was ventilated using the exhaust fans, the air velocity near the PCMs did not show the relationship with the thermal storage during the nighttime. Meanwhile, the outdoor temperature shows a clear relation with the thermal storage of the PCM. As the outdoor temperature decreased, the amount of the thermal storage of the PCM rose. These imply that if air velocity near the PCMs reaches a certain level, the air velocity may not strongly contribute to the increase in thermal storage during nighttime, and ventilation rates to introduce the cool outdoor air to the underfloor space may be more important to increase the thermal storage of the PCM.

4.4.2. Utilization and retention of latent heat thermal storage

In this chapter, when the PCMs were cooled by forced ventilation, the PCMs seemed to solidify completely (Figs. 4.7 and 4.11). Consequently, the thermal storage effect was maintained in the afternoon, even under full-day ventilation conditions. Waqas et al. [4.9] reported that a major proportion of thermal storage (more than 90%) was extracted around melting temperature when the PCM completely solidified. In contrast, if the PCM partially solidified, the extracted thermal storage was reduced to less than 75% at the melting temperature [4.9]. Therefore, ensuring a complete solidification is important for using the thermal storage effect at a specific temperature, that is the melting temperature. This implies that selecting an appropriate phase change temperature influences the retention of the thermal storage effect more than the window-opening condition.

Lizana et al. [4.18] carried out a simulation in the hot summer of Spain. They reported that although the minimum daily temperature often dropped to less than 20 °C, the stored heat of PCM (phase change temperature at 28 °C) cannot be released at night under natural ventilations with a window size of 2 m^2 and air change rates ranging from 3 to 6.5 h^{-1}. According to the recent weather data in Tangerang [4.12], the daily minimum temperature ranged from 24.5–25.3 °C with calm wind conditions. Therefore, there is little possibility that the PCM solidifies under natural ventilation condition. As proposed, forced ventilation for the underfloor space is probably necessary to ensure the solidification of the PCMs if the set-point solidification temperature is close to the average ambient temperature, which is often the case in hot and humid climates. The recent weather data [4.12] and the weather conditions at the experimental site indicate that the set-point solidification temperature of the PCMs was probably appropriate for the proposed system under these climatic conditions.

When the PCMs reached the melting temperature range, the heat absorption increased because of the latent heat, thus, the surface temperature and air temperature near the surface were reduced. For example, on day 2 of Case 5 (May 24), the mean floor surface temperature reduction was 1.65 °C in the afternoon, which was the largest reduction throughout the measurement period. This was primarily because 95% of thermal storage capacity of the PCM could be solidified (Fig. 4.11). Day 2 of Case 5 (May 24) had the hottest outdoor condition during the entire experimental period, with a diurnal mean temperature of 31.9 °C. This condition resulted in an air temperature increase in the underfloor space to 32.0 °C, which was the highest temperature in the underfloor space during the measurement period. Based on the above results, the ambient temperature of PCMs, which is 2–3 °C higher than the set-point melting temperature (29–30 °C), can be roughly recommended to sufficiently utilize the thermal storage effect during the afternoon. To clarify the detailed relationship between the temperature condition and phase state, a long-term evaluation of the PCMs is necessary because PCM is often influenced by the history.

It can be concluded that the thermal storage effect of the latent heat with an appropriate phase change temperature is particularly influential in lowering the floor surface temperature. Neeper [4.19] conducted a simulation in a cold climate and recommended that a phase change temperature can be determined by an average room temperature. However, the recommendation mentioned above may not be insufficient to utilize the thermal storage effect of PCMs in tropics. The daily average air temperatures in the underfloor space were approximately 29.2 °C (Cases 1 and 3) and 28.3 2 °C (Cases 2,4, and 5), and they correspond to the melting and solidification temperatures of the PCM, respectively. Although the mean ambient temperatures of the PCM in all cases corresponded with the phase change temperature of the PCM, the PCM in Cases 1 and 3 (natural ventilation) did not solidify because of low air velocities near the PCMs at night. In Cases 2, 4, and 5, the forced ventilation allowed the cool nocturnal air to enter the underfloor space; therefore, the average diurnal air temperature ranges in the underfloor space increased to 4.7 °C (Cases 2, 4, and 5), compared with the

corresponding temperature range of 3.5 °C in Cases 1 and 3. The present result suggest that when nocturnal forced ventilation was applied in the underfloor space, at least, the diurnal ambient temperature range of 4.7 °C may be required to employ PCMs for a latent heat thermal storage effect. Even though a latent heat thermal storage can be used in small daily temperature ranges in general [4.2], the required diurnal ambient temperature range is approximately 1.5 °C wider than the phase change temperature range of the PCM. Moreover, it can be said that the set-point solidification temperature should correspond to daily average ambient temperature of PCMs, that is, air temperature in the underfloor space, to ensure solidification even under a warmer night and avoid melting in the early part of the day.

4.4.3. Limitation

In the field measurement with the measurement period of three days for each case, some parameter was set to be a constant value. For instance, the flow volume of the fans was set to constant value, that is 0.95 m^3/s, and the operation schedule of the fans and the ventilation rate for the underfloor space were constant. Therefore, further study is necessary to clarify the influence of the ventilation rate of the fans considering the operational schedule. It would be investigated in Chapter 5. Although this chapter clarified the appropriate set point temperature using the results of short-term evaluation and recent weather data, long-term evaluation may be necessary to determine the best operational condition, such as the relationship between temperature and phase state, and would be conducted in Chapter 6.

4.5. Summary

Another field measurement was carried out to clarify the measures to ensure the thermal storage effect of the proposed floor cooling system during the daytime for a naturally ventilated room within a relatively narrow diurnal temperature range in the hot and humid climate of Indonesia. To evaluate the influence of each parameter on the cooling effect of the proposed system, the operation of room windows, louver windows, and exhaust fans were changed in the analysis. The findings are summarized as follows:

- In the hot and humid climates, warm nocturnal outdoor temperatures with calm wind conditions would prevent PCMs from solidifying. However, even when the nighttime outdoor temperature was 0.7–3.2 °C lower than the set-point solidifying temperature and nocturnal wind speed was low (i.e. 0.1–0.8 m/s), forced ventilation for the space attaching PCMs (i.e., underfloor space) was found to be effective to ensure the sufficient solidification of PCMs.

- The floor surface temperature reduction was approximately 0.7–1.5 °C when forced ventilation was adopted for the underfloor space. Cooled air accumulated below FL+0.6 m in the room when the wind speed near the floor surface was less than 0.2 m/s. Nevertheless, the floor surface temperature reduction was obtained stably regardless of window-opening conditions because the thermal storage effect of the floor was influenced more by phase change of PCMs than by convective heat transfer unless the PCMs melt completely.

- In case that the louver windows were opened, and exhaust fans were turned on only at night, the average diurnal outdoor temperature was the highest during the entire experimental period, i.e., 31.9 °C, and the air temperature in the underfloor space, that is, the ambient temperature of the PCMs, reached up to 32.0 °C. However, the mean floor surface temperature reduction was observed at 1.7 °C in the afternoon because 95% of the thermal storage capacity of the PCMs might be utilized. This result suggests that the ambient temperature of PCMs should be 2–3 °C higher than the set-point melting temperature to sufficiently utilize the thermal storage effect during the afternoon.

- The thermal storage effect of latent heat with an appropriate phase change temperature was found to be particularly influential in lowering the floor surface temperature. The phase change temperature for PCMs can be determined based on the average ambient air temperature. A relatively wide diurnal ambient temperature range, at least 4.7 °C, was found to be required to ensure the latent heat thermal storage caused by the supercooling, although the required diurnal ambient temperature range was smaller than typical diurnal temperature ranges in hot and humid climates, such as 8 °C and 6.3 °C in Jakarta (Indonesia) and Penang (Malaysia), respectively.

Chapter 5
Numerical simulation of thermal storage effect through night ventilation

Abstract

Chapter 5 clarifies the key parameters of the radiant floor cooling system using PCMs which cannot be investigated in Chapter 4 because of the limited time and cost. To conduct a sensitivity analysis, Chapter 5 constructed a coupled simulation model of heat balance analysis and computational fluid dynamics (CFD) for naturally ventilated buildings with installed phase change materials (PCMs), and demonstrate a modeling method for the thermal storage effect of PCM in the simulation. The results were validated with field measurements in Chapter 3. The results showed that the coupled simulation model can evaluate both the temperature and heat balance of PCMs in naturally ventilated buildings, where air temperature and air flow distribution are not uniform, with higher accuracy. The temperature and heat flux on the floor surface showed good correlations between the simulation and measurement, with the root mean square errors of 0.3–0.5 ℃ and 4.0 W/m^2, respectively. In particular, coupling with radiative heat transfer calculation increased the simulation accuracy in terms of floor surface and PCM temperatures by 0.3 ℃ when the surface temperature difference between the floor and the other surfaces, i.e., the wall and ceiling, was considerable owing to the thermal storage effect of the PCMs. The following sensitivity analysis which can calculate convective heat transfers owing to the consideration of spatial air flow distribution showed that the air velocity that ensures the solidification of the PCMs in the underfloor space was found to be a key parameter in the proposed system. In addition, the thermal storage of the proposed system was maximized when the operational schedule of the fans was controlled by the outdoor temperature. A PCM thickness of 6 mm and high ventilation rate in the underfloor space during

nighttime are the optimum settings for the radiant floor cooling system under the given hot and humid conditions.

Key words
Thermal storage effect, Night ventilation, Coupled simulation, CFD simulation, Heat balance simulation.

5.1. Introduction

As shown in Chapter 4, to effectively utilize latent heat thermal storage, phase change is required. Previous studies have investigated the factors affecting the melting and solidification process of PCMs, including inlet air temperatures [5.1–5.3], inlet air flow rates [5.1–5.5], thermal properties of PCMs [5.5], and the shape of PCMs [5.4, 5.6]. However, in most of the previous studies, temperatures of inflow were set at a fixed value, such as 29–40 ℃ and 15–24 ℃ for melting and solidification, respectively [5.1–5.6]. Furthermore, the inflow temperature fluctuation over an entire day was rarely considered [5.7]. Liu et al. [5.5] reported that the melting time of PCMs exposed to a fixed inflow temperature was shorter than that when employing a fluctuating inflow temperature. In the field measurement presented in Chapters 3 and 4, the temperature fluctuation was considered through three days evaluation. Although the thermal storage of the PCMs, i.e., heat balance of the PCMs, was evaluated in Chapter 4, a sensitivity analysis considering the thermal storage of the PCMs was limited. Pandey et al. [5.8] indicated that most studies on the thermal storage effect of PCMs focused on evaluating cooling systems incorporating PCMs, such as hear exchanger alone. Few studies investigated the interaction between the heat balance of PCMs, whose response time is much longer than the adjacent fluid, and indoor air temperature and wind distribution in naturally ventilated rooms, owing to the limitations of the measurement methods. Therefore, a modeling method for simulation-based analysis that calculates the thermal storage of the PCMs and their cooling effect on the indoor thermal environment by considering the heat balance and wind distribution is necessary to compensate for the limitation of the measurement method (Chapters 3 and 4).

The results of Chapter 4 showed that the air temperature near the PCMs influenced the heat absorption of the floor cooling system using PCMs more than the room temperature measured in the center of the rooms. Computational fluid dynamics (CFD) considers the ununiformity of airflow and temperature, and thus CFD simulation can calculate convective heat transfer more accurately than thermal energy simulation (TES) which considered one air node in each zone to represent airflow and temperature [5.9]. Nevertheless, heat balance analysis, which considers the influence of radiation, has rarely been conducted in previous studies on CFD simulation, to avoid excessive calculation load [5.10, 5.111]. Owing to the lack of heat balance analysis, including radiant heat transfer, in previous CFD simulations, the

validation results were evaluated in terms of temperature, and few simulation models in previous CFD simulations could properly evaluate the heat balance in the validation process [5.8, 5.12, 5.13]. To fully utilize the thermal storage of PCMs and determine their optimum settings, it is necessary to evaluate the amount of hat stored and released by PCMs because the floor temperature reduction and thermal storage of the PCMs had a strong correlation (see Chapter 4). A validated coupled simulation model can investigate the influence of multiple parameters with limited time and cost compared to field measurements [5.14].

5.1.1. Objective

Chapter 5 determines key parameters of the radiant floor cooling system using PCMs which cannot be investigated in Chapter 4 due to the limited time and cost in the field measurements. To conduct a sensitivity analysis, Chapter 5 construct a novel coupled simulation model of heat balance analysis and CFD for naturally ventilated buildings with installed PCMs to compensate the limitations of commonly used TES and CFD simulation models and demonstrate a modeling method for the thermal storage effect of PCMs in the simulation model. The simulation was conducted for the target building, which installed the proposed floor cooling system and was used in the field measurement (Chapters 3 and 4). The results were validated by comparison with the field measurements in Chapter 3. Using the validated simulation model, a sensitivity analysis was performed in the following sections.

5.2. Methodology

5.2.1 Coupled simulation

To confirm the validation results and clarify the interaction between PCMs and the indoor thermal environment, it is better to investigate the heat balance in the validation process, as well as the temperature [5.15]. Tong et al. [5.16] recommended calculating indoor and outdoor environments within the same computational domain in naturally ventilated buildings because it can capture the dynamic interaction between the outdoor and indoor environments. Straw et al. [5.17] reported that coupled indoor-outdoor simulations provided more accurate results for naturally ventilated rooms. To capture the dynamic interaction of PCMs-indoor-outdoor environments, indoor and outdoor environments were calculated within the same computational domain, because the outdoor environment strongly affects the indoor thermal environment in naturally ventilated buildings compared to highly insulated airtight houses utilizing AC.

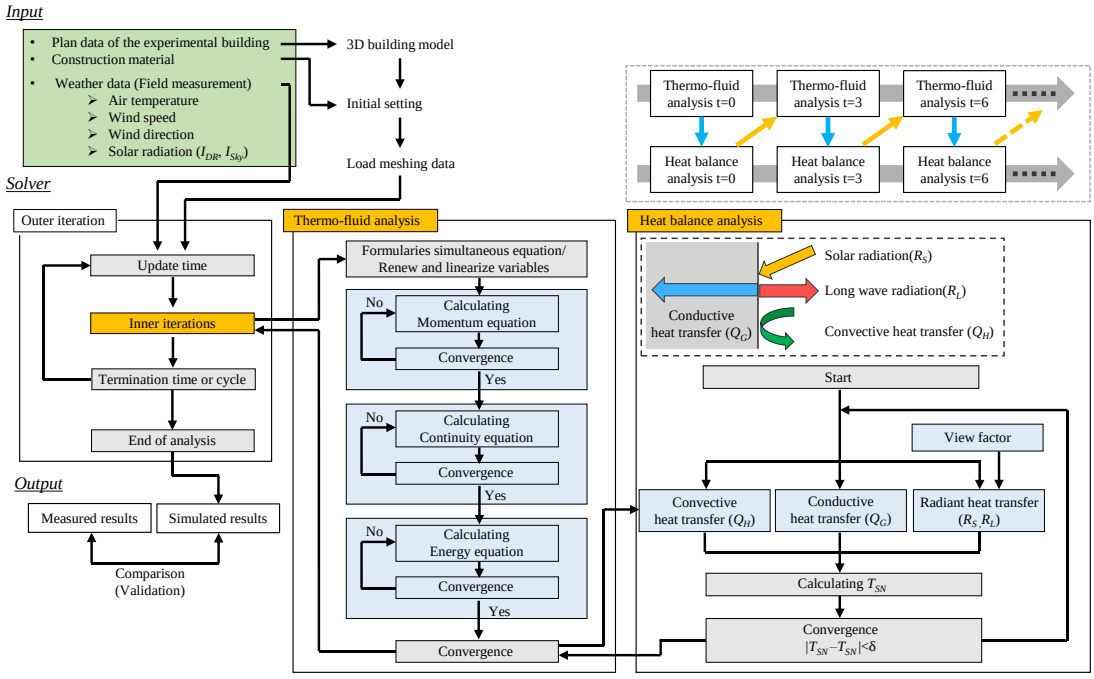

Fig. 5.1. Flow chart of the coupled simulation.

Based on previous simulation models, a CFD simulation coupled with a heat balance analysis was proposed, as mentioned above, to determine the parameters affecting the cooling effect of the radiant floor cooling system using the PCMs. Fig. 5.1 shows the calculation flow for the coupled simulation. Commercial software (scSTREAM v2020, MSC software, Tokyo, Japan) was used to solve the governing equations for momentum, continuity, and energy in the CFD simulation. Intrinsically, variations in outdoor wind speed and direction occur in very short time intervals (tenths of a second to a few seconds), which affects indoor air flow. Regarding transient analysis predicting air flow, large eddy simulation (LES) is regarded as a more accurate method to solve the flow field issue, and has been widely used in recent CFD simulations [5.18]. Nevertheless, it is not always a viable option in research and consultancy, because of its large calculation load [5.19, 5.20]. Therefore, the Reynolds-averaged Navier-Stokes (RANS) approach, in which Reynolds decomposition is used to divide the flow variables into a mean and a fluctuating component, is frequently used [5.21]. In general, the response time of heat transfer at the building surface is much longer than that of the adjacent fluid [5.8]. Pandey et al. [5.8] developed a heat balance simulation coupled with a CFD simulation using the RANS approach, and confirmed its effectiveness in predicting the cooling effect of a PCM-based heat exchanger. Given the calculation load reduction and purpose of this chapter, i.e., evaluation of the thermal storage effect of PCMs, CFD simulation using the

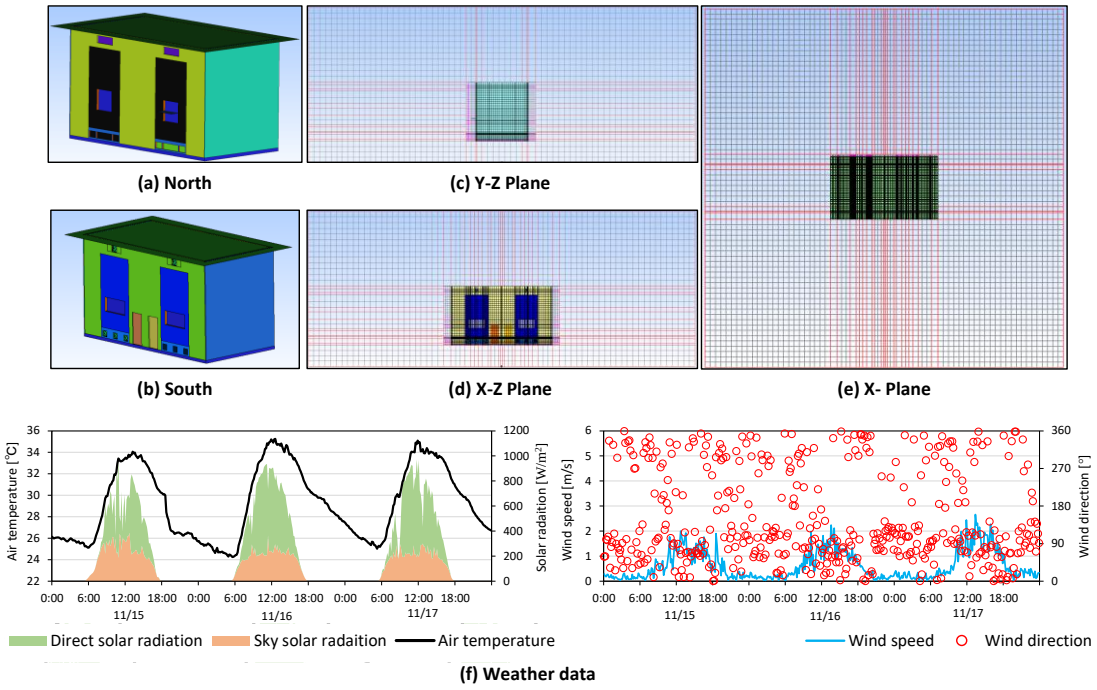

Fig. 5.2. (a, b) Building model, (c–e) Computational domain and fine grid division, and (f) Weather data used for the simulation.

Table 5.1. Thermal properties of materials.

Material	Density [kg/m^3]	Specific heat capacity [J/kg·K]	Latent heat [kJ/kg]	Thermal conductivity [W/m·K]
GRC board	400	1880	-	0.069
Plaster	1560	840	-	0.612
ALC	800	1100	-	0.2
Concrete	2400	900	-	1.637
Glass wool	52	840	-	0.033
Glass	2500	750	-	1.0
Steel deck	7130	400	-	110
Aluminum	2700	880	-	210
Light weight concrete	1600	1100	-	0.53
PCM	800	2000	220	0.2

RANS approach can be a viable option. In this chapter, the CFD simulation used the results of the previous time step as the initial condition of the present time step. For the coupled simulation, the air velocity and air temperature near the solid surface were output from the

Table 5.2. Construction layers of the building envelopes.

Element	Material	Thickness [mm]
Adjacent wall	Glass fiber-reinforced concrete (GRC) board	6
	Plaster	20
	ALC	100
	Plaster	20
	GRC board	6
Ceiling	GRC board	10
Original floor	Ceramic floor	50
	Plaster	25
	Concrete	100
	Metal deck	2
Roof	Glass wool	50
	Metal deck	2
Floor panel	Light weight concrete	25
External wall (North and South)	GRC board	6
	Plaster	20
	ALC	100
	Plaster	20
External wall (East and West)	GRC board	6
	Plaster	20
	ALC	100
	Plaster	20
	Glass wool	50
	Metal deck	2

CFD simulation after the convergence of the CFD, and used as boundary conditions to calculate the radiation, convection, and conduction in the heat balance analysis at the same time step (Fig. 5.1). From the heat balance analysis, the surface temperatures were simulated by transient heat conduction analysis and used as the boundary condition for the next time step of the CFD simulation (Fig. 5.1). The time step for both simulations was three seconds and the number of iterations per time step was 100.

Table 5.3. The mesh size for each domain and the total number of elements.

	Coarse [m]	Medium [m]	Fine [m]
Outer domain	0.6	0.6	0.6
Inner domain	0.4	0.28	0.2
Total elements	273,441	323,829	388,635

5.2.2. Simulation settings

5.2.2.1. Computational geometry, domain, and grid

The target building and system for the coupled simulation were a full-scale experimental building which was used in the previous chapter. The results of the field measurement in Chapter 3 were used for the validation. The geometric model for the experimental building, taking into account the material used to construct it, was developed using a preprocessor (STpre), as shown in Fig. 5.2a, b and Tables 5.1 and 5.2. Based on the literature [5.7, 5.22], this study made the following assumptions to simplify the calculation: (1) the thermal properties of the same material are constant, and (2) all construction materials are homogenous.

Similar to the geometric model, a computational domain was developed based on the experimental field. Since 40 m^2 of the experimental field does not have any obstruction, the computational domain reflects it. Table 5.3 lists the mesh sizes for each domain and the total number of elements. A relationship exists between mesh size and convergence [5.21]. The grid resolutions were increased around the building. The base grid size was 600 mm (outer domain), whereas that around the building was less than 200 mm (inner domain) in the case of a fine mesh, and the inside of the construction material was divided into at least four for the depthwise direction. Three types of mesh divisions were tested to ensure the accuracy of the numerical simulation while minimizing the calculation loads.

5.2.2.2. Boundary conditions for CFD simulation

The flow and wall boundary conditions were set at the interface of the computational domain, i.e., X_{min}, X_{max}, Y_{min}, Y_{max}, Z_{min}, Z_{max}. For the flow boundary, outdoor wind speeds with specified directions and temperatures based on the weather station were set on X_{min} and Y_{min} as inputs, whereas X_{max} and Y_{max} employed a fixed total pressure (i.e., 0 Pa) as the outflow condition. When the wind direction was reversed, the flow boundary settings on X_{min}, Y_{min}, X_{max}

and Y_{max} were opposite to calculate the flow field. Fig. 5.2f shows the weather data for 15–17 November 2020, which were used for validation and subsequent analysis. Although the average diurnal temperature was slightly higher than that at the nearest official weather station, the PCMs were cooled under similar nocturnal temperatures to the mean monthly nocturnal temperature at the nearest official station, with diurnal and nocturnal averages of 31.7 ℃ and 26.6 ℃, respectively. Regarding the wall boundary, the no-slip condition was set to Z_{min} and the building surfaces. Free-slip conditions were employed for the other surfaces in contact with the outside of the computational domain.

5.2.2.3. Heat balance analysis

As discussed above, radiant heat transfer and conductive heat transfer analysis, i.e., heat balance analysis, were conducted for the building surfaces. The following equation shows the fundamental formula of the heat balance analysis for both indoor and outdoor building surfaces:

$$R_s + R_L + Q_G + Q_H = 0 \quad (5.1)$$

where R_S is the net solar radiation [W/m^2], R_L is the net long wave radiation [W/m^2], Q_H is the convective heat transfer [W/m^2], and Q_G is the conductive heat transfer [W/m^2].

The global solar radiation measured in the field experiment was separated into I_{DR} (direct solar radiation) and I_{SR} (sky solar radiation), as shown in Fig. 5.2f. In the hot and humid climate of Indonesia, the quantity of I_{SR} tends to be greater than that in other climatic regions, because of the large cloud cover and humid conditions throughout the year. Huang [5.23] compared 22 solar diffuse fraction models to identify a suitable model for hot and humid conditions in Taiwan, and concluded that the model proposed by Erbs et al. [5.24] performed well in predicting the diffuse fraction. The view factors for radiant heat transfer were calculated using the Monte Carlo ray tracing method (Eqs. 5.2–5.3).

$$R_s = a_{su}(cos\theta \cdot I_{DR} + F_{sky} I_{SR} + I_{RR}) \quad (5.2)$$

$$R_L = \alpha_s \sum_{i=1}^{n} F_i \alpha_{wi} \sigma T_{wi}^4 - F_w \alpha_s \sigma T_s^4 \quad (5.3)$$

where R_S is the net solar radiation [W/m^2], a_{su} is the solar absorptivity [-], θ is the incidence angle of direct solar radiation [rad], I_{DR} is the amount of direct solar radiation [W/m^2], I_{SR} is the amount of sky solar radiation [W/m^2], F is the shape modulus [-], I_{RR} is the amount of reflected solar radiation [W/m^2], R_L is the net long wave radiation [W/m^2], α is the long wave emittance [-], σ is the Stefan Bolzmann constant [W/m^2·K^4], and T is the temperature [K]

Conductive heat transfer based on Fourier's Law was used for the heat balance calculation on the building surface such as walls and ceiling, as follows (Eq. 5.4).

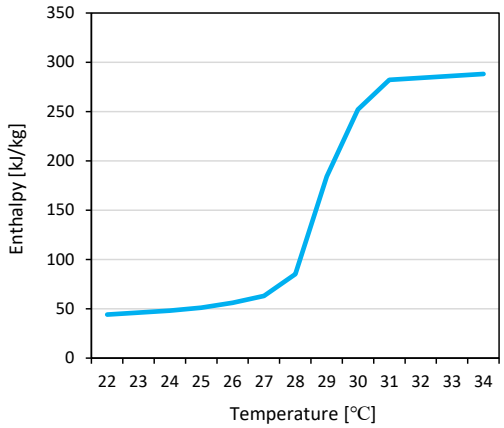

Fig. 5.3. Enthalpy-temperature curve of the PCM.

$$Q_G = -\lambda \frac{\partial T}{\partial x} \tag{5.4}$$

where Q_G is the conductive heat transfer [W/m^2], λ is the heat conductivity [W/m·K], T is the temperature [K], and x is the direction normal to the surfaces [m]. The governing equation of the transient heat conduction for the layer of construction material is as follows (Eq. 5.5).

$$\rho \frac{\partial H}{\partial t} = \frac{\partial}{\partial x_j}\left(\lambda \frac{\partial T}{\partial x_j}\right) \tag{5.5}$$

where ρ is the density [kg/m^3], H is the specific enthalpy [kJ/kg]. λ is the heat conductivity [W/m·K], T is the temperature [K], and x is the direction normal to the surfaces [m].

Fig. 5.3 show the enthalpy-temperature curve of the PCM (paraffin), which freezes with little or no supercooling [5.25]. As with the previous chapter, the phase change temperature of 28–30 °C, with a peak temperature of 29 °C, was selected for this simulation. The latent heat of the PCM, measured by differential scanning calorimetry (DSC) testing with a heating rate of 2 °C/min, was 220 kJ/kg.

In this simulation, the temperature wall function was used to compute the convective heat transfer, instead of low Reynolds number modeling, because it requires an extremely high grid resolution near the surface, and thus significantly increases the calculation load [5.26, 5.27]. Defreye et al. [5.26] verified the effectiveness of the temperature wall function to calculate convective heat transfer practically and accurately by comparing low-Reynolds-number modeling and the temperature wall function. The convective heat transfer of the building surfaces was based on the temperature wall function [5.28], and it was calculated using the following equations (Eqs. 5.6–5.8).

$$Q_H = \frac{\rho c u^*}{T^*}(T - T_s) \tag{5.6}$$

$$T^* = \frac{Pr_t}{K}\ln(Ey^+) + A(Pr, Pr_t) \tag{5.7}$$

$$A(Pr, Pr_t) = 9.24 Pr_t(\frac{Pr}{Pr_t} - 1)(\frac{Pr_t}{Pr})^{0.25} \tag{5.8}$$

where Q_H is the convective heat transfer [W/m^2], ρ is the density [kg/m^3], c is the specific heat capacity [J/kg·K], u* is the friction velocity [m/s], T is the temperature [K], A is the area [m^2], Pr is the Prandtl number [-], Pr_t is the turbulent Prandtl number [-], K is the Karman constant [-], E is the constant in wall function expression [-], and y$^+$ is the distance from the wall n wall normal direction [-]

5.2.2.4. Solver setting

The Reynolds number (*Re*) for indoor space was calculated using Eq. 5.9 based on the air velocity (FL+0.1 m and FL+1.1 m) during the measurement.

$$Re = \frac{\rho u l}{\mu} \tag{5.9}$$

where *Re* is the Reynolds number [-], ρ is the density [kg/m^3], u_i is the velocity [m/s], l is the length [m], and μ is the viscosity coefficient [kg/m·s].

The *Re* ranged from 3476 to 20727, suggesting turbulent flow during most of the measurement period. The finite volume method was used to solve the governing equations for continuity, momentum, energy, turbulent kinetics, and turbulent energy dissipation of three-dimensional incompressible flow and heat (Eqs. 5.10–5.16).

$$\frac{\partial u_i}{\partial x_i} = 0 \tag{5.10}$$

$$\frac{\partial \rho u_i}{\partial t} + \frac{\partial u_j \rho u_i}{\partial x_j} = -\frac{\partial p}{\partial x_i} + \frac{\partial}{\partial x_j}(\mu \frac{\partial u_i}{\partial x_j}) - \rho g_i \beta (T - T_0) \tag{5.11}$$

$$\frac{\partial \rho c T}{\partial t} + \frac{\partial u_j \rho c_p T}{\partial x_j} = \frac{\partial}{\partial x_j}(\lambda \frac{\partial T}{\partial x_j}) + \dot{q} \tag{5.12}$$

$$\frac{\partial \rho k}{\partial t} + \frac{\partial u_i \rho k}{\partial x_i} = \frac{\partial}{\partial x_i}\left(\frac{\mu_t}{\sigma_k}\frac{\partial k}{\partial x_i}\right) + P_k + G_T - \rho\varepsilon \tag{5.13}$$

$$\frac{\partial \rho\varepsilon}{\partial t} + \frac{\partial u_i \rho\varepsilon}{\partial x_i} = \frac{\partial}{\partial x_i}\left(\frac{\mu_t}{\sigma_\varepsilon}\frac{\partial \varepsilon}{\partial x_i}\right) + C_1\frac{\varepsilon}{k}(P_k + G_T)\left(1 + C_3 R_f\right) - C_2\frac{\rho\varepsilon^2}{k} \tag{5.14}$$

$$G_T = g_i \beta \frac{\mu_t}{\sigma_t}\frac{\partial T}{\partial x_i} \tag{5.15}$$

$$R_f = -\frac{G_T}{P_k + G_T} \tag{5.16}$$

where x_i is the coordinate in the object coordinate system [m], u_i is the velocity [m/s], t is the time [s], ρ is the density [kg/m^3], p is the pressure [N/m^2], μ is the viscosity coefficient [kg/m·s], σ_{ij} is the stress tensor [-], g_i is the acceleration [s/m^2], β is the thermal expansion coefficient [1/K], T is the temperature [K], T_0 is the reference temperature [K], c is the specific heat of constant pressure [J/kg·K], λ is the thermal conductivity [W/m·K], $\dot{q}$ is the calorific value [W/m^2], k is the turbulent kinetic energy [m^2/s^2], ε is the turbulent energy dissipation [m^2/s^3], C is the coefficient.

RANS CFD simulation solve the mean flow, whereas the effect of turbulence on the mean flow is modeled using a turbulence model. In this study, modified Launder–Kato (LK) model, which is one of the revised k–ε models, was selected as the turbulence model. Mochida et al. [5.29] pointed out that the standard k–ε model cannot reproduce accurate wind speed near the front corners of a building because the standard k–ε model overestimates production P_k of turbulent kinetic energy k, around the front corners. Therefore, Launder and Kato [5.30] proposed LK model which eliminates the excessive production of k around a stagnation point by modifying the expression for P_k (Eq. 5.17–5.20)

$$P_k = v_t S\Omega \tag{5.17}$$

$$v_t = C_\mu \frac{k^2}{\varepsilon} \tag{5.18}$$

$$S = \sqrt{\frac{1}{2}\left(\frac{\partial u_i}{\partial x_j} + \frac{\partial u_j}{\partial x_i}\right)\left(\frac{\partial u_i}{\partial x_j} + \frac{\partial u_j}{\partial x_i}\right)} \tag{5.19}$$

$$\Omega = \sqrt{\frac{1}{2}\left(\frac{\partial u_i}{\partial x_j} - \frac{\partial u_j}{\partial x_i}\right)\left(\frac{\partial u_i}{\partial x_j} - \frac{\partial u_j}{\partial x_i}\right)} \tag{5.20}$$

The LK model modifies the overestimation of k around the impinging region. However, in the flow field expressed Ω/S , the expression for P_k is inflated compared to that in the standard k-ε model. To avoid this, Tominaga and Mochida [5.31] proposed the modified L-K model which expresses P_k based on Ω/S (Eq. 5.21, 22):

$$P_k = v_t S^2 \qquad (\Omega/S \geq 1) \tag{5.21}$$

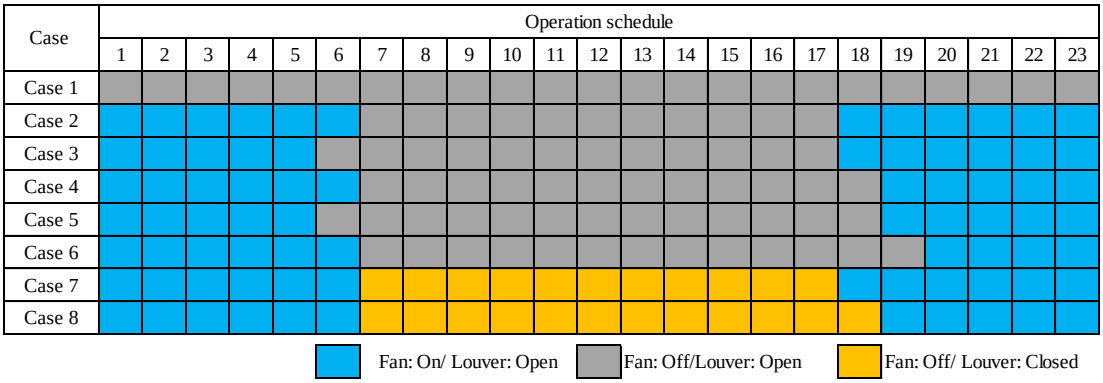

Fig. 5.4. Operation schedule of fan and louver window.

$$P_k = v_t S\Omega \qquad (\Omega/S < 1) \qquad (5.22)$$

Second-order upwind discretization schemes were used for the momentum and turbulence equations. The Quadratic Upstream Interpolation for Convective Kinematics (QUICK) scheme was used for the convection terms. Convergence was assumed to be obtained when the scaled residual leveled off at a minimum of 10^{-6} for momentum and continuity, and 10^{-4} for energy. The first day was set as a spin-up, and the latter two days were used for evaluation.

5.2.3. Criteria for validation

Recent studies have used CFD simulations to model PCM-based systems Growreesunker et al. [5.32] evaluated the effectiveness of PCM clay walls and showed the deviations in air and surface temperatures between the measurement and simulation were 0.7–1.5 ℃ and 0.8–2.0 ℃, respectively. Sun et al. [5.7] investigated the thermal storage effect of a ventilation system containing PCMs using ANSYS FLUENT and demonstrated the influence of the inlet temperature and air flow rate. They confirmed the validity of the simulated air temperature of a PCM air conditioner based on the similarity between the measurement and simulation (R^2>0.92), although the maximum deviation was 2.7 ℃ [5.7]. Based on the previous studies, if the deviation in temperature is less than 2.0 ℃ between the measurement and simulation, with an $R^2 > 0.95$ in the validation process, then the proposed modeling method has relatively high accuracy.

5.2.4. Simulation cases

Table 5.4 and Fig. 5.4 show the simulation cases for the validation and sensitivity analysis. First, a simulation was conducted for the actual conditions of the experimental building, and the simulation model was validated by comparing it with the results of the field measurements. To maintain consistency with the field measurements, Room A (test room) was equipped with a radiant floor cooling system, whereas Room B was set as the reference room without the system (Fig. 3.2). The room window was opened throughout the day. In the following simulation (i.e., sensitivity analysis), only one variable was changed at a time ensure controlled conditions in Room A. The coupled CFD can calculate convective heat transfer more accurately than TES owing to the consideration of spatial air flow distributions. Based on the advantage of the coupled CFD, the flow rate of fan and height of the underfloor space which influence the air velocity near the PCM surface was investigated (Fig. 5.4). Although the opening condition of the louver for the underfloor space was tested in Chapter 4, its influence was not observed clearly. Therefore, the operation schedule of the fan and louver windows was investigated under same weather condition in the simulation. As the amount of PCM installed in buildings strongly affect the latent heat thermal storage, the PCM thickness

Table 5.4. Simulation settings.

Influencing factors	Variables	Constants
Validation	-	1. Fan on: 18:00-7:00 2. Louver: always open 3. Height of underfloor space: 60 mm 4. Flow rate of fan 678 CFM 5. PCM thickness: 6 mm
Operation schedule of fan and louver windows	Illustrated in Fig. 5.4	1. Height of underfloor space: 60 mm 2. Flow rate of fan 678 CFM 3. PCM thickness: 6 mm
Flow rate of fan	100, 200, 300, 400, 500, 600, 700 CFM	1. Fan on: 19:00-7:00 2. Louver close: 7:00-19:00 3. Height of underfloor space: 60 mm 4. PCM thickness 6 mm
Height of underfloor space	60, 100, 200, 300, 400 mm	1. Fan on: 19:00-7:00 2. Louver close: 7:00-19:00 3. Flow rate of fan: 678 CFM 4. PCM thickness 6 mm
PCM thickness	4.5, 6.0, 9.0 mm	1. Fan on: 19:00-7:00 2. Louver close: 7:00-19:00 3. Height of underfloor space: 60 mm 4. Flow rate of fan: 678 CFM

was selected as a test variable to clarify the influence on storing and dissipating the heat during daytime and nighttime, respectively. As shown in Fig. 3.2, Room A (test room) and Room B (reference room) were compared to evaluate the thermal storage effect. The thermal storage effect was evaluated mainly in terms of the surface temperature of the floor, PCMs, and the heat balance of the PCM. Phase states of the PCMs were evaluated based on the PCMs temperature. The thermal storage of PCMs was calculated using the following formula (Eq. 5.23).

$$TS = \int \{H_{lower}(t) - H_{upper}(t)\} dt \quad (5.23)$$

where TS is the thermal storage [kJ/m^2], H_{lower} is the heat flux of the lower side of the PCM [W/m^2], and H_{upper} is the heat flux of the upper side of the PCM [W/m^2].

5.3. Results

5.3.1. Grid sensitivity analysis

The modified LK model with three grid sizes, coarse, medium, and fine meshes, was used for grid sensitivity analysis. Roache [5.33] suggested the grid convergence index (GCI) for evaluating the inaccuracy of outcomes for different mesh sizes using the following equation (Eq. 5.24).

$$\mathrm{GCI} = F_s \left| \frac{r^p \{(u_{Medium} - u_{Fine})/u_H\}}{1 - r^p} \right| \quad (5.24)$$

where F_s is the safety factor [-], r is the liner grid refinement factor [-], u is the air velocity [m/s], and p is the formal order of accuracy [-]

Table 5.5. The results of grid sensitivity analysis for air temperature (AT) and air velocity (AV).

	AT FL+0.1 m		AT FL+1.1 m	
	Room A	Room B	Room A	Room B
Fine-Medium	0.43%	0.42%	0.30%	0.24%
Medium-Coarse	0.53%	0.39%	0.29%	0.27%

	AV FL+0.1 m		AV FL+1.1 m	
	Room A	Room B	Room A	Room B
Fine-Medium	5.89%	9.60%	4.26%	9.11%
Medium-Coarse	8.29%	10.54%	12.94%	13.98%

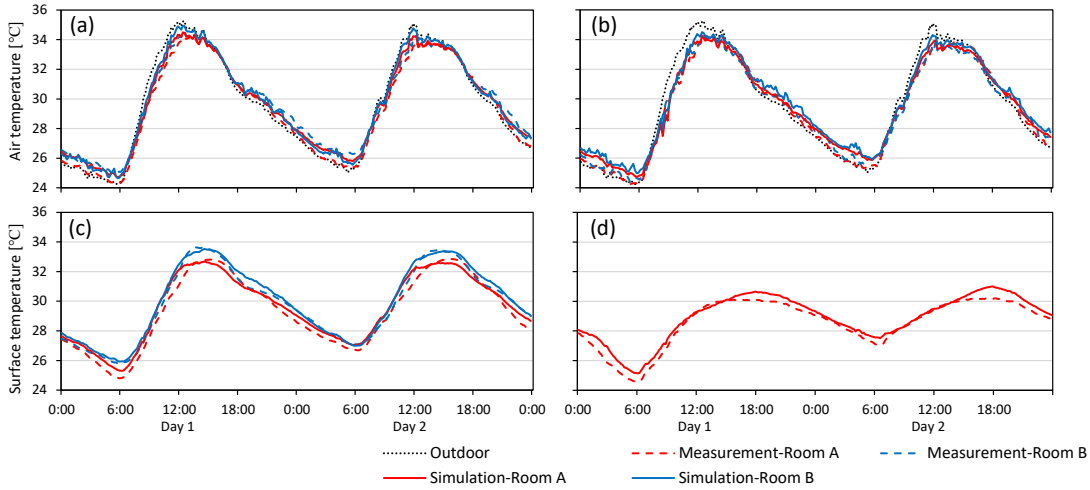

Fig. 5.5. Comparison of (a) air temperature (FL+1.1 m), (b) air temperature (FL+0.1 m), (c) floor surface temperature, and (d) PCM temperature between the field measurement and coupled simulation in Rooms A (PCM) and B (control).

Table 5.5 shows the average GCI for the three types of mesh for air temperature and air velocity at FL+0.1 m and FL+1.1 m in Rooms A and B. For air temperature, the error percentages were relatively small (less than 1.00%), regardless of mesh sizes. The air velocity was greatly influenced by mesh size. Because the horizontal pivot window was installed on the northern wall of Room A and can control the indoor air flow pattern regardless of the outdoor condition, the GCI values in Room A were smaller than those in Room B. Although the GCI value of air velocity was much higher than that of air temperature, it is difficult to adjust to a further finer mesh than in the present setting, because of the practical calculation load. For the fine mesh model, the three-day simulation took three days of actual time. Unlike most of the previously conducted simulations, in this study, the simulation was coupled with heat balance analysis including radiant heat transfer which considerably increases the calculation load. In the previous studies on ventilated rooms, the GCIs typically ranged from 5–17% [5.34–5.37]. Therefore, the GCIs with the fine mesh in this study (0.24–9.60%) were considered still acceptable. The fine mesh was used for further simulations, and the validity of the calculation model was investigated by comparing the results of the field measurements.

5.3.2. Validation

Fig. 5.5 and Table 5.6 show the measurement and simulation results of temperatures at the FL+1.1 m, FL+0.1 m, floor surface and PCM surface at the center of Room A (with the proposed floor cooling system) and B (without the system, as a control). Because the room

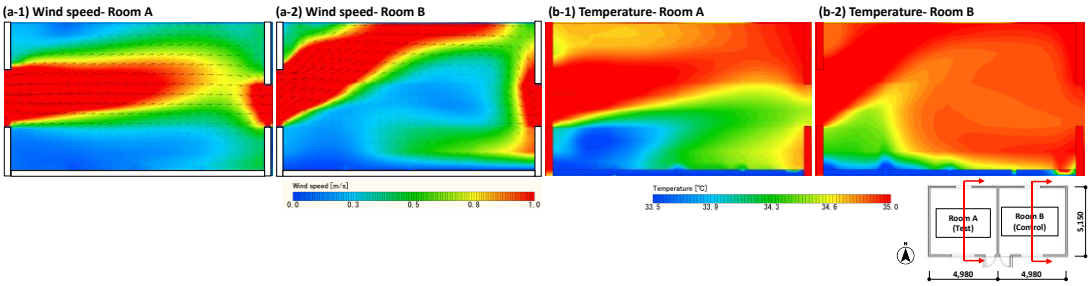

Fig. 5.7. (a) Air velocity and (b) temperature distribution at 14:00, day 1 in Rooms A and B.

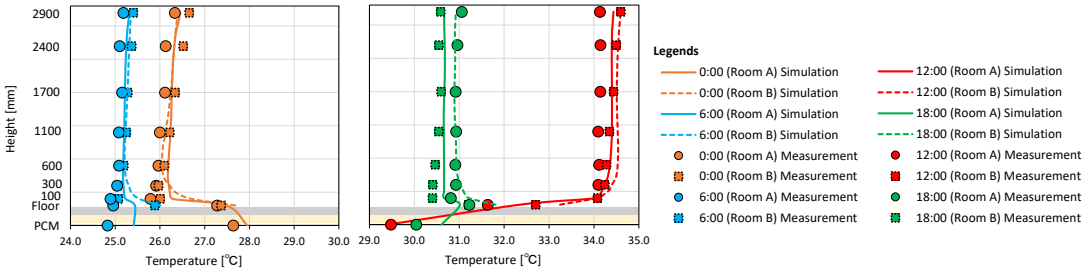

Fig. 5.6. Comparison of air temperatures between the measurement and simulation at 0:00, 6:00, 12:00, and 18:00, day 1 in Rooms A and B.

window was fully opened during the field measurement, the inflow pattern strongly influenced the indoor air temperature distribution, as shown in Fig. 5.6. A relatively high air temperature was observed at high air velocities because hot outdoor air influences the indoor air temperature for both rooms. Furthermore, cool air was observed in the lower part of Room A, due to the proposed system and low air velocity caused by the horizontal pivot window. This is consistent with the results of field measurements presented in Chapter 3. Similar to Room A, the air temperature distribution in Room B was influenced by the inflow pattern. The upper part of Room B tended to have a high temperature because hot outdoor air passes through the upper part of Room B due to upward inflow through the simple opening.

Fig.5.7 shows the hourly averaged air temperature distribution in Rooms A and B, comparing the simulated results with the field measurement results. The deviation in hourly temperatures was less than 1.0 ℃ between FL+ 0 m and 2.9 m. For temporal variation, the simulated air temperatures at FL+0.1 m and FL+1.1 m obtained relatively high accuracy with a root mean square error (RMSE) of 0.4 ℃ (Room A) and 0.4–0.5 ℃ (Room B). The coefficient of determination (R^2) was 0.99. For floor surface temperature, the coefficient of determination in Room A was 0.01 lower than that in Room B, because of the complexity of the phase change processes of the PCMs. The R^2 value of the PCM was 0.97. Nevertheless, the maximum deviation was still smaller than that in the previous studies, with a deviation of

Table 5.6. The validation results.

Room	Variable	Coupled simulation		CFD simulation (without radiant heat transfer)	
		R^2	RMSE [°C]	R^2	RMSE [°C]
Room A	Air temperature (FL+1.1 m)	0.99	0.4	0.99	0.5
	Air temperature (FL+0.1 m)	0.99	0.4	0.97	0.5
	Floor surface temperature	0.98	0.5	0.96	0.8
	PCM temperature	0.97	0.4	0.84	0.7
Room B	Air temperature (FL+1.1 m)	0.99	0.4	0.98	0.4
	Air temperature (FL+0.1 m)	0.99	0.5	0.98	0.5
	Floor surface temperature	0.99	0.3	0.99	0.3

1.2 °C (floor surface in Room A) and 1.2 °C (PCM temperature) (see Section 5.2.3). As shown in Table 5.6, if the simulation does not consider radiant heat transfer, its accuracy decreases. In Room B, the floor surface temperature was almost the same as the other surfaces, i.e., ceiling and wall. Thus, the radiant heat transfer among the surfaces was small. On the other hand, the floor surface temperature and PCM temperature in the case of CFD simulation without considering radiant heat transfer was 0.3 °C higher than that of the coupled simulation. This result implies that the coupled simulation method is preferable when investigating the influence of PCMs on the indoor thermal environment.

Fig. 5.8 shows the heat flux on the floor surface and air velocity at FL+1.1 m and 0.1 m. Although the simulated air velocity at FL+1.1 m was slightly higher than the measured value during the daytime, it did not increase the heat flux on the floor. Between 12:00–17:00

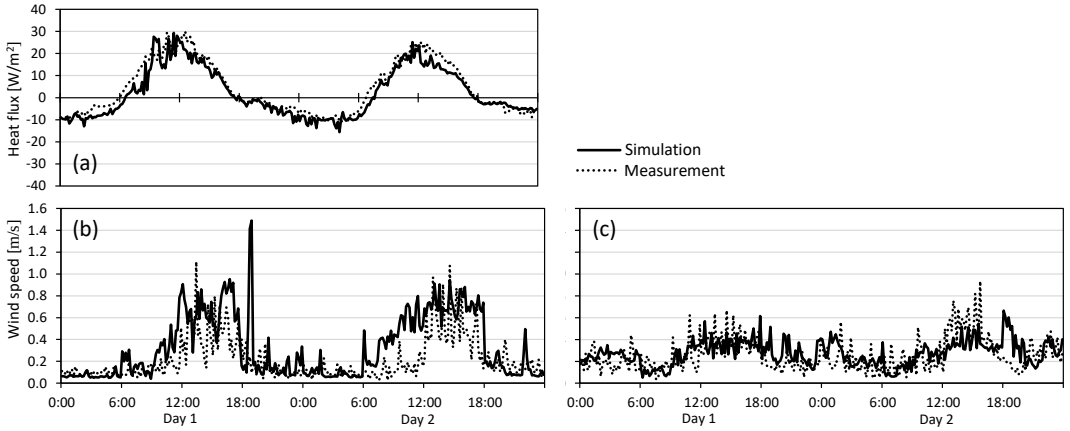

Fig. 5.8. Comparison of (a) heat flux on the floor surface, (b) air velocity (FL+1.1 m), and (c) air velocity (FL+0.1 m) between the field measurement and simulation in Room A (PCM).

(Day 2), the heat flux in the field measurement was 1.0–10.4 W/m^2 larger than the simulated value, because of a 0.0–0.6 m/s higher air velocity near the floor (FL+0.1). Overall, the simulated model showed a relatively high accuracy of the heat flux on the floor surface, with an RMSE of 4.0 W/m^2 and R^2 of 0.92. The present simulation model is more accurate than those in previous studies and is effective for the evaluation of PCM in naturally ventilated buildings.

5.3.3. Effect of operational schedule of louver window and ventilation fans

Fig. 5.9a and 5.9b show the floor and PCM surface temperatures and the average thermal storage of the PCMs for Cases 1–8 with different operation schedules for the louver window and ventilation fans. Compared with the floor surface temperature in Room B (reference), floor surface temperature reduction was 0.2–0.3 ℃ in Case 1, owing to the increased thermal storage of the PCMs without forced ventilation. In addition to the increased thermal storage, forced ventilation for the underfloor space contributed to a floor surface temperature reduction of 0.6–0.8 ℃ in Cases 2–6. Nevertheless, the influence of the operation

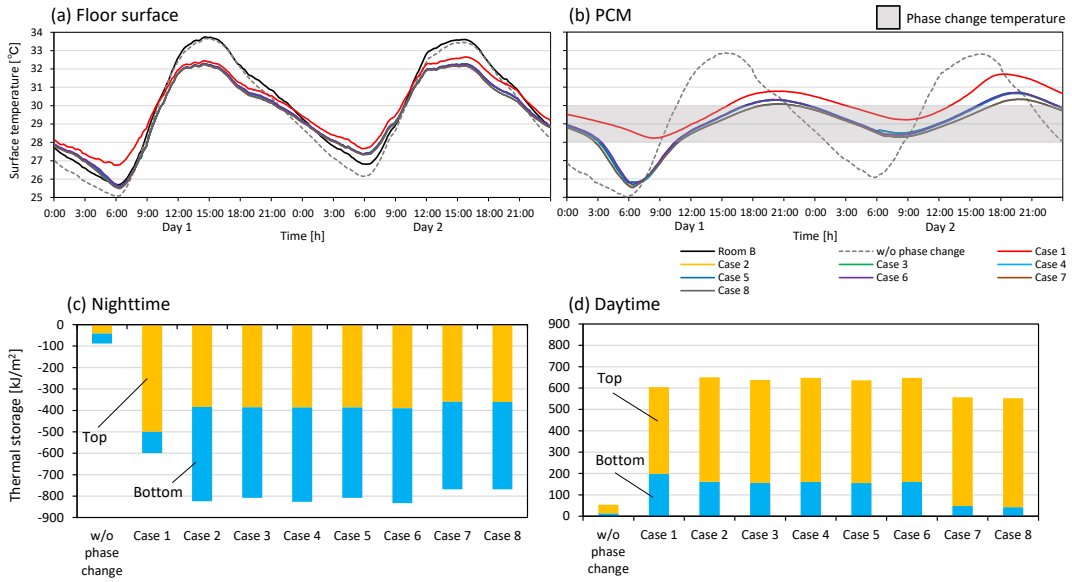

Fig. 5.9. Influence of the operation schedule on (a) floor surface temperature, and (b) PCM surface temperature; (c, d) average thermal storage of the PCMs for each case during the nighttime and daytime.

schedule on floor surface temperature reduction was not observed in Cases 2–6. In Cases 7 and 8, the floor surface temperature was reduced by 0.6–0.9 ℃. The closing louver window improves the thermal storage effect during the daytime.

Fig. 5.9c and 5.9d show the thermal storage of PCMs for each case. Because of history of PCMs, their thermal storage was not necessarily balanced within the elevation term. As a reference, case without phase change of the PCMs, whose phase change temperature was 50 ℃ and operational schedule of the fans was the same as Case 2 is shown in the same figure. In the case, thermal storage of the PCMs was only 88 kJ/m^2 and 54 kJ/m^2 during the nighttime and daytime, respectively, and thus floor surface temperature during the daytime was similar to that in Room B. The specific heat of the PCMs was 2.0 kJ/kg·K, and the PCM temperature ranges in Cases 1−8 were 3.5–5.0 ℃. The contribution of latent heat of the PCMs on thermal storage was more than 90%.

The effect of forced ventilation on the underfloor space was clearly observed at night. In Case 1, i.e., when the fans were turned off throughout the day, the stored thermal storage was 599 kJ/m^2. Nocturnal wind conditions in tropical regions are mostly calm. The average nocturnal air velocity and air temperature in the underfloor space were 0.1 m/s and 28.0 ℃, respectively, due to the insufficient ventilation rate. The coolness stored from the bottom side of the PCMs, which faces the underfloor space, was only 99 kJ/m^2. When forced ventilation with the assistance of a fan was employed (Cases 2–8), the cool outdoor air enters the underfloor space effectively. Therefore, the mean nocturnal temperature in the underfloor space is 0.8–0.9 ℃ lower than that in Case 1. Moreover, the air velocity near the PCMs was maintained at 1.0 m/s. Higher air velocity and lower air temperature in the underfloor space increased the heat dissipation to the underfloor space to 408–440 kJ/m^2 in Cases 2–8. Although the duration of operation of the fans in Case 6 was shorter than that in Cases 2–4, the proposed system retained the highest coolness in Case 6, with thermal storage of 833 kJ/m^2. This is because the outdoor air temperature was still higher than the PCM temperature until approximately 20:00, and operating the fans in the evening of Cases 2–5 assisted heat accumulation. In Cases 2–6, the surface temperature of the PCM became lower than the air temperature at 18:40–19:00 (Day 1) and 19:10–19:50 (Day 2).

Although the PCMs did not fully melt during the daytime on day 1 in Cases 2–6, the heat absorption of the proposed system was 32–45 kJ/m^2 higher than that in Case 1, because of the higher thermal storage during the previous night. In Cases 2–6, approximately 75% of the thermal storage in the PCMs was transferred from their top side to the floor structure. The remainder was released from the bottom side of the PCMs to the underfloor space. Meanwhile, in Cases 7 and 8, the coolness released to the underfloor space was lower than in Cases 2–6, because closing the louvers during daytime maintained temperatures at 1.4–1.9 ℃ lower in the underfloor space. Moreover, the suppressed heat absorption from the underfloor space contributed to increasing the coolness of the PCMs transferred to the floor structure by 22–29

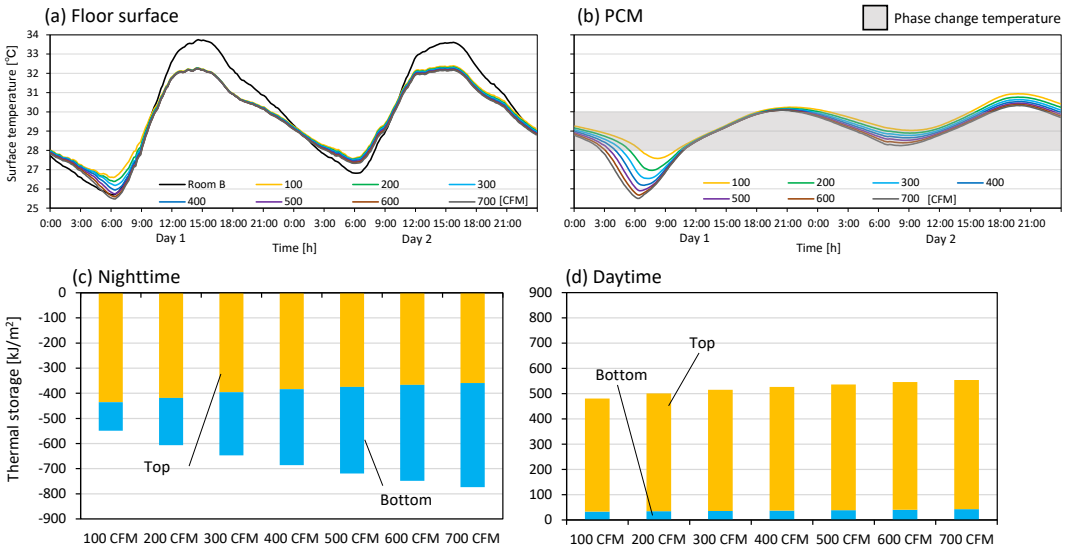

Fig. 5.10. Influence of the flow rate of fan on (a) floor surface temperature and (b) PCM surface temperature (c,d) average thermal storage of the PCMs for each case during the nighttime and daytime.

kJ/m^2. Closing the louvers during the daytime can be effective in increasing the thermal storage effect.

5.3.4. Effect of ventilation rate

Fig. 5.10 shows the floor and PCM surface temperatures and the average thermal storage of the PCMs with an increase in the volumetric flow rate of the fans. On the morning of Day 1, the influence of the flow rate of the fans was clearly observed. In the case of the flow rate of 700 CFM, which was the similar flow rate of the actual case in field measurement (678 CFM), the floor surface temperature was 1.2 ℃ lower than that of 100 CFM at 6:30 owing to a higher air velocity near the PCM. However, on day 1, as the temperature increased during the day, the influence of the air velocity on the floor and PCM surface temperature decreased. In particular, at noon, when the PCM reaches the melting temperature range, the floor surface temperatures were almost the same, although floor surface temperature reduction compared with Room B was up to 1.6 ℃. This is because the thermal storage in the case of 700 CFM was only 63 kJ/m^2 larger than that of 100 CFM. If the PCMs solidify completely, the cooling effect in the afternoon may be the same regardless of the flow rate of the fans because the PCMs tend to maintain a constant temperature. Meanwhile, in the case of partial solidification (day 2), the flow rate of the fans affected the floor surface temperature reduction

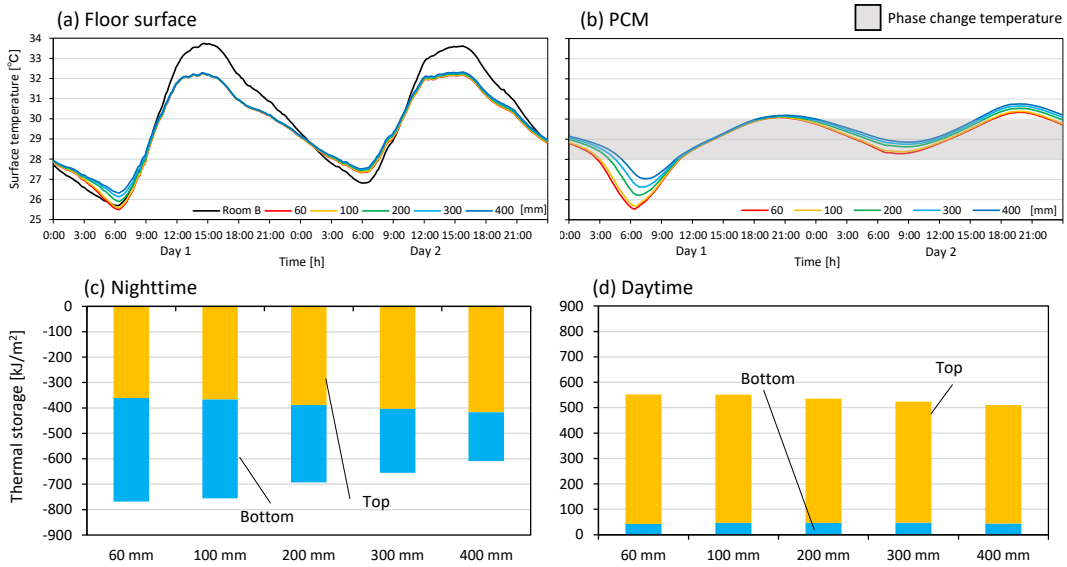

Fig. 5.11. Influence of the height of underfloor space on (a) floor surface temperature and (b) PCM surface temperature; (c, d) average thermal storage of the PCMs during the nighttime and daytime.

even during the daytime. In the peak temperature period, the floor surface temperature reduction with a flow rate of 700 CFM was 0.2–0.3 ℃ larger than that of 100 CFM.

Fig. 5.11 shows the influence of the height of the underfloor space on the floor, PCM surface temperature, and average thermal storage of the PCMs. As the height of the underfloor space increased, both surface temperatures increased because the decrease in the air velocity near the PCM lowered the thermal storage of the PCMs. In the case of the height of 60 mm, the diurnal average floor surface temperature and thermal storage were 30.1–30.6 ℃ and 769 kJ/m^2, respectively. When the height widens to 400 mm, the average diurnal floor surface temperature increases by 0.2 ℃ because the heat dissipation decreases by 159 kJ/m^2 at night. A narrower underfloor space results in a larger convective heat transfer rate; thus, the thermal storage of the PCMs increases. The same conclusion was drawn by Halawa et al. [5.4].

5.3.5. Effect of PCM thickness.

Fig. 5.12 shows the influence of the thickness of the PCM on the floor, PCM surface temperature, and average thermal storage of the PCMs. The increase in the thickness of the PCMs narrows the floor and PCM surface temperature fluctuations. The diurnal floor and PCM temperature fluctuations in the case of a thickness of 9 mm were 0.3–0.6 ℃ and 1.6 ℃ less than those of 4.5 mm, due to the higher thermal storage. When the temperature difference

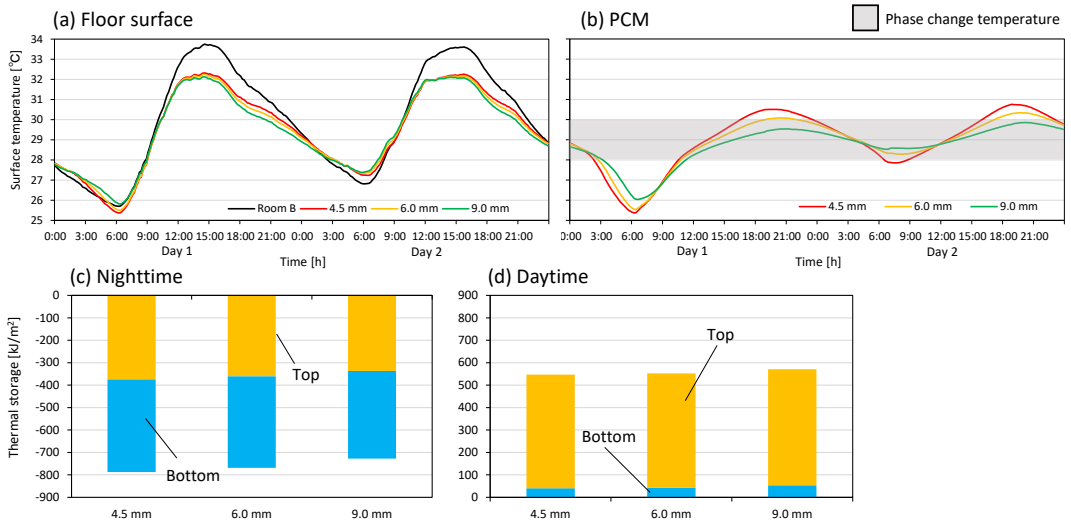

Fig. 5. 12. Influence of the thickness of PCM on (a) floor surface temperature and (b) PCM surface temperature; (c, d) average thermal storage of the PCMs during the nighttime (c) and daytime (d).

of the PCMs between 4.5 mm and 9.0 mm increased, the floor surface temperature difference increased. However, the floor surface temperature reduction in the case of a PCM thickness of 9 mm was similar to that of 4.5 mm in the peak temperature period (12:00–15:00), because a large PCM temperature difference was observed in the late afternoon. For example, a PCM temperature difference of more than 1 °C was observed between 17:00 and 20:00. Zhou et al. [5.38] indicated that low thermal conductivity is a common problem in PCMs, which prolongs the solidification and melting periods. Thicker PCMs delay reaching the melting temperature; therefore, the period of the cooling effect by the latent heat was shifted to a later period compared to thinner PCMs. As shown in Fig. 5.12, the shifted melting temperature period decreased the time required for heat dissipation at night. In this study, although the heat absorption for a PCM thickness of 9.0 mm was 24 kJ/m^2 greater than that of a thickness of 4.5 mm, the heat dissipation in the case of a PCM thickness of 9.0 mm was 60 kJ/m^2 lower during nighttime. A thicker PCM may not necessarily lead to a larger cooling effect.

5.4. Discussion

5.4.1. Validity of the coupled CFD simulation model

Based on the Jürges equation, if an air velocity at FL+1.1 (i.e. center of the indoor space) is used for the heat balance simulation, similar to the TES that uses one air node in each zone, the mean diurnal convective heat transfer would be 0.9 W/m^2K greater compared to the air velocity at FL+0.1. The heat transfer coefficient near the floor surface was more accurate in CFD simulations than in TES because the former can calculate the wind distribution. As with the wind distribution, the relatively high accuracy of the air temperature near the floor surface contributed to improving the heat transfer calculation. Regarding radiative heat transfer, which was considered less in the previous CFD simulations, the coupled simulation improved accuracy when the surface temperature difference between the floor and other surfaces, i.e., the wall and ceiling, was large, owing to the thermal storage effect of the PCMs. These results imply that the coupled method is considered a better option with higher accuracy for evaluating both the temperature and amount of heat stored and released by PCMs in naturally ventilated buildings, where the air temperature and air flow distribution are not uniform.

To simulate the air temperature and airflow distribution in a naturally ventilated room, Straw et al. [5.17] calculated indoor and outdoor environments within the same computational domain and provided accurate results. The indoor air temperature distribution derived from the coupled simulation method was influenced by the wind from the outdoor space (Fig. 8). The coupled simulation is effective in improving the accuracy when the window changes the inflow direction. Nevertheless, for temperature measurement in outdoor spaces, measurement errors of approximately 0.7 ℃ are inevitable [5.39]. Overall, the model validation results in the present study showed a reasonable agreement between the measurement and simulation data, and satisfied the criteria of ASHRAE Guideline 14, with a CVRMSE less than 15% of the average measured value [5.40]. The proposed coupled simulation considers spatial distribution while improving accuracy, even compared with previous studies (see Section 2.3.4).

5.4.2. Limitations of PCM modeling

For modeling of PCM, several studies have proposed PCM modeling methods based on phase change temperature range and latent heat of PCM [5.8, 5.41]. Consequently, inputting the measured thermal properties improves the R^2 of the predicting temperature, because the partial enthalpy of the PCM was not uniformly distributed in the phase change temperature

range. Nevertheless, the heat absorption on the floor in the simulation, based on the heat flux on the floor (Fig. 10a), was 125–137 kJ/m^2 lower than that in the field measurement. Iten et al. [5.42] reported that a heating rate of 10 ℃/min underestimates the latent heat of PCMs, compared to the slower heating rate of 0.2 ℃/min in DSC testing. In this study, the latent heat of the PCMs was measured by DSC testing at a heating rate of 2 ℃/min, which is a much faster heating rate than that in actual environments. In the present study, the latent heat input to the calculation model may have been smaller, and thus may have led to a lower degree of heat absorption in the proposed system. To replicate the PCM temperature and thermal storage effect of the PCM more accurately, an appropriate heating rate based on the target environment must be selected for DSC testing.

5.4.3. Feasibility of the radiant floor cooling system

For the operation schedule of the fans, when comparing Cases 4 and 6 with Cases 3 and 5, the thermal storage in the former was 18–25 kJ/m^2 larger than that in the latter because the temperature difference between the air in the underfloor space and PCM tends to be large in the morning (Fig. 5.9). Waqas et al. [5.3] reported that the phase change of PCMs was more sensitive to their ambient temperature than the air flow rate. Chapter 4 reported that when the outdoor temperature was 0.7–3.2 ℃ lower than the set-point phase change temperature, forced ventilation was found to be effective to ensure the sufficient solidification of PCMs. Recent weather data at the nearest weather station show that the average air temperature at 7:00 was 1.6 ℃ lower than the set-point phase change temperature, and then that at 8:00 exceeded it. Regarding the time to start the fan, the outdoor air temperature of the recent weather data at 19:00 was lower than the set-point phase change temperature. This implies that operating the fans between 19:00 and 7:00 may represent the operation schedule that maximizes the thermal storage of the proposed system under the given weather conditions.

Regarding the effect of ventilation on the underfloor space, comparing two cases of similar ventilation rates, such as 60 mm with 200 CFM (662 ACH) and 200 mm with 678 CFM (674 ACH), the floor and PCM surface temperatures in the latter case were 0.1–0.2 ℃ lower than those in the former case), due to the shape of cross-section of the underfloor space. The friction loss was determined by the airflow volume, cross-sectional area, and length of the flow direction. Moreover, Shui et al. [5.43] concluded that a higher aspect ratio results in a higher friction factor ratio. For instance, the pressure loss of airflow in the 200 mm systems is a quarter of the pressure loss in the 60 mm system. The actual ventilation volume may decrease because of the higher pressure loss, which leads to a reduced cooling effect. In the proposed system, a contraction panel was installed in the underfloor space to accelerate convective heat transfer by narrowing the ventilation space, and its influence was clearly observed. Nevertheless, it may be necessary to choose a ventilation fan with a high external static

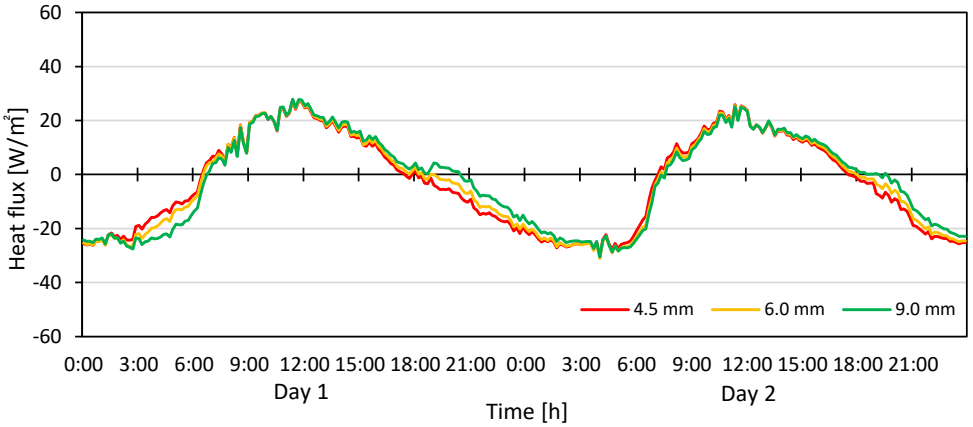

Fig. 5.13. Heat flux of the PCM for different PCM thicknesses.

pressure to maintain the required flow volume within a small cross-sectional area of the ventilation space.

As discussed, the floor surface temperature reduction in the peak temperature period, compared to Room B, was the same, regardless of the PCM thickness. Sato et al. [5.44] reported that an increase in the effective PCM's thickness did not always contribute to reducing the heating load, although it increased the thermal storage of the PCMs. Nevertheless, the surface area of PCMs strongly influences the heating load reduction [5.44]. Similarly, the cooling effect of the proposed system may not change significantly during the peak temperature period; however, the thickness of the PCMs affects the duration of the cooling effect. In the case of PCMs with a thickness of 4.5 mm, the PCM temperature exceeded the phase change temperature of 29 ℃. The PCM temperature reached 30.5 ℃ on day 1 and melted completely. The PCM thickness of 4.5 mm may be too thin to maintain the cooling effect during the daytime under the given weather conditions.

However, when the thickness of PCMs was 6 mm, the maximum PCM temperature on day 1 was 30.1 ℃, and the PCMs almost melted. The mean diurnal outdoor temperature on day 1 was 0.4–2.6 ℃ higher than the recent weather data at the nearest weather station [5.45]. Lei et al. [5.46] conducted a parametric study of PCM in the hot and humid climate of Singapore and concluded that the optimal PCM thickness of the external wall of an air-conditioned room was 10 mm. However, the PCM thickness of 9 mm may be too thick for the proposed system, because closing the louver and turning off the fan suppresses the air temperature rise near the PCMs during the daytime, and the nocturnal indoor temperature was lower in an air-conditioned room than in one without. Moreover, as shown in Fig. 5.13, the heat flux indicates that the period for the heat absorption in the case of a PCMs thickness of 9 mm was approximately two hours longer than that of the thinner PCMs, i.e., 4.5 mm and 6 mm. Thicker PCMs reduce the available time to dissipate their heat, whereas they increase the

time required for dissipating the heat from the PCMs. In tropical climates, including Indonesia, warmer nights limit the time required for heat dissipation. This study implies that a PCM thickness of 6 mm is optimal for the proposed system under hot and humid conditions

5.5. Summary

A coupled simulation model of heat balance analysis and CFD simulation for naturally ventilated buildings was constructed to determines key parameters of the radiant floor cooling system using PCMs. Chapter 5 demonstrates a modeling method for the thermal storage effect of PCMs using the constructed simulation model. The target floor cooling system is composed of PCMs, louver windows, and ventilation fans for underfloor spaces. To evaluate the influence of each component of the floor cooling system, a sensitivity analysis was conducted on the target building in Indonesia based on the validated model. The main findings are summarized as follows.

- In the naturally ventilated room with PCMs, the air temperature distribution and convective heat transfer coefficient are influenced by the indoor airflow patterns. Therefore, the analysis of air temperature and air velocity near the floor surface by the coupled simulation model was found to be more effective in improving the heat transfer calculation compared with the TES. Moreover, coupling with radiative heat transfer calculations increased the accuracy of the simulation when the surface temperature between the floor and the other surface (i.e., wall and ceiling) was large, due to the thermal storage effect of the PCMs. Owing to these improvements, the validation results for the temperature and heat flux showed a good correlation between the simulation and field measurements. The RMSEs were 0.3–0.5 ℃ for the floor surface temperatures and 4.0 W/m^2 for heat flux on the floor, with a coefficient of determination of 0.92–0.99. These results imply that the coupled method is considered a better option for evaluating both the indoor temperature and amount of heat stored and released by PCMs in naturally ventilated buildings, where the air temperature and air flow distribution are not uniform.

- In the proposed system, the air velocity that ensures the solidification of the PCMs in the underfloor space was found to be a key parameter. An increase in air velocity increases the storage of coolness at night. In addition, the thermal storage of the proposed system was maximized when the operational schedule of the fans was controlled by the outdoor temperature. That is, the outdoor air temperature was lower than the set-point phase-change temperature. The

optimum time for fans to operate was between 19:00 and 7:00 under the given hot and humid conditions.

- A contraction panel installed in the underfloor space also increased the air velocity near the PCM by narrowing the ventilation space, and its influence on increasing thermal storage was observed. Nevertheless, a small cross-sectional area with a high aspect ratio increases the pressure loss. To choose the appropriate ventilation fans, the proposed system needs to consider the external static pressure, as well as the flow volume.

- The floor surface temperature reduction of the proposed system in the peak temperature period was the same, regardless of the PCM thickness. This is due to the low thermal conductivity of the PCM, although a thicker PCM increases thermal storage. In tropical climates such as Indonesia, warmer nights limit the time required for heat dissipation. This study implies that a PCM thickness of 6 mm is the optimum thickness for the proposed system under the given hot and humid conditions.

Unlike individual TES or CFD simulations, the coupled simulation method can be applied to thermal comfort evaluation, because air temperature, radiant temperature, and wind distribution can be determined simultaneously. Future studies to optimize the radiant floor cooling system using PCMs for naturally ventilated buildings are required to further improve thermal comfort and energy savings. In the case of free cooling, the thermal storage of PCMs is strongly influenced by weather conditions. An annual simulation of the radiant floor cooling system using weather data from different climate zones of Indonesia is necessary to ensure the thermal storage effect of PCMs throughout the year.

Chapter 6
Annual simulation of phase change materials considering phase state with hysteresis

Abstract

Chapter 6 aims to evaluate the annual performance of the proposed floor cooling system that consider the hysteresis of PCM and to determine its design guidelines and indicators to maximize thermal storage effect of PCMs in the building throughout a year in a hot and humid climate. To evaluate the annual performance of the proposed floor cooling system, Chapter 6 firstly investigated the applicability of a thermal energy simulation (TES) for a naturally ventilated building in which the phase change material (PCM)-based radiant floor cooling system was installed. Based on the results of the full-scale PCM measurement, the EnergyPlus-based TES model was validated by comparing it with the results of field measurement at a full-scale experimental building with natural ventilation and a computational fluid dynamics (CFD) simulation coupled with the heat balance analysis, shown in Chapter 3 and 5, respectively. Good correlations (up to R^2=0.99) were observed in the air and floor surface temperatures between the measurement and TES simulation. Additionally, the TES had a similar accuracy as the coupled CFD, which considers spatial wind and temperature distribution. The results of the annual simulation showed that the proposed PCM-based radiant floor cooling system with night ventilation achieved a thermal comfort period based on the operative temperature (OT) of up to 68.5% a year. Furthermore, the daily maximum and minimum ambient temperatures of the PCMs significantly affected the maximum and

minimum liquid fractions, respectively, and thus it can be a useful guideline for selecting a phase change temperature. A reasonable annual average utilization rate of approximately 70% can be determined to maintain a low floor surface temperature throughout a year.

Key words
Hysteresis, Utilization rate, Condensation, Annual evaluation, Thermal energy simulation.

6.1. Introduction

The results in Chapter 5 showed that the contribution of latent heat of PCMs installed on the floor on thermal storage was more than 90% when the PCMs were ensured a phase change. For effective utilization of latent heat, the thermal behavior of PCMs must be clarified as discussed in Chapter 2. PCMs are classified into three categories: eutectic, inorganic, and organic [6.1]. Paraffin, which is an organic PCM, is widely used for cooling buildings because of its non-corrosiveness, low cost, and availability. Previous studies have reported the unique thermal behavior of paraffin as a PCM, such as latent heat of paraffin was influenced by heating and cooling rate in differential scanning calorimetry (DSC) testing [6.2], as discussed in Chapters 2 and 5. Generally, the size of a specimen in DSC testing is only a few milligrams, which differs in size and shape from PCMs incorporated with building structures; thus, the results of DSC testing are not necessarily representative of the relationship between the temperature and enthalpy of full-scale PCM products [6.3]. To measure the thermal properties of full-scale PCM products, the American Society for Testing and Materials (ASTM) regulates the measurement method, which requires a longer time to maintain the quasistatic condition [6.4]. Nevertheless, few studies have shown the influence of the PCM measurement method on the thermal properties of PCMs and PCM modeling of building simulations. To accurately model PCMs in buildings, it is necessary to measure the thermal properties of full-scale PCMs, in particular the latent heat and phase change temperature, using an appropriate measurement method because previous parametric simulations showed that shifting the phase change temperature by 1 ℃ strongly affects the cooling effect [6.5]. In addition to the measurement, numerical simulations, which can model principles and phenomena, are effective in clarifying the mechanism of the thermal storage effect of PCMs [6.6].

Recently, researchers have applied numerical models of PCMs to several simulation tools to evaluate their thermal storage effects in buildings. The coupled CFD model considering the spatial distributions of air temperature and air velocity compensated for the limitation of thermal energy simulation (TES) caused by the nodal model for each zone and surface [6.7, 6.8]. In Chapter 5, the coupled simulation model of heat balance analysis and CFD was constructed to evaluate the thermal storage effect of the PCMs in terms of heat flux and temperatures for naturally ventilated buildings. Nevertheless, the coupled simulation

requires considerable calculation cost owing to its high spatial resolution. Therefore, the coupled simulation is difficult to apply to the annual simulation. Moreover, regarding the performance evaluation of PCMs using field measurements, limited time and cost can obstruct long-term evaluation. If PCMs are installed in buildings, their thermal behavior under several weather conditions must be investigated through long-term evaluation because the results in Chapters 4 and 5 showed that the history of the PCMs in previous days influenced their thermal storage effect on the following day. In addition to the simulation for high spatial resolution, i.e., coupled CFD, constructing a simulation for long-term evaluation is strongly recommended to determine the effective operation of the proposed system.

A TES is an effective tool for long-term evaluation of the thermal storage effect of PCMs owing to its low calculation load [6.9]. Goia et al. [6.10] validated a hysteresis PCM model in EnergyPlus by comparing it with experimental data. Mohseni et al. [6.11] conducted a sensitivity analysis of PCMs to investigate the thermal storage effect of concrete incorporated with PCMs. The accuracies of a previous TES for building installed PCMs were 0.3–1.1 ℃ for the root mean square error (RMSE) and 0.53–0.99 for the coefficient of determination (R^2) [6.10, 6.12–6.17]. Arıcı et al. [6.18] optimized an external building wall integrated PCM in Turkey to maximize annual energy savings. In previous studies, although closed rooms were often selected, and TESs were rarely implemented to investigate the thermal storage effect of PCMs in naturally ventilated buildings, a TES is a reasonable option for the annual evaluation of naturally ventilated rooms if it has an accuracy similar to that of coupled CFD. Few studies have compared TESs with other simulation models, such as coupled CFD, to calculate the thermal storage effect of PCMs in naturally ventilated buildings. Therefore, the applicability of TESs has not yet been determined.

Information from previous studies on predicting the year-round performance of PCM-based systems integrated into naturally ventilated buildings is limited [6.19]. Al-Absi et al. [6.20] indicated that the advantage of hot and humid climate regions is that the cooling effect of the PCMs can be obtained year-round because of the small annual temperature range (approximately 1.5 ℃ in Jakarta). Therefore, cooling effect of PCM during the daytime and heat dissipation method from PCM during the nighttime can be evaluated even in case of the short-term evaluation (Chapters 3–5). Nevertheless, the sensitive change in latent heat with phase change temperature and seasonal change, i.e., rainy and dry seasons, can affect the year-round performance of PCM-based systems, such as utilization rate and condensation. For instance, the influence of the proposed floor cooling system on condensation which might cause mold and mite problems during rainy season was not investigated in Chapters 3 and 4 because the field measurements were conducted in the dry season and transition season. As discussed, the history of the PCM in previous days affected the thermal storage and utilization rate in following days. Thus, a simulation model is necessary to clarify the influence of the thermal storage effect of PCMs on thermal comfort and building energy consumption throughout a year and to determine a key indicator to maximize the effect.

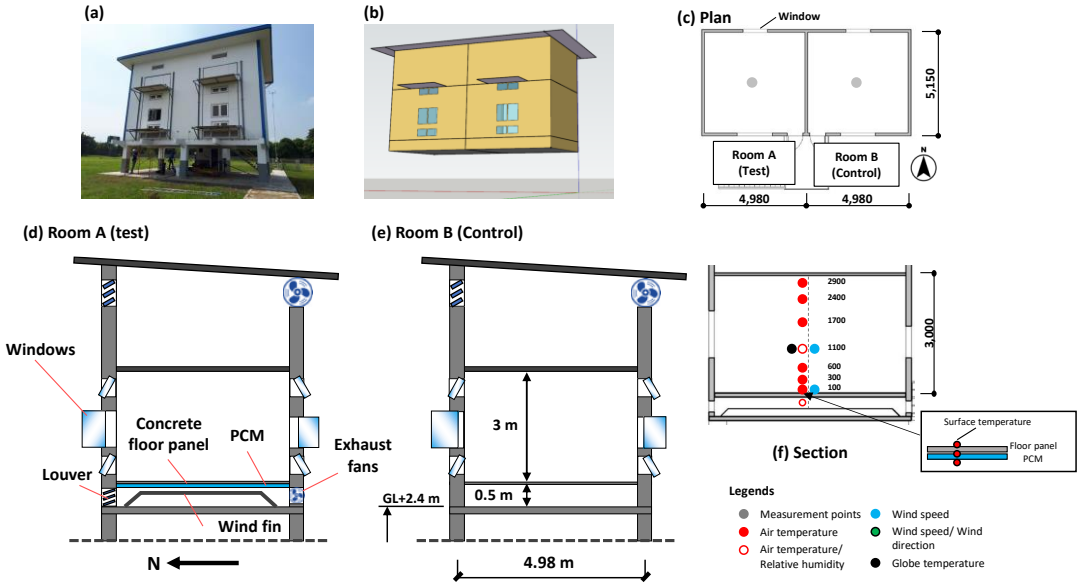

Fig. 6.1. (a) Experimental building in Tangerang, Indonesia, (b) building model in EnergyPlus, (c) plan of the experimental building, (d, e) Description of the experimental building; section of Rooms A and B, and (f) section of sensor setting.

6.1.1. Objective

Chapter 6 aims to evaluate the annual performance of the proposed floor cooling system that consider the hysteresis of PCM and to determine its design guidelines and indicators to maximize thermal storage effect of PCMs in the building throughout a year in a hot and humid climate. To evaluate the annual performance of the proposed floor cooling system, Chapter 6 firstly clarifies the applicability of TESs for and annual simulation of a naturally ventilated building in which the proposed PCM-based radiant floor cooling system was installed. First, the thermal properties of a full-scale PCM product were determined using the heat flow method (HFM). Subsequently, a TES model considering the hysteresis of the PCMs was constructed for a full-scale experimental building in Indonesia, presented in Chapter 3. Second, the TES model was validated by comparing it with the results of the field measurement and CFD simulation coupled with heat balance analysis which constructed in Chapter 5 to show an effectiveness of TES for naturally ventilated buildings installed PCMs. Third, influential factors affecting the thermal storage effect of the PCMs are discussed.

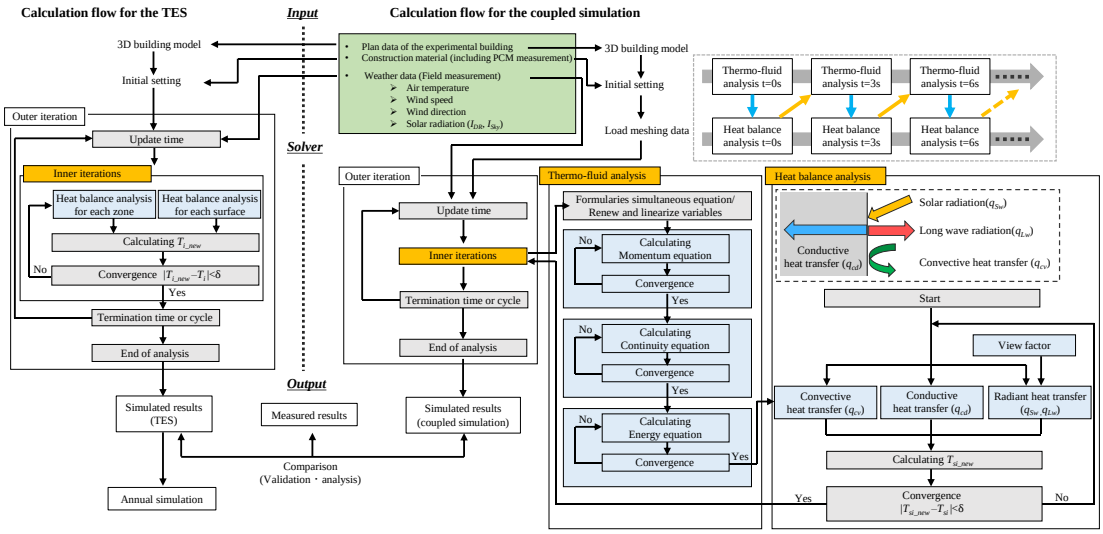

Fig. 6.2. Calculation flow for the TES and coupled CFD simulation.

6.2. Methodology

6.2.1. Outline of the simulation

As with Chapter 5, the full-scale experimental building was selected as the target building for the simulation (Fig. 6.1). The results of the field measurement in Chapter 3 were used for the validation. Fig. 6.2. shows the flow chart for the simulation, i.e., TES and coupled CFD, in Chapters 6 and 5, respectively. Based on the plan data for the experimental building, a three-dimensional building model considering construction material was constructed in both calculation methods. The same weather data were used for the TES and coupled CFD (see Chapter 5) to compare the validation results and analyze the influence of the calculation methods.

Regarding the TES, a whole-building energy simulation program (EnergyPlus 9.5, U.S. Department of Energy), which is a widely used TES tool worldwide, was used to solve the heat balance for each zone and surface. The results of the previous time step were adopted as the initial condition of the present time step. The heat balance analysis was iterated at the same time steps until the convergence of the heat balance analysis (δ=0.002 °C). The time step for the TES was one minute and the number of iterations per time step was 100.

6.2.2. Heat balance analysis

The nodal model calculation in EnergyPlus is based on fundamental heat balance principles. Each zone is assumed to be a node that contains uniform state variables such as temperature, pressure, and density. Empirical coefficients are employed to calculate the state-variable transfer flux between each node. For the one-node temperature T_z of the air for an indoor space, the thermal energy balance is expressed as

$$\rho_{air} C_p C_T \frac{dT_z}{dt} = \sum_{i=1}^{N_s} \frac{Q_i}{dt} + \sum_{i=1}^{N_{surfaces}} h_i A_i (T_{si} - T_z) + \sum_{i=1}^{N_{zones}} \frac{m_i}{dt} C_p (T_{zi} - T_z) + \frac{m_{inf}}{dt} C_p (T_\infty - T_z) \quad (6.1)$$

where ρ_{air} is the density of air [kg/m^3], C_p is the specific heat capacity [J/kg·K], C_T is the sensible heat capacity multiplier [-], T_z is the zone temperature [K], t is the time [s], Q is the convective internal load [W], h_i is the convective heat transfer coefficient [W/m^2·K], A_i is the area [m^2], T_s is the surface temperature [K], m_i is the mass flow rate [kg/s], m_{inf} is the mass flow rate through infiltration [kg/s], and T_∞ is the outside temperature [K].

In Eq. 6.2, the heat transfer coefficients must be set for each surface. The The convective heat transfer coefficients were calculated using the Jürges equation based on the average outdoor wind speeds and indoor air velocities during the measurement period (Chapter 3), and they were confirmed in the coupled CFD simulation (Chapter 5). Values of 12.0 W/m^2·K (daytime) and 8.0 W/m^2·K (nighttime) were applied to the outdoor surfaces. Meanwhile, the convective heat transfer coefficients for indoor surfaces were 10.0 W/m^2·K when the windows were opened and 6.0 W/m^2·K when they were closed. The simulation was performed under unoccupied conditions without any internal heat gain (Eq. 6.2).

$$q_{Sw} + q_{Lw} + q_{cv} + q_{cd} = 0 \quad (6.2)$$

where q_{Sw} is the heat flux through short wave radiation [W/m^2], q_{Lw} is the heat flux through long wave radiation [W/m^2], q_{cv} is the heat flux through convection [W/m^2], and q_{cd} is the heat flux through conduction [W/m^2].

Longwave radiation was calculated using the ScriptF algorithm in EnergyPlus. The ScriptF coefficient between surfaces i and j ($F_{i,j}$) includes all exchanges, i.e., reflection, absorption, and re-emission, and the longwave radiation exchange was calculated using the following formula (Eq. 6.3):

$$q_{LW,ij} = F_{i,j}(T_{si}^4 - T_{sj}^4) \quad (6.3)$$

where q_{Lw} is the heat flux through long wave radiation [W/m^2], $F_{i,j}$ is the ScriptF coefficient [kg/m^{2}K^4], T_{si} is the surface temperature [K].

The convective heat transfer of the internal building surface was calculated using the following equation (Eq. 6.4):

$$q_{cv} = h_i(T_{si} - T_z) \tag{6.4}$$

where q_{cv} is the heat flux through convection [W/m^2], h_i is the convective heat transfer coefficient [W/m^2·K], T_z is the zone temperature [K], and T_z is the zone temperature [K].

The conductive heat transfer on the building surface can be described using Fourier's law as follows (Eq. 6.5):

$$q_{cd} = -\lambda\frac{\partial T}{\partial x} \tag{6.5}$$

where q_{cd} is the heat flux through conduction [W/m^2], λ is the thermal conductivity [W/m·K], T_i is the temperature [K], and x is the length [m].

The time step for the simulation was 1 min based on the recommendation of Ferster et al. [6.21]. The first three days (April 11–13 and November 13–15) were set as spin-up period for the simulation, and the latter two days (April 14–15 and November 16–17) were used to evaluate the validation results. The three-day spin-up period was sufficient for the target building to store heat because of the relatively low thermal mass.

6.2.3. PCM measurement

The thermal properties of the full-scale PCM were measured in an experimental room in Japan to obtain the relationship between the temperature and thermal storage characteristics and to model the thermal storage effect of the PCM in the EnergyPlus

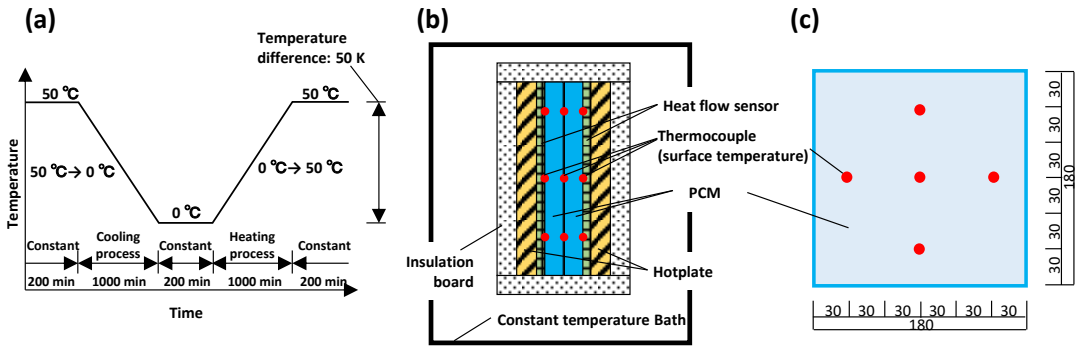

Fig. 6.3. Description of PCM measurement; (a) temperature change speed, (b) section of test apparatus, and (c) temperature measurement point.

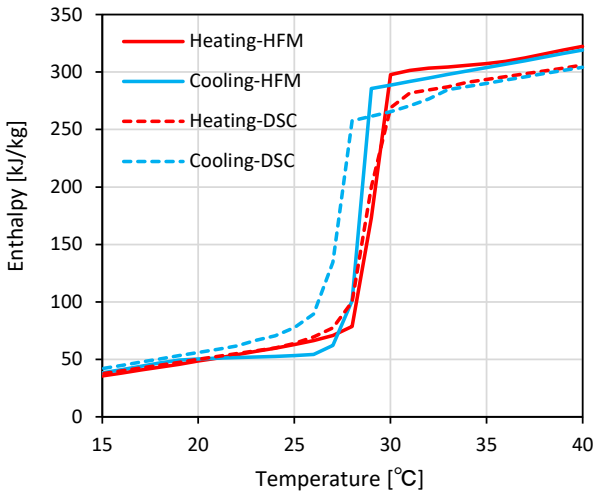

Fig. 6.4. Enthalpy–temperature curve of the PCM

simulation. As shown in Fig. 6.3, the heat flow method (HFM), which was proven to be an effective method for measuring the thermal properties of full-scale PCMs under transient conditions by Saeki et al. [6.22], was adopted. The temperature and heat flux of the PCM were measured while controlling the temperature of the hotplate attached to both sides of the PCM. Serikawa et al. [6.3] reported that the apparent specific heat of PCMs used in a simulation was more accurate for a slow heating or cooling rate (4 ℃/h) than for a fast rate (12 ℃/h). Japan Testing Center for Construction Materials (JSTM) recommended heating and cooling rate of 3 ℃/h as the same reason for measuring thermal storage properties [6.23]. Therefore, heating and cooling rates of 3 ℃/h were adopted for the heating and cooling processes during the measurement. The specimen was covered with thermal insulation boards, and the temperature of the test chamber was the same as that of the hotplate to eliminate thermal influences from the surroundings.

Table 6.1. PCM properties measured using the HFM and DSC.

Property	HFM	DSC
Type of material	Paraffin	
Installed amount	2.54 kg/m^2	
Latent heat	210 kJ/kg	198 kJ/kg
Thermal conductivity	0.2 W/m·K	0.2 W/m·K
Density (Liquid)	790 kg/m^3	790 kg/m^3
Density (Solid)	870 kg/m^3	870 kg/m^3
Specific heat (Liquid)	2.5 kJ/kg·K	2.5 kJ/kg·K
Specific heat (Solid)	3.2 kJ/kg·K	3.8 kJ/kg·K

The enthalpy–temperature curve of the PCM (paraffin), which freezes little or no supercooling [6.24, 6.25], was obtained from the measured value (Fig. 6.4). Here, the value measured using the HFM was compared with that measured by the DSC method at a heating and cooling rate of 2 ℃/min provided by the manufacturer (Lidy Energy Technology Co., Ltd, China). Subsequently, the relationship between temperature and apparent specific heat, including latent heat, was obtained from the resultant curve to model the PCM using the enthalpy–temperature curve method. The latent heat and phase change temperature regions were calculated based on the measured values. As shown in Table 6.1, the specific heat and density of the solid state were different from those of the liquid state owing to the volume change, and these differences were input into the simulation. The peak melting temperatures were 30 and 29 ℃ in the HFM and DSC, respectively, whereas the peak solidification temperatures were 29 and 28 ℃, respectively (see Fig. 6.4). Moreover, the specific enthalpy between 15 and 40 ℃ for the HFM was 12–18 kJ/kg larger than that of DSC. The difference in the measurement method caused the shifting phase change temperature and different latent heat. In this study, the latent heat of the PCM of 210 kJ/kg, measured using the HFM, was employed because Iten et al. [6.2] reported that a high heating rate (10 ℃/min) underestimated the latent heat, compared with the slow heating rate in DSC (0.2 ℃/min), which was still a much higher heating rate than that in this study (0.05 ℃/min). In this study, a measurement method with a slow heating rate, which reflects an actual environment, was employed, and its results were modeled in the simulation.

6.2.4. PCM modeling

A one-dimensional transient heat conduction finite difference (CondFD) solution algorithm was selected to calculate the layer of construction material in the TES [6.26]. The CondFD model compensates for the limitations associated with the conduction heat transfer function (CTF) algorithm, such as the assumption of constant thermal properties and the inability to provide results for the interior of materials [6.27]. Therefore, the CondFD model, which enables the replication of the phase changes of the PCMs in the simulation, consists of four nodes: interior surface, internal, material interface, and external nodes when the TES calculates the conductive heat transfer [6.26]. For CondFD, a fully implicit first-order scheme was selected. Although the Crank–Nicholson second-order scheme can yield more accurate results than the fully implicit scheme, it can produce results that are physically unrealistic with non-bounded results [6.28, 6,29]. For calculating PCMs, several simulation models select the FullyImplicitFirstOrder scheme because of its robustness and unconditional stability over time [6.28, 6,29]. The FullyImplicitFirstOrder model employed in this study is expressed in the following equations (Eq. 6.6–6.8):

$$C_p \rho \Delta x \frac{T_i^{j+1} - T_i^j}{\Delta t} = \lambda_W \frac{T_{i+1}^{j+1} - T_i^{j+1}}{\Delta x} + \lambda_E \frac{T_{i-1}^{j+1} - T_i^{j+1}}{\Delta x} \quad (6.6)$$

$$\lambda_W = \frac{\lambda_{i+1}^{j+1} - \lambda_i^{j+1}}{2} \quad (6.7)$$

$$\lambda_E = \frac{\lambda_{i-1}^{j+1} - \lambda_i^{j+1}}{2} \quad (6.8)$$

where C_p is the specific heat capacity [J/kg·K], ρ is the density [kg/m^3], λ is the thermal conductivity [W/m·K], x is the length [m], T_i is the temperature [K], t is the time [s], λ_W is the thermal conductivity for interface between node i and node i+1[W/m·K], and λ_E is the thermal conductivity for interface between node i and node i-1 [W/m·K].

The time step for this simulation was 1 min, based on the suggestions of Tabres-Velasco et al. [6.30]. The CondFD algorithm model divides all surfaces automatically using the following equations [6.30] (Eq. 6.9, 6.10):

$$\Delta x = \sqrt{c\alpha\Delta t} = \sqrt{\frac{\alpha\Delta t}{F_o}} \quad (6.9)$$

$$F_o = \frac{\alpha\Delta t}{\Delta x^2} \quad (6.10)$$

where x is the length [m], c is the space discretization constant [-], α is the thermal diffusivity [m^2/s], t is the time [s], F_o is the Fourier number [-]

Regarding the modeling of PCMs, the enthalpy–temperature curve method has been widely used in previous studies [6.29]. When PCMs are simulated, the enthalpy is first updated at each iteration and C_p is developed as follows (Eq. 6.11):

$$C_p = \frac{H_{i,new} - H_{i,old}}{T_{i,new} - T_{i,old}} \quad (6.11)$$

where C_p is the specific heat capacity [J/kg·K], H_i is the specific enthalpy [J/kg], and T_i is the temperature [K].

The limitation of the enthalpy–temperature curve method is that it considers only one enthalpy–temperature curve. Therefore, previous studies had to select the freezing or melting curve depending on the research objectives, and accuracy problems occurred when simulating the phase change of PCMs [6.31]. A new method that considers the hysteresis of PCMs was developed (hereafter called the hysteresis method), considering enthalpy temperature curve for respective phase states. In this study, the specific heat considering the hysteresis observed in the measurement at each time step was calculated using the following equation [6.26]

$$C_p = f(T_{i,new}, T_{i,prev}, PhaseState_{new}, PhaseState_{prev}) \quad (6.12)$$

where C_p is the specific heat capacity [J/kg·K], and T_i is the temperature [K].

The solid and liquid states for thermal conductivity and density were inputted to the hysteresis model. Within the transition region of the hysteresis model the average of the two was used. The iteration scheme assures that the correct enthalpy, and therefore, the correct C_p is used in each time step [6.26].

6.2.5. Simulation cases

Table 6.2 lists the simulation cases for the validation and annual simulations. First, the building and PCM simulation models inputting the actual conditions of the experimental building were validated by comparing them with the field measurement results. To maintain consistency with the field measurements, Room A (test room) was equipped with a radiant floor cooling system using the PCMs, whereas Room B was set as the reference room without the system (Fig. 6.1). Different operating patterns for window-opening and underfloor ventilation were selected to validate the simulation model. Based on the PCM measurement, two PCM modeling methods in the TES, i.e., the enthalpy–temperature curve and hysteresis methods, were tested to prove the effectiveness of the PCM measurement for modeling. To replicate the influence of the window-opening pattern of a naturally ventilated house, a constant flow rate of 0.7 m^3/s, which was calculated using the equation of the outdoor wind

Table 6.2. Simulation cases.

Cases	Window opening pattern		Underfloor ventilation	
	Daytime	Nighttime	Daytime	Nighttime
Validation case (Closed window)	Closed	Closed	Yes	Yes
Validation case (Opened window)	Open	Open	No	Yes
Case 1: Full-day ventilation (UF: Nighttime)	Open	Open	No	Yes
Case 2: No ventilation (UF: Nighttime)	Closed	Closed	No	Yes
Case 3: Day ventilation (UF: Nighttime)	Open	Closed	No	Yes
Case 4: Night ventilation (UF: Nighttime)	Closed	Open	No	Yes
Case 5: Full-day ventilation (UF: Always)	Open	Open	Yes	Yes
Case 6: No ventilation (UF: Always)	Closed	Closed	Yes	Yes
Case 7: Day ventilation (UF: Always)	Open	Closed	Yes	Yes
Case 8: Night ventilation (UF: Always)	Closed	Open	Yes	Yes
Case 9: Full-day ventilation (UF: Daytime)	Open	Open	Yes	No
Case 10: No ventilation (UF: Daytime)	Closed	Closed	Yes	No
Case 11: Day ventilation (UF: Daytime)	Open	Closed	Yes	No
Case 12: Night ventilation (UF: Daytime)	Closed	Open	Yes	No

Daytime: 6:00–18:00, Nighttime: 18:00–6:00

condition and opening area proposed by ASHRAE [6.32] was input to the simulation model when the windows were opened (Eq. 6.13, 14).

$$Q_w = C_w A_{opening} V \tag{6.13}$$

$$C_w = 0.55 - \frac{|Direction\ of\ window - Wind\ direction|}{180} \times 0.25 \tag{6.14}$$

where Q_w is the volumetric air flow rate driven by wind [m^3/s], C_w is the opening effectiveness [-], $A_{opening}$ is the opening area [m^2], V is the wind speed [m/s]

A flow rate of 0.025 m^3/s was set as the infiltration rate for the rooms when the windows were closed. In addition, the results of these modeling methods in the TES were compared with those of the CFD simulation coupled with heat balance analysis, which was constructed and calculated in Chapter 5. The coupled CFD simulation used the enthalpy–temperature curve method to model the PCM. As the accuracy of the TES is similar to that of the coupled CFD simulation, we can consider the TES to be an appropriate method of evaluating the cooling effect of the radiant floor cooling system in a naturally ventilated room. The temperatures were averaged every 10 min to maintain consistency with the field measurements. The results of the simulations were evaluated in terms of the root mean square error (RMSE) and the coefficient of determination (R^2), which are the recommended statistical error tests for building simulations [6.33]. The RMSE was calculated using the simulated value (L_{is}), measured value (L_{im}) and number of data points (N) as follows (Eq. 6.15):

$$RMSE = \sqrt{\sum_{i=1}^{N} \frac{(L_{is} - L_{im})^2}{N}} \tag{6.15}$$

In the subsequent annual simulation after the validation, four window-opening patterns and three types of ventilation for the underfloor space were investigated to clarify the influence of the operation of windows and ventilation fans for the underfloor space on the indoor thermal environments and the effectiveness of the radiant floor cooling system throughout the year. The ventilation fans (0.95 m^3/s) for the underfloor space and the PCMs were installed in Room A. The flow rate of the ventilation fan was proved to be effective in Chapter 5. In Room B, which reflected the current condition of a living room in typical Indonesian apartments, the proposed floor cooling system was not installed, and the room windows were opened during the daytime. The thermal storage effect was evaluated in terms of the indoor air, floor surface, and operative temperatures.

6.3. Results

6.3.1 Validation

6.3.1.1. Closed window case

Fig. 6.5 and Table 6.3 show the temperature results at each point between the measurement and simulation for Rooms A and B with windows closed throughout the day. In Room B (control), the RMSEs of the air and floor surface temperatures were both 0.3 ℃ in the TES and 0.4–0.5 ℃ in the coupled CFD. On Day 2, a rapid decrease in air temperature and solar radiation was observed at the weather station around noon. As shown, the simulated curves had similar trends to the experimentally measured curves, and the R^2 values were 0.98 (TES) and 0.97 (coupled CFD). Both the air and floor surface temperatures in the TES had relatively high accuracy.

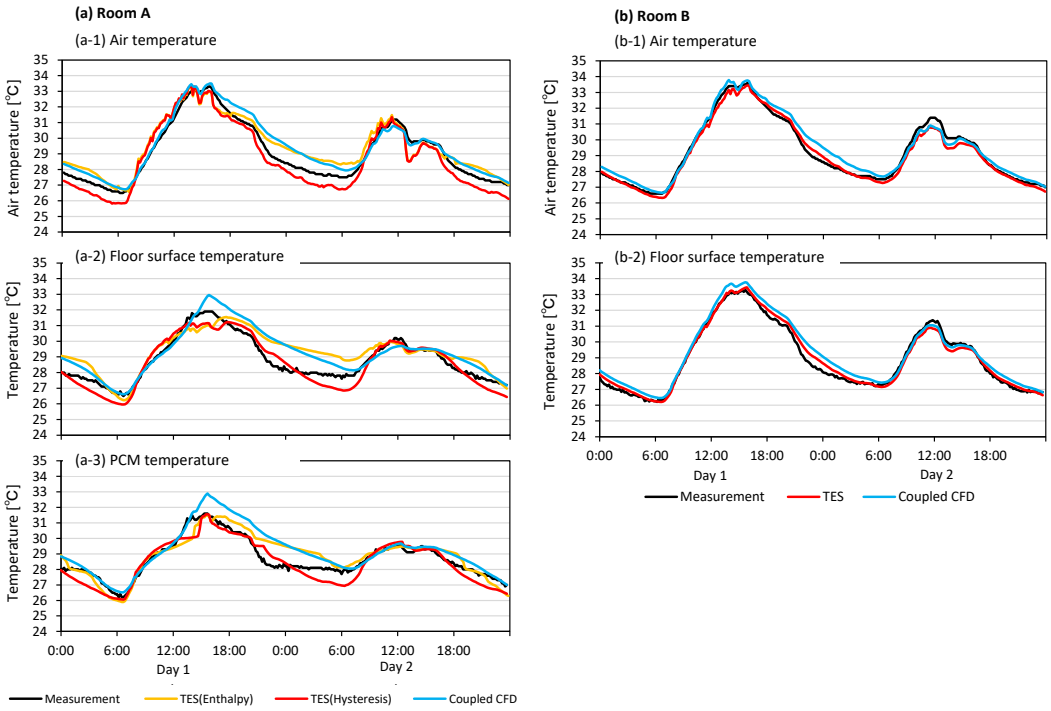

Fig. 6.5. Comparison of (a-1, b-1) air temperature, (a-2, b-2) floor surface temperature, (a-3) PCM temperature in Rooms A (PCM) and B (Control) for closed windows.

Table 6.3. Correlation and deviation of temperature between the field measurement and simulation for closed windows.

Parameter	Room A TES (Enthalpy) RMSE [℃]	Room A TES (Enthalpy) R^2 [-]	Room A TES (Hysteresis) RMSE [℃]	Room A TES (Hysteresis) R^2 [-]	Coupled CFD RMSE [℃]	Coupled CFD R^2 [-]
Air temperature	0.6	0.93	0.6	0.96	0.5	0.96
Floor surface temperature	0.8	0.77	0.5	0.92	0.7	0.85
PCM temperature	0.6	0.81	0.5	0.88	0.7	0.87

	Room B TES RMSE [℃]	Room B TES R^2 [-]	Coupled CFD RMSE [℃]	Coupled CFD R^2 [-]
Air temperature	0.3	0.98	0.4	0.97
Floor surface temperature	0.3	0.98	0.5	0.97

In Room A (PCM), the RMSEs of the air temperature were 0.6 ℃ for both methods in the TES, with an R^2 of 0.93 and 0.96 for the enthalpy–temperature curve and the hysteresis methods, respectively. The diurnal mean floor surface temperatures in Room A were 0.5 ℃ (enthalpy) and 0.7 ℃ (hysteresis) lower than those in Room B in the TES. Compared with Room B, the floor surface temperature rise was slow in both TES and field measurement. In Room A, the delay of the PCM temperature rise around noon (Day 1) affected the large floor surface temperature difference between simulation (TES) and measurement, and it may result in the overestimation the cooling effect. Although the RMSEs in Room A were larger than those in Room B, the overall result demonstrated successful replicability in the cooling effect of the PCM.

For air temperature calculation in Room A, the RMSE of the coupled simulation was 0.1 ℃ lower than that of the TES. Meanwhile, the TES with the hysteresis method had the smallest RMSE and highest R^2 among the three calculation methods for simulating the floor surface and PCM temperatures. In particular, the RMSE in the TES (enthalpy) was 0.2 ℃ larger than that in the TES (hysteresis) during nighttime because the enthalpy temperature curve of the heating process was input to the simulation model. The TES using the hysteresis method had relatively high accuracy when the windows were closed.

6.3.1.2. Opened window case

Fig. 6.6 and Table 6.4 show the temperature comparing the simulation results with the measurement results in Rooms A and B when the windows were opened throughout the day. Because windows were open for an entire day, outdoor air strongly influenced the indoor air temperature in both Rooms A and B. In Room B (control), although the RMSE in the TES was 0.2 ℃ with an R^2 of 0.99, the simulated room air temperature was underestimated in the afternoon when the outdoor wind speed was generally high because a constant ventilation volume (0.7 m^3/s) was input in the calculation model of the TES. Thus, the ventilation volume may have been lower than the actual flow volume in the afternoon. The air and floor surface temperatures may be sensitively influenced by the ventilation volume to a certain level of ventilation volume (see Appendix). For the floor surface temperature, the coupled CFD had a smaller RMSE in the afternoon than the TES because the coupled CFD calculated the air velocity near the floor, and it was used to calculate the convective heat transfer, although the RMSEs of both the coupled CFD and TES were 0.3 ℃. All simulated results of the TES in Room B had relatively high accuracy.

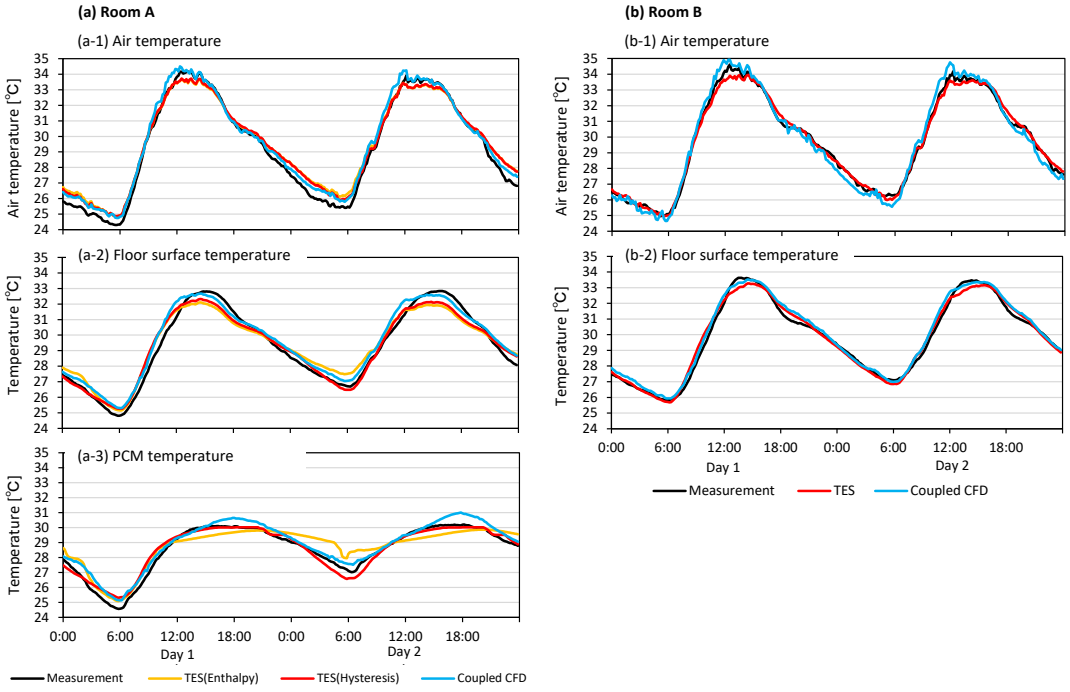

Fig. 6. 6. Comparison of (a-1, b-1) air temperature, (a-2, b-2) floor surface temperature, and (a-3) PCM temperature in Rooms A (PCM) and B (control) for open windows.

Table 6.4. Correlation and deviation of temperature between the field measurement and simulation for open windows.

Parameter	Room A					
	TES (enthalpy)		TES (hysteresis)		Coupled CFD	
	RMSE [℃]	R^2 [-]	RMSE [℃]	R^2 [-]	RMSE [℃]	R^2 [-]
Air temperature	0.6	0.99	0.5	0.99	0.4	0.99
Floor surface temperature	0.6	0.97	0.5	0.97	0.5	0.98
PCM temperature	0.6	0.89	0.3	0.96	0.4	0.97

	Room B			
	TES		Coupled CFD	
	RMSE [℃]	R^2 [-]	RMSE [℃]	R^2 [-]
Air temperature	0.2	0.99	0.4	0.99
Floor surface temperature	0.3	0.99	0.3	0.99

In Room A (PCM), the minimum air and surface temperatures in the early morning were lower than those in Room B owing to the forced nocturnal ventilation for the underfloor space. Even under opened windows case, the cooling effect of the proposed system was observed for both air and floor surface temperatures. The RMSEs of air temperature in Room A were 0.5 ℃ and 0.4 ℃ for the TES using the hysteresis method and the coupled CFD, respectively. As with the results of the control room, the RMSEs of the floor surface temperature in the coupled CFD method were 0.2 ℃ and 0.4 ℃ smaller than those of the TES using the hysteresis method and the enthalpy method, respectively, in the afternoon because the relatively high air velocity of 0.4 m/s, which influenced the convective heat transfer, was observed near the floor surface (FL+0.1 m) during the field measurement period. The maximum floor surface temperature deviation from the measurement results was 1.0 ℃ (coupled CFD) and 1.1 ℃ (TES using the hysteresis method). For the PCM temperature, the RMSE of the TES using the hysteresis method was the smallest among the three calculation methods, with an RMSE of 0.3 ℃ and R^2 of 0.96. The maximum PCM temperature deviation between the TES (hysteresis) and measurement was 0.9 ℃. In both closed and open window cases, the hysteresis method exhibited a smaller RMSE than the enthalpy method in the TES. Hysteresis strongly contributed to the accuracy of calculating the PCM temperature.

Fig. 6.7 shows a comparison of the simulation results with the measurement results in Room A when the windows were opened throughout the day. A constant flow rate of 0.7 m^3/s and variable flow rate calculated every time step were compared. Because the flow rate depends on the outdoor wind speed (V), the nocturnal wind condition was calm, and the flow

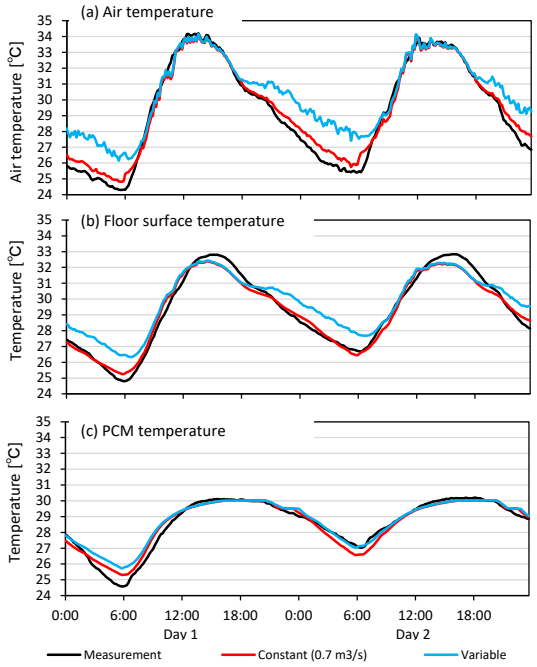

Fig. 6.7. (a) Air temperature, (b) floor surface temperature, and (c) PCM temperature for open windows.

rate was almost zero, the nocturnal air temperature tended to be high compared with the results of a constant flow rate. Based on the RMSE and R^2, a constant flow rate of 0.7 m^3/s, which was determined by the averaged flow rate using the above equation during the measurement period, was more suitable than the variable flow rate at every time step to replicate the full-day ventilation condition. The calculation of the appropriate flow rate will be investigated in a future study.

Although the constant air flow rate for the room was input to the TES model, and the TES does not consider the air flow distribution in naturally ventilated buildings, compared with the coupled CFD, the accuracy of the TES was higher than that of previous studies [6.12–6.17]. The RMSEs of the air temperature calculated using the TES in Rooms A and B were similar to those of the coupled CFD simulation. For the annual simulation of radiant floor cooling systems in naturally ventilated buildings, coupled CFD is unfeasible because of the considerable calculation cost. Considering the calculation cost, the TES model with the hysteresis method was used in the subsequent annual simulation.

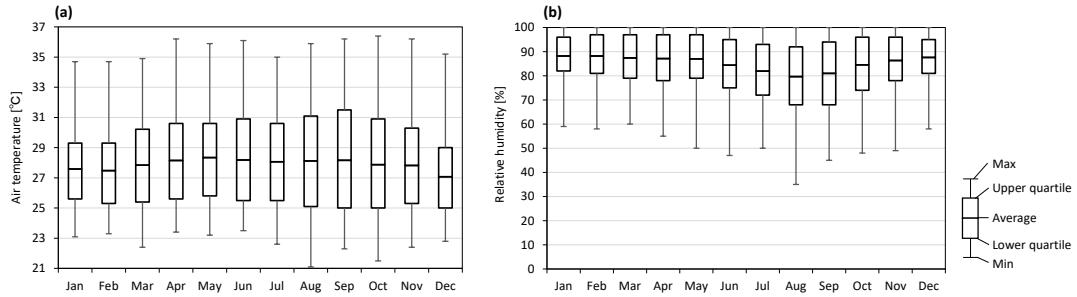

Fig. 6.8. (a) Outdoor air temperature and (b) outdoor relative humidity range in 2020.

6.3.2. Annual simulation

6.3.2.1. Annual weather data

Fig. 6.8 presents the weather data from the experimental field in 2020. Although Indonesia has two seasons (rainy and dry seasons), the annual temperature range is only 1.3 ℃. The outdoor temperature ranged from 21.1 to 36.4 ℃ with diurnal and nocturnal averages of 28.9–31.0 ℃ and 25.2–26.1 ℃, respectively. The outdoor air temperature in the experimental field in 2020 was similar to recent weather observation data (2005–2020) at the nearest official weather station (Tangerang) [6.34]. The average RH was 87.6% and 83.0% during the rainy season (December–May) and dry season (June–November), respectively. The monthly minimum RH was less than 50% during the dry season.

6.3.2.2. Variation in air temperature

Fig. 6.9 shows the variations in the air temperature averaged for each month for Room A under different window-opening patterns and underfloor ventilation (Cases 1–12). The air temperature was lower when the windows were kept closed during the daytime in the presence of the PCM exposed to nighttime underfloor ventilation. In Case 4 (night ventilation), the diurnal temperature was the lowest among the four ventilation modes, and the average diurnal temperature ranged from 28.1 to 28.9 ℃ for a year owing to the opening of the windows at night and closing them during the daytime. In Cases 1–4, the underfloor space was ventilated at night. The largest temperature difference between Cases 1 (full-day ventilation) and 2 (no ventilation) was 1.3 ℃ in September when the highest temperature was observed. Meanwhile, the temperature difference between Cases 1 and 2 in January, February, and

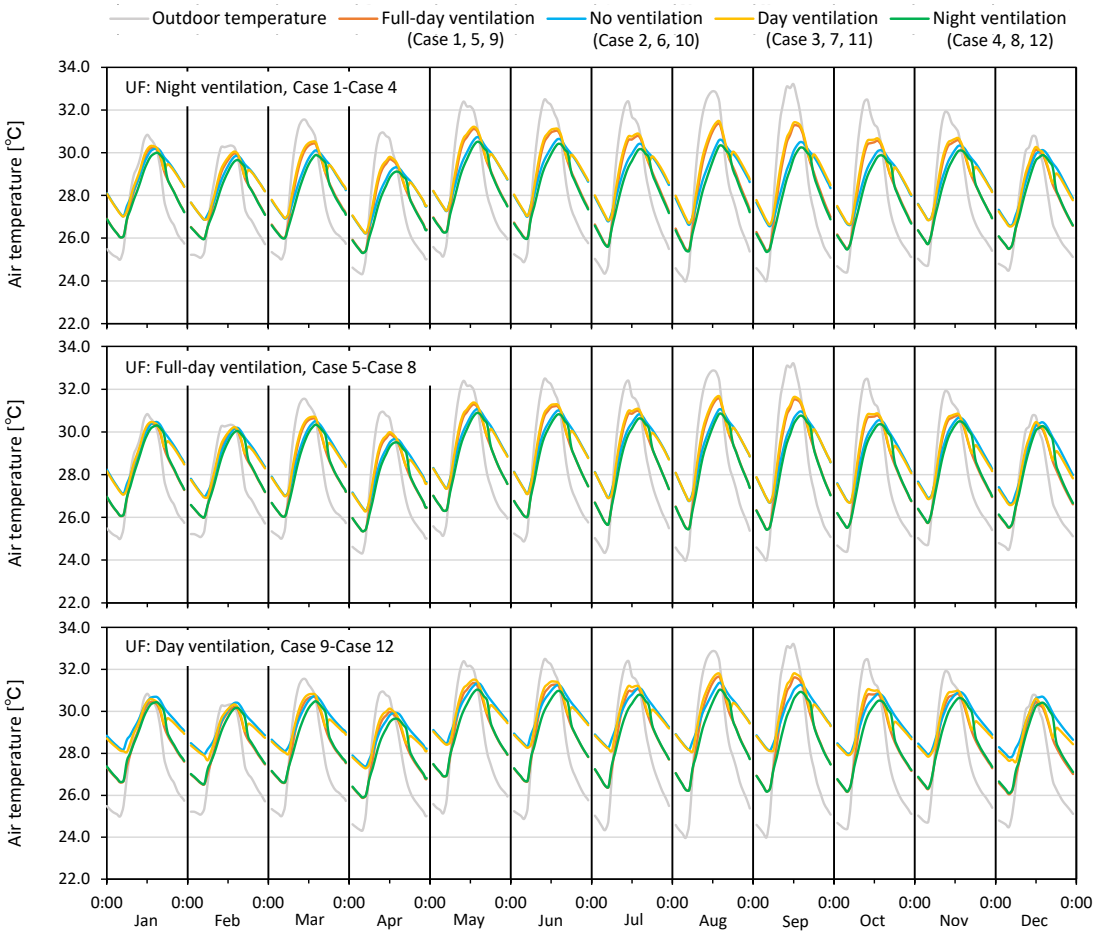

Fig. 6. 9. Air temperature variations for each month in Room A under different types of ventilation for indoor and underfloor spaces.

December, when the diurnal mean outdoor temperature was less than 29.5 °C, was not large. The results in Chapter 4 suggested that the ambient temperature of PCMs should be 2–3 °C higher than the set-point melting temperature to sufficiently utilize the thermal storage effect during the daytime. The temperature difference between September and other relatively cool months was caused by the effectiveness of the PCM thermal storage. The thermal storage was particularly increased because closing the windows during the daytime contributed to the retention of air cooled by the radiant floor cooling system.

When the underfloor space was ventilated throughout the day (Cases 5–8), the daily temperature fluctuations became larger compared with the cases of underfloor night ventilation (Cases 1–4). The daily temperature ranged from 25.3 to 31.3 °C and 25.3 to 31.5 °C in Cases 1 and 5, respectively. The underfloor ventilation during the daytime assisted the heat

accumulation of the PCM; thus, the maximum temperature in Case 5 increased by 0.2 ℃. Owing to the heat accumulation of the PCM, the temperature difference between Cases 5 (full-day ventilation) and 6 (no ventilation) in September was 1.0 ℃. When the windows were closed, the heat accumulation of the PCM was more prominent than when the windows were opened.

Similarly, the day ventilation for the underfloor space (Cases 9–12) increased the air temperature owing to the heat accumulation of the PCM during the daytime. The diurnal average temperatures were 28.8–30.6 ℃ in Cases 9–12. The nocturnal mean air temperature in Case 12 was 0.4–0.6 ℃ higher than that in Case 4 because the radiant floor cooling system could not sufficiently dissipate the heat from the PCM at night. Among all cases, the room and underfloor ventilation settings of Case 4, which employed night ventilation for both the room and underfloor space, had the best performance as it achieved the lowest temperature during the daytime. Several researchers have observed similar conclusions for cooling the indoor thermal environment of hot and humid climates using night ventilation [6.35–6.37]. Moreover, PCMs with night ventilation have been demonstrated to be highly efficient. This proves that the TES can consider the influence of the window-opening pattern on the cooling effect of

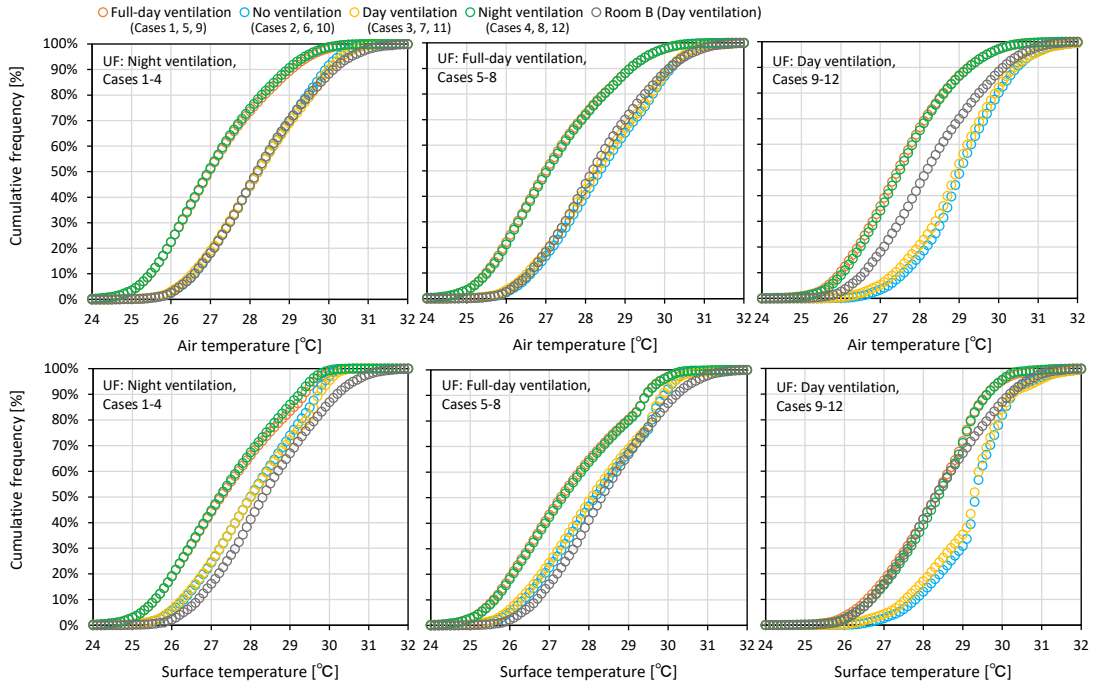

Fig. 6.10. Cumulative frequency of air temperature and floor surface temperature – daytime results 6:00 to 18:00 in Rooms A (test room) and B (control room).

PCMs. Underfloor night ventilation is crucial to improving the thermal storage effect of PCMs throughout a year.

6.3.2.3. Reduction in air and floor surface temperature

Fig. 6.10 presents the cumulative frequency of the air temperature and floor surface temperature for a year during the daytime in Rooms A (test room) and B (control room). Owing to the latent heat of the PCMs, the diurnal average air and floor surface temperatures in Room A was lower than those in Room B in all cases. For Room A, comparing Case 3 (day ventilation) with Case 4 (night ventilation), the maximum differences in the air and floor surface temperature were 0.7 and 0.3 ℃, respectively. Meanwhile, the maximum differences in the air and floor surface temperatures between Cases 11 (day ventilation) and 12 (night ventilation) were 1.1 and 1.1 ℃, respectively. The results of Chapters 3 and 4 indicated that the thermal storage effect of PCMs is influenced more by their thermal mass and cooling strategy at night than by convective heat transfer. These results imply that the influence of the

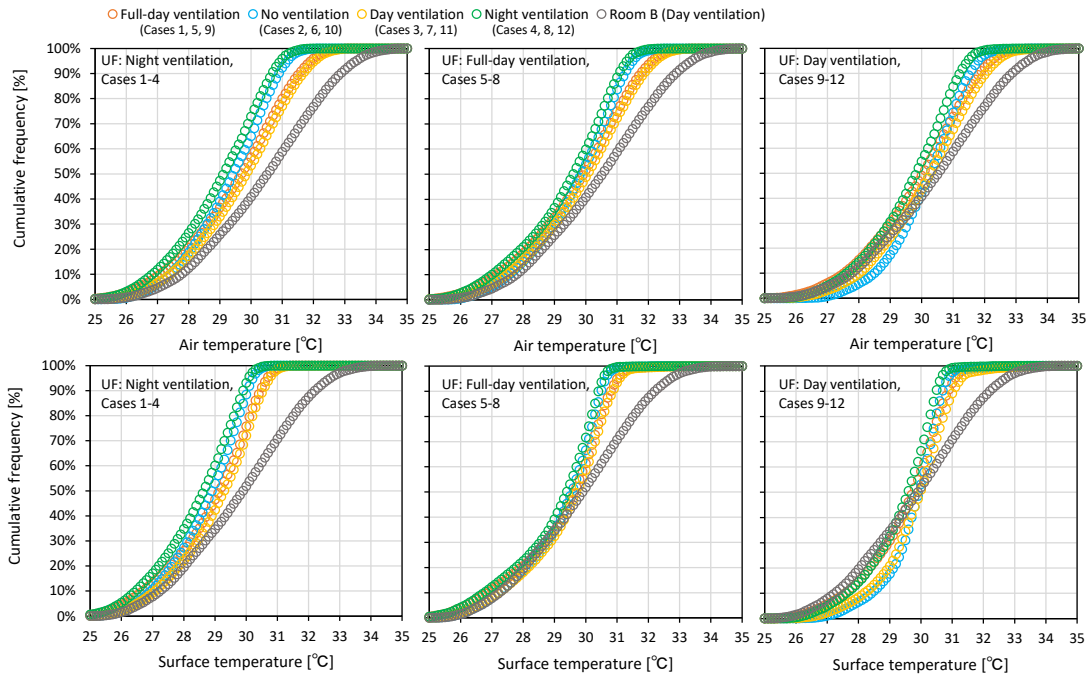

Fig. 6.11. Cumulative frequency of air temperature and floor surface temperature – nighttime results 18:00 to 6:00 in Rooms A (test room) and B (control room).

Table 6. 5. Annual air temperature and floor surface temperature range in Rooms A (test room) and B (control room) during daytime (6:00–18:00) and nighttime (18:00–6:00)

	Air temperature [℃] min–max (avg.)	Floor surface temperature [℃] min–max (avg.)
Daytime		
Room B	24.8–35.0 ℃ (30.4 ℃)	24.5–34.5 ℃ (29.8 ℃)
Case 1	23.2–33.3 ℃ (29.5 ℃)	23.1–31.6 ℃ (28.8 ℃)
Case 2	24.5–32.3 ℃ (29.3 ℃)	24.1–31.1 ℃ (28.7 ℃)
Case 3	24.2–33.4 ℃ (29.7 ℃)	24.1–31.6 ℃ (29.0 ℃)
Case 4	23.1–32.1 ℃ (28.9 ℃)	23.0–30.9 ℃ (28.4 ℃)
Case 5	23.2–33.6 ℃ (29.7 ℃)	23.1–33.4 ℃ (29.2 ℃)
Case 6	24.5–32.8 ℃ (29.6 ℃)	24.2–32.5 ℃ (29.2 ℃)
Case 7	24.3–33.8 ℃ (29.8 ℃)	24.1–33.6 ℃ (29.4 ℃)
Case 8	23.2–32.5 ℃ (29.3 ℃)	23.1–32.1 ℃ (29.0 ℃)
Case 9	24.2–34.0 ℃ (29.8 ℃)	24.4–33.9 ℃ (29.5 ℃)
Case 10	25.5–33.5 ℃ (30.1 ℃)	25.6–33.4 ℃ (29.8 ℃)
Case 11	25.0–34.3 ℃ (30.1 ℃)	25.3–34.1 ℃ (29.8 ℃)
Case 12	24.3–33.1 ℃ (29.6 ℃)	24.5–33.0 ℃ (29.3 ℃)
Nighttime		
Room B	24.5–32.1 ℃ (28.3 ℃)	24.6–32.1 ℃ (28.4 ℃)
Case 1	23.1–31.1 ℃ (27.1 ℃)	23.1–30.6 ℃ (27.4 ℃)
Case 2	24.5–31.4 ℃ (28.2 ℃)	24.1–30.5 ℃ (28.0 ℃)
Case 3	24.4–31.5 ℃ (28.3 ℃)	24.2–30.6 ℃ (28.0 ℃)
Case 4	23.0–31.3 ℃ (27.1 ℃)	23.0–30.5 ℃ (27.3 ℃)
Case 5	23.0–31.8 ℃ (27.1 ℃)	23.0–32.0 ℃ (27.4 ℃)
Case 6	24.5–32.3 ℃ (28.4 ℃)	24.2–32.0 ℃ (28.2 ℃)
Case 7	24.4–32.4 ℃ (28.3 ℃)	24.1–32.1 ℃ (28.1 ℃)
Case 8	23.1–32.1 ℃ (27.2 ℃)	23.1–31.8 ℃ (27.4 ℃)
Case 9	23.8–31.9 ℃ (27.5 ℃)	24.4–32.1 ℃ (28.2 ℃)
Case 10	25.5–32.8 ℃ (29.1 ℃)	25.6–32.5 ℃ (29.2 ℃)
Case 11	25.2–32.6 ℃ (28.9 ℃)	25.4–32.4 ℃ (29.1 ℃)
Case 12	23.9–32.4 ℃ (27.6 ℃)	24.5–32.1 ℃ (28.3 ℃)

window-opening pattern on the floor surface temperature may not be significant compared with air temperature if the PCMs dissipate the heat sufficiently on previous nights.

The maximum floor surface temperatures in Cases 1–4 were 1.2–2.5 ℃ lower than those in Cases 5–12 because of the thermal storage of the PCM and avoidance of the large heat accumulation from the underfloor space during the daytime. In particular, the thermal storage effect of the PCM was more effective in reducing the peak floor surface temperature than the diurnal mean floor surface temperature because the latent heat tended to maintain the constant temperature. Compared with Room B (control room), the peak air and floor surface temperatures in Case 4 decreased by 2.9 and 3.6 ℃, respectively, owing to the PCM.

Fig. 6.11 depicts the cumulative frequency of the nocturnal air and floor surface temperature for a year in Rooms A and B. A previous study indicated that lightweight structures were cooler than high thermal mass structures during the nighttime [6.38]. Nevertheless, the nocturnal average floor surface temperature in Room A (Case 3) was 0.3 ℃ lower than that in Room B because the ventilation fans for the underfloor space dissipated the heat effectively at night.

For the closed windows during the nighttime, both air and floor surface temperatures tended to be high because closing windows at night cannot effectively dissipate the heat from the building structure. In Case 10, which was the hottest case among the 12 cases, the nocturnal average air and floor surface temperatures were 29.1 and 29.2 ℃, respectively. Daytime ventilation for the underfloor space and closing windows during the nighttime should be avoided to maintain a cool indoor thermal environment.

6.3.2.4. Operative temperature evaluation

The resultant indoor thermal comfort in Rooms A (with PCM) and B (without PCM) was evaluated using the operative temperature (OT) to clarify the influence of air and floor

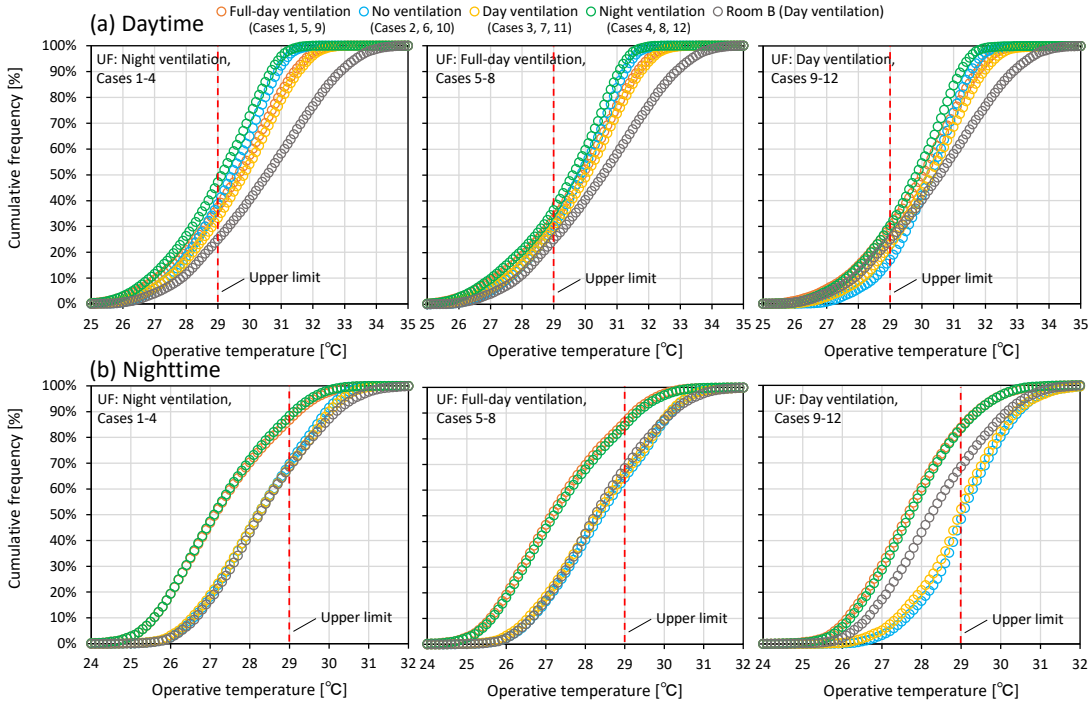

Fig. 6.12. OT with 80% upper comfort limit in Rooms A (test room) and B (control room) during (a) daytime and (b) nighttime.

Table 6.6. Thermal comfort evaluation with OT.

	Daytime	Nighttime
Room B (control room)	25%	69%
Room A (test room)		
Case 1	37%	89%
Case 2	39%	72%
Case 3	33%	71%
Case 4	47%	90%
Case 5	32%	88%
Case 6	30%	68%
Case 7	29%	70%
Case 8	36%	87%
Case 9	29%	85%
Case 10	17%	54%
Case 11	23%	58%
Case 12	30%	84%

surface temperature reduction on thermal comfort. The 80% upper comfort limit of the OT was calculated according to a previous study on naturally ventilated buildings in hot-humid climates, as follows (Eq. 6.16) [6.39].

$$T_{upper} = 0.57T_{outdm} + 13.1 \quad (6.16)$$

where T_{outdm} is the daily mean outdoor air temperature [℃], i.e. the 24-hour arithmetic mean for the day in question, and T_{upper} is upper comfort operative temperature [℃]. Based on the daily upper comfort OT limit calculated using Eq. 6.16 and T_{outdm} obtained from the weather data in the experimental field, the annual average OT limit was estimated as 29.0 ℃.

Fig. 6.12 depicts the annual OT range in Rooms A and B during the daytime and nighttime with the upper comfort unit. In Room B, the diurnal average OT was 30.4 ℃. Meanwhile, in Cases 5–8 (full-day ventilation for the underfloor space), the mean OTs in Room A during the daytime were 29.3–29.8 ℃, because the increased thermal mas of the PCMs reduced the daily air temperature and mean radiant temperature (MRT) fluctuation. In Cases 1–4 (night ventilation for the underfloor space), the diurnal average OT in Room A was 28.9–29.6 ℃. Compared with Case 1, the thermal comfort period in Case 4 increased by 10% during the daytime because minimizing the ventilation prevented the inflow of hot outdoor air. This result was consistent with the findings of Kubota et al. [6.40]. In Case 4, the thermal comfort period was approximately half (47%) that of the daytime and 90% that of the nighttime. Nocturnal ventilation for the room and the underfloor space maximized the thermal comfort period evaluated using the OT.

6.3.2.5. Phase change state for an entire year

Fig. 6.13 shows the utilization rates of the PCM for each case. The PCM utilization rate was employed to evaluate the phase change state in a previous study [6.41]. Based on the PCM temperature, the PCM utilization rate was calculated as follows (Eqs. 6.17–6.18):

$$PCM\ utilization\ rate = (\beta_{max} - \beta_{min}) \times 100 \tag{6.17}$$

$$\beta = \begin{Bmatrix} 0 \\ \frac{T-T_s}{T_l-T_s} \\ 1 \end{Bmatrix}, \begin{matrix} T \le T_s \\ T_s < T < T_l \\ T \ge T_l \end{matrix} \tag{6.18}$$

where β_{min} and β_{max} are the minimum and maximum liquid fractions for each day [-], T is the PCM temperature [℃], T_s is the solidification temperature [℃], and T_l is the melting temperature [℃].

In Cases 1–4 (night ventilation for the underfloor space), the annual mean was 66.2%–72.8%. The annual average outdoor temperature was 27.9 ℃. On February 3, the utilization rate in Cases 1 and 4 was 0% because the lowest daily mean temperature of 26.0 ℃ was observed. The phase state of the PCM was the solid state throughout the day; thus, the radiant floor cooling system could not utilize the latent heat. The maximum utilization rates of the PCM in Cases 1–4 did not reach 100%. This implies that the PCM did not melt completely during the day from the solid condition when the underfloor space was ventilated at night.

When full-day ventilation for the underfloor space was applied (Cases 5–8), the annual average utilization rate increased to 90.7%–91.5%. Approximately 45% of the day for a year, the utilization rate reached 100%, achieving complete solidification and melting within a single day. In Cases 9–12 (day ventilation for the underfloor space), unlike the case of the full-day ventilation for the underfloor space, reaching a utilization rate of 100% was difficult

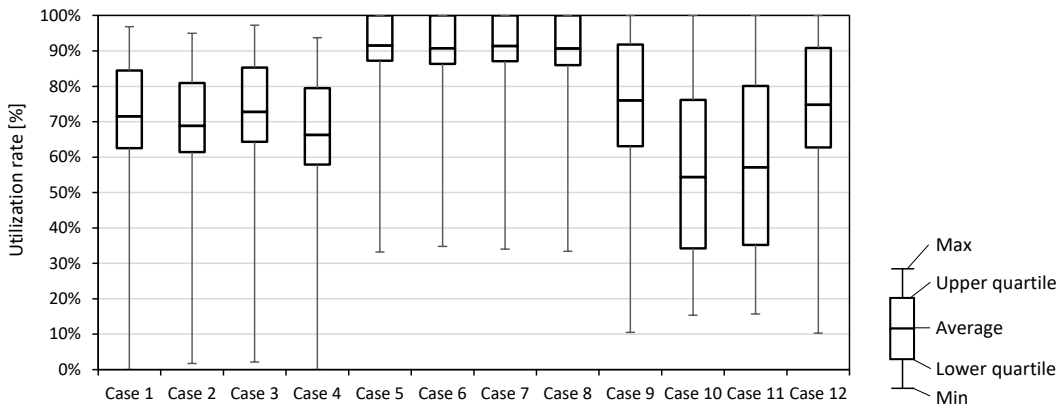

Fig. 6.13. Utilization rate of the PCM for each case.

for several days in succession. To achieve a utilization rate of 100% in Cases 9–12, the utilization rate of the previous days had to be low, which means that the phase state of the PCM tended to be in a solid state in previous days. In Cases 10 and 11, whose floor surface temperature was relatively high compared with the other cases, the annual average utilization rate was 54.3%–57.1%. Nevertheless, the high utilization rate did not necessarily result in a low floor surface temperature because the floor surface temperatures in Cases 5–8 were higher than those in Cases 1–4. Because the cooling effect of the PCM decreased dramatically after a phase change process [6.42], nocturnal ventilation (Cases 1–4), with an annual average utilization rate of approximately 70%, would be an effective ventilation mode for the underfloor space to reduce floor surface temperature while maintaining the cooling effect in the afternoon.

6.3.2.6. Problem of condensation using the radiant floor cooling system

Condensation causes mold and mite problems when radiant cooling systems are installed under hot and humid conditions, including in Indonesia [6.43, 6.44]. In particular, the risk of the problem can be high during the rainy season because of the increase in RH. Fig. 6.14 shows the total time of condensation of the floor surface in a year for each case. The cases that ventilated the underfloor space at night, such as Cases 1, 3, and 4, had a high chance of

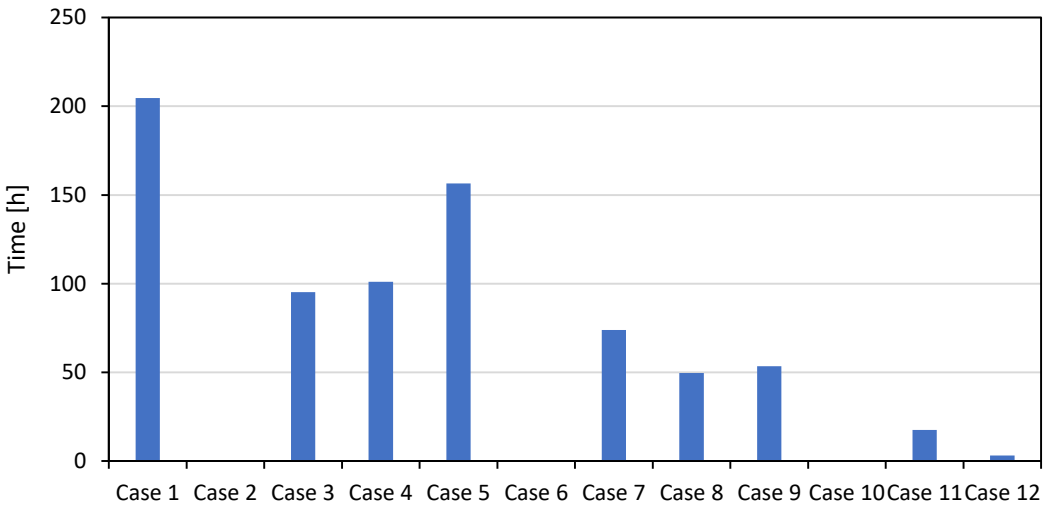

Fig. 6.14. Chances of condensation of floor surface in Room A for each case.

condensation owing to the low floor surface temperature. In Case 1, the longest condensation time of 205 h on the floor was observed. Meanwhile, in Case 2 with closed windows during the daytime, condensation did not occur, although the indoor RH range of 50.6%–96.8% and the floor surface temperature range of 24.1–31.1 ℃ were similar to those in Case 3. Condensation often occurred between 6:00 and 8:00 when the windows were opened during the corresponding periods. Humid outdoor air (more than 90% RH) entered the room if the windows were opened in the morning, causing condensation. Nevertheless, the condensation time was only 0%–2.3% for the year for all cases. The radiant cooling system in the previous study was primarily cooled by chilled water with a supply temperature of 17–22 ℃ [6.43, 6.44]. The risk of condensation in the proposed floor cooling system was much lower than that in the previous study because it utilized free cooling.

6.4. Discussion

6.4.1. PCM modeling

Although the relatively small supercooling is a characteristic of organic PCMs such as paraffin [6.24], the supercooling and peak phase change temperature are dependent on the measurement method and cooling rate, and it strongly affects the calculation results [6.45, 6.46]. Comparing the hysteresis and enthalpy methods, although the supercooling was only 1 ℃, the results of the hysteresis and enthalpy methods exhibited different PCM temperature trends in the simulation, particularly at night. The TES using the hysteresis method improved the accuracy of calculating the PCM temperature.

Both the peak melting and solidification temperatures measured by the HFM were 1 ℃ higher than those measured using DSC. As shown in Fig. 6.6a-3, the PCM temperature in the afternoon tended to remain at 30 ℃ in the field measurement, and the simulated curve was similar to the trend of the field measurement. When the simulation adopted the value measured using DSC, the PCM temperature in the afternoon would decrease by approximately 1 ℃. Meanwhile, the PCM temperature during the night calculated using the TES hysteresis method would also be significantly lower than the measured PCM temperature when the enthalpy–temperature curve based on the DSC was input to the simulation. Measuring the PCM using the HFM contributed to improving the accuracy of calculating the PCM temperature.

6.4.2. Comparison between TES and coupled CFD

In Room B (control), the RMSE of the air temperature in TES was 0.1–0.2 ℃ lower than that in the coupled CFD conducted in Chapter 5, whereas the RMSE of the air temperature calculated using the TES using the hysteresis method was 0.1 ℃ larger than that in the coupled CFD in Room A (PCM). In Room B, the air temperature tended to be uniform in the field measurement presented in Chapter 4; thus, the accuracy even in the TES, which cannot consider the air temperature distribution, was similar to that in the coupled CFD simulation. In contrast, the air temperature gradient was observed in Room A in the measurement shown in Chapter 4 because the radiant floor cooling system cooled the air in the lower part of the room. Therefore, the accuracy of the air temperature using coupled CFD, which considers the heterogeneity of the temperature, was higher than that using the TES. Although the coupled simulation can be used to calculate the air temperature of a room with installed PCMs accurately, the TES can also calculate the air temperature relatively accurately, with an RMSE of less than 0.6 ℃ and an R^2 of more than 0.95.

For the floor surface temperature in Room A (PCM), the coupled CFD had higher accuracy than the TES when the relatively high air velocity (0.4 m/s on average) was observed near the floor surface because the coupled CFD calculated the convective heat transfer coefficient at every time step based on the air velocity near the floor surface. Nevertheless, a clear surface temperature difference between the coupled CFD and TES was not observed at night and in the morning when the air velocity near the floor was low. Moreover, the RMSE in the TES using the hysteresis method was 0.2 ℃ lower than that in the coupled simulation when the windows were closed for an entire day. The coupled CFD employed the modified Launder-Kato model [6.47] with the temperature wall function [6.48] to calculate the convective heat transfer of the building surface. At high Reynolds numbers, CFD simulations are often combined with the wall function; however, their accuracy decreases at high Richardson numbers [6.49]. Pandey et al. [6.19] reported that the EnergyPlus model underpredicted the experimental data during forced convection, compared with coupled CFD using a high Reynolds number model with wall function, whereas no significant difference was observed in the accuracy coupled CFD and TES tools during natural convection. In this study, the influence of forced convection was significant in the target building when the windows were opened and the outdoor wind speed was high, whereas the influence of natural convection was enhanced when the windows were closed. The TES can be used to accurately calculate the floor surface temperature of the radiant floor cooling system using PCMs in rooms influenced by natural convection. Overall, the validation results in the TES showed that the RMSE for open windows was acceptable compared with previous studies [6.10, 6.35–6.37]. We can conclude that the TES with the hysteresis method is widely applicable for evaluating the annual temperature in buildings equipped with PCMs.

6.4.3. Thermal comfort evaluation

In Case 4, the thermal comfort period in Room A, which was assessed using the OT, increased to 68.5% a year when the windows were closed during the daytime and opened during the nighttime, compared with Room B (66.0% a year). Alfata et al. [6.36, 6.37] reported that the thermal comfort period in a modern apartment in Indonesia, which was constructed using a building material similar to that of the target building, was 24%–47% when night ventilation was applied. The thermal comfort period in a naturally ventilated Malaysian terraced house, which consisted of brick walls and reinforced concrete slabs, was 27%–38% [6.51, 6.52]. Compared with the thermal comfort period in Room B and previous studies, the proposed radiant floor cooling system increased the thermal comfort period even when the OT was used for the evaluation.

This study indicated that nocturnal ventilation for the room and underfloor space is the optimum operation to maximize the thermal comfort period evaluated using the OT. Nevertheless, the OT does not consider convective and evaporative heat exchanges through sweating between the occupants and ambient environment. The influence of evaporative heat loss on thermal comfort is considerable under hot conditions, such as in the tropics, including Indonesia. Although the thermal comfort period was 68.5% under night ventilation, enhancing the convective and evaporative heat exchange through natural ventilation can further improve thermal comfort under suitable weather conditions (i.e., higher wind speed and lower air temperature). Therefore, the window-opening patterns should be optimized to control natural ventilation to improve convective and evaporative heat exchange while maintaining the thermal storage effect of the proposed radiant floor cooling system. A simulation method, such as an air flow network model that can evaluate the influence of natural ventilation with light calculation load coupled with TES, should be constructed to evaluate thermal comfort annually in Chapter 7.

6.4.4. Influential factors to utilize the latent heat of the PCM

Among the 12 cases, the lowest floor surface temperature was obtained in Case 4. Based on the results of Case 4, this section discusses the influential factors of the PCM utilization rate, which was determined by the daily liquid fraction difference between the maximum liquid fraction (β_{max}) and minimum liquid fraction (β_{min}) to fully utilize the latent heat of the PCMs. Previous studies have indicated that the ambient temperature of PCMs influences their liquid fraction [6.18, 6.41]. Fig. 6.15a presents the influence of the daily maximum air temperature in the underfloor space on β_{max}, and a strong positive correlation was obtained (R=0.99). In this study, the peak melting temperature of the PCMs was in the range of 29–30 °C. When the daily maximum temperature was 30.4 °C, β_{max} was 95%. This

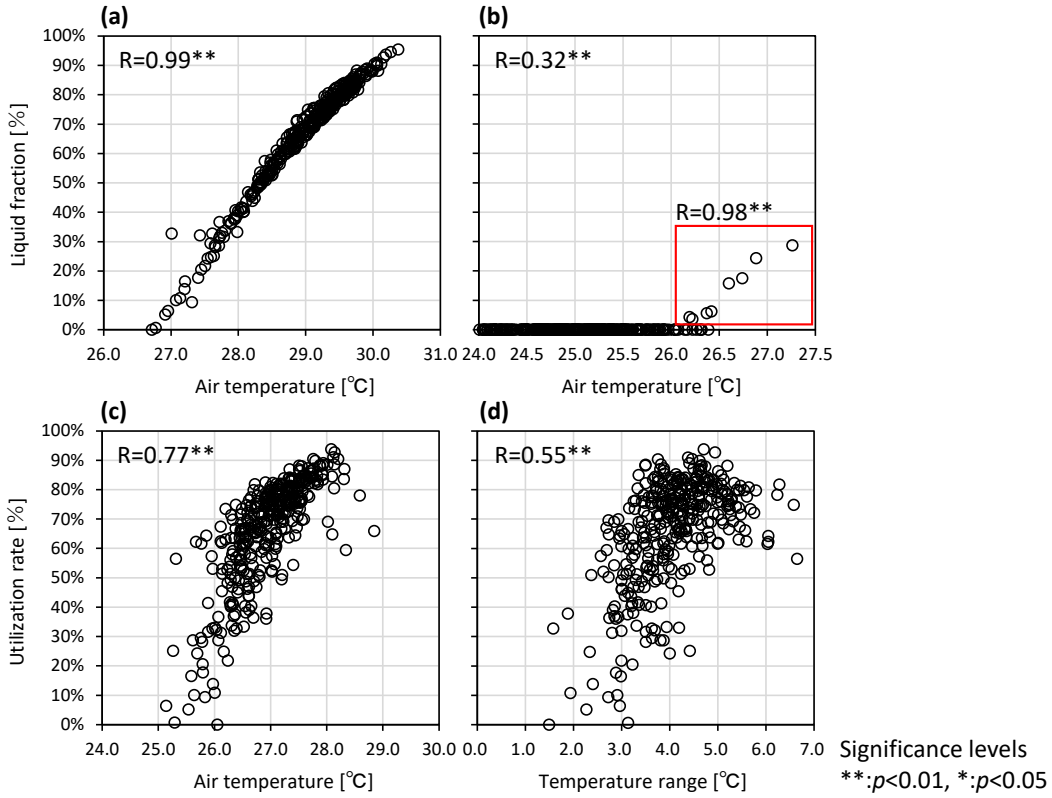

Fig. 6.15. Correlation between (a) β_{max} and daily maximum air temperature in the underfloor space, (b) β_{min} and daily minimum air temperature in the underfloor space, (c) utilization rate and daily mean temperature in the underfloor space, and (d) utilization rate and air temperature range in the underfloor space in Case 4.

implies that if the ambient temperature is approximately 0.5 ℃ higher than the peak melting temperature, most PCMs would melt. Baetens et al. [6.53] reported that the diurnal average temperature affects the melting temperature of PCMs. In this study, the diurnal average temperature had a strong relationship (R=0.82); however, the daily maximum ambient temperature of the PCMs was optimal for selecting a proper melting temperature.

For the solidification temperature of the PCMs, the correlation between β_{min} above 0% and the daily minimum air temperature in the underfloor space, shown in a red rectangle, had a strong relation of 0.98, with a peak solidification temperature of 28–29 ℃. For the PCMs to solidify completely, the phase state during the previous day is also an influential factor. When the daily minimum temperature was 26.2 ℃, β_{max} during the daytime and β_{min} the following night were 91% and 4%, respectively. An ambient temperature of 26 ℃ may be necessary to ensure the solidification of the PCM regardless of β_{max} during the daytime. These

results imply that an ambient temperature range of at least 4.5 ℃ is necessary to fully utilize the latent heat of PCMs. This suggestion is consistent with Chapter 4.

Nevertheless, a moderate relationship (R=0.55) was observed between the PCM utilization rate and diurnal temperature range. The daily average temperature was more influential in maximizing the utilization rate, exhibiting a strong relationship (R=0.77). Previous studies have suggested that the selection of a phase change temperature is based on the daily average temperature [6.54, 6.55]. Lei et al. [6.56] reported that a phase change temperature of approximately 28–29 ℃ is suitable in Singapore, where the reported daily average temperature was 28 ℃, although their simulation did not consider the hysteresis of the PCMs. Therefore, they indicated that accuracy problems may occur if PCMs exhibit hysteresis [6.56]. The result of the annual simulation considering hysteresis suggests that the daily average ambient temperature of PCMs is a suitable criterion for selecting the phase change temperature of PCMs even in hot and humid regions, where the diurnal temperature range is relatively small. If the PCMs have a large temperature difference between the peak melting and solidification temperatures, the daily maximum and minimum ambient temperatures can be another useful guideline for selecting a phase-change temperature. The results for the floor surface temperature in Cases 1–8 indicated that a utilization rate of 100% did not necessarily lead to a low floor surface temperature (see Section 6.3.2.4). Nevertheless, Chapter 4 showed that a higher utilization rate of the latent heat of PCMs results in a large floor surface temperature reduction. In Cases 1–4, β_{max} was 96%–98% throughout the year, and β_{min} decreased to 0% in 94%–98% of the day for a year. The resultant annual average utilization rate was 66%–73%. Meanwhile, in Cases 5–8, β_{max} reached 100% in 47%–53% of the days for a year. Iten et al. [6.42] reported that the cooling effect of PCMs decreased significantly after they melted completely. β_{max} strongly affects the retention of the thermal storage effect of PCMs. To maximize the thermal storage effect of PCMs, a higher utilization rate must be maintained while avoiding a β_{max} of 100%. In this annual simulation, a reasonable annual average utilization rate of approximately 70% was determined to achieve a low floor surface temperature throughout the year. Furthermore, β_{max}, which was influenced by the daily maximum ambient temperature of the PCM, affected the annual utilization rate when the PCM solidified completely at night.

6.5. Summary

Chapter 6 aims to evaluate the annual performance of the proposed floor cooling system that consider the hysteresis of PCM and to determine its design guidelines and indicators to maximize thermal storage effect of PCMs in the building throughout a year in a hot and humid climate. First, the thermal properties of a full-scale PCM product were determined using the heat flow method (HFM). Subsequently, a TES model based on the

results of the PCM measurement was constructed for the full-scale experimental building. The TES model was validated by comparison with the results of field measurements and coupled CFD simulations under naturally ventilated conditions. Using the validated TES model, an annual simulation was conducted for the target building to examine its applicability of the TES model. Influential factors affecting the thermal storage effect of the floor cooling system were analyzed based on the results of the annual simulation. The main findings are summarized as follows.

- The reproducibility of the PCM temperature trend when using the HFM was superior to that of differential scanning calorimetry (DSC) testing. An HFM with slow cooling and heating rates is an appropriate measurement method for PCMs installed in buildings, where the temperature variation is slow, to capture such a sensitive phase change of the PCMs. Although paraffin has a small supercooling, where the peak phase change temperature difference is only 1 ℃ between the melting and solidification states, the difference in PCM temperature between the hysteresis and enthalpy methods was large at night. The PCM temperature calculation was influenced more by the hysteresis than by the accurate convective heat transfer coefficient using coupled CFD in the target system. Under the given building conditions, measuring the PCM using the HFM contributed to improving the accuracy of calculating the PCM temperature.

- The accuracy of the coupled CFD for simulating the floor surface temperature in the room installed with the PCM, i.e., Room A, was superior to that of the TES using the hysteresis method in the period of relatively high air velocity (0.4 m/s on average) near the floor. Nevertheless, there were no significant differences between the coupled CFD and TES during the other periods of opening the windows. In Room A, the RMSE in the TES was 0.2 ℃ lower than that in the coupled CFD using the temperature wall function when the windows were closed throughout the day, and the influence of natural convection was dominant. Given the heavy calculation loads of the coupled CFD, we can conclude that TES with the hysteresis method is applicable to evaluating temperature field in both naturally ventilated and non-ventilated buildings equipped with PCMs annually.

- The radiant floor cooling system contributed to improving thermal comfort owing to the increased thermal mass of the PCMs and forced nocturnal ventilation for the underfloor space, even when the OT was used for the evaluation. In particular, the thermal comfort period was 68.5% for the entire year in Case 4. These results imply that night ventilation for the underfloor

space and room is the optimum ventilation setting for achieving thermal comfort based on the OT.

- The daily maximum and minimum ambient temperatures of the PCMs significantly affected β_{max} and β_{min}, respectively. The daily average temperature was important for maximizing the utilization rate, exhibiting a strong relationship (R=0.77). The result of the annual simulation considering the hysteresis suggests that the daily average ambient temperature of PCMs is a suitable criterion for selecting the phase change temperature of the PCMs, even in hot and humid regions. If a PCM has a large hysteresis between the peak melting and solidification temperatures, the daily maximum and minimum ambient temperatures can be a useful guideline for selecting a phase change temperature as well.

- β_{max} strongly influenced the retention of the thermal storage effect of the PCM because its cooling effect decreased significantly after it melted completely. To maximize the thermal storage effect of the PCM, a higher utilization must be maintained while avoiding a β_{max} of 100%. β_{max}, which was influenced by the daily maximum ambient temperature of the PCM, also affected the annual utilization rate if the PCM solidified completely within a night through nocturnal forced ventilation for the underfloor space. Based on the annual simulation, a reasonable annual average utilization rate of approximately 70% can be determined to maintain a low floor surface temperature throughout the year.

Chapter 7
Thermal comfort evaluation of window-opening control for ventilative cooling and thermal storage effect

Abstract

Chapter 7 aims to determine the optimum window-opening control that maximizes annual thermal comfort using ventilative cooling, i.e., night and comfort ventilation, in naturally ventilated buildings with the floor cooling system. A thermal energy simulation (TES) coupled with an airflow network model was constructed to evaluate the comfort ventilation and thermal storage effects of the PCMs by controlling the window-opening patterns. The EnergyPlus-based coupled TES model was validated by comparing with the field measurement results in Chapter 3. The root-mean-square errors of the temperature and air velocities at the center of the target building ranged from 0.2–0.5 °C and 0.1–0.2 m/s, respectively. The accuracy of the coupled TES was similar to that of computational fluid dynamics coupled with the heat balance analysis, which can simulate the spatial distributions of temperature and air velocities and was constructed in Chapter 5. The annual simulation results showed that prioritizing the thermal storage effect of the PCMs in the morning and comfort ventilation in the afternoon increases the thermal comfort period. For the optimum window-opening control to maximize thermal comfort in the hot and humid climate, an indoor temperature of 27 °C can be considered a criterion to open the windows for comfort ventilation in addition to night ventilation for the thermal storage effect. When this criterion was applied, the thermal comfort period in the room

with PCMs increased to 83.3%. Accordingly, the reduction in electricity consumption for space cooling was 41% less than that in a control room without PCMs.

Key words
Window-opening control, Comfort ventilation, Thermal storage effect, Air flow network, Coupled simulation.

7.1. Introduction

The results in Chapter 6 showed that the thermal storage effect can be utilized throughout the year because the forced ventilation near the PCM ensures solidification at night. The thermal storage of PCMs employing night ventilation increased the annual thermal comfort period based on the operative temperature (OT) by up to 68.5%. Nevertheless, the thermal storage effect of the radiant floor cooling system alone makes it difficult to achieve thermal comfort during the peak temperature period. Therefore, it is necessary to consider the influence of airflow on the convective and sweat-evaporative heat loss of the human body using comfort ventilation, as indicated in Chapter 3. Tanabe et al. [7.1] indicated that adequate air movement, i.e., comfort ventilation, can compensate for increased air temperature and humidity. The cooling effect of comfort ventilation largely depends on outdoor conditions in naturally ventilated buildings [7.2]. Although the influence of comfort ventilation tends to be low when the air velocity is low, the accumulation of coolness and temperature reduction near the floor from the thermal storage effect has been observed in Chapter 4. Therefore, the combined effects of comfort ventilation and thermal storage of PCMs must be investigated to maximize indoor thermal comfort in hot and humid conditions.

Window-opening control can be important in utilizing both comfort ventilation and thermal storage effect through night ventilation Sorgato et al. [7.3] established a night ventilation control method by referencing the indoor operative and outdoor temperatures in Brazil. Psomas et al. [7.4] evaluated the risk of thermal discomfort when an automated window-opening control system was used for comfort ventilation in Denmark. Wang et al. [7.5] simulated the influence of window-opening operations on building energy consumption in the United States. However, most previous studies on window-opening control utilized air-conditioning systems in temperate climates, and few studies have constructed a window-opening control method that solely employs passive cooling methods in hot and humid climates.

Furthermore, previous studies on window-opening control systems have primarily focused on reducing cooling loads and energy consumption using thermal energy simulation (TES). However, annual analysis methods that evaluate indoor thermal comfort by considering both comfort ventilation, i.e., air velocity, and thermal storage effect has posed challenges [7.6, 7.7]. The CFD simulation coupled with a heat balance analysis, which simultaneously

evaluates the comfort ventilation and thermal storage effects of PCMs, was constructed in Chapter 5. However, the application of the coupled CFD to long-term evaluations is difficult owing to its high calculation load. For instance, the constructed coupled CFD took three days for the three-day simulation. TES can be a suitable method to analyze the thermal storage effect of PCMs, which must consider the influence of long-term history owing to its low calculation load, as presented in Chapter 6. However, considering the TES for the spatial distribution of air velocity is difficult due to the nodal model for each zone [7.8, 7.9]. Therefore, a TES-based annual coupled simulation method that considers the PCM history of the long-term thermal storage effect and the influence of comfort ventilation, i.e., air velocity, is required because the complex relationship between the thermal storage effect of PCMs and comfort ventilation through window-opening controls must be clarified to maximize thermal comfort under various outdoor conditions.

7.1.1. Objective

In Chapters 3–6, the window system, PCMs, and cooling method of the PCMs were investigated. Using a TES-based annual coupled simulation, Chapter 7 aims to determine the optimum window-opening control that maximizes the annual thermal comfort using the thermal storage effect of the PCMs and comfort ventilation in naturally ventilated buildings. First, a TES coupled with an airflow network (AFN) model that calculates the air flow rate and indoor air velocity to evaluate the influence of comfort ventilation was developed, followed by the construction of a simulation model for a full-scale experimental building used in Chapters 3–6. Second, the coupled TES model was validated by comparing it with the results of the field measurements and with the coupled CFD developed in Chapter 5. Third, annual simulations with different window-opening controls were conducted to maximize the thermal comfort period using the thermal storage effect of the PCMs and comfort ventilation, as well as to reduce energy consumption. The relationship (including the trade-off relationship) between the thermal storage effect and comfort ventilation was discussed to determine the optimum window-opening control based on the simulation results.

7.2. Methodology

7.2.1. Coupled TES

In Chapter 7, the EnergyPlus-based model developed in Chapter 6 was modified. Fig. 7.1 shows the calculation flow for the coupled TES constructed in this chapter. Regarding the

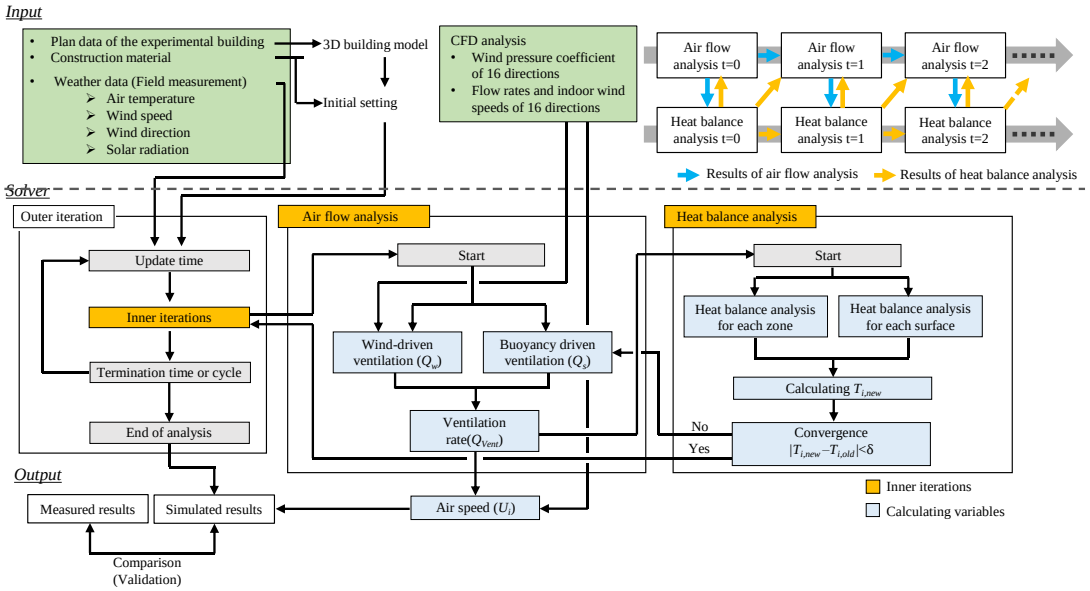

Fig. 7.1. Flow chart of the coupled TES.

calculation method for the heat balance analysis was almost the same as that in Chapter 6 (see section 6.2.2). In Chapter 7, the TES was coupled with the AFN model. In the coupled simulation (coupled TES), the results of the previous time step were employed as the initial condition of the present time step. First, the airflow was analyzed using the AFN, and the airflow rate for each zone was outputted for the heat balance analysis. The heat balance of each node was then calculated using the TES. The airflow and heat balance analyses were iterated in the same time steps until the heat balance analysis converged. The time step for the coupled simulations was 1 min and the number of iterations per time step was 100.

7.2.1.1. Air flow analysis

In the coupled TES using EnergyPlus, the airflow rate for each zone was calculated using the AFN model based on the airflow balance. The following equations show the fundamental formula for the airflow balance in each zone (Eq. 7.1):

$$\sum_{i=1}^{N} m_i = \sum_{i=1}^{N} \rho_{air} Q_{flow} = 0 \qquad (7.1)$$

where m_i is the mass flow rate [kg/s], ρ_{air} is the density of the air [kg/m^3], and Q_{flow} is the flow rate [m^3/s].

To calculate the airflow rate for an indoor space, the AFN considers two types of ventilation: buoyancy-driven and wind-driven. In this study, the airflow rate for each zone was calculated as the root sum square of both ventilation types and is expressed as follows (Eqs. 7.2–7.5):

$$Q_{flow} = \sqrt{Q_s^2 + Q_w^2} \tag{7.2}$$

$$Q_{s,w} = c_d A \sqrt{\frac{2\Delta P_{s,w}}{\rho}} \tag{7.3}$$

$$\Delta P_s = \frac{\rho g x (T_z - T_\infty)}{T_z} \tag{7.4}$$

$$\Delta P_w = (c_{w1} - c_{w2}) \frac{1}{2} \rho U_{ref}^2 \tag{7.5}$$

where Q_{flow} is the flow rate [m^3/s], Q_s is the buoyancy-driven flow rate [m^3/s], Q_w is the wind-driven flow rate [m^3/s], c_d is the discharge coefficient [-], P_i is the pressure [Pa], A_i is the area [m^2], g is the gravitational acceleration [m^2/s], U_{ref} is the air velocity at reference point [m/s], T_s is the surface temperature [K], T_∞ is the outside temperature [K], and c_w is the wind-pressure coefficient [-].

Prior to the airflow analysis in EnergyPlus, a CFD simulation of the target building was performed to obtain the wind-pressure coefficient (c_w) of the external walls and discharge coefficient (c_d) of the openings. For the CFD simulation, a commercial software (scSTREAM v2021; MSC software, Tokyo, Japan) was used to solve the governing equations for momentum and continuity. The simulation settings were based on the best-practice guidelines for CFD simulations provided by Franke et al. [7.10], Tominaga et al. [7.11], and Blocken [7.12]. The three-dimensional steady Reynolds-averaged Navier–Stokes (RANS) equation was solved, and the renormalization group k–ε model (RNG k–ε) [7.13, 7.14] was selected as the turbulence model. Second-order upwind discretization schemes were employed for the momentum and turbulence equations. Convergence was assumed when the scaled residual leveled off at a minimum of 10^{-5} for all variables.

The dimensions of the calculation domain were 132 × 132 × 68.7 m (W×D×H), which was discretized by a hexahedral mesh of 258 × 235 × 116 for the outer domain and 210 × 143 × 89 for the inner domain. The influence of mesh size was examined using the grid convergence index (GCI), as suggested by Roache [7.15]. The GCI between the medium-mesh model (9,705,750 elements) and the coarse-mesh model (4,862,769 elements) was 2.7% and that between the medium-mesh model and the fine-mesh model (18,213,551 elements) was 1.4%. Based on the results of the grid sensitivity analysis, the medium-mesh model (9,705,750 elements) was selected for this analysis.

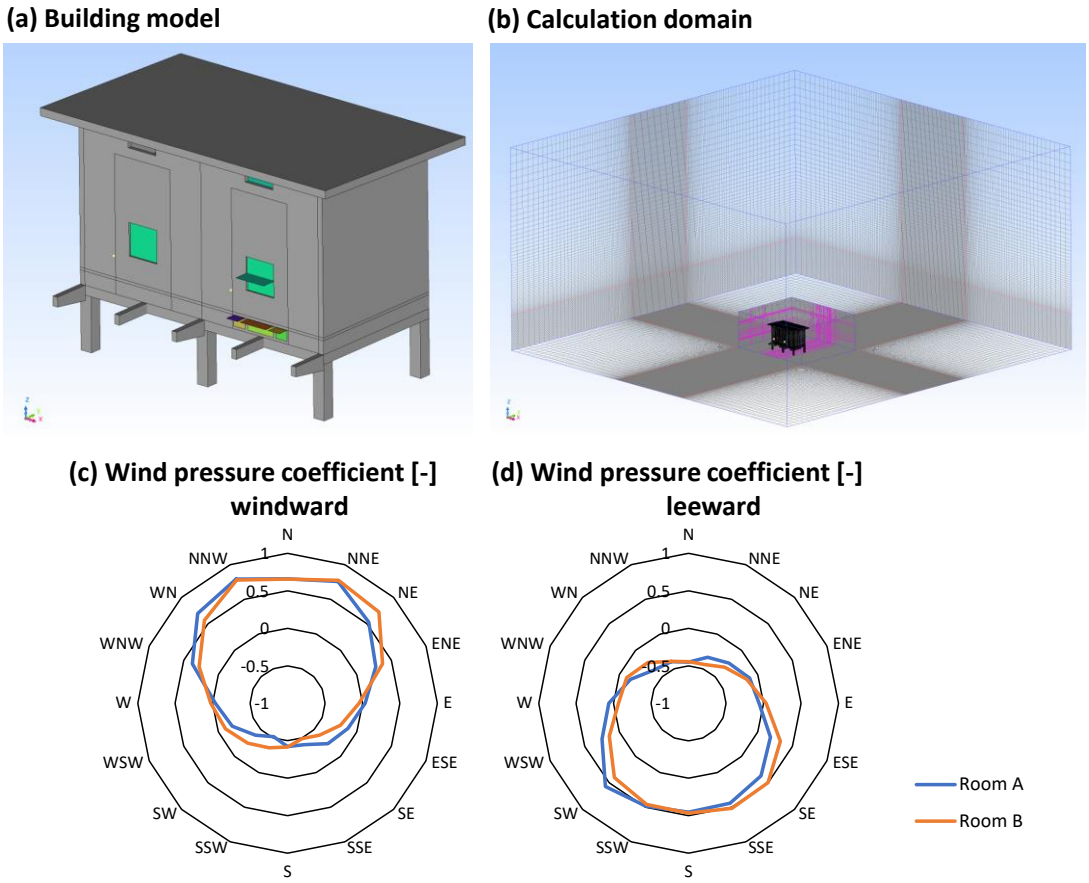

Fig. 7.2. (a) Building model in the CFD; (b) calculation domain; and (c) wind-pressure coefficients on the windward side and (d) leeward side for Rooms A and B.

The flow and wall boundary conditions were set at the interfaces of the computational domain, that is, X_{min}, X_{max}, Y_{min}, Y_{max}, Z_{min}, and Z_{max}. Regarding the wall boundary condition, the log low condition was considered for the building and Z_{min} [7.16]. For the flow boundary, the inflow from 16 directions (every 22.5°) was calculated to determine c_w and c_d for all wind directions. A wind speed of 3 m/s at the reference height (H=10 m) was set at X_{min} and Y_{min} as the inputs, whereas a fixed total pressure (0 Pa) was set at X_{max} and Y_{max} as the outflow condition. When the wind direction was reversed, the flow boundary settings X_{min}, X_{max}, Y_{min}, and Y_{max} were reversed to calculate the flow field. The power-law exponent for the inflow determined by the terrain category was 0.2, which considers the environment surrounding the experimental building [7.17]. Fig. 7.2 presents c_w for the windward and leeward sides of Rooms A and B. The c_d for openings was approximately 0.6–0.7 in previous

studies [7.18–7.20]. Based on the previous studies and the results of the flow rate in the CFD, a c_d of 0.6 was adopted for the air flow analysis in this chapter.

7.2.1.2. Air velocity estimation using the air flow network model

The AFN model cannot be used to calculate the indoor air velocity. Tanabe et al. [7.21] showed that the airflow rate could be predicted using the air velocity at a naturally ventilated opening. Horikawa et al. [7.22] found a strong correlation between the air velocity at a naturally ventilated opening and the air velocity at an occupied level 15 m away from the opening. In the present study, a linear regression formula between the airflow rate and the air velocity at a specific measurement point was constructed to calculate the indoor air velocity using the AFN model. A linear regression formula was obtained based on the CFD simulation results as follows (Eq. 7.6):

$$U_i = aQ_{vent} + b \tag{7.6}$$

where U_i is the air velocity [m/s], Q_{vent} is the ventilation rate [m^3/s], a and b are the coefficients [-].

Table 7.1 presents the coefficient of Eq. 7.6, which was obtained from the simulation results to calculate the air velocity in the middle of the rooms (FL+1.1 m). As the opening type affects the indoor air flow pattern shown in Chapter 3, a linear regression formula must be developed for each window type and measurement point. In the target building, a horizontal pivot window, which is a preferable window type for comfort ventilation under hot and humid conditions, was installed in Room A, and a simple opening was used in Room B. A simple opening used in Room A was investigated in the annual simulation to clarify the influence of the window type. The measurement position was at the center of the rooms at a height of 1.1 m above the floor. The coefficient of a in case of the horizontal pivot window was higher than that of the simple opening because the horizontal pivot window controls the inflow vertically and contributes to increasing the air velocity at the occupied level (FL+1.1 m). Therefore, even when the air flow rate was the same, the air velocity at occupied level in case of the horizontal pivot window was higher than that of the simple opening.

Table 7.1. Coefficients of linear regression.

Window type and Height	a	b	R^2
Horizontal pivot in Room A (FL+1.1 m)	0.4103	0.0834	0.69
※Simple opening in Room A (FL+1.1 m)	0.2767	-0.0436	0.79
Simple opening in Room B (FL+1.1 m)	0.2825	0.0458	0.84

※ comparison of the window types in Room A

In the case of the horizontal pivot window and simple opening, the R^2 values of the linear regression formula for air velocities at FL+1.1 were 0.69 and 0.84, respectively. Moon et al. [7.23] concluded that a coefficient of determination (R^2) more than 0.6 represents a high correlation, and this criterion is generally accepted as a key index for evaluating the reliability of simple regression statistical models.

Because both buoyancy and wind-driven ventilation affect the indoor airflow, the flow field characteristics based on the experimental results need to be clarified [7.24]. Archimedes number (Ar) is the ratio of the external forces to the internal viscous form, which describes the flow field characteristics. The Ar during November 13–17, when the windows were opened throughout the day, was calculated using the following equation (Eq. 7.7) [7.25]:

$$Ar = \frac{g\beta x|T_{FL+1.1} - T_{out}|}{U^2} \quad (7.7)$$

where Ar is the Archimedes number [-], g is the gravitational acceleration [m^2/s], β is the thermal expansion rate [-], x is the length [m], $T_{FL+1.1}$ is the room air temperature at 1.1 m above the floor [K], T_{out} is the outdoor temperature [K], and U_i is the air velocity [m/s].

The average Ar values were 0.05 and 0.08 in Rooms A and B, respectively. Therefore, the influence of wind-driven ventilation was dominant on the indoor airflow compared with that of buoyancy-driven ventilation. Moreover, the prevailing wind direction in the experimental field was uniform throughout the year because of the sea and land breezes. The results in Chapter 3 showed that the indoor air flow patterns using the horizontal pivot window were mostly similar, regardless of the outdoor wind conditions. A low Ar, stable outdoor wind direction, and influence of the opening type resulted in an acceptable simple regression statistical model for calculating the indoor air velocity based on the flow rate.

7.2.2. Validation process of the coupled TES

The simulation results were compared with field measurement to validate the constructed model. Room A (test room) was installed with the radiant floor cooling system using PCMs, whereas Room B was set as the reference room without the radiant floor cooling system to maintain consistency with the field measurement in Chapter 3. The ventilation fans (0.95 m^3/s) for the underfloor space in Room A were turned on between 18:00 and 7:00, referring the results in Chapters 5 and 6 to maximize the thermal storage effect of PCMs. The field measurement (Chapter 4) and annual simulation (Chapter 6) have confirmed the validity of the phase change temperature of 28–30 °C under the weather conditions of the experimental field in Tangerang, Indonesia. As mentioned, the opening types in Rooms A and B were assumed to be the horizontal pivot window which is a preferable window type for comfort

ventilation as discussed in Chapter 3 and simple opening, respectively, for airflow analysis, and the windows were opened throughout the day.

The indoor air velocity calculated using Eq. 7.6 and the air flow rate in the coupled TES. The result of the coupled TES was compared with that of the TES with a constant flow rate (0.7 m^3/s) constructed in Chapter 6 based on the equation of the outdoor wind condition and opening area proposed by the American Society of Heating and Air-Conditioning Engineers (ASHRAE) [7.26]. Furthermore, the results of the coupled TES were compared with those of the CFD simulation coupled with the heat balance analysis (coupled CFD simulation) constructed in Chapter 5 to discuss the calculation results of the indoor air velocity for thermal comfort evaluation. If the accuracy of the coupled TES is similar to that of the coupled CFD simulation, it can be inferred that the coupled TES is an appropriate calculation method for evaluating the indoor thermal comfort of naturally ventilated buildings with window systems and radiant floor cooling systems. Because of the low calculation load, coupled TES can be a more feasible calculation method than coupled CFD for annual thermal comfort evaluation if the coupled TES model is validated. The temperatures were averaged every 10 min to maintain consistency with the field measurement. The simulation results were evaluated in terms of the root-mean-square error (RMSE) and R^2. Moreover, Coakley et al. [7.27] proposed the coefficient of variation of the RMSE (CVRMSE). Chapter 7 employed CVRMSE for evaluating the validation results, regardless of the unit as follows (Eq. 7.8):

$$CVRMSE = \frac{\sqrt{\sum_{i=1}^{N} \frac{(L_{is}-L_{im})^2}{N}}}{\overline{L_m}} \tag{7.8}$$

where L_{is} is the simulated value, L_{im} is the measured value, and N is the number of data points.

7.2.3. Window-control and simulation setting

Table 7.2 presents the simulation cases with window-control methods for annual simulation. Ideally, the windows should be closed when the indoor temperature is low to maintain the thermal storage effect. As the indoor temperature or outdoor wind speed increases, the windows should be opened to provide comfort ventilation. Furthermore, windows should be opened at night to effectively dissipate the heat accumulated during daytime in the PCM through night ventilation, as discussed in Chapter 6. The conditional criteria for opening the windows in this simulation included four basic ventilation modes: full-day ventilation, no ventilation, day ventilation, and night ventilation. The indoor air temperature, outdoor air temperature, and outdoor wind speed were selected as conditional criteria to determine the optimal control setting because they are relatively easy to measure and can be used to determine the time required to control the windows in practical applications. In the control

Table 7.2. Simulation cases of window-control methods with conditional criteria.

Window-opening control method	Conditional criteria for opening window
Ventilation mode	full day, no, daytime, and nighttime
Indoor air temperature	above 27, 28, 29, 30 ℃
Indoor air temperature + night ventilation (NV)	nighttime OR above 27, 28, 29, and 30 ℃ during daytime
Outdoor air temperature	above 26, 27, 28, 29, 30, and 31 ℃
Indoor air temperature + NV	nighttime OR above 26, 27, 28, 29, 30, and 31 ℃ during daytime
Outdoor wind speed	above 0.5, 1.0, 1.5, 2.0, and 2.5 m/s
Outdoor wind speed + NV	nighttime OR above 0.5, 1.0, 1.5, 2.0, and 2.5 m/s during daytime

※Nighttime: 18:00–6:00; daytime: 6:00–18:00

settings, the windows were closed when the indoor temperature was low to maintain a low indoor temperature and thermal storage effect. When the indoor air temperatures exceeded the threshold temperatures (i.e., 27, 28, 29, and 30 °C), the room windows were opened at the next time step for comfort ventilation because the thermal storage effect alone tends to make it difficult to achieve thermal comfort. Similar to the indoor air temperature, the threshold temperatures based on the outdoor air temperature (i.e., 26, 27, 28, 29, 30, and 31 °C), which were employed for the window-opening control in a previous study [7.3], were set for the simulation cases. Although increased temperatures accumulate heat in building structures, adequate comfort ventilation during the daytime compensates for the increased air temperature and reduces the thermal storage effect. Therefore, as another setting with the wind speed, the hourly averaged wind speed was compared with the threshold wind speed (i.e., 0.5, 1.0, 1.5, 2.0, and 2.5 m/s). When the hourly average wind speed exceeded the threshold wind speed, the room windows were opened at the next time step. As listed in Table 7.2, these conditional criteria for opening windows combined with the night ventilation were also investigated.

7.2.4. Evaluation criteria

The optimum window-opening control was determined using the evaluation criteria of the standard effective temperature (SET*). The metabolic rate was set to 1.0 met (seated position), and the clothing worn was assumed to be 0.5 clo, representing the clothing worn in naturally ventilated buildings in the tropics [7.28]. The upper comfort limit (80% acceptance) was set for the evaluation based on the previous studies of the thermal comfort model conducted on naturally ventilated buildings in the tropics [7.29]. The upper comfort limit of SET* was set to 29.9 ℃ [7.29].

7.3. Results

7.3.1. Validation

Fig. 7.3 and Table 7.3 show the results of the temperature at each point between the measurement and the simulation for Rooms A and B in the case of open windows throughout the day. In Room B, the air temperature was calculated using the TES, coupled TES, and coupled CFD, with RMSEs of less than 0.4 ℃ and R^2 of 0.99. Although the RMSEs of the floor surface temperature in the TES and coupled TES were 0.3 ℃ and 0.2 ℃ for the entire calculation period, respectively, the RMSE in the coupled CFD was 0.1 ℃ smaller than that of the TES and coupled TES when the relatively high air velocity (0.4 m/s on average) was observed near the floor surface. Calculating the convective heat transfer coefficient at every time step in the coupled CFD model improved the floor surface temperature. Pandey et al. [7.30] indicated that the coupled CFD had better prediction accuracy for temperatures than the TES under forced convection; however, temperatures calculated using the TES were similar to those calculated using the coupled CFD under natural convection. In this study, at night and in the morning, the influence of natural convection became large compared with the period of high wind speed; thus, the floor surface temperature difference among the three simulation methods could not be clearly observed in Room B.

In Room A, the air temperature difference among the three calculation methods (i.e., TES, coupled TES, and coupled CFD) could not be observed clearly because of the significant influence of outdoor conditions with the horizontal pivot window. Fin et al. [7.31] reported that an increase in the ventilation rate beyond 10 air changes per hour (ACH) did not strongly affect the indoor air temperature. A constant ventilation rate of 0.7 m^3/s, which equals 32.8 ACH, was applied to calculate the TES in this study. Although outdoor weather conditions in hot and humid climatic regions tend to be calm, the nocturnal air flow rate was approximately 0.2 m^3/s, which was equivalent to 9.6 ACH, because the experimental building had the opening on the north and south sides that faced prevailing wind directions. Therefore, the accuracy of the TES with the constant flow volume is similar to that of the coupled TES and CFD for calculating the air temperature. For the floor surface temperature, the thermal storage effect of the PCMs during the daytime was observed in both the field measurement and simulations, that is, TES, coupled TES, and coupled CFD. The diurnal floor surface temperature in Room A was 0.6 ℃ (measured) and 0.4–0.7 ℃ (simulated) lower than that in Room B (control room) because of the thermal storage effect of PCMs. When the PCMs reached the melting temperature of 30 °C, they maintained a constant temperature in both field measurement and simulations, resulting in a lower floor surface temperature. The RMSE and R^2 of the PCM

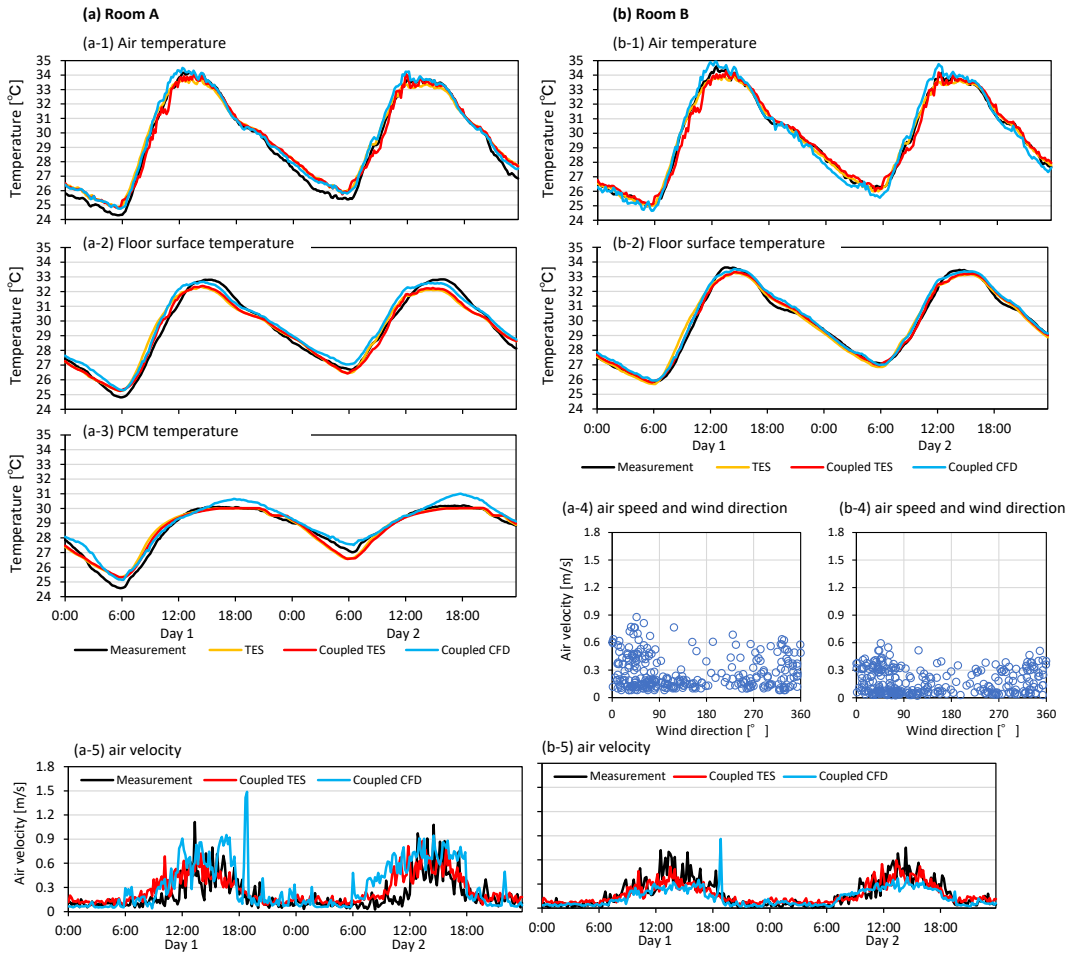

Fig. 7.3. Comparison of the (a-1, b-1) air temperature, (a-2, b-2) floor surface temperature, and (a-3) PCM temperature; (a-4, b-4) relationship between the indoor air velocity and the outdoor wind direction; and (a-5, b-5) indoor air velocities in Rooms A (PCM) and B (control).

temperature in the coupled TES were 0.3 °C and 0.96, respectively. Nageler et al. [7.32] compared the RMSEs using four TES tools, namely Dymola, EnergyPlus, IDA ICE, and TRANSYS, and the RMSEs for the air temperature in the test chamber ranged from 0.2–2.3 °C. Mazzeo et al. [7.33] reported the simulation accuracy using EnergyPlus, IDA ICE, and TRANSYS; the R^2 of the air temperature in the test chamber ranged from 0.92–0.99. Compared with the accuracy of the temperature calculations in the previous studies using TES tools, the results of the coupled TES were relatively accurate.

Fig. 7.3(a-5, b-5) presents the results of the air velocity in the middle of Rooms A and B (FL+1.1 m). In the field measurement, the air velocity in Room A tended to be higher than that in Room B during the day because of the influence of the horizontal pivot window.

Table 7.3. Correlation and deviation of temperature between the field measurement and the simulation.

Parameter	Room A					
	TES		Coupled TES		Coupled CFD	
	RMSE [°C]	R^2 [-]	RMSE [°C]	R^2 [-]	RMSE [°C]	R^2 [-]
Air temperature	0.5	0.99	0.5	0.99	0.4	0.99
Floor surface temperature	0.5	0.97	0.4	0.98	0.5	0.98
PCM temperature	0.3	0.96	0.3	0.96	0.4	0.97
	Room B					
	TES		Coupled TES		Coupled CFD	
	RMSE [°C]	R^2 [-]	RMSE [°C]	R^2 [-]	RMSE [°C]	R^2 [-]
Air temperature	0.2	0.99	0.4	0.99	0.4	0.99
Floor surface temperature	0.3	0.99	0.2	0.99	0.3	0.99

The simulated results replicated the influence of the opening type on the indoor air velocity. Although using the coupled TES to replicate the air velocity at each time step may be difficult and the indoor air velocity in the presence of cross winds (i.e., 90° and 270°) did not reach zero (Fig. 7.3(a-4, b-4)), it reproduced the overall trend of the indoor air velocity. During the daytime, indoor air velocity tended to be high owing to the sea breeze from the north. Meanwhile, the nocturnal wind condition was calm. Compared with the coupled CFD proposed in Chapter 5, the RMSEs of the air velocity ranged from 0.1–0.2 m/s (coupled TES) and 0.1–0.2 m/s (coupled CFD) for both Rooms A and B in this study. The results of a previous study using the AFN model showed that the CVRMSE of the flow rate ranged from 0.1%–44.4% [7.34]. The American Society for Testing Materials (ASTM) D5157 Standard [7.35] suggests that the CVRMSE should be less than 25% for the statistical evaluation of indoor air quality models, including the calculation of the flow rate. The CVRMSE of the air velocity using the result of the airflow rate ranged from 14.5%–22.4% in the coupled TES. Moreover, the validation results of the coupled TES were similar to those of the coupled CFD, which had a significantly higher calculation load. Given the calculation load and accuracy, coupled TES was used for the subsequent analysis to evaluate the annual thermal comfort.

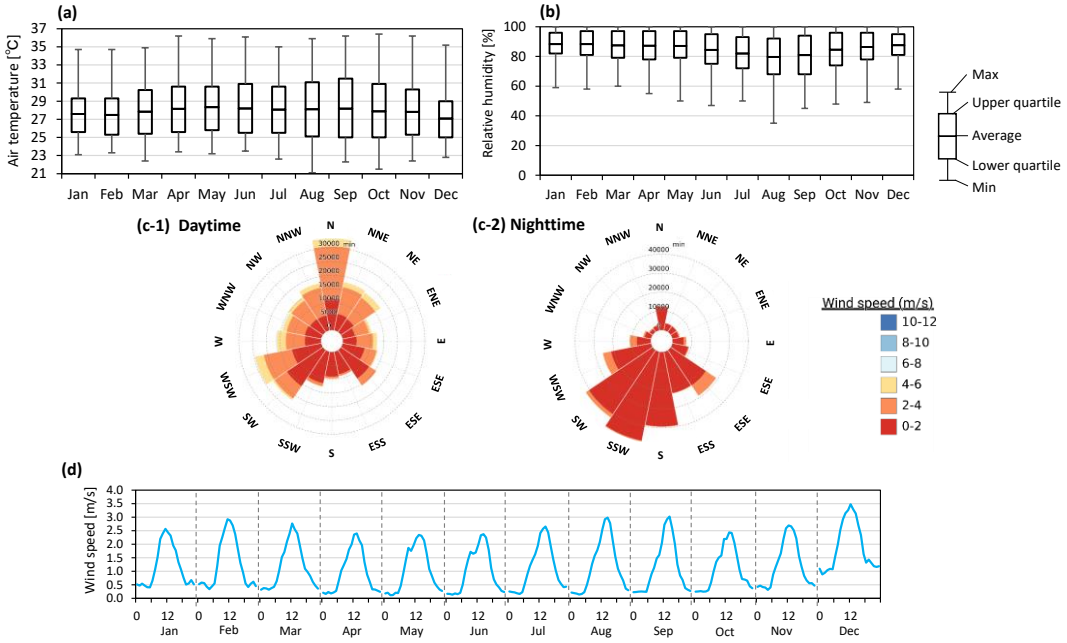

Fig. 7.4. (a) Outdoor air temperature range, (b) outdoor relative humidity range, (c) wind rise in 2020, and (d) monthly averaged daily patterns of the outdoor wind speed.

7.3.2. Annual simulation

7.3.2.1. Annual weather data

Fig. 7.4 shows the outdoor air temperature, relative humidity, wind speed, and wind direction measured in the experimental field in 2020. Overall, a small annual temperature range of 1.3 ℃ and high relative humidity (more than 80% on monthly average), which are the features of hot and humid climatic regions, were observed. The outdoor air temperature in the experimental field was similar to the recent weather observation data (2005–2020) at the nearest official weather station (Tangerang) [7.36], with diurnal and nocturnal averages of 28.9–31.0 ℃ and 25.2–26.1 ℃, respectively.

As Tangerang is a coastal city, the prevailing wind direction was north during the day owing to the sea breeze, whereas it was south at night. The diurnal and nocturnal mean wind speeds ranged from 1.6–2.7 m/s and 0.3–1.1 m/s, respectively. The wind speed in December was relatively high, compared to that in the other month.

7.3.2.2. Influence of the ventilation mode

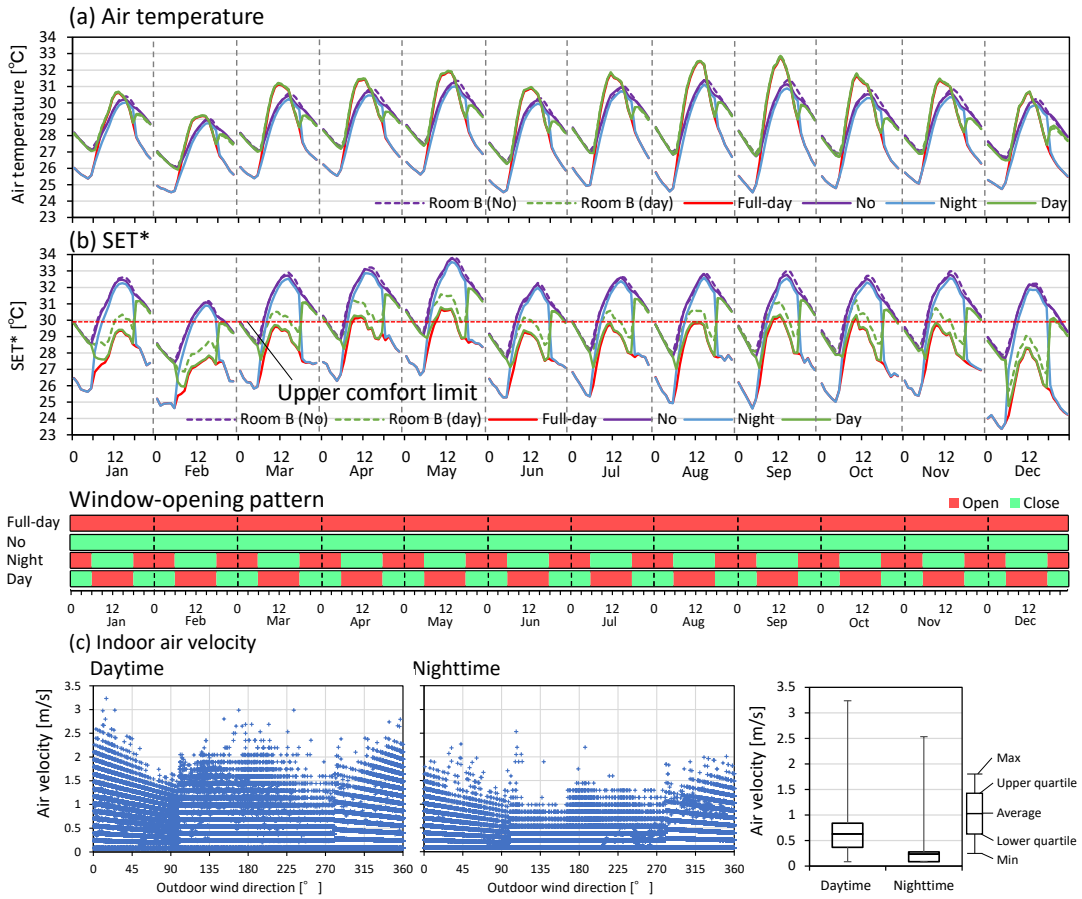

Fig. 7.5. (a,b) Monthly averaged daily patterns of indoor air temperature and SET* with changing ventilation modes and (c) indoor velocities and outdoor wind directions in Room A under full-day ventilation condition.

Fig. 7.5ab presents the monthly averaged daily patterns of the air temperature and SET* for each ventilation mode. Table 7.4 shows the hourly SET* range with comfort evaluation. Four basic ventilation modes were applied to the window-opening patterns in Room A. As a reference, the window-opening pattern in Room B (control) was no ventilation and day ventilation, which is the major window-opening pattern in the hot and humid climates of Indonesia and Malaysia [7.36, 7.37]. In Room B without ventilation, the diurnal average SET* was 31.7 °C. The SET*-based comfort period in Room B (no ventilation) was 31.1% per year. When day ventilation was applied to Room B, the comfort period increased to 50.3% per year owing to comfort ventilation during the daytime.

Table 7.4. Hourly SET* range with thermal comfort evaluation and changing ventilation modes.

	Nighttime		Daytime		Whole
	SET*[℃] min–max (avg)	Comfort period [%]	SET*[℃] min–max (avg)	Comfort period [%]	Comfort period [%]
Room B (No ventilation)	25.0–34.6 ℃ (30.0 ℃)	48.7%	25.7–35.7 ℃ (31.7 ℃)	13.5%	31.1%
Room B (Day ventilation)	24.8–34.2 ℃ (29.8 ℃)	51.9%	20.7–34.7 ℃ (29.7 ℃)	48.6%	50.2%
Full-day ventilation	19.9–32.4 ℃ (26.6 ℃)	95.2%	19.9–33.4 ℃ (28.6 ℃)	71.0%	83.1%
No ventilation	24.8–34.3 ℃ (29.9 ℃)	49.2%	25.2–35.6 ℃ (31.6 ℃)	14.9%	32.1%
Night ventilation	19.9–32.5 ℃ (26.7 ℃)	95.3%	23.2–35.5 ℃ (31.2 ℃)	22.6%	58.9%
Day ventilation	24.5–34.0 ℃ (29.8 ℃)	51.8%	20.0–33.5 ℃ (28.8 ℃)	67.7%	59.8%

※ Nighttime: 18:00–6:00; Daytime: 6:00–18:00

In Room A, without ventilative cooling through the windows, the diurnal average SET* was 0.1 ℃ lower than that in Room B (no ventilation) because of the thermal storage effect from the radiant floor cooling system. The air temperature in Room A (no ventilation) was 0.1–0.5 ℃ lower than that in Room B (no ventilation) in the afternoon. In the case of full-day ventilation for Room A, the diurnal average SET* was 28.6 ℃, with an annual comfort period of 71.0% during the daytime. Fig. 7.5c shows the results of air velocity in the case of full-day ventilation condition for the middle of Room A (FL+1.1 m). The mean diurnal and nocturnal air velocities were 0.6 m/s and 0.2 m/s, respectively. The relatively high air velocity was observed when the outdoor wind direction was north and south which was perpendicular to the façade of experimental building. Switching the window operations (i.e., closing and opening) strongly affected the SET*. In particular, when day ventilation was stopped and night ventilation was started, the SET* differences between 17:00 and 18:00 ranged from 2.3–4.8 ℃. Moreover, when the windows in Room A were closed, the air temperature in Room A sharply increased by 0.5–1.1 ℃ due to the stored heat emission into the room. Nevertheless, the comfort period for day ventilation was 0.8% longer than that for night ventilation. Because the daytime wind speed tended to be higher than the nocturnal wind speed at the experimental site, the influence of day ventilation on extending the comfort period was slightly greater than that of night ventilation. The diurnal average SET* in Room A (day ventilation) was reduced by 0.9 ℃ than that in room B (day ventilation) owing to the radiant floor cooling system and horizontal pivot window, which is the preferable window type for improving the thermal comfort in a hot and humid climate.

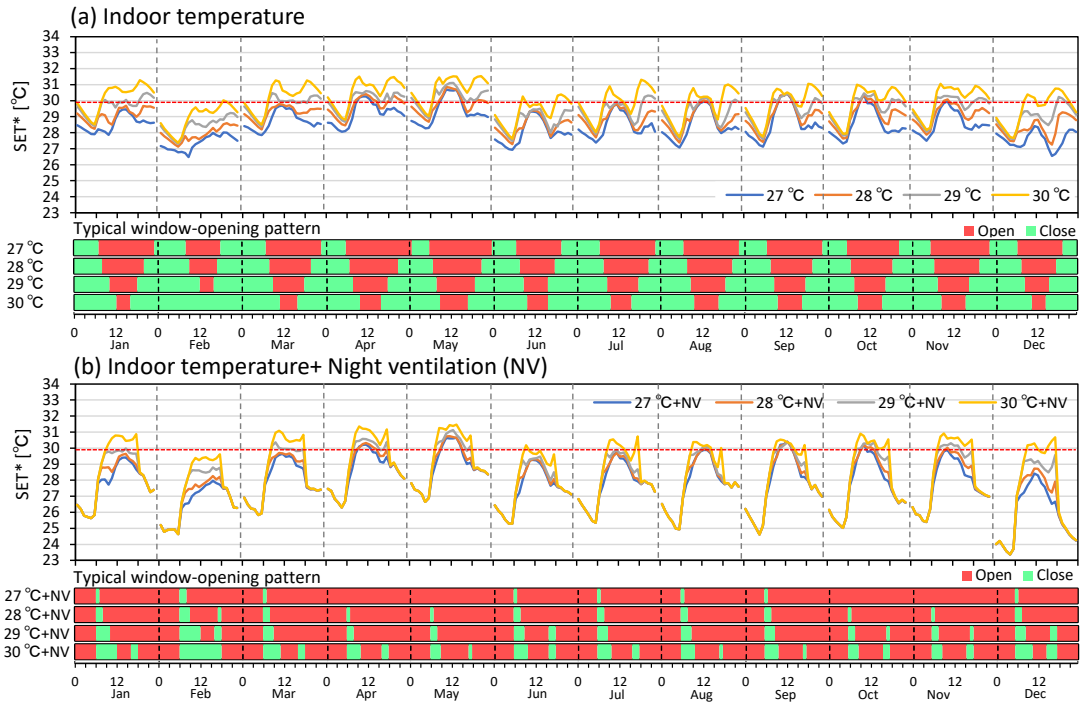

Fig. 7.6. Monthly averaged daily patterns of SET* controlled by the (a) indoor air temperature and (b) indoor air temperature and night ventilation (NV).

7.3.2.3. Window-opening control based on the indoor air temperature

Focusing on window-opening control based on the indoor air temperature, Fig. 7.6 presents the monthly averaged daily patterns of SET*, and Table 7.5 depicts the hourly SET* ranges with comfort evaluation. The median switching time for window opening was presented as a typical window-opening pattern in the simulation, as shown in Fig. 7.6. A low indoor air temperature threshold resulted in a low annual average SET*. The annual average SET* in the case of threshold indoor temperatures of 27 °C and 30 °C were 29.0 °C and 30.4 °C, respectively. Around 6:00, the SET* difference among the four cases was relatively small because of the low air velocity. As the indoor temperature increased in the morning, the SET* difference between the cases increased from the lower threshold because of comfort ventilation obtained by opening the windows (Fig. 7.6c). The SET* in the case of threshold temperatures of 29 °C and 30 °C tended to exceed the comfort limit in the late evening because closing the windows prevented ventilative cooling and the building structures could not dissipate the heat sufficiently. The duration of opening the windows in the case of the threshold indoor

Table 7.5. Hourly SET* ranges with thermal comfort evaluation controlled by the (a) indoor air temperature and (b) indoor air temperature and night ventilation (NV)

	Nighttime		Daytime		Whole
	SET*[℃] min–max (avg)	Comfort period [%]	SET*[℃] min–max (avg)	Comfort period [%]	Comfort period [%]
27 ℃	24.5–32.4 ℃ (28.2 ℃)	95.1%	24.4–33.4 ℃ (29.0 ℃)	69.6%	82.4%
28 ℃	24.7–32.4 ℃ (28.9 ℃)	85.6%	24.6–33.4 ℃ (29.3 ℃)	66.4%	76.0%
29 ℃	24.8–32.4 ℃ (29.4 ℃)	59.7%	25.1–33.4 ℃ (29.8 ℃)	50.9%	55.3%
30 ℃	24.8–33.0 ℃ (29.8 ℃)	49.7%	25.2–33.4 ℃ (30.4 ℃)	33.2%	41.4%
27 ℃+NV	19.9–32.4 ℃ (26.7 ℃)	95.2%	23.2–33.4 ℃ (28.9 ℃)	71.3%	83.3%
28 ℃+NV	19.9–32.4 ℃ (26.7 ℃)	95.2%	23.2–33.4 ℃ (29.1 ℃)	69.6%	82.4%
29 ℃+NV	19.9–32.4 ℃ (26.7 ℃)	95.2%	23.2–33.4 ℃ (29.6 ℃)	55.1%	75.2%
30 ℃+NV	19.9–32.4 ℃ (26.7 ℃)	95.2%	23.2–33.4 ℃ (30.1 ℃)	39.5%	67.3%

※Nighttime: 18:00–6:00; Daytime: 6:00–18:00
Bold: the longest annual comfort period among the 34 cases in this study.

temperature of 27 °C was 3587 h longer than that at 30 °C, and the window-opening pattern difference, that is, closed and opened, frequently occurred in the morning and late evening.

Combining the indoor temperature threshold with night ventilation (NV) increased the thermal comfort period. The temporal variation in the SET* at night was almost the same regardless of the threshold temperature. Thermal comfort periods were 95.2% for all cases during the nighttime. Meanwhile, the thermal comfort period during the daytime increased by 1.8%–6.3% compared with that in the corresponding cases without night ventilation. In particular, the night ventilation reduced the SET* and extended the thermal comfort period in the morning because of a reduction in the air temperature and mean radiant temperature owing to the thermal storage effect. The case of the indoor temperature threshold of 27 °C and night ventilation was the optimum window-opening control among the 34 cases with an annual comfort period of 83.3%. This implies that indoor thermal comfort can be achieved for most of the year without the use of air-conditioning systems if the radiant floor cooling system and horizontal pivot window with optimum window-opening control are employed.

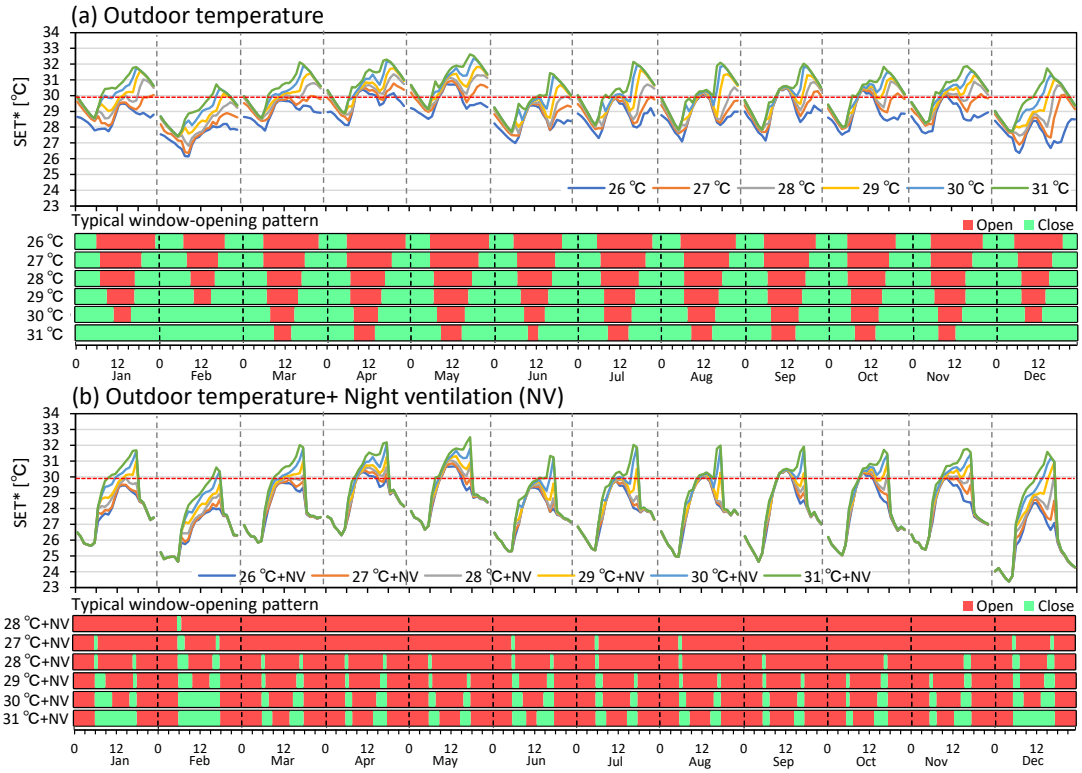

Fig. 7.7. Monthly averaged daily patterns of SET* controlled by the (a) outdoor air temperature and (b) outdoor air temperature and night ventilation (NV).

7.3.2.4. Window-opening control based on the outdoor air temperature

Focusing on window-opening control based on the outdoor air temperature, Fig. 7.7 presents the monthly averaged daily patterns of SET*, and Table 7.6 depicts the hourly SET* range with comfort evaluation. Similar to the window-opening controlled through the indoor temperature threshold, the low threshold of the outdoor air temperature resulted in a low annual average SET* owing to the significant influence of comfort ventilation during the daytime. The annual average SET* in the case of the threshold temperature of 26 °C was 1.6 °C lower than that at 31 °C.

In the case of a threshold temperature of more than 27 °C, the maximum SET* was frequently observed in the evening. Previous studies [7.38] reported that the indoor temperature peak was delayed by a few hours compared with that in outdoors in buildings with

Table 7.6. Hourly SET* ranges with thermal comfort evaluation controlled by the (a) outdoor air temperature and (b) outdoor air temperature and night ventilation (NV)

	Nighttime		Daytime		Entire
	SET* [℃] min–max (avg)	Comfort period [%]	SET* [℃] min–max (avg)	Comfort period [%]	Comfort period [%]
26 ℃	23.3–32.4 ℃ (28.6 ℃)	87.6%	23.1–33.4 ℃ (29.0 ℃)	67.5%	77.5%
27 ℃	24.7–32.6 ℃ (29.3 ℃)	63.5%	24.6–33.5 ℃ (29.2 ℃)	63.7%	63.6%
28 ℃	24.8–33.1 ℃ (29.7 ℃)	52.2%	25.3–33.6 ℃ (29.5 ℃)	58.2%	55.2%
29 ℃	24.8–33.7 ℃ (30.0 ℃)	47.7%	25.3–33.8 ℃ (29.8 ℃)	50.5%	49.1%
30 ℃	24.8–34.1 ℃ (30.0 ℃)	46.5%	25.3–34.0 ℃ (30.3 ℃)	38.7%	42.6%
31 ℃	24.8–34.4 ℃ (30.0 ℃)	46.5%	25.3–34.8 ℃ (30.7 ℃)	27.2%	36.9%
26 ℃+NV	19.9–32.4 ℃ (26.7 ℃)	95.1%	23.1–33.4 ℃ (28.8 ℃)	69.7%	82.4%
27 ℃+NV	19.9–32.4 ℃ (26.7 ℃)	95.1%	23.2–33.4 ℃ (29.0 ℃)	66.9%	81.0%
28 ℃+NV	19.9–32.4 ℃ (26.7 ℃)	95.0%	23.2–33.5 ℃ (29.3 ℃)	62.5%	78.8%
29 ℃+NV	19.9–32.4 ℃ (26.7 ℃)	94.9%	23.2–33.7 ℃ (29.6 ℃)	56.4%	75.6%
30 ℃+NV	19.9–32.5 ℃ (26.7 ℃)	94.7%	23.2–33.8 ℃ (30.0 ℃)	47.1%	70.9%
31 ℃+NV	19.9–32.5 ℃ (26.7 ℃)	94.6%	23.2–34.7 ℃ (30.3 ℃)	36.7%	65.7%

※Nighttime: 18:00–6:00; Daytime: 6:00–18:00

a high thermal mass. The outdoor temperature drop was faster than the indoor temperature drop. Moreover, the radiant floor cooling system, which increased the thermal storage of the target building using PCMs, released the heat into the indoor and underfloor spaces in the evening. In cases where the threshold outdoor temperature was more than 28 ℃, the windows were often closed before 18:00. Even when night ventilation was included, an increase in the SET* in the late afternoon was observed because of the temperature peak shift between the outdoor and indoor environments. Therefore, window-opening control using outdoor temperatures may not be a suitable control method for buildings with PCMs.

7.3.2.5. Window-opening control based on the outdoor wind speed

Focusing on window-opening control based on the outdoor wind speed, Fig. 7.8 presents the monthly averaged daily patterns of SET*, and Table 7.7 depicts the hourly SET* ranges with comfort evaluation. The monthly average SET* in December was 0.1–3.8 ℃ lower than that in the other months (January to November) because the monthly average

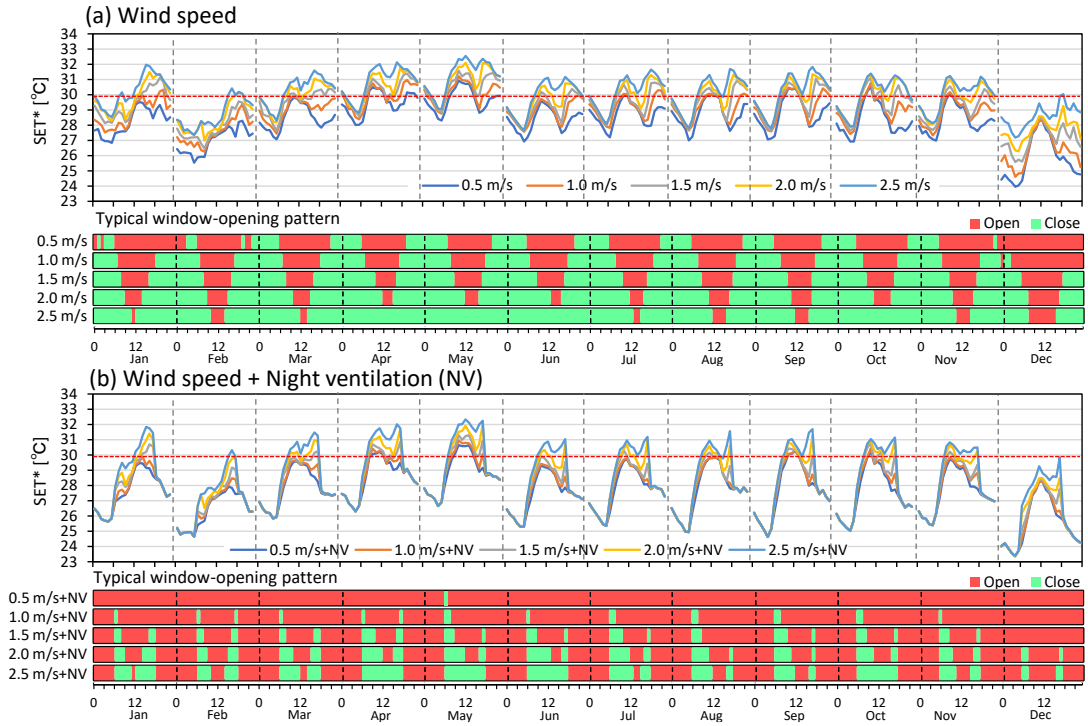

Fig. 7.8. Monthly averaged daily patterns of SET* controlled by the (a) outdoor wind speed and (b) outdoor wind speed and night ventilation (NV).

outdoor wind speeds in December were 0.6–1.1 m/s (daytime) and 0.6–0.9 m/s (nighttime) higher than those in the other months (Fig. 7.4d). In the afternoon, when the outdoor speed tended to be more than 0.5 m/s, the threshold wind speed strongly influenced the SET*. Thus, the diurnal average SET* in the case of the threshold of 0.5 m/s was 1.8 °C lower than that of 2.5 m/s.

The nocturnal average SET* ranged from 28.1–29.8 °C, with a comfort period of 50.1%–76.5%. The nocturnal wind conditions at the experimental site were calm, similar to typical weather conditions in hot and humid regions. Even in the case of a threshold wind speed of 0.5 m/s, the windows tended to be closed at night, and the indoor space could not dissipate heat effectively. Therefore, combining the threshold wind speed with night ventilation dramatically increased the thermal comfort period to 94.9%–95.2% at night. Similarly, windows were often closed in the morning owing to the low wind speed. The diurnal SET* when combining the threshold with night ventilation was 0.2–0.4 °C lower than that without night ventilation. When the window opening was controlled by the outdoor wind speed, the window-opening time affected the expansion of the thermal comfort period owing to the dominant influence of wind speed on thermal comfort in the hot and humid climate. The case

Table 7. 7. Hourly SET* ranges with thermal comfort evaluation controlled by the (a) outdoor wind speed and (b) outdoor wind speed and night ventilation (NV).

	Nighttime		Daytime		Whole
	SET*[℃] min–max (avg)	Comfort period [%]	SET*[℃] min–max (avg)	Comfort period [%]	Comfort period [%]
0.5 m/s	19.9–33.7 ℃ (28.1 ℃)	76.5%	19.9–34.2 ℃ (28.8 ℃)	65.2%	70.8%
1.0 m/s	20.2–33.8 ℃ (28.8 ℃)	63.7%	19.9–34.5 ℃ (29.1 ℃)	59.8%	61.7%
1.5 m/s	20.3–34.2 ℃ (29.3 ℃)	56.1%	19.9–34.8 ℃ (29.6 ℃)	52.5%	54.3%
2.0 m/s	20.3–34.2 ℃ (29.6 ℃)	52.0%	19.9–34.8 ℃ (30.0 ℃)	43.4%	47.7%
2.5 m/s	20.4–34.3 ℃ (29.8 ℃)	50.1%	19.9–35.3 ℃ (30.6 ℃)	33.9%	42.0%
0.5 m/s + NV	19.9–32.5 ℃ (26.7 ℃)	95.2%	19.9–33.8℃ (28.6 ℃)	70.0%	82.6%
1.0 m/s + NV	19.9–32.5 ℃ (26.7 ℃)	95.0%	19.9–34.2 ℃ (28.9 ℃)	65.7%	80.4%
1.5 m/s + NV	19.9–32.5 ℃ (26.7 ℃)	95.0%	19.9–34.7 ℃ (29.3 ℃)	58.8%	76.9%
2.0 m/s + NV	19.9–32.5 ℃ (26.7 ℃)	94.9%	19.9–34.7 ℃ (29.7 ℃)	50.7%	72.8%
2.5 m/s + NV	19.9–32.5 ℃ (26.7 ℃)	94.9%	19.9–35.1 ℃ (30.2 ℃)	41.4%	68.1%

※Nighttime: 18:00–6:00; Daytime: 6:00–18:00

of a threshold wind speed of 0.5 m/s achieved the lowest SET* throughout the year among the five types of threshold wind speeds. The SET* decreased further when combined with night ventilation.

7.3.2.6. Evaluation of electricity consumption

Fig. 7.9a depicts the simulation results of the monthly electricity consumption for space cooling. The thermostat in Room B was set to 27 ℃, which is the comfort temperature standard recommended by the Indonesian National Standard (SNI) [7.39], to calculate the cooling load in Room B. The annual performance factor (APF) of air conditioners in the room was assumed to be 5.7 based on a catalog study for room air conditioners [7.40], and the energy consumption was calculated by cooling load and performance factor of air conditioners. The annual electricity consumption for space cooling in Room B (without the radiant floor cooling system and ventilation), which was constructed using typical construction materials for Indonesian apartments, was 1588 kWh, although the simulation was conducted under unoccupied conditions without any internal heat gain. According to the results of a field survey in Jakarta, the average annual electricity consumption for space cooling was 1591 kWh [7.41].

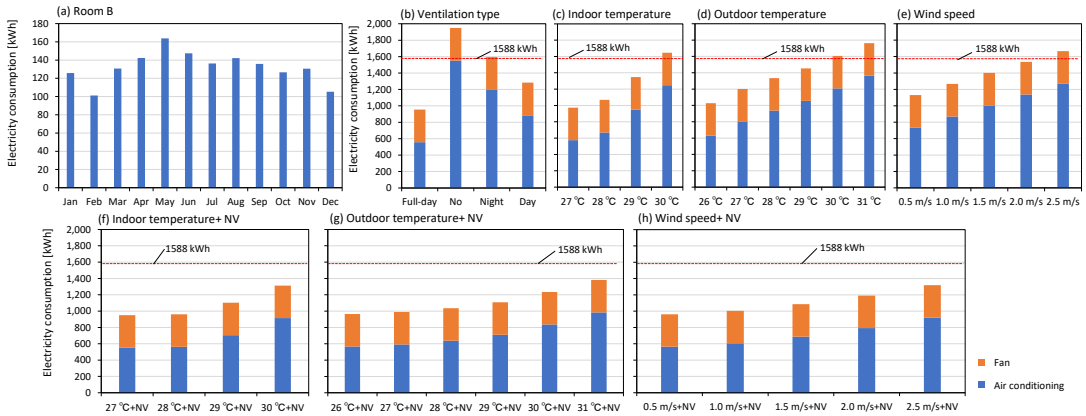

Fig. 7.9. (a) Monthly electricity consumption in Room B (without the radiant floor cooling system and ventilation) and (b–f) annual electricity consumption in Room A (with the radiant floor cooling system).

For the electricity consumption evaluation in Room A, the air conditioner was turned on, and the windows were closed when the SET* did not satisfy the thermal comfort range. Moreover, the electricity consumption of the ventilation fans for the underfloor space (393 kWh) which referred to the specification of the fan used in the field measurements (Chapters 3 and 4) was added to compare it with the electricity consumption in Room B and to demonstrate the total energy efficiency of the proposed system.

Figs. 7.9(b)–(f) show the annual electricity consumption for each case. In the case of no ventilation, the annual electricity consumption in Room A was 362 kWh higher than that in Room B because of the electricity consumption of the fan for the underfloor space. Without ventilative cooling, it may be difficult to dramatically reduce electricity consumption. Compared with no ventilation, night ventilation reduced the electricity consumption by 356 kWh. As discussed above, the SET* in Room A rapidly decreased immediately after opening the windows at 18:00 owing to ventilative cooling and, thus, contributed to reduced electricity consumption. Nevertheless, ventilative cooling at night did not significantly influence the reduction in electricity consumption owing to the small cooling load at night. The influence of ventilative cooling during the daytime was larger than that at night because the electricity consumption of day ventilation was 311 kWh lower than that of night ventilation. Full-day ventilation was the best window-opening pattern among the four basic ventilation modes for decreasing electricity consumption, with an annual electricity consumption of 955 kWh (Fig. 7.9b). The combination of the radiant floor cooling system and ventilative cooling throughout the day reduced the electricity consumption by 40% compared with the electricity consumption in Room B. Overall, the radiant floor cooling system reduced the electricity

consumption for cooling and ventilative cooling by opening the window, thus significantly contributing to the further reduction in electricity consumption.

When windows were opened based on the indoor air temperature, a lower threshold of the indoor air temperature resulted in lower electricity consumption, primarily because of ventilative cooling. For the indoor temperature threshold of 27 °C, the annual electricity consumption was 972 kWh. Applying night ventilation further reduced the electricity consumption owing to the retention of the thermal storage effect in the morning. The lowest annual electricity consumption of 951 kWh among the 34 cases was observed in the case of the combination of the threshold indoor temperature of 27 °C and night ventilation. In this annual simulation, this window-opening control minimized annual electricity consumption while maximizing the annual thermal comfort period.

Similar to the threshold indoor temperature, a lower threshold outdoor temperature and wind speed resulted in lower electricity consumption. Compared with the threshold temperature or wind speed alone, the addition of night ventilation reduced the electricity consumption by 22–370 kWh. Although Solgi et al. [7.42] indicated that warm nights and calm nocturnal wind conditions decreased the cooling effect of night ventilation in hot and humid regions, the annual simulation showed that night ventilation strongly contributed to a reduction in annual electricity consumption.

7.4. Discussion

7.4.1. Thermal comfort evaluation

Compared with the thermal comfort period in Room B (day ventilation), which is considered the typical context of apartments in Indonesia, the proposed system installed in Room A increased the thermal comfort period by up to 33% per year. Hasse et al. [7.43] reported that the annual potential of ventilative cooling to satisfy thermal comfort in major cities of Southeast Asia, such as Singapore, Kuala Lumpur, Bangkok, and Hanoi, ranged from 27%–50%. Wang et al. [7.44] showed that the annual thermal comfort period, which was defined as a 70% acceptance rate in a naturally ventilated building with various thermal properties of construction materials in Singapore, was approximately 85%. Compared with the systems proposed in previous studies, the proposed system in the present study strongly contributed to improving thermal comfort, which was 83.3% and 95.9% over a year, as evaluated using 80% and 70% acceptance rates, respectively (Table 7.4).

The ASHRAE Standard 55 indicates that the upper limit of the air velocity shall be 0.8 m/s when the OT is above 25.5 °C [7.45]. Deng et al. [7.46] suggested that a small opening area that reduces the influence of the outdoors can be effective in achieving thermal comfort.

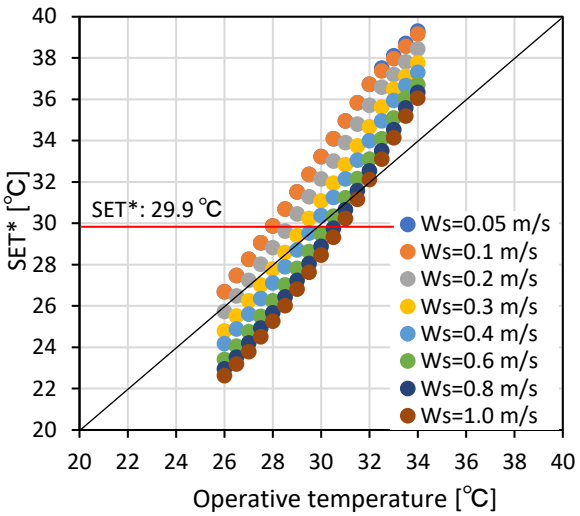

Fig. 7.10. Relationship between the operative temperature (OT) and SET* at various air velocities (80% RH, 0.5 clo, and 1.0 met).

It is difficult to achieve thermal comfort by closing the windows without sweat evaporation and convective heat transfer assisted by sufficient airflow in tropical climates. Therefore, occupants living in hot and humid climatic regions tend to prefer higher air velocities than those living in other climatic regions. Meita et al. [7.47] conducted a questionnaire survey on individuals living in apartments in Indonesia, and the results showed that more than 70% of the respondents felt that indoor airflow was high. Nevertheless, approximately 80% preferred higher wind conditions. Cândido et al. [7.48] found the minimum preferred air velocities in hot and humid climates to be 0.9 m/s for an OT of 30 ℃. Fig. 7.10 shows the relationship between OT and SET* at various air velocities, relative humidity of 80%, metabolic rate of 1.0 met, and clothing worn of 0.5 clo. When the OT is 30 ℃, an air velocity of more than 0.6 m/s is necessary to satisfy thermal comfort. In the case of full-day ventilation, the average air velocity was 0.7 m/s when the OT was approximately 30 ℃. The proposed system with the pivot window tended to supply the required airflow that satisfied the thermal comfort while reducing the indoor air temperature through the thermal storage effect of the PCMs (Fig. 7.10). However, when the OT exceeded 31 ℃, it may be difficult to achieve thermal comfort even with sufficient airflow, that is, an air velocity of 1.0 m/s (Fig. 7.10). Hence, other passive cooling methods that can reduce the OT and increase the air velocity should be investigated in future studies to further improve thermal comfort under higher temperature conditions

As discussed above, the annual average outdoor temperature and wind speed in the experimental field were 27.9 ℃ and 1.2 m/s, respectively. Putra et al. [7.49] classified the climate zones using passive cooling methods in Indonesia. The weather conditions in the experimental field were similar to those in the highest-temperature and lowest–wind speed

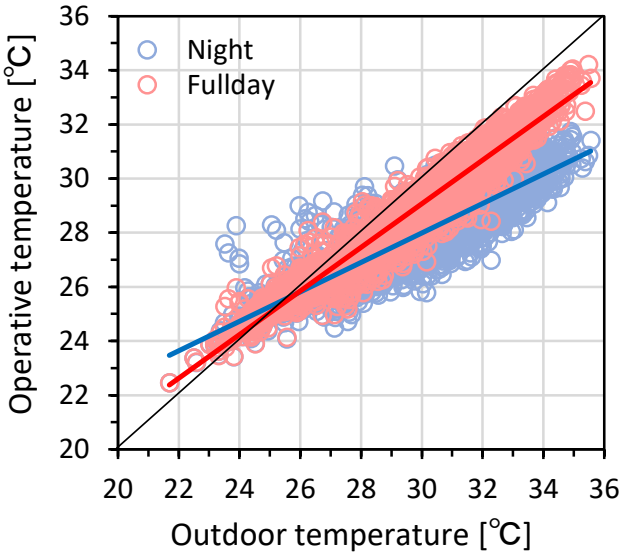

Fig. 7.11. Relationship between the outdoor temperature and the OT in the morning (6:00–12:00) in Room A (full day and night)

zones in the climate zone. This indicates that the experimental field in Tangerang has the harshest weather conditions for achieving thermal comfort using thermal storage and ventilation. Nevertheless, the longest comfort duration of the proposed system was 7293 h per year (8760 h). Although the phase change temperature of the PCMs must be adjusted for each climate zone, the proposed system, that is, the radiant floor cooling system and horizontal pivot window with optimum window-opening control, can be an effective passive cooling method for achieving thermal comfort across Indonesia.

7.4.2. Window-opening control method

Overall, night ventilation strongly contributed to satisfying the thermal comfort owing to heat dissipation at night and the thermal storage effect in the morning. The thermal comfort period during the nighttime and daytime in cases of night ventilation increased by 0.1%–48.1% and 1.8%–9.4% compared with those in the corresponding cases without night ventilation, respectively. Sorgato et al. [7.3] set a night ventilation operation control as the indoor OT is higher than the outdoor temperature. In the present study, the period of night ventilation was from 18:00–6:00, although the period during which the OT was higher than the outdoor temperature was from 15:00–6:00 on average. In the optimum case, that is, a threshold indoor temperature of 27 °C with night ventilation, the windows were generally opened during that period. Meanwhile, the indoor temperature was maintained by closing the

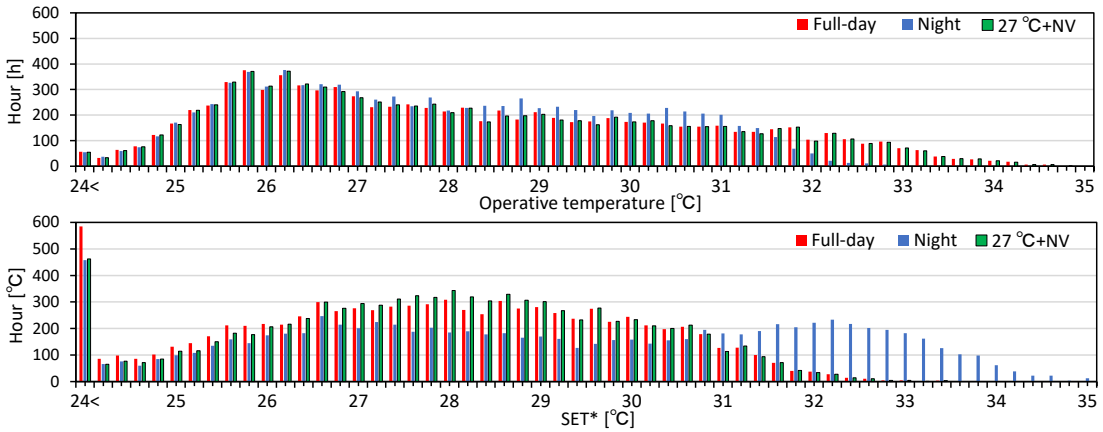

Fig. 7.12. The frequency of OT and SET*.

windows at 6:00 when the outdoor temperature tended to be the lowest throughout the day. This implies that a window-opening period from 15:00–6:00 was effective for night ventilation in hot and humid climates.

In the case of window-opening control with a threshold outdoor temperature, the thermal discomfort period often occurs in the afternoon owing to the peak temperature shift in buildings with a high thermal mass. Although fewer monitoring points employ the outdoor temperature, compared with the indoor air temperature and its reduced installation cost and simplified control system in an actual building management system (BMS) [7.50], window-opening controlled by the outdoor temperature may not be a suitable control method for naturally ventilated buildings installed with PCMs.

Regarding the windows controlled by the outdoor wind speed, a drop in the SET* was observed in the afternoon when the outdoor wind speed tended to be high. Calm wind conditions in the evening led to frequent increases in the SET*. As discussed above, the influence of airflow on thermal comfort (i.e., SET*) was significant in this study. Although the wind conditions in the experimental field were almost stable owing to sea and land breezes throughout the year, sudden fluctuations in the wind speed can increase the frequency of window opening and closing. Opening the windows in the morning may dissipate the coolness stored at night. Hence, controlling the window opening based on the outdoor wind speed is not an appropriate method for the proposed system because it does not consider the thermal storage effect of the radiant floor cooling system.

Fig. 7.11 shows the relationship between the outdoor temperature and OT in the morning (6:00–12:00) in Room A (full day and night ventilation). As discussed above, night ventilation effectively dissipated the heat and decreased the indoor temperature at night. Thus, the decrease in the OT when employing night ventilation in the following morning was gentler than that in the case of full-day ventilation.

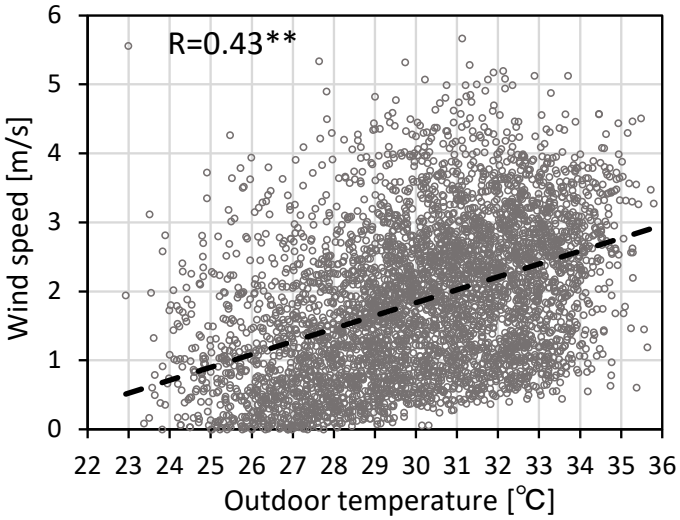

Fig. 7.13. Relationship between diurnal outdoor temperature and wind speed in the experimental site (2020).

Fig. 7.12 shows the frequency of the OT and SET* in Room A in cases of full-day ventilation, night ventilation, and the indoor temperature threshold of 27 °C with night ventilation, which showed the longest annual thermal comfort period in this study. The OT range for night ventilation was narrower than that for the full-day ventilation (Fig. 7.12). As shown in Fig. 7.10, the OT of 27 °C achieved thermal comfort even when the air velocity was approximately zero. A threshold indoor temperature of 27 °C can be considered the upper limit to satisfy the thermal comfort in the case of a closed window and high humidity, that is, a relative humidity of approximately 80%. Previous study showed that natural ventilation system often combined multiple conditions, such as indoor temperature, outdoor temperature, outdoor wind speed, and dew points, to allow the outdoor air to enter the room [7.51]. Meanwhile, a threshold indoor temperature of 27 °C proposed in this study is much more simple criteria for opening windows.

Closing the windows until the indoor temperature exceeded 27 °C extended the thermal comfort period owing to the thermal storage effect of the radiant floor cooling system. Closing the window in the morning increased the time of the OT below 27 °C by 35–95 h compared with full-day ventilation (Fig. 7.12). In the case of the optimum window-opening control, closing the windows in the morning, which maintained the thermal storage effect, increased the frequency of SET* from 27–30 °C (Fig. 7.12). Although the optimum window-opening control cannot reduce the minimum SET* (such as less than 24 °C) similar to that achieved with full-day ventilation because of the absence of comfort ventilation in the morning, it contributed to stabilizing the SET* owing to the maintenance of the thermal storage effect, regardless of the outdoor condition. Based on the relationship between the operative and

outdoor temperatures, we found that the thermal storage effect of the system was effective in achieving thermal comfort until the outdoor temperature reached approximately 28 °C (Fig. 7.11). Meanwhile, the outdoor wind speed increased as the temperature increased (Fig. 7.13); thus, the influence of comfort ventilation became sufficiently large to open the windows. This trend in the wind speed and temperature has been observed in Indonesia [7.49, 7.52]. These results imply that opening the windows in the case of a threshold indoor temperature of 27 °C with night ventilation can maximize the annual thermal comfort of the proposed system in the hot and humid climates.

7.4.2.1. Feasibility of window-opening control

Table 7.8 presents the hourly SET* ranges in the case of applying a simple opening in Room A. Compared with the horizontal pivot window, simple opening decreased the annual thermal comfort period by 17.2% because of lower air velocities. Nevertheless, even in the case of the simple opening, opening the windows when the indoor temperature exceeded 27 °C with night ventilation increased the thermal comfort period compared with that with full-day ventilation. Therefore, optimum window-opening control can improve thermal comfort, regardless of the window type.

Table 7.8. Hourly SET* ranges with thermal comfort evaluation in Room A installed with a horizontal pivot window and simple opening

	Nighttime		Daytime		Whole
	SET*[℃] min–max (avg)	Comfort period [%]	SET*[℃] min–max (avg)	Comfort period [%]	Comfort period [%]
Horizontal pivot window in Room A					
Full-day	19.9–32.4 ℃ (26.6 ℃)	95.2%	19.9–33.4 ℃ (28.6 ℃)	71.0%	83.1%
27 ℃+NV	19.9–32.4 ℃ (26.7 ℃)	95.2%	23.2–33.4 ℃ (28.9 ℃)	71.3%	83.3%
Simple opening in Room A					
Full-day	21.2–32.8 ℃ (27.4 ℃)	88.9%	20.8–35.1 ℃ (30.0 ℃)	42.9%	65.9%
27 ℃+NV	21.2–32.8 ℃ (27.4 ℃)	88.9%	23.2–35.1 ℃ (30.1 ℃)	44.0%	66.4%
Simple opening in Room A, assumed in the built-up area					
Full-day	21.7–32.8 ℃ (27.5 ℃)	87.8%	21.4–35.1 ℃ (30.4 ℃)	35.5%	61.7%
27 ℃+NV	21.7–32.8 ℃ (27.5 ℃)	87.8%	23.2–35.1 ℃ (30.4 ℃)	37.2%	62.5%

※Nighttime: 18:00–6:00; Daytime: 6:00–18:00

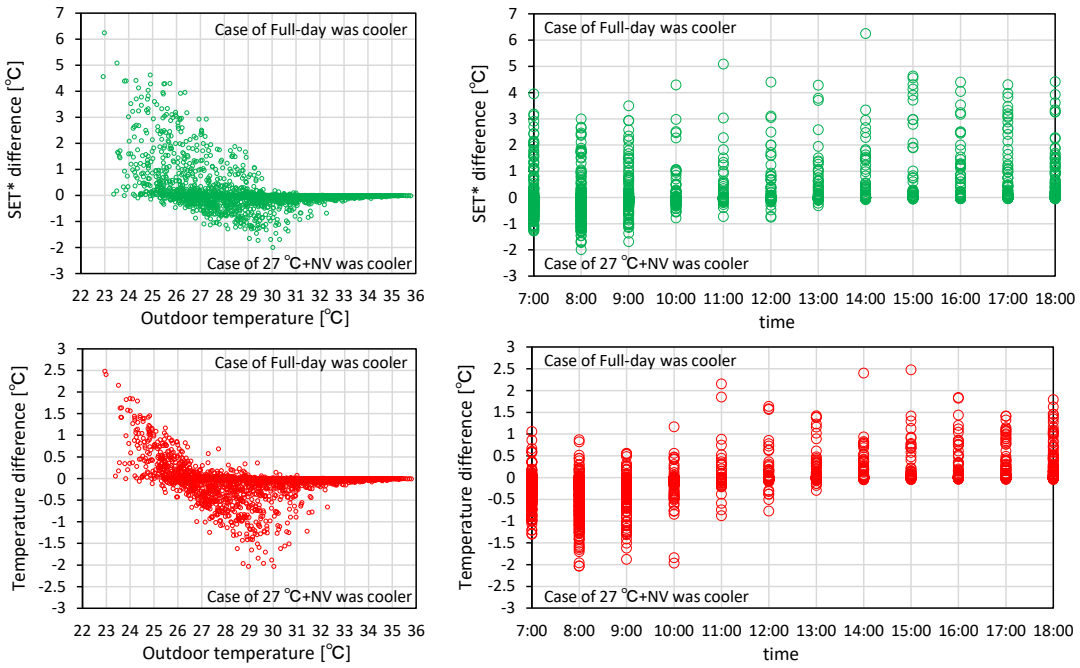

Fig. 7.14. SET* and temperature difference between the case of full-day ventilation and case of threshold indoor temperature of 27 °C with night ventilation during the daytime.

Although the threshold indoor temperature of 27 °C with night ventilation demonstrated the longest thermal comfort period, the difference in the annual thermal comfort period compared with the case of full-day ventilation was only 0.2% in case of the horizontal pivot window. The large influence of comfort ventilation during the daytime through the horizontal pivot window, which is the preferred window type for comfort ventilation, may have resulted in a small difference. Meanwhile, the difference of thermal comfort period between the case of full-day ventilation and case of threshold indoor temperature of 27 °C with night ventilation during the daytime increased by 0.8% when the simple opening was installed in Room A, compared to the horizontal pivot window due to the decrease in the influence of comfort ventilation. Here, thermal comfort in cased on the reduced influence of comfort ventilation was evaluated. Taniguchi and Akamine [7.53] reported that the wind pressure coefficient in a build-up area (gross building coverage ratio of 43%) was decreased by approximately 20%, compared with the area with the gross building coverage ratio of 33%. The building model using the simple opening with the decreased wind pressure coefficient, i.e., 80% of the original model, was constructed. Table 7.8 shows the results of the thermal comfort period in case of the simple opening with the built-up area. The difference of the diurnal thermal comfort period between two cases increased to 1.7%.

Fig. 7.14 presents the SET* and temperature difference between the case of full-day ventilation and case of threshold indoor temperature of 27 °C with night ventilation during the daytime. As discussed in Chapter 6, closing the windows prevented from dissipating the cool air through thermal storage effect. In case of window-opening controlled by the threshold indoor temperature of 27 °C with night ventilation, the indoor air temperature tended to be cooler than that of the full-day ventilation in the morning (until 10:00), and thus the reduced air temperature contributed to the SET* reduction. The largest air temperature difference was observed when the outdoor temperature was approximately 29–30 °C, which corresponds with a peak melting temperature of the PCMs. The aforementioned window-opening control method that improve thermal comfort may be more suitable for buildings in the built-up area, where the outdoor wind speed tends to be lower than that in the open area or cooler outdoor temperature area compared with the experimental field (Tangerang) if a phase change temperature of PCMs is adjusted to the weather condition.

7.4.3. Limitation

For airflow analysis, a regression equation was created between the airflow rate for the room and the air velocity in the middle of the rooms. The R^2 of the regression equation was relatively high, that is, 0.69–0.84, because the large influence of sea and land breezes in the experimental field stabilized the diurnal and nocturnal prevailing wind directions, which were perpendicular to the northern and southern openings. Nevertheless, it may be difficult to use the linear regression equation and same coefficients as those in the equation shown in Table 7.1 to calculate the indoor air velocity if the outdoor wind direction changes frequently, as observed in multi-story buildings and built-up areas. As shown in Fig. 7.3, the replication of the indoor air velocity from cross winds needs to be improved in future studies. Even in the case of a same window type, that is, simple opening, the coefficient was changed owing to the room position (Table 7.1). Because the indoor airflow pattern through wind-driven ventilation depends on the building shape, window type, and outdoor wind condition [7.54], creating a regression equation for each designated point and above-mentioned condition is necessary.

7.5. Summary

In Chapter 7, a coupled simulation model of thermal energy simulation (TES) and airflow network (AFN) was constructed for naturally ventilated buildings, wherein a comprehensive radiant floor cooling system, including window systems, window-opening control, and PCMs, was installed in a hot and humid climate. Chapter 7 clarified the influence of window-opening control on the thermal storage effect of the PCMs and ventilative cooling,

i.e., comfort ventilation and night ventilation, such that thermal comfort is maximized while reducing energy consumption throughout the year. The coupled TES model was validated by comparing it with the results of the field measurement conducted in the hot and humid climate of Indonesia, along with the coupled CFD simulation under naturally ventilated conditions. Using the validated coupled TES model, an annual simulation was conducted for the target building, and the relationship between the thermal storage effect of PCMs and ventilative cooling was investigated to determine the optimum window-opening control method. The main findings are summarized as follows:

- The validation results showed that the RMSEs of the temperature ranged from 0.2–0.5 ℃, with an R^2 of 0.96–0.99 in the coupled TES. Compared with the coupled CFD, which calculates the convective heat transfer coefficient based on the air velocity near the construction surfaces, the RMSE in the coupled TES tended to be large when a relatively high air velocity (0.4 m/s on average) was observed because of the dominant influence of forced convection. At night and in the morning, the temperature differences between the coupled TES and the coupled CFD could not be identified because of the influence of natural convection. Overall, the results of the coupled TES had relatively high accuracy.

- A linear regression method was constructed to calculate the indoor air velocities based on the airflow rates. The RMSE of the air velocities ranged from 0.1–0.2 m/s in the coupled TES with the regression method. Although the coupled TES was used to calculate a single air velocity for each node with a low calculation load, it demonstrated a similar accuracy compared with the coupled CFD and is considered an effective calculation method for annual thermal comfort evaluation.

- The floor cooling system and horizontal pivot window with optimum window-opening control increased the thermal comfort period based on the SET* by up to 83.3% throughout the year. The weather conditions of the experimental field with an annual outdoor temperature of 27.9 ℃ and a wind speed of 1.2 m/s were similar to those of the highest-temperature and lowest–wind speed climate zones in Indonesia. This implies that the proposed system is an effective passive cooling method to achieve thermal comfort in the hot and humid climates.

- In addition to thermal comfort, the annual electricity consumption for space cooling in Room A (test) was reduced by 41% compared with that of Room B (control) when the window opening was controlled by a threshold indoor temperature of 27 ℃ and night ventilation. In the morning, the thermal storage effect of PCMs using night ventilation extended the thermal comfort period and reduced the cooling load. As the outdoor temperature increased, the outdoor

wind speed tended to increase, and the comfort ventilation compensated for the increased room temperature. Considering the influences of room temperature and air velocity on the SET*, opening the windows when the indoor temperature exceeds 27 °C with night ventilation can maximize the annual thermal comfort and reduce energy consumption in the hot and humid climate.

Chapter 8
Conclusion

8.1. Conclusion

The main objective of this study is to clarify the thermal performance of residential buildings with an effective combination of passive cooling methods for hot and humid climates in terms of thermal comfort. In particular, this study focuses on the combination of natural ventilation and phase change material (PCM), and then evaluates its cooling effect on residential buildings. The conclusions of this study are as follows:

In Chapter 1 "Introduction",
context of passive cooling methods that reduce the energy consumption and satisfy thermal comfort was described. In particular, implementing passive cooling in developing tropical countries can be effective because the demand for space cooling was occurred throughout a year. Nevertheless, using a single passive cooling method alone is difficult to achieve thermal comfort in hot and humid climates. Based on these, the objective of this study and the framework of the thesis was described.

In Chapter 2 "A review and proposal of passive cooling methods",
the comprehensive overview of the passive cooling methods in hot and humid climates was shown using text mining-based bibliometric analysis method The results using 39,604 publications showed that natural ventilation took a vital role in passive cooling methods improving thermal comfort in hot and humid climates and the number of studies on PCM has rapidly increased since the 2010s. Although the combination of natural ventilation and PCM was not observed in the co-occurrence networks and previous research, the combination of the

comfort ventilation and the thermal storage effect improved the thermal environment in the traditional Dutch colonial buildings. Given the research gap and traditional knowledge, a novel floor cooling system using phase change materials (PCMs) for naturally ventilated buildings was finally proposed.

In Chapter 3 "Optimum window design for ventilative cooling with radiant floor cooling systems",
a field measurement was conducted to determine the effective window design for ventilative cooling with the floor cooling system proposed in Chapter 2. The results showed that the horizontal pivot window increased the air velocity at the occupied level (FL+1.1 m), while reducing it near the floor. Consequently, the horizontal pivot window and floor cooling system reduced the standard effective temperature (SET*) by 0.8 ℃ at the middle of the room. Although the decreased air velocity near the floor surface reduced the heat transfer coefficient by 1.5 W/m^{2}K, the high thermal storage floor strongly influenced the retention of thermal storage effect. The results in Chapter 3 indicate that the most essential point of window design in the proposed system is not to reduce the air flow near the floor structure, but to improve the comfort ventilation at the occupied level.

In Chapter 4 "Field measurement of thermal storage effect of phase change materials",
another field measurement was conducted to ensure the thermal storage effects. The floor surface temperature reduction, compared with the reference room, was approximately 0.7–1.5 °C when forced ventilation was adopted for the underfloor space at night. The floor surface temperature reduction was stable regardless of window-opening conditions because the PCM fusion was the influential factor of the thermal storage effect during the daytime. Moreover, cooled air accumulated below FL+0.6 m in the room when the wind speed near the floor surface was less than 0.2 m/s.

In Chapter 5 "Numerical simulation of thermal storage effect through night ventilation",
a coupled simulation of heat balance analysis and CFD simulation was conducted to clarify the influence of each component, i.e., louver, ventilation fans, and height of the underfloor space, which cannot be investigated in Chapter 4 because of the limited time and cost. The coupled CFD was validated with the field measurement in Chapter 3. The results of the sensitivity analysis showed that the air velocity that ensures the solidification of the PCMs in the underfloor space was found to be a key parameter in the proposed system. An increase in the air velocity increases the storage of coolness at night. In addition, the thermal storage of the proposed floor cooling system was maximized when the operational schedule of the fans was controlled by the outdoor temperature.

In Chapter 6 "Annual simulation of phase change materials considering phase state with hysteresis",
the thermal energy simulation (TES) was developed in Chapter 6 to evaluate the annual performance of the proposed floor cooling system that consider the hysteresis of PCM and to determine its design guidelines and indicators, referring to the results in Chapter 5. The annual evaluation indicated that the risk of condensation which is the problem for implementing radiant cooling systems in hot and humid climates in the proposed floor cooling system was much lower than that of the conventional radiant cooling systems. Further annual analysis showed that the daily maximum and minimum ambient temperatures of the PCMs significantly affected the maximum and minimum liquid fractions indicating the phase states of the PCMs, respectively. A reasonable annual average PCM utilization rate that is calculated liquid fractions was approximately 70% to maintain a low floor surface temperature throughout the year.

In Chapter 7 "Thermal comfort evaluation of window-opening control for ventilative cooling and thermal storage effect",
the annual TES was conducted to determine the optimum window-opening control that maximizes annual thermal comfort using the optimum window system and PCMs with the optimum operation. The TES model developed in Chapter 6 was modified by coupling with the air flow network model to clarify the influence of window-opening control on the thermal storage effect of the PCMs and ventilative cooling. For the optimum window-opening control to maximize thermal comfort in the hot and humid climate, an indoor temperature of 27 °C can be considered as a criterion to open the windows for comfort ventilation in addition to night ventilation for the thermal storage effect. When this criterion was applied, the thermal comfort period in the room with PCMs increased to 83.3%, while the annual electricity consumption for space cooling in the test room (the proposed system) was reduced by 41% compared with that of the control room.

Three simulation methods, i.e., CFD simulation coupled with heat balance analysis, thermal energy simulation (TES), and TES coupled with air flow network (AFN), were constructed in Chapters 5–7 to evaluate the influence of the phase state of the PCMs, night ventilation, thermal storage effects, and comfort ventilation. When the above-mentioned findings for the combination of natural ventilation and PCM were applied, occupants in hot and humid climates can spend most of the year comfortably without ACs, and thus reducing energy consumption. The results of the field measurements and simulation models constructed in this study can be used as a guideline for the installation of PCMs to naturally ventilated buildings in hot and humid climates.

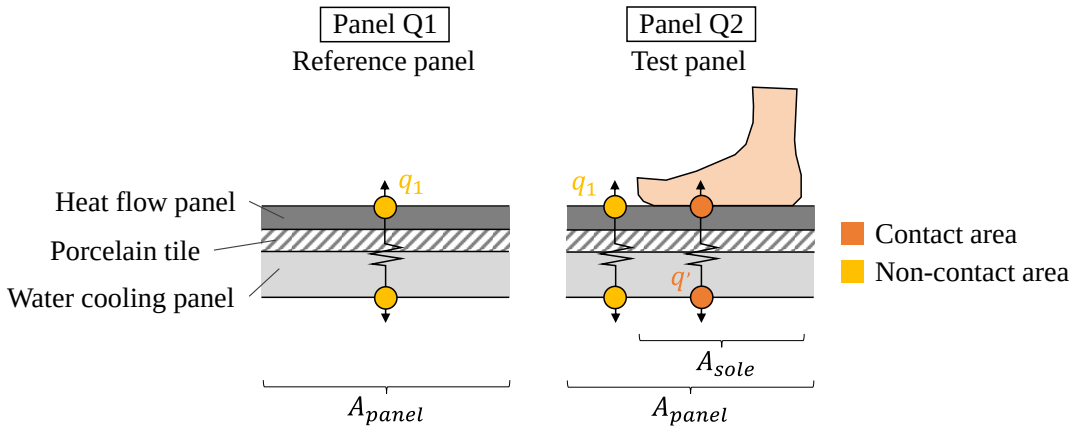

Fig. 8.1. Method for calculating the heat flow of the entire sole.

8.2. Future work

8.2.1. Thermal comfort evaluation

In this study, the influence of the proposed floor cooling system on thermal comfort was evaluated mainly in terms of SET*. However, in the tropics, people tend to stay directly on the floor structure in bare feet, which is often made of ceramic tiles without any cover, such as a carpet [8.1, 8.2]. Sakuragawa [8.3] figure out a negative correlation between the thermal conductivity of materials and thermal sensation when subjects contacted with building materials. As the thermal conductivities of ceramic tiles are higher than those of wood and carpets [8.4], it would be easier for bare feet to feel cool. This implies that the proposed floor cooling system can improve thermal comfort further, considering the conductive heat transfer. Under these circumstances, thermal comfort should be determined differently, putting more emphasis on conductive heat transfer through direct contact. A comprehensive thermal comfort index that considers the conductive heat transfer is necessary to evaluate the proposed floor cooling system.

8.2.2. Hybrid floor cooling system

The results of the proposed system showed that occupants in hot and humid climates can spend most of the year comfortably without ACs. Based on the findings of this study, the implementation of the system that considers the local lifestyle is necessary. Figs. 8.2 and 8.3

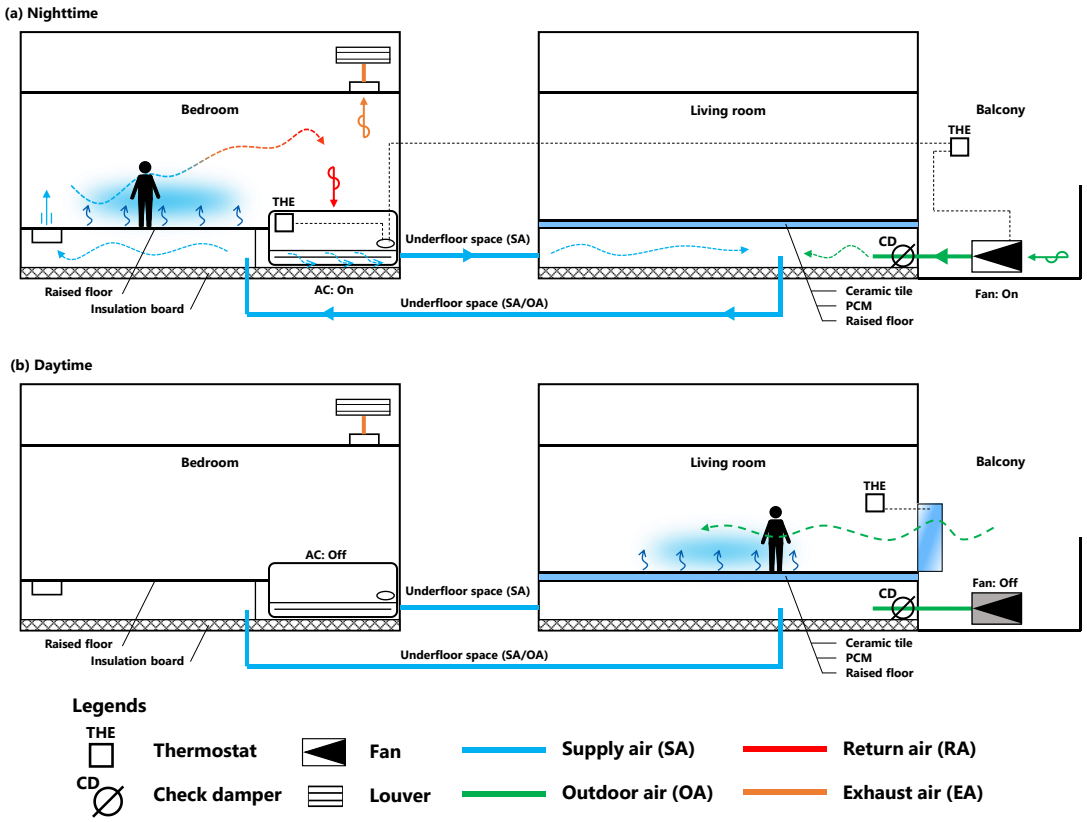

Fig. 8.2. Schematic diagram of the hybrid floor cooling system during (a) nighttime and (b) daytime.

show the hybrid floor cooling systems that may increase thermal storage effect further as an example of implementation, while considering the typical lifestyle in Southeast Asia. The relatively small cooling effect of the thermal storage of the PCMs, compared with comfort ventilation, was the limitation of this study. Adopting a lower phase change temperature, such as 20–27 °C which correspond to comfort temperature range recommended by Saffari et al. [8.5], can increase the cooling effect because a lower melting temperature results in lower floor surface temperature when the PCMs melt. Nevertheless, cool nocturnal conditions are required to solidify the PCMs if the lower phase change temperature is adopted. Meanwhile, turning on ACs at night is a typical AC usage pattern in Southeast Asia, such as Indonesia and Malaysia because occupants firstly install the AC in their bedroom [8.6, 8.7].

The main idea of the hybrid cooling system is to subsidiarily cool the PCM during nighttime (Fig. 8.2a). The ACs and supply air inlets are installed in the underfloor space and on the floor, respectively. As discussed, occupants tend to use the ACs during nighttime in the bedrooms. Therefore, the ACs cool the PCM installed in the living room as well as the air in

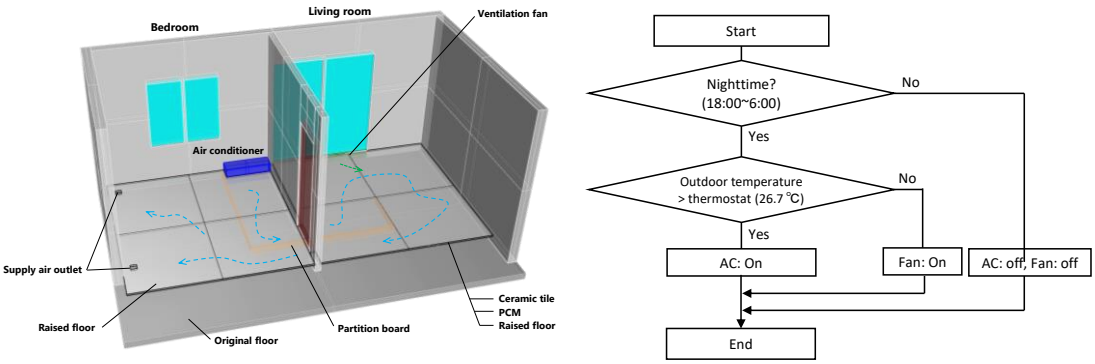

Fig. 8.3. Example of layout for hybrid floor cooling system and logic flow chart for controlling AC and ventilation fans.

the bedroom. As the temperature of the supply air from the ACs is much lower than the outdoor temperature in the evening, the proposed hybrid system may select a PCM with a cooler phase change temperature, regardless of the outdoor conditions. Nevertheless, using the ACs can increase the energy consumption. In the proposed hybrid system, the operation of ACs can be switched to that of ventilation fans when the outdoor air temperature reaches a set point temperature to reduce the duration of AC usage (Fig. 8.3). Controlling the operation of ACs and fans may contribute to reducing the energy consumption, while maintaining thermal comfort.

Meanwhile, the proposed window-opening control for thermal storage effect and comfort ventilation is adopted during daytime (Fig. 8.2b). The enhanced thermal storage effect by a lower phase change temperature and subsidiary AC usage can extend the period of closing windows, and thus it may improve thermal comfort further. Moreover, even if the operation of ACs during daytime is demanded, the thermal storage effect can contribute to reducing the peak cooling loads and cooling capacity of ACs.

References

Chapter 1

[1.1] UN (2019) World Population Prospects 2019: Data Booklet, United Nations, Department of Economic and Social Affairs, Population Divisio.

[1.2] EIA (2019) International Energy Outlook 2019 with projections to 2050. Energy Information Administration, Washington DC, USA.

[1.3] X. Cao, X. Dai,J. Liu, Building energy-consumption status worldwide and the state-of-the-art technologies for zero-energy buildings during the past decade, Energy Build. 128 (2016) 198-213. https://doi.org/10.1016/j.enbuild.2016.06.089

[1.4] IPCC (2014) IPCC Working Group Ⅲ - Mitigation of Climate Change Chapter 9: Buildings, Cambridge University Press, Cambridge, UK and New York, USA.

[1.5] UNEP (2009) Buildings and Climate Change, Summery for decision-makers, United Nations Environment Programme, Nairobi, Kenya.

[1.6] Bappenas, BPS, UNFPA (2018) Proyeksi Penduduk Indonesia; Indonesia Population Projection 2015-2045, Indonesia.

[1.7] National Energy Council (2019) Indonesia Energy Outlook 2019, Jakarta, Indonesia.

[1.8] U. Surahman and T Kubota (2012) Life cycle energy and CO_2 emissions in unplanned buildings of Indonesia, PLEA2012, Lima, Peru.

[1.9] International Energy Agency (2019) Southeast Asia Energy Outlook, International Energy Agency, Paris, France.

[1.10] S.E. Belcher, J.N. Hacker, D.S. Powell, Constructing design weather data for future climates, Build. Serv. Eng. Res. Technol. 26 (2005) 49-61.

[1.11] BP (2019) BP Statistical Review 2019; Indonesia's energy market in 2018, UK.

[1.12] World Bank (2020) World Bank East Asia and Pacific Economic Update: East Asia and Pacific in the Time of COVID-19, pp.172.

[1.13] Coordinating Ministry for Economic Affairs (2011) Masterplan for Acceleration and Expansion of Indonesia Economic Development 2011-2025, Jakarta, Indonesia.

[1.14] World Bank (2019) Time to ACT Realizing Indonesia's Urban Potential, M. Roberts, G. Sander and S. Tiwari (Eds.), Washington DC, USA.

[1.15] SMF Indonesia (2017) SMF Highlight, Indonesia.

[1.16] N. Kumer, T. Kubota, Y. Tominaga, M. Shirzadi, R. Bardhan, CFD simulations of wind-induced ventilation in apartment buildings with vertical voids: Effects of pilotis and wind fin on ventilation performance, Build. Environ. 194 (2021) 107666. https://doi.org/10.1016/j.buildenv.2021.107666

[1.17] N.Y. Nugroho, S. Triyadi, S. Wonorahardjo, Effect of high-rise buildings on the surrounding thermal environment, Build. Environ. 207 (2022) 108393. https://doi.org/10.1016/j.buildenv.2021.108393

[1.18] R. Debnath, G.M.F. Simoes, R. Bardhan, S.M. Leder, R. Lamberts, M. Sunikka-Blank, Energy justice in slum rehabilitation housing: an empirical exploration of built environment effects on socio-cultural energy demand, Sustain. 12 (2020) 3027. https://doi.org/10.3390/su12073027

[1.19] R. Bardhan, R. Debnath, J. Malik, A. Sarkar, Low-income housing layouts under socio-architectural complexities: a parametric study for sustainable slum rehabilitation, Sustain. Cities Soc. 41 (2018) 126–138. https://doi.org/10.1016/j.scs.2018.04.038

[1.20] J. Lueker, R. Bardhan, A. Sarkar, L. Norford, Indoor air quality among Mumbai's resettled populations: comparing Dharavi slum to nearby rehabilitation sites, Build. Environ. 167 (2020) 106419. https://doi.org/10.1016/j.buildenv.2019.106419

[1.21] M.N.F. Alfata, N. Hirata, T. Kubota, A.M. Nugroho, T. Uno, S.N. Ekasiwi, I.G.N. Antaryama, Field investigation of indoor thermal environments in apartments of Surabaya, Indonesia: Potential passive cooling strategies for middle-class apartments. Energy Procedia. 78 (2015) 2947-2952. https://doi.org/10.1016/j.egypro.2015.11.674

[1.22] M.N.F. Alfata, N. Hirata, T. Kubota, A.M. Nugroho, T. Uno, I.G.N. Antaryama, S.N. Ekasiwi, Thermal comfort in naturally ventilated apartments in Surabaya, Indonesia, Procedia Eng. 121 (2015) 459-467. https://doi.org/10.1016/j.proeng.2015.08.1093

[1.23] H. Mori, T. Kubota, I.G.N. Antaryama, S.N.N. Ekasiwi, Analysis of window-opening patterns and air conditioning usage of urban residences in tropical Southeast Asia, Sustain. 12 (2020) 10650. https://doi.org/10.3390/su122410650

[1.24] V.K. Venkiteswaran, J. Liman, S.A. Alkaff, Comparative study of passive cooling methods for reducing cooling load. Energy Procedia. 142 (2017) 2689-2697. https://doi.org/10.1016/j.egypro.2017.12.212

[1.25] D.K. Bhamare, M.K. Rathod, J. Banerjee, Passive cooling techniques for building and their applicability in different climatic zones - The state of art, Energy Build. 198 (2019) 467-490. https://doi.org/10.1016/j.enbuild.2019.06.023

[1.26] N.B. Greetha, R. Velraj, Passive cooling methods for energy efficient buildings with and without thermal energy storage – A review, Energy Educ. Sci. Technol. Part A: Energy Sci. Res. 29 (2012) 913-946.

[1.27] K. Panchabikesan, K. Vellaisamy, V. Ramalingam, Passive cooling potential in buildings under various climatic conditions in India, Renew. Sustain. Energy Rev. 78 (2017) 1236-1252. https://doi.org/10.1016/j.rser.2017.05.030

[1.28] A. Tejero-González, M. Andrés-Chicote, P. García-Ibáñez, E. Velasco-Gómez, F.J. Rey-Martínez, Assessing the applicability of passive cooling and heating techniques through climate factors: An overview, Renew. Sustain. Energy Rev. 65 (2016) 727-742. https://doi.org/10.1016/j.rser.2016.06.077

[1.29] S.B. Sadineni, S. Madala, R.F. Boehm, Passive building energy savings: A review of building envelope components. Renew. Sustain. Energy Rev. 15 (2011) 3617-3631. https://doi.org/10.1016/j.rser.2011.07.014

[1.30] S. Mirrahimi, M.F. Mohamed, L.C. Haw, N.L.N. Ibrahim, W.F.M. Yusoff, A. Aflaki, The effect of building envelope on the thermal comfort and energy saving for high-rise buildings in hot-humid climate, Renew. Sustain. Energy Rev. 53 (2016) 1508-1519. https://doi.org/10.1016/j.rser.2015.09.055

[1.31] A.S. Bachrun, T.Z. Ming, A. Cinthya, Building envelope component to control thermal indoor environment in sustainable building: A review, Sinergy. 23 (2019) 79-98. http://doi.org/10.22441/sinergi.2019.2.001

[1.32] N.A. Azmi, S.H. Ibrahim, A comprehensive review on thermal performance and envelope thermal design of mosque building. Build. Environ. 185 (2020) 107305. https://doi.org/10.1016/j.buildenv.2020.107305

[1.33] W.F.M. Yusoff, M.I. Shaharil, M.F. Mohamed, M.R.M. Rasani, A.R. Sapian, N.D. Dahlan, Review of openings with shading devices at naturally ventilated buildings, Archit. Eng. Des. Manag. (2022) https://doi.org/10.1080/17452007.2022.2095553

[1.34] S.M. Al-Masrani, K.M. Al-Obaidi, N.A. Zalin, M.I.A. Isma, Design optimization of solar shading systems for tropical office buildings: Challenges and future trends, Sol. Energy. 170 (2018) 849-872. https://doi.org/10.1016/j.solener.2018.04.047

[1.35] A.Z. Zulkarnain, M.N.M. Salleh, Z.A. Aziz, Thermal-daylighting balance through building shading devices: A review on factors and methods, Malaysian J. Sustain. Environ. 8 (2021) 157-178. https://doi.org/10.24191/myse.v8i3.15894

[1.36] Suhendri, M. Hu, Y. Su, S. Riffat, J. Darkwa J. Implementation of passive radiative cooling technology in Buildings: A review, Build. 10 (2020) 215. https://doi.org/10.3390/buildings10120215

[1.37] D.G.L. Samuel, S.M.S. Nagendra, M.P. Maiya, Passive altanatives to mechanical air conditioning of building: A review. Build. Environ. 66 (2013) 54-64. https://doi.org/10.1016/j.buildenv.2013.04.016

[1.38] A. Tejero-González, A. Franco-Salas, Optimal operation of evaporative cooling pads: A review, Renew. Sustain. Energy Rev. 151 (2021) 111632. https://doi.org/10.1016/j.rser.2021.111632

[1.39] P.M. Cuce, S. Riffat, A state of the art review of evaporative cooling systems for building applications, Renew. Sustain. Energy Rev. 54 (2016) 1240-1249. http://dx.doi.org/10.1016/j.rser.2015.10.066

[1.40] M. Santamouris, D. Kolokotsa, Passive cooling dissipation techniques for buildings and other structures: The state of the art. Energy Build. 57 (2013) 74-94. https://doi.org/10.1016/j.enbuild.2012.11.002

[1.41] A. Aflaki, N. Mahyuddin, Z.A. Mahmoud, M.R. Baharum, A review on natural ventilation applications through building façade components and ventilation openings in tropical climates. Energy Build. 101 (2015) 153-162. https://doi.org/10.1016/j.enbuild.2015.04.033

[1.42] T. Ahmed, P. Kumar, L. Mottet, Natural ventilation in warm climates: The challenges of thermal comfort, heatwave resilience and indoor air quality. Renew. Sustain. Energy Rev. 138 (2021) 110669. https://doi.org/10.1016/j.rser.2020.110669

[1.43] N. Izadyar, W. Miller, B. Rismanchi, V. Garcia-Hansen, Impacts of façade openings' geometry on natural ventilation and occupants' perception: A review. Build. Environ. 170 (2020) 106613. https://doi.org/10.1016/j.buildenv.2019.106613

[1.44] E. Solgi, Z. Hamedani, R. Fernando, H. Skates, N.E. Orji, A literature review of night ventilation strategies in buildings. Energy Build. 173 (2018) 337-352. https://doi.org/10.1016/j.enbuild.2018.05.052

[1.45] N. Khan, Y. Su, S.B. Riffat, A review on wind driven ventilation techniques. Energy Build. 40 (2008) 1586-1604. https://doi.org/10.1016/j.enbuild.2008.02.015

[1.46] X. Guo, C. Yang, L. Chen, N. Lu, A. Li, F. Meng, Review on buoyancy-driven natural ventilation in an enclosure with various types of heat sources. E3S Web Conf. 356 (2022) 03062. https://doi.org/10.1051/e3sconf/202235603062

[1.47] K.T. Andersen, Semi-empirical models for buoyancy-driven ventilation – A literature study. Int. J. Vent. 14 (2015) 77-90. https://doi.org/10.1080/14733315.2015.11684071

[1.48] B.M. Jones, M.J. Cook, S.D. Fitzgerald, C.R. Iddon, A review of ventilation opening area terminology. Energy Build. 118 (2016) 249-258. https://doi.org/10.1016/j.enbuild.2016.02.053

[1.49] F. Jomehzadeh, P. Nejat, J.K. Calautit, M.B.M. Yusof, S.A. Zaki, B.R. Hughes, M.N.A.W.M. Yazid, A review on windcatcher for passive cooling and natural ventilation in buildings, Part 1: Indoor air quality and thermal comfort assessment. Renew. Sustain. Energy Rev. 70 (2017) 736-756. https://doi.org/10.1016/j.rser.2016.11.254

[1.50] F. Jomehzadeh, H.M. Hussen, J.K. Calautit, P. Nejat. M.S. Ferwati, Natural ventilation by windcatcher (Badgir): A review on the impacts of geometry, microclimate and macroclimate. Energy Build. 226 (2020) 110396. https://doi.org/10.1016/j.enbuild.2020.110396

[1.51] N.W. Tuck, S.A. Zaki, A. Hagishima, H.B. Rijal, M.A. Zakaria, F. Yakub, Effectiveness of free running passive cooling strategies for indoor thermal environments: Example from a two-story corner terrace house in Malaysia. Build Environ. 160 (2019) 106214. https://doi.org/10.1016/j.buildenv.2019.106214

[1.52] N.W. Tuck, S.A. Zaki, A. Hagishima, H.B. Rijal, F. Yakub, Affordable retrofitting methods to achieve thermal comfort for a terrace house in Malaysia with a hot-humid climate. Energy Build. 223 (2020) 110072. https://doi.org/10.1016/j.enbuild.2020.110072

Chapter 2

[2.1] S.D Turi, F. Ruggiero, Re-interpretation of an ancient passive cooling strategy: a new system of wooden lattice opening, Energy Procedia. 126 (2017) 289-296. https://doi.org/10.1016/j.egypro.2017.08.159

[2.2] N.B. Greetha, R. Velraj, Passive cooling methods for energy efficient buildings with and without thermal energy storage – A review, Energy Educ. Sci. Technol. Part A: Energy Sci. Res. 29 (2012) 913-946.

[2.3] D.K. Bhamare, M.K. Rathod, J. Banerjee, Passive cooling techniques for building and their applicability in different climatic zones - The state of art, Energy Build. 198 (2019) 467-490. https://doi.org/10.1016/j.enbuild.2019.06.023

[2.4] H. M. Taleb, Using passive cooling strategies to improve thermal performance and reduce energy consumption of residential buildings in U.A.E. buildings, Front. Archit. Res. 3 (2014) 154-165. https://doi.org/10.1016/j.foar.2014.01.002

[2.5] R. Sharma, J. Jang, J. Hu, Phase-change materials in concrete: Opportunities and challenges for sustainable construction and building materials, Mater. 15 (2022) 335. https://doi.org/10.3390/ma15010335

[2.6] M. Antinucci, D. Asian, B.Fleury, J. Lopez, E. Maldonado, M. Santamouris, A. Tombazis, S. Yannas, Passive and hybrid cooling of buildings – State of the art. Int. J. Sol. Energy. 11 (1992) 251-271. https://doi.org/10.1080/01425919208909744A

[2.7] A. Tejero-González, M. Andrés-Chicote, P. García-Ibáñez, E. Velasco-Gómez, F.J. Rey-Martínez, Assessing the applicability of passive cooling and heating techniques through climate factors: An overview, Renew. Sustain. Energy Rev. 65 (2016) 727-742. https://doi.org/10.1016/j.rser.2016.06.077

[2.8] K. Panchabikesan, K. Vellaisamy, V. Ramalingam, Passive cooling potential in buildings under various climatic conditions in India. Renew. Sustain. Energy. Rev. 78 (2017) 1236-1252. https://doi.org/10.1016/j.rser.2017.05.030

[2.9] N.D. Miranda, R. Renaldi, R. Khosla, M.D. McCulloch, Bibliometric analysis and landscape of actors in passive cooling research. Renew. Sustain. Energy Rev. 149 (2021) 111406. https://doi.org/10.1016/j.rser.2021.111406

[2.10] B. Nie, S. Sun, Using text mining techniques to identify research trends: A case study of design research, Appl. Sci. 7 (2017) 401. https://doi.org/10.3390/app7040401

[2.11] N. Donthu, S. Kumar, D. Pattnaik, Forty-five years of Journal of Business Research: A bibliometric analysis. J. Bus. Res. 109 (2020) 1-14. https://doi.org/10.1016/j.jbusres.2019.10.039

[2.12] T. Hao, X. Chen, G. Li, J. Yan, A bibliometric analysis of text mining in medical research. Soft. Comput. 22 (2018) 7875-7892. https://doi.org/10.1007/s00500-018-3511-4

[2.13] G.O. White III, O. Guldiken, T.A. Hemphil, W. He, M.S. Khoobdeh, Trends in international strategic management research from 2000 to 2013: Text mining and bibliometric analyses. Manag. Int. Rev. 56 (2016) 35-65. https://doi.org/10.1007/s11575-015-0260-9

[2.14] M. Vanhala, C. Lu, J. Peltonen, S. Sundqvist, J. Nummenmaa, K. Järvelin, The usage of large data sets in online consumer behavior: A bibliometric and computational text-mining-driven analysis of previous research. J. Bus. Res. 106 (2020) 46-59. https://doi.org/10.1016/j.jbusres.2019.09.009

[2.15] Z. Ding, Z. Li, C. Fan, Building energy savings: Analysis of research trends based on text mining. Autom. Constr. 96 (2018) 398-410. https://doi.org/10.1016/j.autcon.2018.10.008

[2.16] I. Cañas-Guerrero, F.R. Mazarrón, C. Calleja-Perucho, A. Pou-Merina, Bibliometric analysis in the international context of the "construction and building Technology" category from the Web of Science database. Constr. Build. Mater. 53 (2014) 13-25. https://doi.org/10.1016/j.conbuildmat.2013.10.098

[2.17] A. Martín-Martín, M. Thelwall, E. Orduna-Malea, E.D. López-Cózar, Google Scholar, Microsoft Academic, Scopus, Dimensions, Web of Science, and OpenCitations' COCI: a multidisciplinary comparison of coverage via citations. Scientometr. 126 (2021) 871-906. https://doi.org/10.1007/s11192-020-03690-4

[2.18] A. Martín-Martín, E. Orduna-Malea, M. Thelwall, E.D. López-Cózar, Google Scholar, Web of Science, and Scopus: A systematic comparison of citations in 252 subject categories. J. Informetr 12 (2018) 1160-1177. https://doi.org/10.1016/j.joi.2018.09.002

[2.19] A.H. McGinn, B.J. Taylor, M. McColgan, J. McQuilkin, Social work literature searching current issues with databases and online search engines. Res. Soc. Work Pract. 26 (2016) 266-277. https://doi.10.1177/1049731514549423

[2.20] A.S. Pullin, G.B. Stewart, Guidelines for systematic review in conservation and environmental management. Conserv. Biol. 20 (2006) 1647-1656. https://doi.org/10.1111/j.1523-1739.2006.00485.x

[2.21] A. Liberati, D.G. Altman, J. Tetzlaff, C. Mulrow, G. Gøtzsche, J.P.A. Ioannidis, M. Clarke, Devereaux, P.J. Kleijnen, D. Moher, The PRISMA statement for reporting systematic reviews and meta-analyses of studies that evaluate healthcare interventions: explanation and elaboration, J. Clin. Epidemiol. 62 (2009) e1-e34. https://doi.org/10.1016/j.jclinepi.2009.06.006

[2.22] J.B. Kruskal, Multidimensional scaling by optimizing goodness of fit to a nonmetric hypothesis. Psychom. 29 (1964) 1-27.

[2.23] J.B. Kruskal, Nonmetric multidimensional scaling: A numerical method, Psychom. 29 (1964) 115-129.

[2.24] H. Nakagawa, H. Yumoto, T. Mori, Term extraction based on occurrence and concatenation. J. Nat. Lang. Process. 10 (2003) 27-45. https://doi.org/10.5715/jnlp.10.27

[2.25] L.C. Freeman, A set of measures of centrality based on betweenness. Sociam. 40 (1977) 35-41. https://doi.org/10.2307/3033543

[2.26] K. Higuchi, A Two-step approach to quantitative content analysis: KH Coder tutorial using Anne of Green Gabels (Part 1), Ritsumeikan Soc. Sci. Rev. 52 (2016) 77-91.

[2.27] K. Higuchi, A Two-step approach to quantitative content analysis: KH Coder tutorial using Anne of Green Gabels (Part 2), Ritsumeikan Soc. Sci. Rev. 53 (2017) 137-147.

[2.28] M. Santamouris, D. Kolokotsa, Passive cooling dissipation technique for buildings and other structures: The state of the art, Energy Build. 57 (2013) 74-94. https://doi.org/10.1016/j.enbuild.2012.11.002

[2.29] Suhendri, M. Hu, Y. Su, Riffat, J. Darkwa, S. Riffat, Implementation of passive radiative cooling technology in Buildings: A review. Build. 10 (2020) 215. https://doi.org/10.3390/buildings10120215

[2.30] D.G.L. Samuel, S.M.S. Nagendra, M.P. Maiya, Passive altanatives to mechanical air conditioning of building: A review. Build. Environ. 66 (2013) 54-64. https://doi.org/10.1016/j.buildenv.2013.04.016

[2.31] A. Tejero-González, A. Franco-Salas, Optimal operation of evaporative cooling pads: A review. Renew. Sustain. Energy Rev. 151 (2021) 111632. https://doi.org/10.1016/j.rser.2021.111632

[2.32] P.M. Cuce, S. Riffat, A state of the art review of evaporative cooling systems for building applications. Renew. Sustain. Energy Rev. 54 (2016) 1240-1249. http://dx.doi.org/10.1016/j.rser.2015.10.066

[2.33] A.S. Farooq, P. Zhang, Y. Guo, R. Gulfam, Emerging radiative materials and prospective applications of radiative sky cooling- A review. Renew. Sustain. Energy Rev. 144 (2021) 110910. https://doi.org/10.1016/j.rser.2021.110910

[2.34] D. Xing, N. Li, C. Zhang, P. Heiselberg, A critical review of passive condensation prevention for radiant cooling. Build. Environ. 205 (2021) 108230. https://doi.org/10.1016/j.buildenv.2021.108230

[2.35] Z. Emdadi, N. Asim, M.A. Yarmo, R. Shamsudin, M. Mohammad, K. Sopian, Green material prospects for passive evaporative cooling system: Geopolymers. Energies. 9 (2016) 586. https://doi.org/10.3390/en9080586

[2.36] Z.A. Al-Absi, M.I.M. Hafizal, M. Ismail, Experimental study on the thermal performance of PCM-based panels developed for exterior finishes of building walls, J. Build. Eng. 52 (2022) 104379. https://doi.org/10.1016/j.jobe.2022.104379

[2.37] Z.A. Al-Absi, M.I.M. Hafizal, M. Ismail, A. Mardiana, A. Ghazali, Peak indoor air temperature reduction for buildings in hot-humid climate using phase change materials, Case Study Therm. Eng. 22 (2020) 100762. https://doi.org/10.1016/j.csite.2020.100762

[2.38] Z.A. Al-Absi, M.I.M. Hafizal, M. Ismail, A. Ghazali, Towards sustainable development: Building's retrofitting with PCMs to enhance the indoor thermal comfort in tropical climate, Malaysia. Sustain. 13 (2021) 3614. https://doi.org/10.3390/su13073614

[2.39] R. Hwang, B. Chen, W. Chen, Analysis of incorporating a phase change material in a roof for the thermal management of school buildings in hot-humid climates, build. 11 (2021) 248. https://doi.org/10.3390/buildings11060248

[2.40] A. Gallardo, U Berardi, Evaluation of the energy flexibility potential of radiant ceiling panels with thermal energy storage, Energy. 254 (2022) 124447. https://doi.org/10.1016/j.energy.2022.124447

[2.41] F. Souayfane, F. Fadoun, P Biwole, Phase change materials (PCM) for cooling applications in buildings: A review, Energy Build. 129 (2016) 396-431. https://doi.org/10.1016/j.enbuild.2016.04.006

[2.42] D.H.C. Toe, T. Kubota Development of an adaptive thermal comfort equation for naturally ventilated buildings in hot-humid climates using ASHRAE RP-884 data base. Front. Archit. Res. 2 (2013) 278-291. https://doi.org/10.1016/j.foar.2013.06.003

[2.43] A.T. Nguyen, M.K. Singh, S. Reiter, An adaptive thermal comfort model for hot humid South-East Asia, Build. Environ. 56 (2012) 291-300. https://doi.org/10.1016/j.buildenv.2012.03.021

[2.44] Y. Zhang, J. Wang, H. Chen, J. Zhang, Q. Meng, Thermal comfort in naturally ventilated buildings in hot-humid area of China. Build. Environ. 45 (2010) 2562-2570. https://doi.org/10.1016/j.buildenv.2010.05.024

[2.45] M.N.F. Alfata, N. Hirata, T. Kubota, A.M. Nugroho, T. Uno, I.G.N. Antaryama, S.N. Ekasiwi, Thermal comfort in naturally ventilated apartments in Surabaya, Indonesia, Procedia Eng. 121 (2015) 459-467. https://doi.org/10.1016/j.proeng.2015.08.1093

[2.46] M.N.F. Alfata, N. Hirata, T. Kubota, A.M. Nugroho, T. Uno, S.N. Ekasiwi, I.G.N. Antaryama, Field investigation of indoor thermal environments in apartments of Surabaya, Indonesia: Potential passive cooling strategies for middle-class apartments. Energy Procedia. 78 (2015) 2947-2952. https://doi.org/10.1016/j.egypro.2015.11.674

[2.47] N.W. Tuck, S.A. Zaki, A. Hagishima, H.B. Rijal, M.Z. Zakaria, F. Yakub, Effectiveness of free running passive cooling strategies for indoor thermal environments: Example from a two-story corner terrace house in Malaysia, Build. Environ. 160 (2019) 106214, https://doi.org/10.1016/j.buildenv.2019.106214

[2.48] N.W. Tuck, S.A. Zaki, A. Hagishima, H.B. Rijal, F. Yakub, Affordable retrofitting methods to achieve thermal comfort for terraced house in Malaysia with a hot-humid climate, Energy Build. 223 (2020) 110072, https://doi.org/10.1016/j.enbuild.2020.110072

[2.49] A. Aflaki, N. Mahyuddin, Z.A. Mahmoud, M.R. Baharum, A review on natural ventilation applications through building façade components and ventilation openings in tropical climates, Energy Build. 101 (2015) 153-162. https://doi.org/10.1016/j.enbuild.2015.04.033

[2.50] T. Ahmed, P. Kumar, L. Mottet, Natural ventilation in warm climates: The challenges of thermal comfort, heatwave resilience and indoor air quality, Renew. Sustain. Energy Rev. 138 (2021) 110669. https://doi.org/10.1016/j.rser.2020.110669

[2.51] N. Izadyar, W. Miller, B. Rismanchi, V. Garcia-Hansen, Impacts of façade openings' geometry on natural ventilation and occupants' perception: A review. Build. Environ. 170 (2020) 106613. https://doi.org/10.1016/j.buildenv.2019.106613

[2.52] P.V. Nielsen, Fifty years of CFD for room air distribution. Build. Environ. 91 (2015) 78-90. http://dx.doi.org/10.1016/j.buildenv.2015.02.035

[2.53] D.R. Chapman, Computational aerodynamics development and outlook, AIAA. J. 17 (1979) 1293-1313. https://doi.org/10.2514/3.61311

[2.54] H. Wang, Z. Zhai, Advances in building simulation and computational techniques: A review between 1987 and 2014. Energy Build. 128 (2016) 319-335. http://dx.doi.org/10.1016/j.enbuild.2016.0

[2.55] D. Crawley, L.K. Lawrie, F.C. Winkelmann, W.F. Buhl, Y.J. Huang, C.O. Pedersen, R.K. Strand, R.J. Liesen, D.E. Fisher, M.J. Witte, J. Glazer, EnergyPlus: creating a new-generation building energy simulation program, Energy Build. 33 (2001) 319-331. https://doi.org/10.1016/S0378-7788(00)00114-6

[2.56] P.A. Strachan, G. Kokogiannakis, I.A. Macdonald, History and development of validation with the ESP-r simulation program. Build. Environ. 43 (2008) 601-609. https://doi.org/10.1016/j.buildenv.2006.06.025

[2.57] N. Fumo, P. Mago, R. Luck, Methodology to estimate building energy consumption using EnergyPlus benckmark models, Energy Build. 42 (2010) 2331-2337. https://doi.org/10.1016/j.enbuild.2010.07.027

[2.58] A.A.A. Gassar, C. Koo, T.W. Kim, S.H. Cha, Performance optimization studies on heating, cooling and lighting energy system of buildings during the design stage: a review. Sustain. 13 (2021) 9815. https://doi.org/10.3390/su13179815

[2.59] K. Suga, S. Kato, K. Hiyama, Structural analysis of Pareto-optimal solution sets for multi-objective optimization: An application to outer window design problems using Multiple Objective Genetic Algorithms. Build. Environ. 45 (2010) 1144-1152. https://doi.org/10.1016/j.buildenv.2009.10.021

[2.60] K. Deb, Unveiling innovative design principles by means of multiple conflicting objectives, Eng. Optim. 35 (2003) 445-470. https://doi.org/10.1080/0305215031000151256

[2.61] M. Khoroshiltseva, D. Slanzi, I.A. Poli, Pareto-based multi-objective optimization algorithm to design energy-efficient shading devices, Appl. Energy 184 (2016) 1400-1410. http://dx.doi.org/10.1016/j.apenergy.2016.05.015

[2.62] Y. Zhai, Y. Wang, Y. Huang, X. Meng, A multi-objective optimization methodology for window design considering energy consumption, thermal environment and visual performance, Renew. Energy. 134 (2019) 1190-1199. https://doi.org/10.1016/j.renene.2018.09.024

[2.63] N.R.M. Sakiyama, J.C. Carrlo, J. Frick, H. Garrecht, Perspective of naturally ventilated buildings: A review. Renew. Sustain. Energy Rev. 130 (2020) 109933. https://doi.org/10.1016/j.rser.2020.109933

[2.64] H. Homma, M. Yakiyama, Experimental study on free convection caused by metabolic heat of occupants in room, J. Archit. Plan. Environ. Eng. Trans. AIJ 375 (1987) 39048. https://doi.org/10.3130/aijax.375.0_39

[2.65] R. Ooka, Heat and human body, Wind Eng. JAWE. 97 (2003) 37-41. https://doi.org/10.5359/jawe.2003.97_37

[2.66] S. Murakami, S. Kato, J. Zeng, Combined simulation of airflow, radiation and moisture transport for heat release from a human body, Build. Environ. 35 (2000) 489-500. https://doi.org/10.1016/S0360-1323(99)00033-5

[2.67] S. Zhang, Z. Lin, Predicted mean vote with skin wittedness from standard effective temperature model, Build. Environ. 17 (2021) 107412. https://doi.org/10.1016/j.buildenv.2020.107412

[2.68] H. Wang, S. Hu, Experimental study on thermal sensation of people in moderate activities, Build. Environ. 100 (2016) 127-134. http://dx.doi.org/10.1016/j.buildenv.2016.02.016

[2.69] C. Lee, A.K. Melikov, H. Homma, An experimental study on convective heat transfer coefficient distribution on thermal manikin by air flow with various velocities and turbulence intensities, J. Archit. Plan. Environ. Eng. Trans. AIJ. 429 (1991) 25-31. https://doi.org/10.3130/aijax.429.0_25

[2.70] Y. Sun, W.J. Jasper, Numerical modeling of heat and moisture transfer in a wearable convective cooling system for human comfort, Build. Environ. 93 (2015) 50-62. http://dx.doi.org/10.1016/j.buildenv.2015.06.008

[2.71] M.T. Arethusa, T. Kubota, A.M. Nugroho, I.G.N. Antaryama, S.N. Ekasiwi, T. Uno, A field survey of window-opening behavior and thermal conditions in apartment of Surabaya, Indonesia, Intercult. Underst. 4 (2014) 17-25. https://doi.org/10.14993/00000850

[2.72] C. Cândido, R.J. de Dear, R. Lamberts, L. Bettencourt, Air movement acceptability limits and thermal comfort in Brazil's hot humid climate zone, Build. Environ. 46 (2010) 222-229. https://doi.org/10.1016/j.buildenv.2009.06.005

[2.73] H. Mori, T. Kubota, I.G.N. Antaryama, S.N.N. Ekasiwi, Analysis of window-opening patterns and air conditioning usage of urban residences in tropical Southeast Asia, Sustain. 12 (2020) 10650. https://doi.org/10.3390/su122410650

[2.74] P. Devaux, M.M. Farid, Benefits of PCM underfloor heating with PCM wallboards for space heating in winter, Appl. Energy 191 (2017) 593-602. https://doi.org/10.1016/j.apenergy.2017.01.060

[2.75] S. Liu, M. Iten, A. Shukla, Numerical study on the performance of an air – Multiple PCMs unit for free cooling and ventilation, Energy Build. 151 (2017) 520-533. https://doi.org/10.1016/j.enbuild.2017.07.005

[2.76] M. Iten, S. Liu, S. Shukla, P.D. Silva, Investigating the impact of C_p-T values determined by DSC on the PCM-CFD model. Appl. Therm. Eng. 117 (2017) 65-75. https://doi.org/10.1016/j.applthermaleng.2017.02.021

[2.77] A. Gallardo, U. Berardi, Analysis of the energy and thermal performance of a radiant cooling panel system with integrated phase change materials in very hot and humid

conditions, IOP Conf. Ser. Mater. Sci. Eng. 609 (2019) 052025. https://doi:10.1088/1757-899X/609/5/052025

[2.78] H. Tang, T. Zhang, X. Liu, C. Li, A novel pulse width modification for metal radiant panels to control the condensation risk in a hot and humid environment, Build. Environ.196 (2021) 107802. https://doi.org/10.1016/j.buildenv.2021.107802

[2.79] Y.L. Yin, R.Z. Wang, X.Q. Zhai, T.F. Ishugah, Experimental investigation on the heat transfer performance and water condensation phenomenon of radiant cooling panels, Build. Environ. 71 (2014) 15-23. http://dx.doi.org/10.1016/j.buildenv.2013.09.016

[2.80] National Centers for Environmental Information, NOAA, USA, integrated surface dataset, 2020 https://www.ncei.noaa.gov/access/search/data-search/global-hourly, Accessed date November 10 2020

[2.81] D.H.C. Toe, T. Kubota, Comparative assessment of vernacular passive cooling techniques for improving indoor thermal comfort of modern terraced houses in hot-humid climate of Malaysia, Sol. Energy. 114 (2015) 229–258. http://dx.doi.org/10.1016/j.solener.2015.01.035

[2.82] J. Ran, M. Tang, Passive cooling of the green roofs combined with night-time ventilation and walls insulation in hot and humid regions. Sustain. Cities Soc. 38 (2018) 466-475. https://doi.org/10.1016/j.scs.2018.01.027

[2.83] Y. Chen, Z. Tong, A. Malkawi, Investigating natural ventilation potentials across the globe: Regional and climatic variations, Build. Environ. 122 (2017) 386-396. https://doi.org/10.1016/j.buildenv.2017.06.026

[2.84] C. Yuan, R. Shan, A.S. Adelia, A. Tablada, S.K. Lau, S.S. Lau, Effect of vertical farming on natural ventilation of residential buildings, Energy Build. 185 (2019) 316-325. https://doi.org/10.1016/j.enbuild.2018.12.028

[2.85] P. Scriver, Constructing colonial and contemporary South Asia, Fabric. 19 (2010) 34-57, https://doi.org/10.1080/10331867.2010.10539657

[2.86] M.N.F. Alfata, Fundamental study on indoor thermal environments in high-rise apartments in hot-humid climates of Indonesia, Ph.D thesis, Hiroshima University, 2018.

[2.87] J. Widodo, Modern Indonesian architecture: Transplantation, adaptation, accommodation and hybridization, The past in the present, Architecture in Indonesia, Ed. Nas, J.M. Leiden, KITLV Press, 2007.

[2.88] C. Passchier, Colonial architecture in Indonesia, References and Developments, The past in the present, Architecture in Indonesia, Ed. Nas, J.M. Leiden, KITLV Press, 2007.

[2.89] A. Abhat, Low temperature latent heat thermal energy storage: heat storage materials, Sol. Energy, 30 (1983) 313-32. https://doi.org/10.1016/0038-092X(83)90186-X

[2.90] D. Zhou, C.Y. Zhao, Y. Tian, Review on thermal energy storage with phase change materials (PCMs) in building applications, Appl. Energy. 92 (2012) 593-605. https://doi.org/10.1016/j.apenergy.2011.08.025

[2.91] A. Shukla, D. Buddhi, R.L. Sawhney, Thermal cycle test of few selected inorganic and organic phase change material, Renew. Energy. 33 (2008) 2606-2614. https://doi.org/10.1016/j.renene.2008.02.026

[2.92] D.W. Hawes, D. Feldman, D. Banu, Latent heat storage in building materials, Energy Build. 20 (1993) 77-86. https://doi.org/10.1016/0378-7788(93)90040-2

[2.93] J. Lei, K. Kumarasamy, K.T. Zingre, J. Yang, M.P. Wan, E.H. Yang, Cool colored coating and phase change materials as complementary cooling strategies for building cooling load reduction in tropics, Appl. Energy 190 (2017) 57–63. https://doi.org/10.1016/j.apenergy.2016.12.114

[2.94] American Society of Heating, Refrigerating and Air Conditioning Engineers, 2017 ASHRAE, Handbook- Fundamentals, Heat, Air, and Moisture Control in Building Assemblies- Material Properties, ASHRAE, Atlanta, 2017.

[2.95] V.A.A. Raj, R. Velraj, Review on free cooling of buildings using phase change materials, Renew. Sustain. Energy Rev. 14 (2010) 2819–2829, https://doi.org/10.1016/j.rser.2010.07.004

[2.96] A. Wapas, Z.U. Din, Phase change materials (PCM) storage for free cooling of buildings – A review. Renew. Sustain. Energy Rev. 18 (2013) 607-625. https://doi.org/10.1016/j.rser.2012.10.034

[2.97] M. Iten, S. Liu, A. Shukla, Experimental study on the thermal performance of air-PCM unit, Build. Environ. 105 (2016) 128–139, https://doi.org/10.1016/j.buildenv.2016.05.035

[2.98] H. Djamila, C. M. Chu, S. Kumaresan, Field study of thermal comfort in residential buildings in the equatorial hot-humid climate of Malaysia, Build. Environ. 62 (2013) 133-142, http://dx.doi.org/10.1016/j.buildenv.2013.01.017

[2.99] B. W. Olesen, K. C. Parsons, Introduction to thermal comfort standards and to the proposed new version of EN ISO 7730, Energy Build. 34 (2002) 537-548, https://doi.org/10.1016/S0378-7788(02)00004-X

Chapter 3

[3.1] A. Tungka Sangkeradi, R. Syafriny, Thermal comfort comparison of traditional architecture and modern style housing in north Sulawesi-Indonesia, Proc. Int. semin. (2008) 1-9. SENVAR 9th & ISESEE 2nd, Kuala Lumpur.

[3.2] T. Kubota, D.H.C. Toe, S. Ahmad, The effect of night ventilation technique on indoor thermal environment for residential buildings in hot-humid climate of Malaysia, Energy Build. 41 (2009) 829-839. https://doi.org/10.1016/j.enbuild.2009.03.008

[3.3] H. Mori, T. Kubota, I.G.N. Antaryama, S.N.N. Ekasiwi, Analysis of window-opening patterns and air conditioning usage of urban residences in tropical Southeast Asia, Sustain. 12 (2020) 10650. https://doi.org/10.3390/su122410650

[3.4] S.A. Zaki, N.F.N. Hanip, A. Hagishima, F. Yakub, M.S.M. Ali, Survey of resident behavior related to air conditioner operation in low-cost apartments of Kuala Lumpur, Chem. Eng. Trans. 63 (2018) 259-264. https://doi.org/10.3303/CET1863044

[3.5] H. Wang, S. Hu, Experimental study on thermal sensation of people in moderate activities. Build. Environ. 100 (2016) 127-134. http://dx.doi.org/10.1016/j.buildenv.2016.02.016

[3.6] C. Lee, A.K. Melikov, H. Homma, An experimental study on convective heat transfer coefficient distribution on thermal manikin by air flow with various velocities and turbulence intensities. J. Archit. Plan. Environ. Eng. Trans. AIJ. 429 (1991) 25-31. https://doi.org/10.3130/aijax.429.0_25

[3.7] T. Ogawa, evaporative heat loss, Thermophysiology, Ed. T. Nakayama, Jupiter publishing, Japan, 2014.

[3.8] American National Standard Institute (ANSI), Thermal Environmental Conditions for Human Occupancy (ANSI/ASHRAE Standard 55-2020), ASHRAE, USA, 2020. ISSN 1041-2336.

[3.9] J. Yam, Y. Li, Z. Zheng, Nonlinear coupling between thermal mass and natural ventilation in buildings, Int. J. Heat Mass Tran. 46 (2003) 1251-1264. https://doi.org/10.1016/S0017-9310(02)00379-4

[3.10] H. Shetavivash, Investigation of opening position and shape on the natural cross ventilation, Energy Build. 93 (2015) 1-15. https://doi.org/10.1016/j.enbuild.2014.12.053

[3.11] T. Liu, W.L. Lee, Using response surface regression method to evaluate the influence of window types on ventilation performance of Hong Kong residential buildings, Build. Environ. 154 (2019) 167-181. https://doi.org/10.1016/j.buildenv.2019.02.043

[3.12] C.F. Gao, W.L. Lee, Evaluating the influence of openings configutation on natural ventilation performance of residential units in Hong Kong, Build. Environ. 46 (2011) 961-969. https://doi.org/10.1016/j.buildenv.2010.10.029

[3.13] C. Tantasavasdi, J. Srebric, Q. Chen, Natural ventilation design for houses in Thailand, 33 (2001) 815-824. https://doi.org/10.1016/S0378-7788(01)00073-1

[3.14] M. J. Lei, J. Yang, E.H. Yang, Energy performance of building envelopes integrated with phase change materials for cooling load reduction in tropical Singapore, Appl. Energy 162 (2016) 207–217, https://doi.org/10.1016/j.apenergy.2015.10.031

[3.15] E. Prianto, P. Depecker, Characteristic of air flow as the effect of balcony, opening design and internal division on indoor velocity A case study of traditional. Dwelling in urban living quarter in tropical humid region, Energy Build. 34 (2002) 401–409, https://doi.org/10.1016/S0378-7788(01)00124-4

[3.16] 日本建築学会環境工学委員会熱小委員会 温熱感 WG・同測定法 SWG, 室内温熱環境測定法学術規準, http://news-sv.aij.or.jp/kankyo/s8/old_hp/PDF/acasuta.pdf

[3.17] ASHRAE (2017) *2017 ASHRAE Handbook – Fundamentals (SI Edition)*, American Society of Heating, Refrigerating and Air-conditioning Engineers. Inc., Atlanta, USA, ISBN 978-1-939200-58-7

[3.18] International Organization for Standardization (ISO) (2001) *Ergonomics of the Thermal Environment. Instruments for Measuring Physical Quantities (BS EN ISO 7726:2001)*, BSI, London, UK, ISBN 0-580-38651-1.

[3.19] National Center for Environmental Information (2020) National Oceanic and Atmospheric Administration, USA. (https://www.ncei.noaa.gov/access/search/data-search/global-hourly)

[3.20] S.A. Damiati, S.A. Zaki, H.B. Rijal S. Wonorahardjo, Field study on adaptive thermal comfort in office buildings in Malaysia, Indonesia, Singapore, and Japan during hot and humid season. Build. Environ. 109 (2016) 208-223. https://doi.org/10.1016/j.buildenv.2016.09.024

[3.21] G.M. Stavrakakis, M.K. Koukou, M.G. Vrachopoulos, N.C. Markatos, Natural cross-ventilation in buildings: Building-sale experiments, numerical simulation and thermal comfort evaluation. Energy Build. 40 (2008) 1666-1681. https://doi.org/10.1016/j.enbuild.2008.02.022

[3.22] Y. Jiang, Q.Chen, Study of natural ventilation in buildings by large eddy simulation. J. Wind Eng. Ind. Aerodynamics. 89 (2001) 1155-1178. https://doi.org/10.1016/S0167-6105(01)00106-4

[3.23] T.R. Oke Boundary layer climates, Second ed., Taylor&Francis, New York, 1987

[3.24] C.M. Chiang, N.T. Chen, P.C Chou, Y.Y. Li, I.C. Lien, A study on the influence of horizontal louvers on natural ventilation in a dwelling unit, Proc. Indoor air 2005, Beijing (2005) 3142-3147.

[3.25] A. Hagishima, J. Tanimoto, K. Narita, Review of the former researches on the convective heat transfer coefficient of urban surfaces, J. Japan Soc. Hydrol. Water Resour. 17 (2004) 536-554.

[3.26] T. Ogasawara, T. Kurabuchi, N. Ohira, Study on measurement method of convective heat transfer coefficient in a Room and measurement in residential house, Proc. 2012 JSRAE Annual Conf. Sapporo (2012) 1077-1080. https://doi.org/10.18948/shasetaikai.2012.1.0_1077

[3.27] K. Narita, I. Morioka, T. Sawachi, H. Seto, Y. Ishikawa, N. Kiyota, Measurement of heat transfer coefficient on cross ventilated indoor surface using full-scale model in a wind tunnel, AIJ J. Technol. Des. 11 (2005) 259-262. https://doi.org/10.3130/aijt.11.259

[3.28] R. Sato, T. Lee, T. Asawa, H. Kawai, Y. Hirayama, I. Ohta, Y. Sato and S. Ishiguro (2016) Study on the passive cooling effect of thermal storage material with automatic ventilative cooling in Summer. *AIJ Annual meeting*, Kyushu, 21-24.

[3.29] T. Cholewa, M. Rosinski, Z. Spik, M.R. Dudzinska, A. Siuta-Olcha, On the heat transfer coefficients between heated/cooled radiant floor and room, Energy Build. 66 (2013) 599-606. https://doi.org/10.1016/j.enbuild.2013.07.065

[3.30] EN 15377-1, Heating System in Buildings – Design of Embedded Water Based Surface Heating and Cooling systems – Part 1: Determination of the Design Heating and Cooling Capacity, 2008.

[3.31] W. Jürges, Der Wärmeübergang (1925) an einer ebenen Wand (Heat transfer at a plane wall) Beiheft Nr. 19 zum "Gesundh.- Ing." (1924), appearing in Gesundheits-Ingenieur 9. Heft, 48. Jahrg., 105.

[3.32] B. Olesen, Radiant floor cooling systems, ASHRAE J. 50 (2008) 16-22.

[3.33] S. Vogel, Living in a physical world. V. Maintaining temperature, *J. Biosci.* 30 (2005) 581-590.

[3.34] T.H. Karyono, E. Siri, J.G. Sulistiawan, Y. Triswanti, Thermal comfort studies in naturally ventilated buildings in Jakarta, Indonesia, Buildings. 5 (2015) 917-932. https://doi.org/10.3390/buildings5030917

[3.35] T. Sakoi, T. Mochida, K. Nagano, K. Shimakura Characteristics and consideration of required sweat rate standard of the previous ISO 7933, J. human environ. system, 9 (2006) 19-29.

[3.36] International Organization for Standardization (ISO) (1989) ISO 7933 Hot Environments-Analytical determination and interpretation of heat stress using calculation of required sweat rate.

[3.37] D.H.C. Toe, T. Kubota Development of an adaptive thermal comfort equation for naturally ventilated buildings in hot-humid climates using ASHRAE RP-884 data base. Front. Archit. Res. 2 (2013) 278-291. https://doi.org/10.1016/j.foar.2013.06.003

[3.38] M. Vellei, J.Le Dreau A novel model for evaluating dynamic thermal comfort under demand response events. Build. Environ. 160 (2019) 106215. https://doi.org/10.1016/j.buildenv.2019.106215

[3.39] A.T. Nguyen, M.K. Singh, S. Reiter, An adaptive thermal comfort model for hot humid South-East Asia, Build. Environ. 56 (2012) 291-300. https://doi.org/10.1016/j.buildenv.2012.03.021

[3.40] E. Solgi, B.M. Kari, R. Fayaz, H. Taheri, The impact of phase change materials assisted night purge ventilation on the indoor thermal conditions of office buildings in hot-arid climates, Energy Build. 150 (2017) 488-497. http://dx.doi.org/10.1016/j.enbuild.2017.06.035

[3.41] M.T. Arethusa, T. Kubota, A.M. Nugroho, I.G.N. Antaryama, S.N. Ekasiwi, T. Uno, A field survey of window-opening behavior and thermal conditions in apartment of Surabaya, Indonesia, Intercult. Underst. 4 (2014) 17-25. https://doi.org/10.14993/00000850

[3.42] C. Cândido, R.J. de Dear, R. Lamberts, L. Bettencourt, Air movement acceptability limits and thermal comfort in Brazil's hot humid climate zone, Build. Environ. 46 (2010) 222-229. https://doi.org/10.1016/j.buildenv.2009.06.005

[3.43] X. Deng, P. Cooper, Z. Ma, G. Kokogiannakis, Numerical analysis of indoor thermal comfort in a cross-ventilated space with top-hung windows, Energy Procedia 121 (2017) 222-229. https://doi.org/10.1016/j.egypro.2017.08.021

[3.44] S. Tanabe, K. Kimura, Effects of air temperature, humidity, and air movement on thermal comfort under hot and humid conditions, ASHARAE Transactions. 100 (1994) 953-969.

[3.45] E. Prianto, P. Depecker, Optimization of architectural design elements in tropical humid region with thermal comfort approach, Energy Build. 35 (2003) 273-280. https://doi.org/10.1016/S0378-7788(02)00089-0

Chapter 4

[4.1] A. Maccarini, G. Hultmark, N.C. Bergsøe, A. Afshari, Free cooling potential of a PCM-based heat exchanger coupled with a novel HVAC system for simultaneous heating and cooling of buildings, Sustain. Cities Soc. 42 (2018) 384-395. https://doi.org/10.1016/j.scs.2018.06.016.

[4.2] V.A.A. Raj, R. Velraj, Review on free cooling of buildings using phase change materials, Renew. Sustain. Energy Rev. 14 (2010) 2819–2829. https://doi.org/10.1016/j.rser.2010.07.004

[4.3] S. Wonorahardjo, I.M. Sutjahja, E. Tunçbilek, R.A. Achsani, M. Arıcı, N. Rahmah, PCM-based passive air conditioner in urban house for the tropical climates: an experimental analysis on the stratum air circulation, Build. Environ. 192 (2021) 107632, https://doi.org/10.1016/j.buildenv.2021.107632

[4.4] P.K.S. Rathre, S.K. Shula, N.K. Gupta, Yearly analysis of peak temperature, thermal amplitude, time lag and decrement factor of a building envelope in tropical climate, J. Build. Eng. 31 (2020) 101459, https://doi.org/10.1016/j.jobe.2020.101459

[4.5] Z.A. Al-Absi, M.I.M. Hafizal, M. Ismail, A. Mardiana, A. Ghazali, Peak indoor air temperature reduction for buildings in hot-humid climate using phase change materials, Case study Therm. Eng. 22 (2020) 100762, https://doi.org/10.1016/j. csite.2020.100762.

[4.6] L. Navarro, A. de Gracia, A. Castell, L.F. Cabeza, Experimental evaluation of a concrete core slab with phase change materials for cooling purposes, Energy Build. 116 (2016) 411–419, https://doi.org/10.1016/j.enbuild.2016.01.026

[4.7] H. Weinl¨ader, W. K¨orner, B. Strieder, A ventilated cooling ceiling with integrated latent heat storage-Monitoring results, Energy Build. 82 (2014) 65–72. https://doi.org/10.1016/j.enbuild.2014.07.013

[4.8] F. Kuznik, J. Virgone, J. Roux, Energetic efficiency of room wall containing PCM wallboard: a full-scale experimental investigation, Energy Build. 40 (2008) 148–156, https://doi.org/10.1016/j.enbuild.2007.01.022

[4.9] A. Waqas, S. Kumar, Thermal performance of latent heat storage for free cooling of buildings in a dry and hot climate: An experimental study, Energy Build. 43 (2011) 2621–2630. https://doi.org/10.1016/j.enbuild.2011.06.015

[4.10] M. Iten, S. Liu, A. Shukla, Experimental study on the thermal performance of air-PCM unit, Build. Environ. 105 (2016) 128–139. https://doi.org/10.1016/j.buildenv.2016.05.035

[4.11] W. Sun, R. Huang, Z. Ling, X. Fang, Z. Zhang, Numerical simulation on the thermal performance of a PCM-containing ventilation system with a continuous change in inlet air temperature, Renew. Energy, 145 (2020) 1608-1619. https://doi.org/10.1016/j.renene.2019.07.089

[4.12] National Centers for Environmental Information, NOAA, USA, integrated surface dataset, 2020 https://www.ncei.noaa.gov/access/search/data-search/global-hourly, Accessed date November 10 2020

[4.13] T. Lee, R. Sato, T. Asawa, H. Kawai, Y. Hirayama, I. Ohta, Y. Sato, Y. Hayashi, Study on cold storage of phase change material on the floor of a house with night natural ventilation, J. Environ. Eng. AIJ 82 (2017) 1025–1034. https://doi.org/10.3130/aije.82.1025

[4.14] S. Kobayashi, Characteristics of heat transfer in room interior (1) temperature and naturl convection in non ventilated room, Trans. Arch. Inst. Japan, 282 (1979)139-147.

[4.15] D.H.C. Toe, T. Kubota, Comparative assessment of vernacular passive cooling techniques for improving indoor thermal comfort of modern terraced houses in hot-humid climate of Malaysia, Sol. Energy 114 (2015) 229–258. http://dx.doi.org/10.1016/j.solener.2015.01.035

[4.16] T. Kubota, M.A. Zakaria, S. Abe, D.H.C. Toe, Thermal functions of internal courtyards in traditional Chinese shophouses in the hot-humid climate of Malaysia, Build. Environ. 112 (2017) 115–131. https://doi.org/10.1016/j.buildenv.2016.11.005

[4.17] D.H.C. Toe, T. Kubota, Field measurement on thermal comfort in traditional Malay houses, AIJ J. Technol. Des. 19 (2013) 219–224. https://doi.org/10.3130/aijt.19.219

[4.18] J. Lizana, M. de-Borja-Torrejon, A. Barrios-Padura, T. Auer, R. Chacartegui, Passive cooling through phase change materials in buildings. A critical study of implementation alternatives, Appl. Energy 254 (2019) 113658. https://doi.org/10.1016/j.apenergy.2019.113658

[4.19] D.A. Neeper, Thermal dynamics of wallboard with latent heat storage, Sol. Energy 68 (2000) 393–403. https://doi.org/10.1016/S0038-092X(00)00012-8

Chapter 5

[5.1] A.A. Rabienataj Darzi, S.M. Moosania, F.L. Tan, M. Farhadi, Numerial investigation of free-cooling system using plate type PCM storage, Int. Commun. Heat Mass Transf. 48 (2013) 155-163. https://doi.org/10.1016/j.icheatmasstransfer.2013.08.025

[5.2] S.A. Nada, W.G. Alshaer, R.M. Saleh, Thermal characteristics and energy saving of charging/discharging processes of PCM in air free cooling with minimal temperature differences, Alexandria, Eng. J. 58 (2019) 1175-1190. https://doi.org/10.1016/j.aej.2019.10.002

[5.3] A. Waqas, S. Kumar, Thermal performance of latent heat storage for free cooling of buildings in a dry and hot climate: An experimental study, Energy Build. 43 (2011) 2621–2630. https://doi.org/10.1016/j.enbuild.2011.06.015

[5.4] E. Halawa, W. Saman, Thermal performance analysis of a phase change thermal storage unit for space heating, Renew. Energy, 36 (2011) 259-264. https://doi.org/10.1016/j.renene.2010.06.029

[5.5] S. Liu, M. Iten, A. Shukla, Numerical study on the performance of an air – Multiple PCMs unit for free cooling and ventilation, Energy Build. 151 (2017) 520-533. https://doi.org/10.1016/j.enbuild.2017.07.005

[5.6] M.R. Hajizadeh E. Abohamzeh, A.K. Tiwari, M.A. Sheremet, Z. Li, Q.V. Bach, Discharging of PCM for ventilation system incorporating nanoparticles, J. Mol. Liq. 315 (2020) 113696. https://doi.org/10.1016/j.molliq.2020.113696

[5.7] W. Sun, R. Huang, Z. Ling, X. Fang, Z. Zhang, Numerical simulation on the thermal performance of a PCM-containing ventilation system with a continuous change in inlet air temperature, Renew. Energy, 145 (2020) 1608-1619. https://doi.org/10.1016/j.renene.2019.07.089

[5.8] B. Pandey, R. Banerjee, A. Sharma, Coupled EnergyPlus and CFD analysis of PCM for thermal management of buildings, Energy Build. 231 (2021) 110598., https://doi.org/10.1016/j.enbuild.2020.110598

[5.9] A.T. Jones, D.P. Finn, Co-simulation of a HVAC system-integrated phase change material thermal storage unit, J. Build. Perform. Simul. 10 (2017) 313-325. https://doi.org/10.1080/19401493.2016.1257068

[5.10] K. Chow, A.E. Holdo, On the influence of boundary conditions and thermal radiation on predictive accuracy in numerical simulations of indoor ventilation, Build. Environ. 45 (2010) 437-444. https://doi.org/10.1016/j.buildenv.2009.06.021

[5.11] X. Meng, Y. Wang, T. Liu, X. Xing, Y. Cao, J. Zhao, Influence of radiation on predictive accuracy in numerical simulations of the thermal environment in industrial buildings with buoyancy-driven natural ventilation, Appl. Therm. Eng. 96 (2016) 473-480. https://doi.org/10.1016/j.applthermaleng.2015.11.105

[5.12] M. Jaworski, P. Lapka, P. Furmanski, Numerical modeling and experimental studies of thermal behavior of building integrated thermal energy storage unit in a form of a ceiling

panel, Appl. Energy, 113 (2014) 548-557, https://doi.org/10.1016/j.apenergy.2013.07.068

[5.13] L. Royon, L. Karim, A. Bontemps, Optimization of PCM embedded in a floor panel developed for thermal management of the lightweight envelope of buildings, Energy Build., 82 (2014) 385-390, https://doi.org/10.1016/j.enbuild.2014.07.012

[5.14] Y. Toparlar, B. Blocken, B. Maiheu, G.J.F. van Heijst, A review on the CFD analysis of urban microclimate, Renew. Sustain. Energy Rev. 80 (2017) 1613-1640. https://doi.org/10.1016/j.rser.2017.05.248

[5.15] H. Ling, C. Chen, S. Wei, Y. Guan, C. Ma, G. Xie, N. Li, Z. Chen, Effect of phase change materials on indoor thermal environment under different weather conditions and over a long time, Appl. Energy, 140 (2015) 329-337, https://doi.org/10.1016/j.apenergy.2014.11.078

[5.16] Z. Tong, Y. Chen, A. Malkawi, Defining the influence region in neighborhood-scale CFD simulations for natural ventilation design, Appl. Energy, 182 (2016) 625-633. https://doi.org/10.1016/j.apenergy.2016.08.098

[5.17] M.P. Straw, C.J. Baker, A.P. Robertson, Experimental measurements and computations of the wind-induced ventilation of a cubic structure, J. Wind Eng. Ind. Aerodyn. 88 (2000) 213-230. https://doi.org/10.1016/S0167-6105(00)00050-7

[5.18] T. van Hoff, B. Blocken, Y. Tominaga, On the accuracy of CFD simulations of cross-ventilation flows for a generic isolated building: Comparison of RANS, LES and experiments, Build. Environ. 114 (2017) 148-165. https://doi.org/10.1016/j.buildenv.2016.12.019

[5.19] Y. Tominaga, A. Mochida, R. Yoshie, H. Kataoka, T. Nozu, M. Yoshikawa, T. Shirasawa, AIJ guidelines for practical applications of CFD to pedestrian wind environment around buildings. J. Wind Eng. Ind. Aerodyn. 96 (2008) 1749-1761. https://doi.org/10.1016/j.jweia.2008.02.058

[5.20] B. Blocken, LES over RANS in building simulation for outdoor and indoor applications: A foregone conclusion? Build. Simul. 11 (2018) 821-870. https://doi.org/10.1007/s12273-018-0459-3

[5.21] B. Blocken, 50 years of computational wind engineering: past, present and future, J. Wind Eng. Ind. Aerodyn. 129 (2014) 69-102. https://doi.org/10.1016/j.jweia.2014.03.008

[5.22] C. Buratti, D. Palladino, E. Moretti, Prediction of indoor conditions and thermal comfort using CFD simulations: A case study based on experimental data, Energy Procedia, 126 (2017) 115-122. https://doi.org/10.1016/j.egypro.2017.08.130

[5.23] K. Huang, Identifying a suitable hourly solar diffuse fraction model to generate the typical meteorological year for building energy simulation application, Renew. Energy, 157 (2020) 1102-1115. https://doi.org/10.1016/j.renene.2020.05.094

[5.24] D.G. Erbs, S.A. Klein, J.A. Duffie, Estimation of the diffuse radiation fraction for hourly, daily and monthly average global radiation, Sol. Energy, 28 (1982) 293-302. https://doi.org/10.1016/0038-092X(82)90302-4

[5.25] F. Souayfane, F. Fadoun, P Biwole, Phase change materials (PCM) for cooling applications in buildings: A review, Energy Build. 129 (2016) 396-431. https://doi.org/10.1016/j.enbuild.2016.04.006

[5.26] T. Defraeye, B. Blocken, J. Cameliet, An adjusted temperature wall function for turbulent forced convective heat transfer for bluff bodies in the atmospheric boundary layer, Build. Environ. 46 (2011) 2130-2141. https://doi.org/10.1016/j.buildenv.2011.04.013

[5.27] T. Asawa, A. Hoyano, High-resolution heat balance simulation for building and urban surfaces by combining the 3D CAD-based thermal environment simulator and CFD, In Proceedings of Building Simulation 2011, Sydney, Australia, 14-16 November 2011, 2565-2572.

[5.28] The Japan Society of Mechanical Engineers, Heat Transfer, JSME, Tokyo, 2009. ISBN：978-4-88898-184-2

[5.29] A. Mochida, S. Murakami, Y. Hayashi, Comparison between k-ε model and LES for turbulence structure around cube, J. Archit. Planning Environ. Eng. (Transaction of AIJ), 423 (1991) 23-31.

[5.30] B.E. Launder, M. Kato, Modeling flow-induced oscillations in turbulent flow arpund square cylinder, ASME Fluid Eng. Conf. (1993) pp.20.

[5.31] Y. Tominaga, A. Mochida, CFD prediction of flowfield and snowdrift around a building complex in a snowy region, J. Wind Eng. Ind. Aerodynamics,81 (1999) 273-282. https://doi.org/10.1016/S0167-6105(99)00023-9

[5.32] B.L. Growreesunker, S.A. Tassou, Effectiveness of CFD simulation for the performance prediction of phase change building boards in the thermal environment control of Indoor space, Build. Environ. 59 (2013) 612-625. https://doi.org/10.1016/j.buildenv.2012.10.004

[5.33] P.J. Roache, Quantification of uncertainty in computational fluid dynamics, Annu. Rev. Fluid. Mech. 29 (1997) 123-160. https://doi.org/10.1146/annurev.fluid.29.1.123

[5.34] D. Micallef, V. Buhagiar, Simon P. Borg, Cross-ventilation of a room in a courtyard building. Energy Build. 133 (2016) 658-669. https://doi.org/10.1016/j.enbuild.2016.09.053

[5.35] W. Shan, D. Rim, Thermal and ventilation performance of combined passive chilled beam and displacement ventilation systems, Energy Build. 158 (2018) 466-475. https://doi.org/10.1016/j.enbuild.2017.10.010

[5.36] Y. Wang, T. Zhao, Z. Cao, C. Zhai, S. Wu, C. Zhang, Q. Zhang, W. Lv, The influence of indoor thermal conditions on ventilation flow and pollutant dispersion in downstream industrial workshop, Build. Environ. 187 (2021) 107400. https://doi.org/10.1016/j.buildenv.2020.107400

[5.37] H. Ahn, D. Rim, L.J. Lo, Ventilation and energy performance of partitioned indoor spaces under mixing and displacement ventilation, Build. Simul. 11 (2018) 561-574. https://doi.org/10.1007/s12273-017-0410-z

[5.38] D. Zhou, C.Y. Zhao, Y. Tian, Review on thermal energy storage with phase change materials (PCMs) in building applications, Appl. Energy, 92 (2012) 593-605. https://doi.org/10.1016/j.apenergy.2011.08.025

[5.39] T.C. Lee, T. Asawa, H. Kawai, R. Sato, Y. Hirayama, I. Ohta, Multipoint measurement method for air temperature in outdoor spaces and application to microclimate and passive cooling studies for a house, Build. Environ. 114 (2017) 267-280. https://doi.org/10.1016/j.buildenv.2016.12.030

[5.40] American Society of Heating, Refrigerating and Air Conditioning Engineers, ASHRAE Guideline 14-2014: measurement of energy, demand, and water savings, ASHRAE, Atlanta, 2014.

[5.41] Y. Hu, R. Guo, P.K Heiselberg, H. Johra, Modeling PCM phase change temperature and hysteresis in ventilation cooling and heating applications, Energies, 13 (2020) 6455. https://doi.org/10.3390/en13236455

[5.42] M. Iten, S. Liu, A. Shukla, P.D. Silva, Investigating the impact of C_p-T values determined by DSC on the PCM-CFD model, Appl. Therm. Eng., 117 (2017) 65-75, https://doi.org/10.1016/j.applthermaleng.2017.02.021

[5.43] L. Shui, J. Gao, X. Shi, J. Liu, Effect of duct aspect ratio on heat transfer and friction in steam-cooled ducts with 60° angled rib turbulators, Exp. Therm. Fluid Sci. 49 (2013) 123-134. https://doi.org/10.1016/j.expthermflusci.2013.04.010

[5.44] Y. Sato, A. Osaki, T. Nakamura, Y. Hayashi, S. Ishiguro, Research on the reduction effect of the space heating load by latent heat storage interior building material, J. Environ. Eng. 77 (2012) 651-659. https://doi.org/10.3130/aije.77.651

[5.45] National Centers for Environmental Information, NOAA, USA, integrated surface dataset, 2020 https://www.ncei.noaa.gov/access/search/data-search/global-hourly, Accessed date November 10 2020

[5.46] J. Lei, J. Yang, E.H. Yang, Energy performance of building envelopes integrated with phase change materials for cooling load reduction in tropical Singapore, Appl. Energy, 162 (2016) 207-217. https://doi.org/10.1016/j.apenergy.2015.10.031

Chapter 6

[6.1] S. Rostami, M. Afrand, A. Shahsavar, M. Sheikholeslami, R. Kalbasi, S. Aghakhani, M.S. Shadloo, H. F. Oztop, A review of melting and freezing processes of PCM/nano-PCM and their application in energy storage, Energy 211 (2020) 118698. https://doi.org/10.1016/j.energy.2020.118698

[6.2] M. Iten, S. Liu, A. Shukla, P.D. Silva, Investigating the impact of C_p-T values determined by DSC on the PCM-CFD model, Appl. Therm. Eng., 117 (2017) 65-75, https://doi.org/10.1016/j.applthermaleng.2017.02.021

[6.3] M. Serikawa, T. Saeki, M. Mae, Study on accuracy of specific heat measurement of phase change materials by calculation, AIJ J. Technol. Des. 25 (2019) 223-228, http://doi.org/10.3130/aijt.25.223

[6.4] American Society for Testing and Materials, ASTM C 1784, Standard test method for using a heat flow meter apparatus for measuring thermal storage properties of phase change materials and products, ASTM, Pennsylvania, 2020.

[6.5] E. Solgi, Z. Hamedani, R. Fernando, B.M. Kari, H. Skates, A parametric study of phase change material behavior when used with night ventilation in different climatic zones, Build. Environ. 147 (2019) 327-336, https://doi.org/10.1016/j.buildenv.2018.10.031

[6.6] K. Chen, T. Asawa, H. Oshio, Formation factors of microclimate around a high-rise building in winter season -Examining by coupled analysis of heat balance simulation and CFD, J. Heat Isl. Inst. Int. 12 (2017) 9-20.

[6.7] F. Guarino, A. Athienitis, M. Cellura, D. Bastien, PCM thermal storage design in buildings: Experimental studies and applications to solaria in cold climates, Appl. Energy, 185 (2017) 95-106. https://doi.org/10.1016/j.apenergy.2016.10.046

[6.8] M.E. Poulad, A.S. Fung, D. Naylor, Effects of convective heat transfer coefficient on the ability of PCM to reduce building energy demand, in: Proc. 12th int. IBSPA conf., 2011.

[6.9] Y. Yu, A.C. Megri, S. Jiang, A review of the development of airflow models used in building load calculation and energy simulation, Build. Simul. 12 (2019) 347-363, https://doi.org/10.1007/s12273-018-0494-0

[6.10] F. Goia, G. Chaudhary, S. Fantucci, Modeling and experimental validation of an algorithm for simulation of hysteresis effect in phase change materials for building components, Energy Build. 174 (2018) 54-67, https://doi.org/10.1016/j.enbuild.2018.06.001

[6.11] E. Mohseni, W. Tang, Parametric analysis and optimization of energy efficiency of a lightweight building integrated with different configurations and types of PCM, Renew. Energy, 168 (2021) 865-877, https://doi.org/10.1016/j.renene.2020.12.112

[6.12] D. Mazzeo, N. Matera, C. Cornaro, G. Oliveti, P. Romagnoni, L.D. Santoli, EnergyPlus, IDA ICE and TRNSYS predictive simulation accuracy for building thermal behavior evaluation by using an experimental campaign in solar test boxes with and without a PCM module, Energy Build. 212 (2020) 109812, https://doi.org/10.1016/j.enbuild.2020.109812

[6.13] H. Jamil, M. Alam, J. Sanjayan, J. Wilson, Investigation of PCM as retrofitting option to enhance occupant thermal comfort in a modern residential building, Energy Build. 133 (2016) 217-229, http://dx.doi.org/10.1016/j.enbuild.2016.09.064

[6.14] Y. Hu, R. Guo, P.K. Heiselberg, Performance and control strategy development of a PCM enhanced ventilated window system by a combined experimental and numerical study, Renew. Energy, 155 (2020) 134-152, https://doi.org/10.1016/j.renene.2020.03.137

[6.15] W. Sun, Z. Zhang, Z. Wu, Y. Xu, Numerical modeling and optimization of annual thermal characteristics of an office room with PCM active-passive coupling system, Energy Build. 254 (2022) 11629, https://doi.org/10.1016/j.enbuild.2021.111629

[6.16] A. Jayalath, L. Aye, P. Mendis, T. Ngo, Effects of phase change material roof layers on thermal performance of a residential building in Melbourne and Sydney, Energy Build. 121 (2016) 152-158, http://dx.doi.org/10.1016/j.enbuild.2016.04.007

[6.17] M. Alam, J. Sanjayan, P.X.W. Zou, S. Ramakrishnan, J. Wilson, A comparative study on the effectiveness of passive and free cooling application methods of phase change materials for energy efficient retrofitting in residential buildings, Procedia Eng. 180 (2017) 993-1002, https://doi.org/10.1016/j.proeng.2017.04.259

[6.18] M. Arıcı, F. Bilgin, S. Nižetić, H. Karabay. PCM integrated to external building walls: An optimization study on maximum activation of latent heat, Appl. Therm. Eng. 165 (2020) 114560. https://doi.org/10.1016/j.applthermaleng.2019.114560

[6.19] B. Pandey, R. Banerjee, A. Sharma, Coupled EnergyPlus and CFD analysis of PCM for thermal management of buildings, Energy Build. 231 (2021) 110598, https://doi.org/10.1016/j.enbuild.2020.110598

[6.20] Z.A. Al-Absi, M.I.M. Hafizal, M. Ismail, A. Mardiana, A. Ghazali, Peak indoor air temperature reduction for buildings in hot-humid climate using phase change materials, Case Study Therm. Eng. 22 (2020) 100762, https://doi.org/10.1016/j.csite.2020.100762

[6.21] B. Ferster, H. Shen, J.D. Rendall, PCM (phase change material) optimization modeling for passive cooling in south Texas, in: Proc. 15th int. IBSPA conf., 2017. https://doi.org/10.26868/25222708.2017.255

[6.22] T. Saeki, S. Hagihara, T. Tasaka, K. Mabuchi, Development of the measurement method of thermal storage properties for phase change material, Japan J. Therm. Prop. 34 (2020) 56-63.

[6.23] Japan Testing Center for Construction Materials. JSTM O 6101, Test method for the thermal storage properties of building materials using phase change materials, JSTM, Tokyo, 2020.

[6.24] F. Souayfane, F. Fadoun, P. Biwole, Phase change materials (PCM) for cooling applications in buildings: A review, Energy Build. 129 (2016) 396-431, https://doi.org/10.1016/j.enbuild.2016.04.006

[6.25] Y. Sato, A. Osaki, T. Nakamura, Y. Hayashi, S. Ishiguro, Research on the reduction effect of the space heating load by latent heat storage interior building material, J. Environ. Eng. 77 (2012) 651-659. https://doi.org/10.3130/aije.77.651

[6.26] U.S. Department of Energy. EnergyPlus Engineering Reference, 2022.

[6.27] P.C. Tabares-Velasco, B. Griffith, Diagnostic test cases for verifying surface heat transfer algorithms and boundary conditions in building energy simulation programs, J. Build. Perform. Simul. 5 (2011) 329-346, https://doi.org/10.1080/19401493.2011.595501

[6.28] H.K. Versteeg, W. Malalasekera, An Introduction of computational fluid dynamics, Person Education Limited, Harlow, 1995.

[6.29] A. Al-Janabi, M. Kavgic, Application and sensitivity analysis of the phase change material hysteresis method in EnergyPlus: A case study, Appl. Therm. Eng. 162 (2019) 114222, https://doi.org/10.1016/j.applthermaleng.2019.114222

[6.30] P.C. Tabares-Velasco, C. Christensen, M. Bianchi, Verification and validation of EnergyPlus phase change material model for opaque wall assemblies, Build. Environ. 54 (2012) 186-196, https://doi.org/10.1016/j.buildenv.2012.02.019

[6.31] S. Medved, C. Arkar, Correlation between the local climate and the free-cooling potential of latent heat storage, Energy Build. 40 (2008) 429-437, https://doi.org/10.1016/j.enbuild.2007.03.011

[6.32] American Society of Heating, Refrigerating and Air Conditioning Engineers, 2017 ASHRAE, Handbook – Fundamentals, Heat, Air, and Moisture Control in Building Assemblies – Material Properties, ASHRAE, Atlanta, 2017.

[6.33] S. Diamond, B. Hunn, Comparison of DOE-2 computer program simulations to metered data for seven commercial buildings, ASHRAE Trans. 87 (1981) 1222-1231.

[6.34] National Centers for Environmental Information, NOAA, USA, integrated surface dataset, 2020 https://www.ncei.noaa.gov/access/search/data-search/global-hourly, Accessed date November 10 2020.

[6.35] T. Kubota, D.H.C. Chyee, A. Ahmad, The effect of night ventilation technique on indoor thermal environment for residential buildings in hot-humid climate of Malaysia, Energy Build. 41 (2009) 829-839, https://doi.org/10.1016/j. enbuild.2009.03.008

[6.36] M.N.F. Alfata, N. Hirata, T. Kubota, A.M. Nugroho, T. Uno, S.N. Ekasiwi, I.G.N. Antaryama, Field investigation of indoor thermal environments in apartments of Surabaya, Indonesia: potential passive cooling strategies for middle-class apartments, Energy Procedia 78 (2015) 2947–2952, https://doi.org/10.1016/j. egypro.2015.11.674

[6.37] M.N.F. Alfata, N. Hirata, T. Kubota, A.M. Nugroho, T. Uno, I.G.N. Antaryama, S. N. Ekasiwi, Thermal comfort in naturally ventilated apartments in Surabaya, Indonesia, Procedia Eng. 121 (2015) 459–467, https://doi.org/10.1016/j. proeng.2015.08.1093

[6.38] D.H.C. Toe, T. Kubota, Comparative assessment of vernacular passive cooling techniques for improving indoor thermal comfort of modern terraced houses in hot-humid climate of Malaysia, Sol. Energy, 114 (2015) 229-258, https://doi.org/10.1016/j.solener.2015.01.035

[6.39] D.H.C. Toe, T. Kubota, Development of an adaptive thermal comfort equation for naturally ventilated buildings in hot-humid climates using ASHRAE RP-884 database, Front. Archit. Res. 2 (2013) 278-291, https://doi.org/10.1016/j.foar.2013.06.003

[6.40] T. Kubota, D.H.C. Chyee, A. Ahmad, The effect of night ventilation technique on indoor thermal environment for residential buildings in hot-humid climate of Malaysia, Energy Build. 41 (2009) 829-839, https://doi.org/10.1016/j. enbuild.2009.03.008

[6.41] W. Sun, R. Huang, Z. Ling, X. Fang, Z. Zhang, Numerical simulation on the thermal performance of a PCM-containing ventilation system with a continuous change in inlet air temperature, Renew. Energy, 145 (2020) 1608-1619. https://doi.org/10.1016/j.renene.2019.07.089

[6.42] M. Iten, S. Liu, A. Shukla, Experimental study on the thermal performance of air – PCM unit, Build. Environ. 105 (2016) 128–139, https://doi.org/10.1016/j.buildenv.2016.05.035

[6.43] H. Tang, T. Zhang, X. Liu, C. Li, A novel pulse width modification for metal radiant panels to control the condensation risk in a hot and humid environment, Build. Environ. 196 (2021) 107802, https://doi.org/10.1016/j.buildenv.2021.107802

[6.44] Y.L. Yin, R.Z. Wang, X.Q. Zhai, T.F. Ishugah, Experimental investigation on the heat transfer performance and water condensation phenomenon of radiant cooling panels, Build. Environ. 71 (2014) 15-23, http://dx.doi.org/10.1016/j.buildenv.2013.09.016

[6.45] A. Safari, R. Saidur, F.A. Sulaiman, Y. Xu, J. Dong, A review on supercooling of phase change materials in thermal energy storage systems, Renew. Sustain. Energy Rev. 70 (2017) 905-919, http://dx.doi.org/10.1016/j.rser.2016.11.272

[6.46] M. Thonon, G. Fraisse, L. Zalewski, M. Pailha, Analytical modeling of PCM supercooling including recalescence for complete and partial heating/cooling cycles. Appl. Therm. Eng. 190 (2021) 116751, https://doi.org/10.1016/j.applthermaleng.2021.116751

[6.47] Y. Tominaga, A. Mochida, CFD prediction of flowfield and snowdrift around a building complex in a snowy region, J. Wind Eng. Ind. Aerodyn., 81 (1999) 273-282. https://doi.org/10.1016/S0167-6105(99)00023-9

[6.48] The Japan Society of Mechanical Engineers, Heat Transfer, JSME, Tokyo, 2009. ISBN：978-4-88898-184-2

[6.49] T. Defraeye, B. Blocken, J. Carmeliet, CFD simulation of heat transfer at surfaces of bluff bodies in turbulent boundary layers: Evaluation of a forced-convective temperature wall function for mixed convection, J. Wind Eng. Ind. Aerodyn. 104-106 (2012) 439-446, https://doi.org/10.1016/j.jweia.2012.02.001

[6.50] F. Goia, G. Chaudhary, S. Fantucci, Modeling and experimental validation of an algorithm for simulation of hysteresis effect in phase change materials for building components, Energy Build. 174 (2018) 54-67, https://doi.org/10.1016/j.enbuild.2018.06.001

[6.51] N.W. Tuck, S.A. Zaki, A. Hagishima, H.B. Rijal, M.Z. Zakaria, F. Yakub, Effectiveness of free running passive cooling strategies for indoor thermal environments: Example from a two-story corner terrace house in Malaysia, Build. Environ. 160 (2019) 106214, https://doi.org/10.1016/j.buildenv.2019.106214

[6.52] N.W. Tuck, S.A. Zaki, A. Hagishima, H.B. Rijal, F. Yakub, Affordable retrofitting methods to achieve thermal comfort for terraced house in Malaysia with a hot-humid climate, Energy Build. 223 (2020) 110072, https://doi.org/10.1016/j.enbuild.2020.110072

[6.53] R. Baetens, B.P. Jelle, A. Gustavsen, Phase change materials for building applications: A state-of-the-art review, Energy Build. 42 (2010) 1361-1368, https://doi.org/10.1016/j.enbuild.2010.03.026

[6.54] D.A. Neeper, Thermal dynamics of wallboard with latent heat storage, Sol. Energy, 68 (2008) 393-403, https://doi.org/10.1016/s0038-092x(00)00012-8

[6.55] J. Koo, H. So, S.W. Hong, H. Hong, Effect of wallboard design parameters on the thermal storage in buildings, Energy Build. 43 (2011) 1947-1951, https://doi.org/10.1016/j.enbuild.2011.03.038

[6.56] J. Lei, J. Yang, E.H. Yang, Energy performance of building envelopes integrated with phase change materials for cooling load reduction in tropical Singapore, Appl. Energy, 162 (2016) 207-217, https://doi.org/10.1016/j.apenergy.2015.10.031

Chapter 7

[7.1] S. Tanabe, K. Kimura, Effect of air temperature, humidity, and air movement on thermal comfort under hot and humid conditions, ASHRAE Transactions. 100 (1994) 953-969.

[7.2] M. Santamouris, Cooling the buildings – past, present and future, Energy Build. 128 (2016) 617–638. https://doi.org/10.1016/j.enbuild.2016.07.034

[7.3] M.J. Sorgato, A.P. Melo, R. Lamberts, The effect of window opening ventilation control on residential building energy consumption, Energy Build. 133 (2016) 1–13. http://dx.doi.org/10.1016/j.enbuild.2016.09.059

[7.4] T. Psomas, M. Fiorentini, G. Kokogiannakis, P. Heiselberg, Ventilative cooling through automated window opening control systems to address thermal discomfort risk during the summer period: Framework, simulation and parametric analysis, Energy Build. 153 (2017) 18–30. http://dx.doi.org/10.1016/j.enbuild.2017.07.088

[7.5] L. Wang, S. Greenberg, Window operation and impacts on building energy consumption, Energy Build. 92 (2015) 313–321. http://dx.doi.org/10.1016/j.enbuild.2015.01.060

[7.6] S. Kato, W. Zhang, A review: coupled simulation of CFD and network model for heat and contaminant transport in a building, J. Asia Archit. Build. Eng. 13 (2014) 231-238. https://doi.org/10.3130/jaabe.13.231

[7.7] A.S. Andelkovi´c, I. Mujan, S. Daki´c, Experimental validation of a EnergyPlus model: application of a multi-story naturally ventilated double skin façade, Energy Build. 118 (2016) 27–36, https://doi.org/10.1016/j.enbuild.2016.02.045

[7.8] Y. Yu, A.C. Megri, S. Jiang, A review of the development of airflow models used in building load calculation and energy simulation, Build. Simul. 12 (2019) 347–363. https://doi.org/10.1007/s12273-018-0494-0

[7.9] M.E. Poulad, A.S. Fung, D. Naylor, Effects of convective heat transfer coefficient on the ability of PCM to reduce building energy demand, in: Proc. 12th int. IBSPA conf., 2011. http://ibpsa.org/proceedings/BS2011/P_1202.pdf

[7.10] J. Franke, A. Baklanov, Best practice guideline for the CFD simulation of flows in the urban environment: COST action 732 quality assurance and improvement of microscale meteorological models, Meteorological Inst. Hamburg, Germany, 2007. https://www.researchgate.net/publication/257762102_Best_Practice_Guideline_for_the_CFD_Simulation_of_Flows_in_the_Urban_Environment_COST_Action_732_Quality_Assurance_and_Improvement_of_Microscale_Meteorological_Models

[7.11] Y. Tominaga, A. Mochida, R. Yoshie, H. Kataoka, T. Nozu, M. Yoshikawa, T. Shirasawa, AIJ guidelines for practical applications of CFD pedestrian wind environment around buildings, J. Wind Eng. Ind. Aerodyn. 96 (2008) 1749–1761. https://doi.org/10.1016/j.jweia.2008.02.058

[7.12] R. Blocken, Computational fluid dynamics for urban physics: Importance, scales, possibilities, limitations and ten tips and tricks towards accurate and reliable simulations, Build. Environ. 91 (2015) 219–245. https://doi.org/10.1016/j.buildenv.2015.02.015

[7.13] V. Yakhot, S.A. Orszag, S. Thangam, T.B. Gatski, C.G. Speziale, Development of turbulence models for shear flows by a double expansion technique, Phys. Fluids. 4 (1992) 1510–1520. https://doi.org/10.1063/1.858424

[7.14] D. Choudhury, Introduction to the renormalization group method and turbulence modeling, Fluent Incorporated, 1973. https://books.google.co.in/books?id=mKWEQwAACAAJ

[7.15] P.J. Roache, Quantification of uncertainty in computational fluid dynamics, Annu. Rev. Fluid Mech. 29 (1997) 123–160. https://doi.org/10.1146/annurev.fluid.29.1.123

[7.16] B.E. Launder, D.B. Spalding, The numerical computation of turbulent flows, Pergamon Press Ltd., 1983. https://doi.org/10.1016/b978-0-08-030937-8.50016-7

[7.17] H. Kataoka, Numericla simulations of a wind-induced vibrating square cylinder within turbulent boundary layer, J. Wind Eng. Ind. Aerodyn. 96 (2008) 1985–1997. https://doi.org/10.1016/j.jweia.2008.02.061

[7.18] P. Karava, T. Stathopoulos, A.K. Athienitis, Wind-induced natural ventilation analysis, Sol. Energy. 81 (2007) 20–30. https://doi.org/10.1016/j.solener.2006.06.013

[7.19] M. Shirzadi, P.A. Mirzaei, M. Naghashzadegan, Development of an adaptive discharge coefficient to improve the accuracy of cross-ventilation airflow calculation in building energy simulation tools, Build. Environ. 127 (2018) 277–290. https://doi.org/10.1016/j.buildenv.2017.10.019

[7.20] T. Kurabuchi, M. Ohba, T. Endo, Y. Akamine, Local dynamic similarity concept and underlaying wind tunnel tests-Prediction accuracy of flow rate of cross-ventilate buildings (Part 1), J. Environ. Eng. Trans. AIJ. 71 (2006) 37–41. https://doi.org/10.3130/aije.71.37_2

[7.21] S. Tanabe, T. Yamanaka, Y. Momoi, K. Sagara, Natural ventilation performance of high-rise office buildings with corner voids. Part 1- Ventilation rate by differential pressure measurement, Trans. Soc. Heating Air conditioning Sanit. Eng. Japan. 45 (2020) 41–47. https://doi.org/10.18948/shase.45.283_41

[7.22] S. Horikawa, K. Sagara, T. Yamanaka, H. Kotani, E. Lim, M. Yamagiwa, S. Ischiyama, T. Yamashita, T. Ushio, Task ambient air conditioning system with natural ventilation for high rise office building. Part 8: field measurements of indoor thermal environment in spring and fall, Tech. Paper Annu. Meet. Soc. Heating Air conditioning Sanit. Eng. Japan. (2006) 1373–1376. https://doi.org/10.18948/shasetaikai.2006.2.0_1373

[7.23] S. Moon, H. Yun, Y. Seo, Suggestion of advanced regression model on friction angle of fault gouge in South Korea, J. Rock Mech. Geotech. Eng. 13 (2021) 1368–1379. https://doi.org/10.1016/j.jrmge.2021.07.010

[7.24] G.M. Stavrakakis, M.K. Koukou, M.Gr. Vrachopoulos, N.C. Markatos, Natural cross-ventilation in buildings: Building-scale experiments, numerical simulation and thermal comfort evaluation, Energy Build. 40(9) (2008) 1666–1681. https://doi.org/10.1016/j.enbuild.2008.02.022

[7.25] Y. Jiang, Q. Chen, Study of natural ventilation in buildings by large eddy simulation, J. Wind. Eng. Ind. Aerod. 89(13) (2001) 1155–1178. https://doi.org/10.1016/S0167-6105(01)00106-4

[7.26] American Society of Heating, Refrigerating and Air Conditioning Engineers, 2017 ASHRAE, Handbook- Fundamentals, Heat, Air, and Moisture Control in Building Assemblies- Material Properties, ASHRAE, Atlanta, 2017.

[7.27] D. Coakley, P. Raftery, K. Marcus, A review of methods to match building energy simulation models to measured data, Renew. Sustain. Energy Rev. 37 (2014) 123–141. https://doi.org/10.1016/j.rser.2014.05.007

[7.28] T.H. Katyono, E. Siri, J.G. Sulistiawan, Y. Triswanti, Thermal comfort studies in naturally ventilated buildings in Jakarta, Indonesia, Buildings. 5 (2015) 917–932. https://doi.org/10.3390/buildings5030917

[7.29] A.T. Nguyen, M.K. Singh, S. Reiter, An adaptive thermal comfort model for humid South-East Asia, Build. Environ. 56 (2012) 291–300. https://doi.org/10.1016/j.buildenv.2012.03.021

[7.30] B. Pandey, R. Banerjee, A. Sharma, Coupled EnergyPlus and CFD analysis of PCM for thermal management of buildings, Energy Build. 231 (2021) 110598. https://doi.org/10.1016/j.enbuild.2020.110598

[7.31] D.P. Fin, D. Connolly, P. Kenny, Sensitivity analysis of a maritime located night ventilated library building, Sol. Energy. 81 (2007) 697–710. https://doi.org/10.1016/j.solener.2006.10.008

[7.32] P. Nageler, G. Schweiger, M. Pichler, D. Brandl, T. Mach, R. Heimrath, H. Schranzhofer, C. Hochenauer, Validation of dynamic building energy simulation tools based on a rea text-box with thermally activated building systems (TABS), Energy Build. 168 (2018) 42–55. https://doi.org/10.1016/j.enbuild.2018.03.025

[7.33] D. Mazzeo, N. Matera, C. Cornaro, G. Oliveti, P. Romagnoni, L.D. Santoli, EnergyPlus IDA ICE and TRANSYS predictive simulation accuracy for building thermal behavior evaluation by using an experimental campaign in solar test boxes with and without a PCM module, Energy Build. 212 (2020) 109812. https://doi.org/10.1016/j.enbuild.2020.109812

[7.34] G.B. Porsani, C.F. Bandera, A case study of empirical validation of EnergyPlus infiltration models based on different wind data, Build. 13 (2023) 511. https://doi.org/10.3390/buildings13020511

[7.35] American Society for Testing and Materials, ASTM D 5157, Standard guide for statistical evaluation of indoor air quality models, ASTM, Pennsylvania, 2019.

[7.36] National Centers for Environmental Information, NOAA, USA, integrated surface dataset, 2020 https://www.ncei.noaa.gov/access/search/data-search/global-hourly, Accessed 10 November 2020.

[7.37] H. Mori, T. Kubota, I.G.N. Antaryama, S.N.N. Ekasiwi, Analysis of window-opening patterns and air conditioning usage of urban residences in tropical Southeast Asia, Sustain. 12 (2020) 10650. https://doi.org/10.3390/su122410650

[7.38] T. Kubota, D.H.C. Toe, S. Ahmad, The effect of night ventilation technique on indoor thermal environment for residential buildings in hot-humid climate of Malaysia, Energy Build. 41 (2009) 829-839. https://doi.org/10.1016/j.enbuild.2009.03.008

[7.39] T.H. Karyono, Predicting comfort temperature in Indonesia, an initial step to reduce cooling energy consumption, Buildings. 5 (2015) 802–813. https://doi:10.3390/buildings5030802

[7.40] S. Akabayashi, J. Sakaguchi, T. Oshima, H. Ichikawa, Y. Arinami, A study on the current status of COP of residential air conditioners and regional characteristics of APF, Architectural Institute of Japan Technical Reports 20 (2014) 187–190. https://doi.org/10.3130/aijt.20.187

[7.41] U. Surahman, T. Kubota, O. Higashi, Life cycle assessment of energy and CO_2 emissions for residential buildings in Jakarta and Bandung, Indonesia, Buildings. 5 (2015) 1131–1155. https://doi.org/10.3390/buildings5041131

[7.42] E. Solgi, Z. Hamedani, R. Fernando, H. Skates, N.E. Orji, A literature review of night ventilation strategies in buildings, Energy Build. 173 (2018) 337–352. https://doi.org/10.1016/j.enbuild.2018.05.052

[7.43] M. Haase, A. Amato, An investigation of the potential for natural ventilation and building orientation to achieve thermal comfort in warm and humid climates, Sol. Energy. 83 (2009) 389–399. https://doi:10.1016/j.solener.2008.08.015

[7.44] W. Liping, W.N. Hien, The impacts of ventilation strategies and façade on indoor thermal environment for naturally ventilated residential buildings in Singapore, Build. Environ. 42 (2007) 4006–4015. https://doi:10.1016/j.buildenv.2006.06.027

[7.45] American National Standard Institute (ANSI), Thermal Environmental Conditions for Human Occupancy (ANSI/ASHRAE Standard 55-2020), ASHRAE, USA, 2022. ISSN 1041-2336

[7.46] X. Deng, P. Cooper, Z. Ma, G. Kokogiannakis, Numerical analysis of indoor thermal comfort in a cross-ventilated space with top-hung windows, Energy Procedia. 121 (2017) 222–229. https://doi.org/10.1016/j.egypro.2017.08.021

[7.47] M.T. Arethusa, T. Kubota, A.M. Nugroho, I.G.N. Antaryama, S.N. Ekasiwi, T. Uno, A field survey of window-opening behavior and thermal conditions in apartment of Surabaya, Indonesia, Intercult. Underst. 4 (2014) 17–25.

[7.48] C. Cândido C, R.J. de Dear, R. Lamberts, L. Bittencourt, Air movement acceptability limits and thermal comfort in Brazil's hot humid climate zone, Build. Environ. 41 (2010) 222–229. https://doi.org/10.1016/j.buildenv.2009.06.005

[7.49] I.D.G.A. Putra, H. Nimiya, A. Sopaheluwakan, T. Kubota, H.S. Lee, R.P. Pradana, M.N.F. Alfata, R.B. Perdana, D.S. Permana, N.F. Riama, Development of climate zones for passive cooling techniques in the hot and humid climate of Indonesia, Build. Environ. 226 (2022) 109698. https://doi.org/10.1016/j.buildenv.2022.109698

[7.50] B. Painter, N. Brown, M.J. Cook, Practical application of a sensor overlay system for building monitoring and commissioning, Energy Build. 48 (2012) 29–39. https://doi.org/10.1016/j.enbuild.2012.01.003

[7.51] Y. Yamamoto, M. Kuboki, H. Suzuki, S. Tanabe, Investigation on management of natural ventilation system, J. Environ. Eng. AIJ. 619 (2007) 9-16. https://doi.org/10.3130/aije.72.9_7

[7.52] H. Kitagawa, A. Tanimoto, T. Kubota, K. Koyama, M.N.F. Alfata, A field experiment on green walls taking into consideration wind flow in the hot-humid climate of Indonesia. IOP Conf. Ser. Earth Environ. Sci. 294 (2019) 012088. https://doi:10.1088/1755-1315/294/1/012088

[7.53] K. Taniguchi, Y. Akamine, Wind pressure coefficient distribution of detached houses in a dense residential block, J. Environ. Eng. AIJ. 83 (2018) 679-689. https://doi.org/10.3130/aije.83.679

[7.54] E. Prianto, P. Depecker, Characteristic of air flow as the effect of balcony, opening design and internal division on indoor velocity A case study of traditional dwelling in urban living quarter in tropical humid region, Energy Build. 34 (2002) 401–409. https://doi.org/10.1016/S0378-7788(01)00124-4

Chapter 8

[8.1] H. Djamila, C. M. Chu, S. Kumaresan, Field study of thermal comfort in residential buildings in the equatorial hot-humid climate of Malaysia, Build. Environ. 62 (2013) 133-142, http://dx.doi.org/10.1016/j.buildenv.2013.01.017

[8.2] B. W. Olesen, K. C. Parsons, Introduction to thermal comfort standards and to the proposed new version of EN ISO 7730, Energy Build. 34 (2002) 537-548, https://doi.org/10.1016/S0378-7788(02)00004-X

[8.3] S. Sakuragawa, The tactile warmth/coldness sensation of wood, Mokuzai no sesshoku onreikan (in Japanese), Wood Ind. 70 (2015) 376-381.

[8.4] American Society of Heating, Refrigerating and Air Conditioning Engineers, 2017 ASHRAE, Handbook- Fundamentals, Heat, Air, and Moisture Control in Building Assemblies- Material Properties, ASHRAE, Atlanta, 2017.

[8.5] M. Saffari, A. de Gracia, S. Ushak, L.F. Cabeza, Economic impact of integrating PCM as passive system in buildings under Fanger comfort model, Energy Build. 112 (2016) 159-172. https://doi.org/10.1016/j.enbuild.2015.12.006

[8.6] H. Mori, T. Kubota, I.G.N. Antaryama, S.N.N. Ekasiwi, Analysis of window-opening patterns and air conditioning usage of urban residences in tropical Southeast Asia, Sustain. 12 (2020) 10650. https://doi.org/10.3390/su122410650

[8.7] T. Kubota, D.H.C. Toe, S. Ahmad, The effect of night ventilation technique on indoor thermal environment for residential buildings in hot-humid climate of Malaysia, Energy Build. 41 (2009) 829-839. https://doi.org/10.1016/j.enbuild.2009.03.008

List of Publication

【Journal paper】

1-1. **H. Kitagawa,** T. Asawa, Y. Hirayama, Optimum window-opening control for naturally ventilated buildings installed phase change materials in the hot and humid climate of Indonesia, Building and Environment 245 (2023) 110898. https://doi.org/10.1016/j.buildenv.2023.110898

1-2. **H. Kitagawa,** T. Asawa, M.A. Del Rio, T. Kubota, A.R. Trihamdani, Thermal energy Simulation of PCM-based radiant floor cooling systems for naturally ventilated buildings in a hot and humid climate, Building and Environment, 238 (2023) 110351. https://doi.org/10.1016/j.buildenv.2023.110351

1-3. **H. Kitagawa**, T. Asawa, T. Kubota, A.R. Trihamdani, Numerical simulation of radiant floor cooling systems using PCM for naturally ventilated buildings in a hot and humid climate, Building and Environment, 226 (2022) 109762. https://doi.org/10.1016/j.buildenv.2022.109762

1-4. **H. Kitagawa**, T. Asawa, T. Kubota, A.R. Trihamdani, H. Mori, Thermal storage effect of radiant floor cooling system using phase change materials in the hot and humid climate of Indonesia, Building and Environment, 207 (2022) 108442. https://doi.org/10.1016/j.buildenv.2021.108442

1-5. **H. Kitagawa**, T. Asawa, T. Kubota, A.R. Trihmdani, K. Sakurada, H. Mori, Optimization of window design for ventilative cooling with radiant floor cooling systems in the hot and humid climate of Indonesia, Building and Environment, 188 (2021) 107483 https://doi.org/10.1016/j.buildenv.2020.107483

1-6. **H. Kitagawa,** A. Tanimoto, T. Kubota, K. Koyama, M.N.F. Alfata, A field experiment on green walls taking into consideration wind flow in the hot-humid climate of

Indonesia, IOP Conf. Series: Earth and Environment Science, 294 (2019) 012088, https://doi:10.1088/1755-1315/294/1/012088

1-7. K. Hakamada, T. Asawa, **H. Kitagawa**, H. Aoshima, R. Kawamura, Contact cooling for bare feet using floor cooling systems: Experiment on human thermal physiology and sensation in Japanese hot environment, Building and Environment, (2024) 111256, https://doi.org/10.1016/j.buildenv.2024.111256

1-8. M. Nagasue, **H. Kitagawa**, T. Asawa, T. Kubota, A systematic review of passive cooling methods in hot and humid climates using a text mining-based bibliometric approach, Sustainability, 16 (2024) 1420, https://doi.org/10.3390/su16041420

1-9. **H. Kitagawa**, T. Asawa, T. Kubota, Y. Hirayama, T. Maeda, N. Kumar, M.N.F. Alfata, Natural ventilation performance for midrise double-loaded apartments with a vertical void in the hot and humid climate of Indonesia, Building and Environment, (will be submitted)

1-10. T. Zhang, **H. Kitagawa**, T. Asawa, Dynamic coupling simulation method between CFD and building energy simulation for studying radiant floor cooling systems in naturally ventilated buildings, Building and Environment, (will be submitted)

【International Conference】

2-1. N. Kumar, **H. Kitagawa**, M.N.F. Alfata, T. Maeda, T. Kubota, T. Asawa, Y. Hirayama, A.R. Trihamdani, D. Nakahara, Experimental study on vertical void for improving natural ventilation in midrise double-loaded apartments, 11th international conference on indoor air quality, ventilation & energy conservation in buildings, IAQVEC 2023, pp.1-8. C000256. 2023. 5, Tokyo. https://doi.org/10.1051/e3sconf/202339602024

2-2. T. Maeda, T. Kubota, N. Kumar, **H. Kitagawa**, T. Asawa, H. Mori, A.R. Trihamdani, CFD analysis on window design to improve indoor thermal comfort of residential buildings in the tropics. 11th international conference on indoor air quality, ventilation & energy conservation in buildings, IAQVEC 2023, C000169. 2023. 5, Tokyo

2-3. **H. Kitagawa**, K. Sakurada, A.R. Trihamdani, T. Asawa, T. Kubota, H. Mori, Optimization of window systems to achieve thermal comfort in the hot and humid climate of Indonesia, 16th Conference of the International Society of Indoor Air Quality & Climate, Indoor Air 2020, pp.1-6, 2020. 11, Online.

2-4. A.R. Trihamdani, A. Tanimoto, T. Kubota, H. Mori, T. Asawa, **H. Kitagawa**, Development of radiant floor cooling system using phase change material in the hot and humid climate of Indonesia, 16th Conference of the International Society of Indoor Air Quality & Climate, Indoor Air 2020, pp.1-6, 2020. 11, Online.

2-5. **H. Kitagawa,** A. Tanimoto, T. Kubota, K. Koyama, M.N.F. Alfata, A field experiment on green walls taking into consideration wind flow in the hot-humid climate of Indonesia, Sustainable Build Environment Conference 2019 Tokyo, SBE19, 2019. 8, Tokyo.

2-6. T. Kubota, H. Shima, H. Sani, N. Kumar, **H. Kitagawa**, T. Asawa, M.N.F. Alfata, Effects of closed vertical void on natural ventilation in double-loaded apartment building, 44th AIVC conference, 2024.10, Dublin. (Under review)

【Domestic Conference】

3-1. **北川遼**, 浅輪貴史, 久保田徹, 高温多湿気候のインドネシアにおける潜熱蓄熱材を用いた自然換気住宅の性能評価に関する研究　その 1 床冷却システムの蓄冷性能の年間評価, 日本建築学会大会（近畿）学術講演会, p. 829-830, 2023. 9.

3-2. 浅輪貴史, **北川遼**, 久保田徹, 高温多湿気候のインドネシアにおける潜熱蓄熱材を用いた自然換気住宅の性能評価に関する研究　その 2 窓開閉制御最適条件の検討, 日本建築学会大会（近畿）学術講演会, p. 831-832, 2023. 9.

3-3. T. Kubota, N. Kumar, **H. Kitagawa**, T. Maeda, T. Asawa, Field experiment on effects of vertical void on natural ventilation in double-loaded apartments, 日本建築学会大会（近畿）学術講演会, p. 833-834, 2023. 9

3-4. **北川遼**, 永末百々日, 浅輪貴史, 久保田徹, テキストマイニングを用いた高温多湿気候に適応するパッシブクーリング技術の系統的整理と分析, 日本建築学会関東支部研究発表会, p.1-4, 2023.2.

3-5. 牛塚功大, 平山由佳理, 河本陸, 浅輪貴史, 久保田徹, Nikhil Kumar, **北川遼**, ボイドを有する集合住宅における自然通風の評価, 日本建築学会関東支部研究発表会, p.5-8, 2023.2.

3-6. **H. Kitagawa**, T. Asawa, T. Kubota, A.R. Trihamdani, H. Mori, Optimization of radiant floor cooling systems using phase change materials for naturally ventilated residential buildings in the hot and humid climate of Indonesia, 日本建築学会大会（東海）学術講演会, p.2419-2422, 2021. 9.

3-7. A.R. Trihamdani, K. Sakurada, T. Kubota, T. Asawa, **H. Kitagawa**, H. Mori, Control methods of vertical airflow distribution through window design for naturally ventilated residential buildings in the hot and humid climate, 日本建築学会大会（東海）学術講演会, p.2415-2418, 2021. 9.

3-8. K. Sakurada, A. Tanimoto, T. Kubota, H. Mori, T. Asawa, **H. Kitagawa**, Effect of radiant floor cooling using phase change material on thermal comfort in hot-humid climate, 日本建築学会大会（関東）学術講演会, p. 2563-2566, 2020.9.

3-9. **H. Kitagawa**, K. Sakurada, T. Asawa, T. Kubota, H. Mori, A field experiment on

window systems to achieve thermal comfort with ventilative cooling in the hot-humid climate of Indonesia, 日本建築学会大会（関東）学術講演会, p. 2555-2558, 2020.9.

3-10. **北川遼**, 櫻田葵香, A.R. Trihamdani, 浅輪貴史, 久保田徹, 森博史, 高温多湿気候のインドネシアに適応する自然換気住宅の窓設計及び性能評価, 日本建築学会関東支部研究発表会, p.139-142, 2020.3.

3-11. **H. Kitagawa**, T. Kubota, A field experiment on effects of green walls on indoor thermal comfort in the hot and humid climate, 日本建築学会大会（北陸）学術講演会, p. 985-988, 2019.9.

3-12. **北川遼,** 浅輪貴史, Nikhil Kumar, 久保田徹, 平山由佳理, 牛塚功大, 高温多湿気候のボイドを有する集合住宅の温度・気流性状に関する実験的検討, 日本建築学会関東支部研究発表会, 2024.3. (発表申し込み済)

3-13. 吉池秀太, 平山由佳理, 牛塚功大, 浅輪貴史, **北川遼**, 久保田徹, Nikhil Kumar, 高温多湿気候のボイドを有する集合住宅における窓開閉条件に関する数値解析, 日本建築学会関東支部研究発表会, 2024.3. (発表申し込み済)

【Award】

4-1. 2022 年度 日本建築学会関東支部研究発表会 若手優秀発表賞 2023.3

4-2. 2019 年度大会 日本建築学会大会（北陸）学術講演会 環境工学委員会 若手優秀発表賞 2019.12

4-3. 広島大学 学術研究活動 工学部・工学研究科学生表彰 2019.3

Acknowledgement

This thesis was made possible with the greatest kind and continuous support from many people and organizations. First and foremost, I would like to thank Associate Professor Takashi Asawa for giving me fine opportunity to conduct the research at Asawa lab in the School of Environment and Society, Tokyo Institute of Technology. Throughout the research, Associate Prof. Takashi Asawa has provided invaluable advice, knowledge, meaningful discussion. He kindly gave me an opportunity to conducting research on passive cooling methods adapting hot and humid climates. When I faced problems, his deep and extensive knowledge helped me to overcome them. Without his assistance, I could not complete the doctoral course within two years. In the mid-term presentation and EE seminar, Professor Naoki Kagi, Professor Masasi Matsuoka, Associate Professor Tsubasa Okaze, Associate Professor Kazuhiro Yuasa, and Assistant Professor Wataru Umishio gave me valuable comments to improve the research further.

In this thesis, all field measurements were carried out in YKK AP R&D Center, PT. YKK AP INDONESIA as a part of joint research. I feel gratitude to YKK AP Inc. for the permission to use the experimental building and research grants. I really appreciate Dr. Hiroshi Mori and Dr. Andhang Rakhmat Trihamdani for supports in the field measurements.

This research was conducted as a part of the research project of the Science and Technology Research Partnership for Sustainable Development (SATREPS). I would like to thank Professor Tetsu Kubota of Hiroshima University (HU) for invaluable advice, Processor Hideyo Nimiya of Kagoshima University, Associate Professor Tomonori Sakoi of Shinshu University, Professor Hiroto Takaguchi of Waseda University, Associate Professor Yukari Hirayama of Kogakuin University, Dr. Nikhil Kumar (HU), and Dr. Muhammad Nur Fajri Alfata (PUPR). I feel gratitude to Japan Science and Technology Agency (JST) and Japan International Cooperation Agency (JICA) for their financial supports. I thank Mrs. Eiko Takahashi (HU) for her kind support and assistance when I went to Indonesia.

I wish to thank Mrs. Chie Usuba who is a secretary of Asawa lab for kind support in our life of the lab. I had the opportunity to work with many fellow students in Asawa lab, Mrs. Maria Alejandra Del Rio, Ms. Momoka Nagasue, Ms. Kaho Hakamada, Mr. Hiroki Aoshima, Mr. Rei Kawamura, Mr. Zhang Tianxing, and Mr. Muhammad Emir Hanif Rasyadi. I am pleased to work together and submit papers.

Finally, I am most indebted to my wife and parents for their assistance and encouragement. They always supported what I want to do. Above all, I greatly thank for the wonderful journey.

January 2024
Haruka Kitagawa